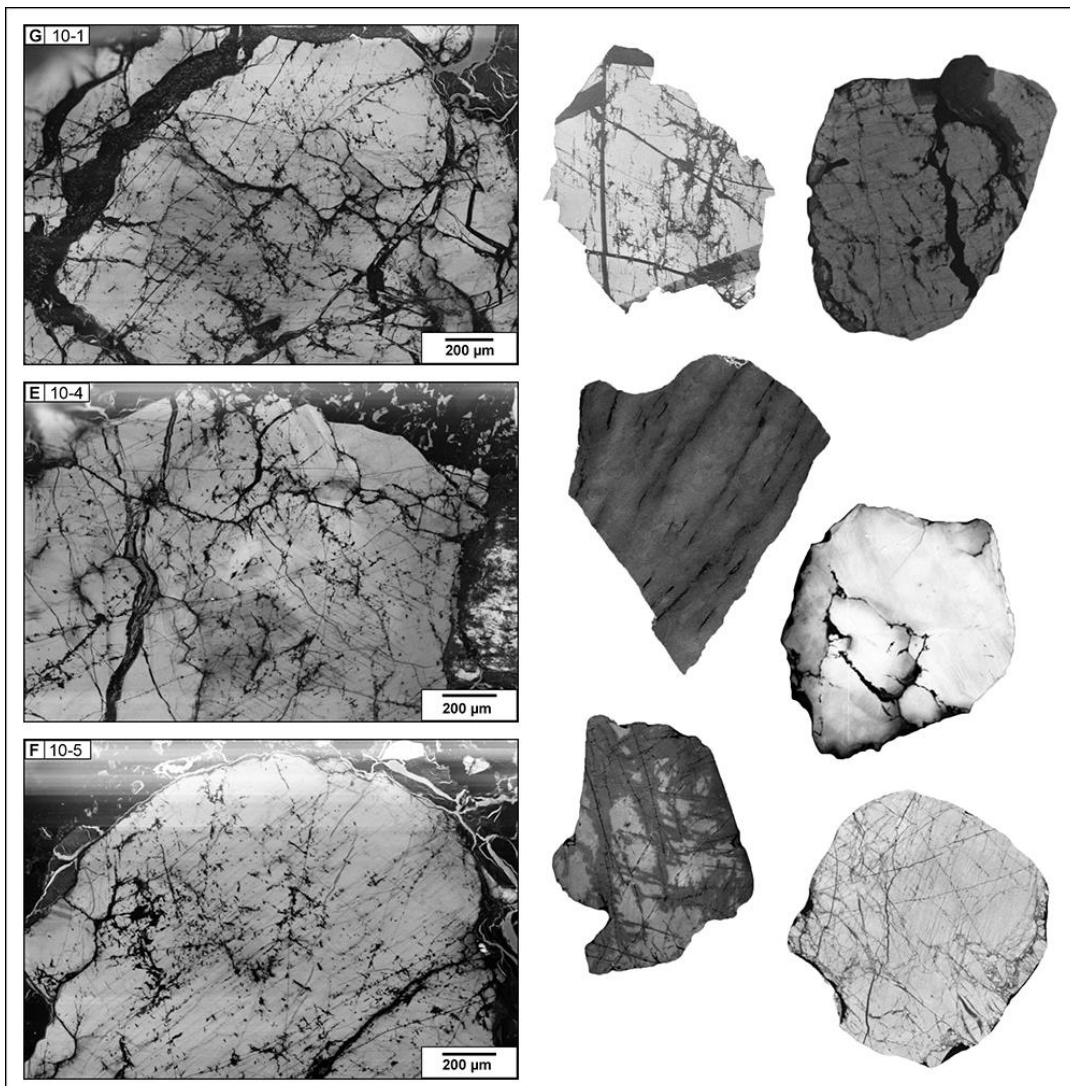


Tracking the sources of marine sediments on the Norwegian Sea continental shelf by using geochemical properties of detrital quartz

—
Sebastian Eugen Worm
Master thesis in Geology (GEO-3900)
May 2016



Faculty of Science and Technology

Department of Geology



**Tracking the sources of marine sediments
on the Norwegian Sea continental shelf
by using geochemical properties of detrital quartz**

*Master thesis in Sedimentology and Quaternary Geology
Submitted in partial fulfilment of the requirements for the degree of
MASTER OF SCIENCE*

Presented by
Sebastian Eugen Worm

Tromsø, May 2016

ABSTRACT

Provenance studies reconstruct the erosion and transport history of sediments based on character and composition of deposited sedimentological records with implications for uplift and subsidence of the investigated area. This Master thesis presents a new combination of in situ analytical methods for qualitative provenance studies exemplified on siliciclastic sediments from three offshore exploration wells in the Miocene Molo Formation on the Norwegian Sea continental shelf (wells 6610/3-1, 6610/7-1, 6510/2-1). The first method applied was scanning electron microscope backscattered electron and cathodoluminescence (CL) imaging. The second method was high-resolution trace element analysis by means of laser ablation combined with inductively coupled plasma mass spectrometry. The study focused on Al, Ti, Li, and Ge, which are among the most common trace elements in quartz and indicative for their crystallization environment. Based on CL and trace element properties, individual quartz grains were characterized and seven generic types of plutonic and metamorphic quartz grains were distinguished. These are indicative of different magmatic/metamorphic histories. The geochemical properties were used for a comparison with quartz grains in rocks sampled from Precambrian basement at saprolitic outcrops on Hadseløya and Hamarøy as well as with weathered bedrock samples from the Froan Basin (6408/12-U-01), and Ribban Basin (6814/4-U-1). An overlap of the quartz types within particular wells and among the three sampled wells implies common provenance and hence common sediment catchment areas for a depositional area comprising 130 km horizontally and 500 m vertically. The subtypes show various local basement provenance signatures and the classification implies a main provenance of granitic plutonic rocks. The properties of the quartz grains sampled offshore do not correspond to those from quartz in saprolitic sand and mangerite thin sections sampled on Hadseløya and Hamarøy. This implies that the locations did not act as sediment source for the Molo Formation but rather for the overlying Plio-Pleistocene Naust Formation. Best match between source and sink material was found among deeply weathered bedrock sampled from the Froan Basin and the Molo Formation, suggesting an alongshore south to north-eastern sediment transport direction.

Key words: Provenance study, quartz, cathodoluminescence, laser ablation, trace elements, saprolite, uplift, Norwegian Sea continental shelf, Molo Formation, Miocene

Acknowledgements

First and foremost I would like to thank my supervisors Jochen Knies and Axel Müller for their help and for giving me the opportunity to work within the *BASE* project.

My sincere thanks are due to Martin Worm and Simone Bechtold, who reviewed the manuscript critically and gave useful feedback on how to improve the quality of the thesis.

I wish to express my gratitude to all of my fellow students, especially to Lea Canzler, for their friendship and company throughout the time of our Master studies.

Above all, I am very thankful to my parents Ferdinand Worm and Cäcilia Brendieck-Worm for their generous support and encouragement during my entire university education.

Sebastian Worm

Tromsø, May 2016

Table of Contents

ABSTRACT	1
Acknowledgements.....	3
Table of Contents	5
Table of Figures	8
Abbreviations	10
Preface.....	11
1. INTRODUCTION AND OBJECTIVES	13
1.1 Leading geological question.....	13
1.2 Background.....	13
1.3 Tropical weathering in Norway – Saprolites	15
1.4 Properties and applicability of quartz	22
1.4.1 Physical and chemical properties.....	23
1.4.2 General applications.....	23
1.4.3 Occurrence of quartz.....	24
1.4.4 Trace elements in quartz.....	26
1.4.5 Laser ablation and trace element analysis.....	28
1.4.6 Cathodoluminescence properties of quartz	29
2. PHYSIOGEOGRAPHIC AND GEOLOGICAL SETTING	33
2.1 Hinterland and Oceanography	34
2.2 Geological background.....	38
2.2.1 Onshore geology	38
2.2.1.1 Geology north and south of Vestfjorden/Ofotfjorden	44
2.2.1.1.1 Geology north of Vestfjorden/Ofotfjorden.....	44
2.2.1.1.2 Geology south of Vestfjorden/Ofotfjorden	46
2.2.2 Offshore geology	49
2.2.3 Uplift of Fennoscandia	56
3. MATERIALS AND METHODS	61
3.1 Materials.....	61
3.1.1 Image data.....	61
3.1.2 Offshore samples	62
3.1.3 Offshore samples in detail	62
Well 6610/7-1: Sample 2, 3, 4.....	62
Well 6610/3-1: Sample 6 and 1.....	64

3.1.4. Onshore/basement samples	64
3.1.5 Onshore samples in detail.....	65
Hadseløya: Sample 5, 89415, 89418	65
Hamarøy: Sample 89421	65
Tysfjord, Hundholmen: Sample 47802.....	65
Well 6408/12-U-01 (32.42 m): Sample 10	65
Well 6814/4-U-1 (174.48 m): Sample 25	66
3.2 Methods	68
3.2.1 Specimen preparation.....	68
3.2.2 Scanning electron microscope: Backscattered electron.....	69
3.2.3 Cathodoluminescence imaging	70
3.2.4 Laser Ablation Inductively Coupled Plasma Mass Spectrometry.....	71
3.2.4.1 The ablation process in detail	73
3.2.4.2 LA-ICP-MS analysis and trace element evaluation.....	75
3.2.5 Classification and grouping of individual quartz grains	76
4. RESULTS.....	83
4.1 General cathodoluminescence observations.....	83
4.2 LA-ICP-MS analysis: Trace element content	84
4.3. Offshore samples.....	85
4.3.1 Cathodoluminescence properties of the offshore quartz grains.....	85
4.3.2 The seven quartz grain types in detail	87
4.3.4 The offshore samples in detail	91
Well 6610/7-1 (900 m): Sample 2	91
Well 6610/7-1 (920 m): Sample 3	95
Well 6610/7-1 (940 m): Sample 4	97
Well 6610/3-1 (460 m): Sample 1	99
Well 6610/3-1 (480 m): Sample 6	100
Well 6510/2-1 (441 m): Sample 3a	102
4.4 Onshore/basement samples	104
4.4.1 Cathodoluminescence properties of the onshore/basement samples	104
4.4.2 The onshore/basement samples in detail.....	104
Hadseløya: Sample 5	104
Hadseløya: Sample 89415	105
Hadseløya: Sample 89418	108
Hamarøy: Sample 89421	109

Tysfjord, Hundholmen: Sample 47802.....	110
Well 6408/12-U-01 (32.42 m): Sample 10	110
Well 6814/4-U-1 (174.48 m): Sample 25	112
5. DISCUSSION	115
5.1 General CL and LA-ICP-MS findings.....	116
5.2 The quartz grain classification.....	117
5.2.1 Features used for classification.....	119
5.2.2 Interpretation of features used for classification	119
5.2.3 Quartz type comparison with Svalbard.....	120
5.3 Cathodoluminescence properties of the offshore samples.....	121
5.3.1 Classification difficulties.....	122
5.3.1.1 Fluid and mineral inclusions versus structurally bound trace elements	125
5.4. Cathodoluminescence properties of the onshore/basement samples	126
5.5 Onshore - offshore comparison	127
Hadseløya: Sample 5	127
Hadseløya: Sample 89415	128
Hadseløya: Sample 89418 and Hamarøy: Sample 89421	131
Tysfjord, Hundholmen: Sample 47802.....	131
Well 6814/4-U-1 (174.48 m): Sample 25	133
Well 6408/12-U-01 (32.42 m): Sample 10	136
5.6 Discussion of the Onshore - offshore comparison.....	142
5.7 Absence of saprolitic sand in the Molo Formation	143
5.8 Preservation of saprolites in Norway	143
5.9 Sedimentation of the Molo Formation	145
5.10 Age of the saprolites	148
5.11 Critical consideration of the data.....	149
6. SYNTHESIS AND OUTLOOK	151
6.1 Summary and conclusion	151
6.2 Outlook.....	153
7. REFERENCES	157
8. APPENDIX.....	171

Table of Figures

Figure 1: World map showing the present distribution of deep tropical weathering	17
Figure 2: Modelled plate tectonic drift pattern of Norway	17
Figure 3: Schematic relief differentiation model	19
Figure 4: Idealized weathering profile of granitic bedrock under tropical climate.	20
Figure 5: Saprolitic profile on Hadseløya, south-west Vesterålen.....	21
Figure 6: Weathered basement and corestone development on Hadseløya.....	21
Figure 7: Metamorphic facies	25
Figure 8: Average concentration and variations of trace elements in natural quartz	27
Figure 9: Schematic quartz structure	28
Figure 10: Schematic representation of electron-beam response	29
Figure 11: Cathodoluminescence micrographs in comparison BSE micrographs	31
Figure 12: Overview map of the study area.....	33
Figure 13: Overview map of the Lofoten-Vesterålen area.	34
Figure 14: Near-surface Ocean currents of the North Atlantic.	35
Figure 15: Reconstruction of ice flow patterns and fast-flowing ice streams.	37
Figure 16: Overview map of the major geological subdivisions of the Baltic Shield.....	39
Figure 17: Simplified tectonic map of the Scandinavian Caledonides.....	44
Figure 18: Bedrock geology map of the Lofoten-Vesterålen archipelago.	45
Figure 19: Main geological provinces around the Froan Basin.....	47
Figure 20: Tectonostratigraphic map of Norway and its passive continental margin.....	48
Figure 21: Overview map of Oligocene to Pliocene wells at the NCS.....	50
Figure 22: Isopach map of the Molo Formation	51
Figure 23: Seismic representation of the Naust Fm, Brygge Fm, and Molo Fm.	53
Figure 24: Seismic profiles across the mid-Norwegian shelf	54
Figure 25: Idealized sketch illustrating uplift and subsidence mechanisms.....	57
Figure 26: Exemplary true-colour scan of an offshore sample.....	63
Figure 27: Exemplary true-colour scan of a basement sample	66
Figure 28: Software interface of New Wave Research – Laser Ablation System	73
Figure 29: Scans demonstrating the laser ablation procedure.....	74
Figure 30: Micrographs showing specimen preparation-induced cracks.....	77
Figure 31: Most common artefacts that occur in CL scanning.	79
Figure 32: Quartz grains scanned with CL with indicated primary and secondary features... ..	79
Figure 33: CL micrographs showing contrast features used for classification	80
Figure 34: CL micrographs showing features used for classification and grouping	81
Figure 35: Grain roundness distribution of all offshore sediment samples	84
Figure 36: Average lattice-bound trace element concentrations of LA-ICP-MS analyses.	85
Figure 37: Percentages of the quartz grain types	87
Figure 38: Example of a Type A grain.....	87
Figure 39: Example of a Type B grain.....	88
Figure 40: Example of a Type C grain.....	88
Figure 41: Example of a Type D grain.....	88
Figure 42: Example of a Type E grain.....	89
Figure 43: Example of a Type F grain	89
Figure 44: Example of a Type G grain	90
Figure 45: Trace element concentrations plotted with respect to quartz type	90

Figure 46: Trace element signature of plutonic and metamorphic grains..	91
Figure 47: Different types of quartz grains found in sample 2	92
Figure 48: Medium-grade metamorphic quartz grains found sample 2	92
Figure 49: Different types of low-grade metamorphic quartz grains found in sample 2.	93
Figure 50: Plutonic quartz grains of sample 2.	94
Figure 51: Trace element variation of offshore sample 2.	94
Figure 52: Different types of plutonic quartz grains found sample 3.	95
Figure 53: Examples of plutonic grains attributed to Type A, found in sample 3	96
Figure 54: Examples of metamorphic quartz grains of sample 3.	96
Figure 55: Examples of plutonic quartz grains from sample 4.	97
Figure 56: Different types of plutonic quartz grains found sample 4.	98
Figure 57: Low-grade metamorphic quartz grains found in sample 4.	98
Figure 58: Different plutonic quartz grain types found in sample 1.	99
Figure 59: Plotted trace element concentrations of sample 1	100
Figure 60: Different plutonic quartz grain types found in sample 6.	101
Figure 61: Different metamorphic quartz grain types found in sample 6.	101
Figure 62: Different plutonic quartz grain types found in sample 3a.	102
Figure 63: Different plutonic quartz grain types found in sample 3a.	103
Figure 64: SEM-CL and corresponding BSE micrographs of sample 5	105
Figure 65: SEM-CL and BSE micrographs of sample 89415.	106
Figure 66: Plotted trace element concentrations of sample 89415 and 89421.	107
Figure 67: CL and BSE micrographs of sample 89418.	108
Figure 68: Representative quartz grains found in Sample 89421.	109
Figure 69: Representative thin section details of sample 47802.	110
Figure 70: SEM-CL and BSE micrographs of deformed quartz crystals in sample 10	111
Figure 71: SEM-CL micrographs of deformed quartz crystals in sample 25.	112
Figure 72: Plotted trace element concentrations of all 5 onshore/basement samples.	113
Figure 73: Summarized classification of metamorphic quartz grains.	117
Figure 74: Summarized classification of plutonic quartz grains	118
Figure 75: Examples of grains with domains that potentially can represent other grains....	124
Figure 76: Representative grain selection showing dark staining along micro-fractures	125
Figure 77: Closest matches of the onshore - offshore comparison of sample 5	128
Figure 78: Closest matches of the onshore - offshore comparison of sample 89415.	129
Figure 79: Trace element concentrations of sample 89415 compared with Type F grains ..	130
Figure 80: Closest matches of the onshore - offshore comparison of sample 47802.	132
Figure 81: Closest matches of the onshore - offshore comparison of sample 25.	134
Figure 82: LA-ICP-MS data of Type A grains.	135
Figure 83: Closest matches of the onshore - offshore comparison of sample 10.	137
Figure 84: Trace element concentrations of sample 10 in comparison	138
Figure 85: Trace element data of Li and Al for all offshore grains in comparison.	139
Figure 86: Summarized results of the onshore - offshore comparison from sample 25.	140
Figure 87: Summarized results of the onshore - offshore comparison from sample 10.	141
Figure 88: Palaeogeographical interpretation of the Late Miocene.	147

Abbreviations

Ab	albite, a plagioclase feldspar
µm	micrometre, one millionth of a metre
BAM	<i>Bundesanstalt für Materialforschung und -prüfung (Federal Institute for Materials Research and Testing)</i>
BSE	backscatter electron
CCD	charge coupled device
CL	cathodoluminescence
e.g.	exempli gratia, for example
EPMA	electron microprobe analysis
et al.	et alia, and others
Fm	formation
Fs	feldspar
Ga	gigaannum, billion years
GW	gigawatt, one billion watts (joule per second)
Hz	hertz, one cycle per second
i.e.	id est, that is
ICP	inductively coupled plasma
IR	infrared
IRD	ice rafted debris
Kbar	kilobar
Kfs	K-feldspar, potassium feldspar
LA	laser ablation
Laser	light amplification by stimulated emission of radiation
LOD	limit of detection
m a.s.l.	metres above sea level
Ma	megaannus, million years (ago)
MS	mass spectrometry
NCS	Norwegian Sea continental shelf
NGU	<i>Norges Geologiske Undersøkelse (Geological Survey of Norway)</i>
NIST	<i>National Institute of Standards and Technology</i>
NPD	<i>Norwegian Petroleum Directorate</i>
nm	nanometre, one billionth of a metre
ppm	parts per million
QAPF	Quartz, Alkali feldspar, Plagioclase, Feldspathoid
Qtz	quartz
RKB	rotary Kelly bushing (metres below rig floor)
SEM	scanning electron microscope
SRM	standard reference material
TIB	Transscandinavian Igneous Belt
TWIN	Tropical Weathering in Norway
UHP	ultra high pressure
UV	ultraviolet
WGR	Western Gneiss Region
Z	atomic number (from German: Zahl)

Preface

This study is part of the project *Basement fracturing and weathering on- and offshore Norway - Genesis, age, and landscape development* (BASE), a joined research program implemented by four teams at the *Geological Survey of Norway* (NGU) and *SINTEF Petroleum Research*, both located in Trondheim, Norway. The project, designated for four years (2013-2017), investigates age, present distribution, former extend, and relevance of fractured and weathered basement rocks in Norway. It is funded by the following gas and oil companies: *Lundin Petroleum*, *Det Norske Oljeselskap*, *Maersk Oil*, and *Wintershall*.

1. INTRODUCTION AND OBJECTIVES

1.1 Leading geological question

This Master thesis aims to illustrate and critically examine a new multi-methodological approach for sediment provenance studies using geochemical and luminescence properties of individual quartz grains in siliciclastic sediments.

A combination of analytical methods is applied to identify specific characteristics of sediment particles that can be used to track their source area, defined as the location the original material was first exposed to weathering and erosion. The methods include imaging with a scanning electron microscope (SEM) equipped with a cathodoluminescence (CL) detector, as well as mass spectrometry (MS) combined with laser ablation (LA).

The question will be addressed as to whether quartz particles found within Miocene sediment layers on the Norwegian Sea continental shelf are directly derived from saprolitic outcrops of basement rocks presently preserved on the mainland of northern Norway. The practicality to match the sediment grains to this specific source will be tested and alternative sediment provenance consulted.

1.2 Background

Extensive offshore drilling by numerous gas and oil companies on the Norwegian Sea continental shelf (NCS) has contributed to an abundance of geological data over the last few decades (e.g. Ottesen et al., 2009). These data, combined with countless seismic profiles, enabled a reasonable understanding of the subsurface and revealed a long succession of geological history represented in sedimentary layers deposited on the continental shelf. However, most of those ancient layers are sparsely represented on the mainland of Norway or even completely absent today. Uplift and glacial erosion in the Cenozoic Era erased most geologic evidence (e.g. Riis, 1996; Stuevold & Eldholm, 1996). It might be obvious to assume that all deposited sediments offshore originate from the elevated, proximal hinterland. However, sedimentary transport is complex, influenced by various processes and has to be studied in detail before an authoritative conclusion can be drawn.

At only one known locality on mainland Norway Mesozoic remnants of rocks and sediments have been preserved (see Ørving, 1960; Dalland, 1975; and Bøe et al., 2010 for a review). This locality allows insights into past geologic times of elsewhere eroded material and is of significant importance for sediment provenance studies and the overall geological history of Norway and its continental margin.

Likewise scarce but more common than rocks of actual Mesozoic age are locations with preserved remnants of basement rocks that were affected by Mesozoic weathering. For this Master thesis, samples taken from such locations in northern Norway serve as potential source material for sediments today buried deep within the adjacent continental shelf. The objective is to link source and sink by a systematic comparison of on- and offshore sediment and solid rock samples. The required data for the investigation was obtained by a number of destructive and non-destructive analytical methods which will be illustrated in detail (chapter 3). The study utilizes CL signal properties and chemical trace element content data gathered by laser ablation inductively coupled plasma mass spectrometry (LA-ICP-MS). By this means, luminescent and geochemical characteristics of sediment grains were identified and representative categories within the investigated samples developed accordingly. Sediment grains that show similarities in terms of CL signal and trace element content are interpreted to represent a common source as the properties are the result of a common crystallization and/or metamorphic history. The method allows, in theory, an allocation of sediments to their source area if the properties identified emerge in source- and sink sediments equally.

This chapter provides a theoretical background of the methods and introduces the main types of the investigated material. In order to provide sufficient background knowledge that allows a placement of the study sites with its sampled material in a vertical, horizontal, and temporal context, important general properties and geologic relevance of both source and sink area material are presented first.

After a subsequent presentation of the study area and the stratigraphy of the NCS (chapter 2), the applied methodology as well as the equipment used will be illustrated. The quartz grain categories and relevant trace element data will then be presented and interpreted. Finally, the overall applicability of the multi-methodological approach for provenance studies will be discussed.

In the following, the potential source material, i.e. saprolitic corestones and derived sand taken from the mainland will be introduced. This subchapter is followed by a general description of the mineral quartz, which is the object of investigation for the entire study. The suitability of the mineral will be emphasized and discussed. Both subchapters contain explanations of the most important geological and geomorphological processes involved, especially weathering and sedimentation.

1.3 Tropical weathering in Norway – Saprolites

Weathering is the main process that leads to disintegration of solid rock material and is requisite for clastic sediments (Nesbitt et al., 1997). The process is driven by a variety of agents that operate in different ways depending on the prevailing climate or latitude, respectively. The rates of weathering are controlled by the source rock composition and may vary according to changes in the tectonic setting (Nesbitt et al., 1997; Nesbitt, 2003). All of these factors have a strong influence on the production and composition of sediments.

Solid crystalline bedrock is influenced by atmospheric processes causing weathering as soon as it is exposed at the Earth's surface. However, under certain circumstances, weathering can affect the basement or bedrock that is still buried under sediments or soil. Or, put another way, the weathering surface can be shifted downwards when loose material stays on top of it. Erosion, the removal and transport of the weathered particles, usually takes over and eventually the material is deposited as sediment remotely when transport ceases. Whether or not erosion takes place depends on the availability of transport agents and the relief at and around the weathered material. In the course of geologic time, deposition of once weathered and eroded material has built up thick sediment packages especially on shelves of passive continental margins. At the mid-Norwegian shelf, this package reaches a thickness of more than 2000 m (Smelror et al., 2007). Tectonically undisturbed weathering and erosion eventually form a flat, slightly undulating planation surface called peneplain (Reusch, 1901; 1903). This is the last state of the erosion cycle and can be defined as a state where the base level is equal or close to sea level.

Deep chemical weathering, as opposed to physical weathering on exposed rocks, is usually assigned to tropical and subtropical latitudes (see Fig. 1) in areas where warmer climate with a higher humidity favour chemical reactions (White & Blum, 1995; White et al., 1999; Nesbitt,

2003). An extensive vegetation cover might also facilitate chemical weathering (Drever, 1994; Nesbitt, 2003). Constant percolation of potentially acidic rainwater is reduced in higher latitudes due to the temporary storage of precipitation as snow and ice. Rates of chemical weathering are therefore reduced (Nesbitt, 2003). The presence of deeply weathered layers or remains of such layers that have been found on the mainland of Norway (Olesen, 2012), presently lying at high latitudes with temperate to arctic climate, brings up the question of how these layers have evolved (see Fig. 2).

The primary agents of chemical weathering are water charged with CO₂ and organic acids (Nesbitt & Young, 1984). Deep weathering profiles develop when erosion rates are low and acid input (e.g. through precipitation or released by roots) is high (Nesbitt et al., 1997). Chemical weathering of feldspars (or other primary minerals) leads to the formation of clay minerals, referred to as secondary weathering products. Certain clay minerals as for example smectite, kaolinite, or gibbsite in particular are indicative of strong weathering that occurred most probably in a warm and humid climate (Roaldset et al., 1982) (Fig. 3 & 4).

The general importance of deep weathering as a process formative for the relief, especially on bedrock, has long been recognized and was mainly observed and studied in regions actually featuring tropical climate (e.g. Thomas, 1966, and references therein). The idea that deep chemical weathering was a major process that also extensively shaped the Scandinavian landscape was introduced by Lidmar-Bergström (1982; 1988) and mainly studied and demonstrated in southern Sweden.

Weathering in Norway of supposedly pre-glacial age was already described around 100 years ago (Schetelig, 1918, cited in Låg, 1945). Låg (1945) noted that thick layers of residual soil or weathered rocks are not expected to be found in Fennoscandia, referring to the recent glaciations. Similar observations have been made in Finland (Kejonen, 1985) and Scotland (Fitzpatrick, 1963; Hall, 1985). The thickness and position of the weathered profiles suggested that the material has somehow survived glacial erosion. However, the sole presence of these profiles does not necessarily exclude the possibility that the weathering occurred more recently during post-glacial times (Peulvast, 1985; 1988; Sørensen, 1988). Kejonen (1985) in fact clearly sees the weathering to be of pre-glacial origin but also states that the observed type of weathering, called *grusification*, could also have developed in the present climate. Peulvast (1985; 1988) came to a similar conclusion for his study of in situ weathered rocks in the Lofoten-Vesterålen area in northern Norway.

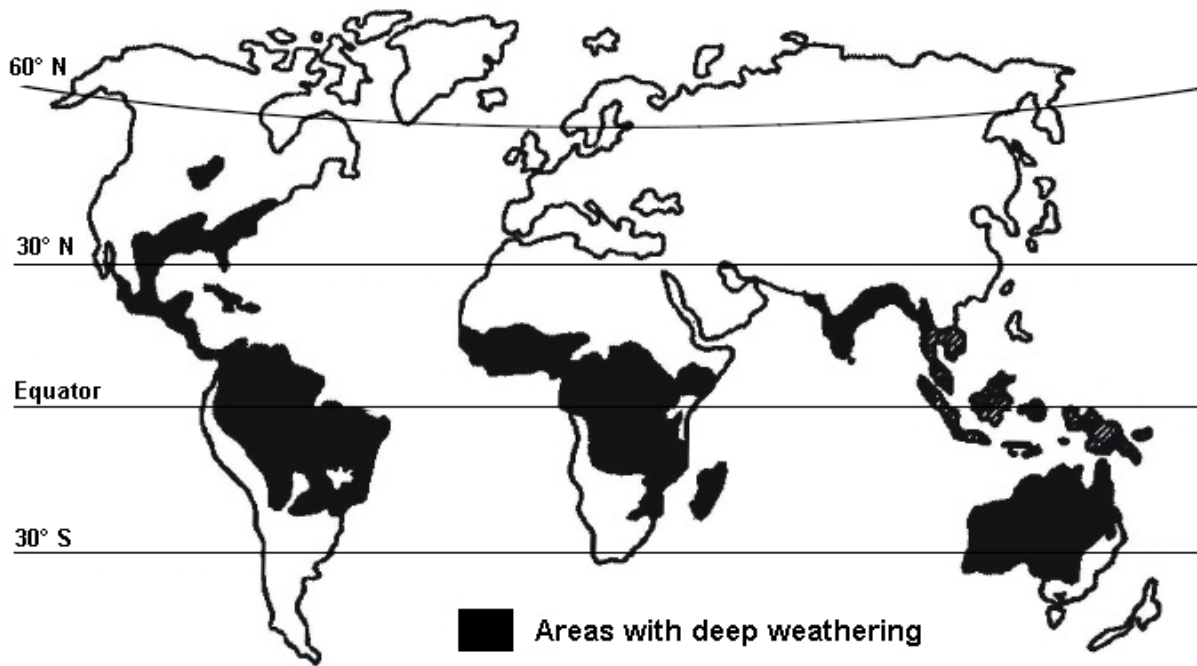


Figure 1: World map showing the present distribution of deep tropical weathering. Modified after Büdel (1982).

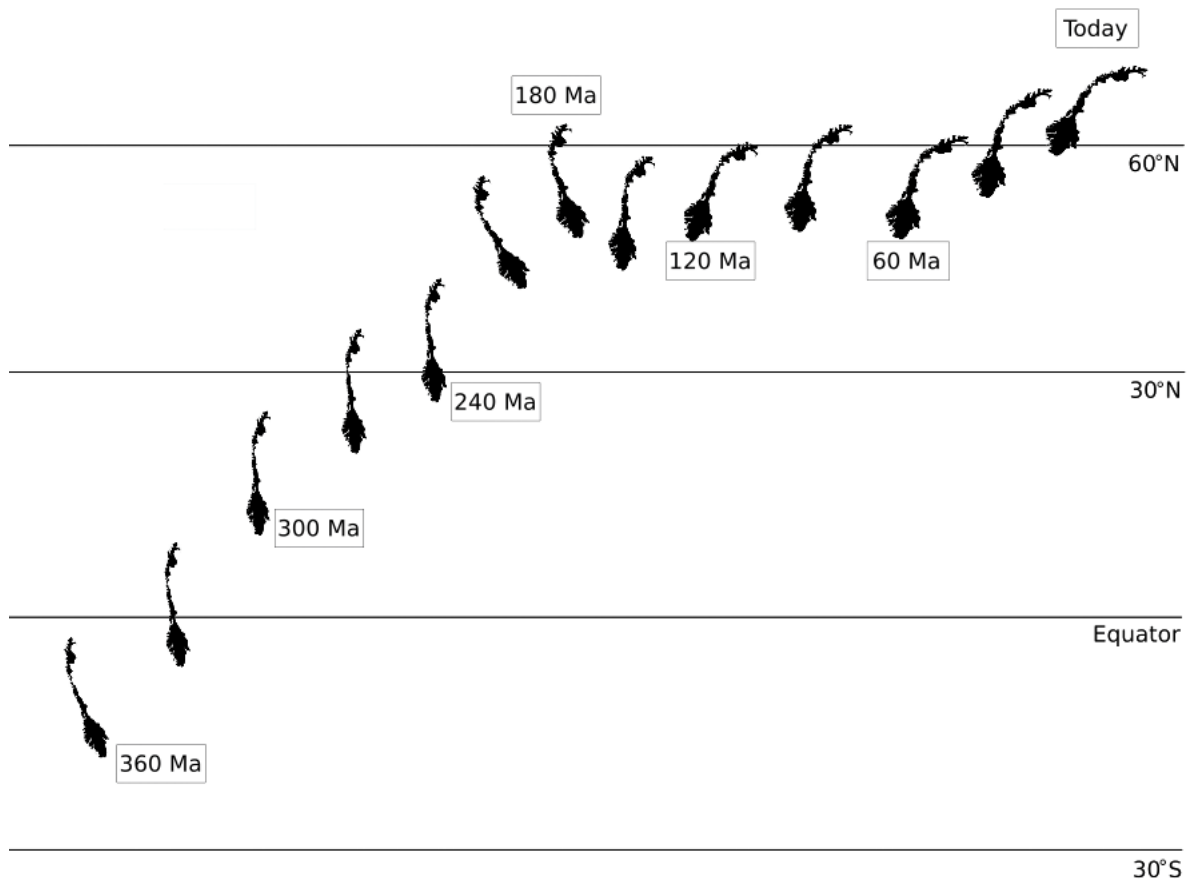


Figure 2: Modelled plate tectonic drift pattern of Norway from Carboniferous to the present day. The model indicates that the part of the Baltic Shield that comprises Norway today was situated at tropical latitudes at least until Triassic times. Figure modified after R. J. Watson, based on data from Torsvik & Cocks (2016). Source: NGU (2015).

Pre-glacial weathering in a tropical climate is questioned mainly because of the low clay content at some investigated localities of deep weathering (Peulvast, 1985; 1988). However, Roaldset et al. (1982) investigated weathered gabbro and granite in western Norway and found high amounts of clay minerals indicative of lateritic weathering. Lateritic weathering has been known to occur under tropical climate conditions and according to Roaldset et al. (1982), the findings suggest an age of at least late Neogene. Nesje et al. (1988) also report clay minerals indicative of pre-glacial weathering and agree with Roaldset et al. (1982).

The majority of authors favour the idea that the deep weathering occurred in pre-glacial, warmer climate and that the profiles have been preserved throughout the Pleistocene glaciations. A major contribution to the subject was done by Lidmar-Bergström (1982; 1988; 1995; 1999), who linked deep weathering processes to many of the landscape surface characteristics of Scandinavia that were usually seen as the result of glacial erosion. According to Lidmar-Bergström (1995), glacial erosion and differences in bedrock alone cannot explain the vertical relief variations on the Baltic Shield. In Sweden, the Precambrian basement shows regional variations independent of rock type. According to Lidmar-Bergström (1995), the time of basement surface exposure and weathering intensity during the Phanerozoic are the most important factors that shaped the diverse relief rather than the eroding force of the ice sheet and glaciers (Lidmar-Bergström, 1995). The joint valleys in southern Sweden were formed in the Neogene as a result of denudation of Mesozoic weathered basement that developed in faults and fractures (Lidmar-Bergström, 1995). The character of this relief is also present in Norway (Olesen et al., 1997) and an extension of this explanation for the landscape development to Norway seems reasonable (Olesen et al., 2012; Olesen et al., 2013).

Tropical Weathering In Norway (TWIN) is the name of a joint research project that predominantly studied saprolites (i.e. weathered bedrock) on- and offshore Norway and ties on the results of Lidmar-Bergström acquired in Sweden. The TWIN project was established in 2009 as a collaboration of the *Geological Survey of Norway (NGU)* and the *Norwegian Petroleum Directorate (NPD)*. The main results are summarized in a comprehensive report authored by Olesen et al. (2012). The project established a database containing all known locations of deep weathering in Norway and investigated selected localities of saprolite occurrences in southern and northern Norway. Two of those localities were also sampled, studied, and discussed for this thesis.

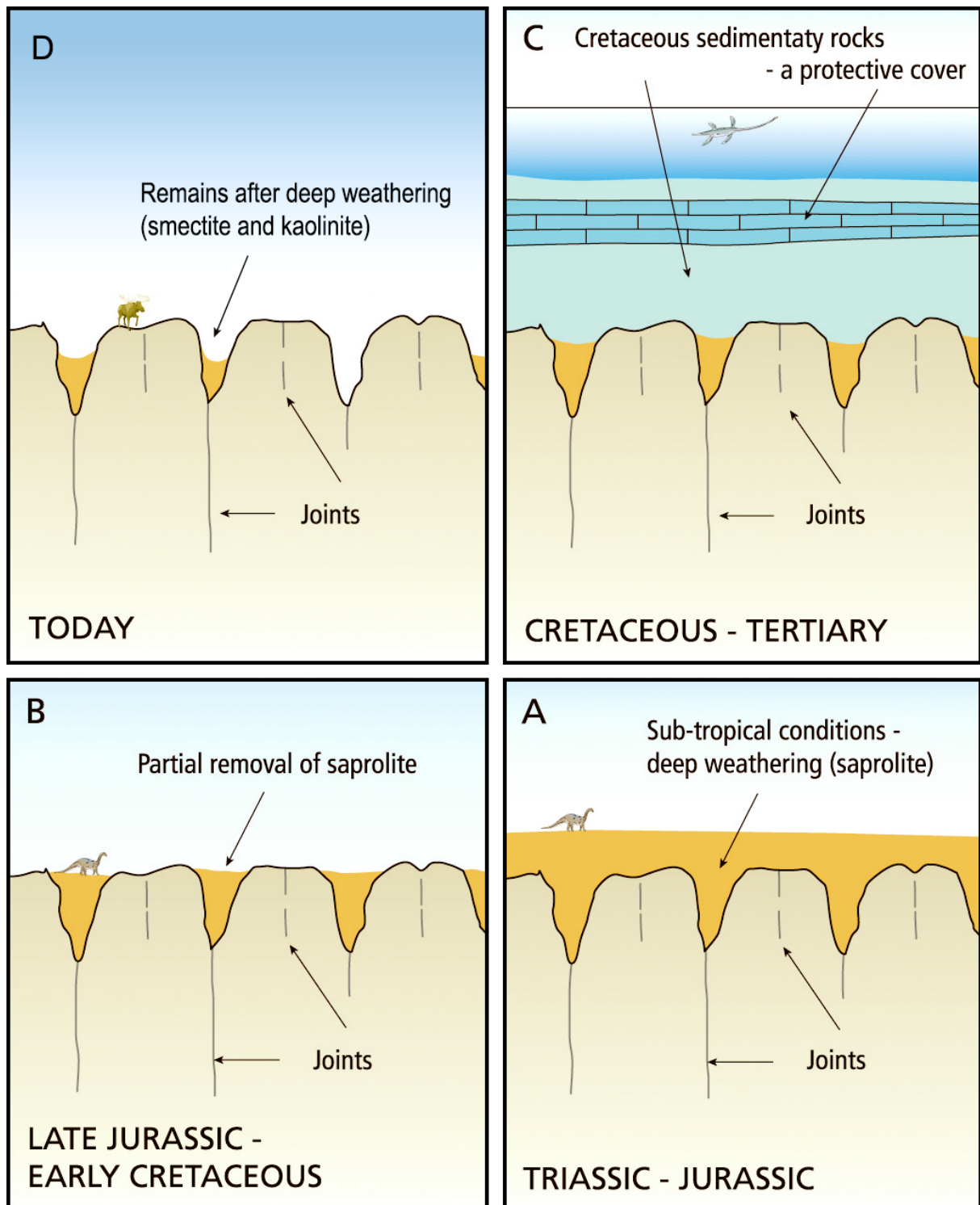


Figure 3: Schematic relief differentiation model suggesting a possible development of weathering surfaces on the Baltic Shield. **A:** Sub-tropical weathering dissolves bedrock especially along pre-existing fractures (indicated joints). **B:** Removal of the weathered material by erosion. **C:** Preservation of the developed landscape due to relative sea level rise and associated sedimentation of marine sediments on top of it. **D:** Present situation. Neogene uplift and associated erosion proceed relief differentiation. Erosion of the weathered material has increased relief amplitude. The model is based on Lidmar-Bergström (1995); here modified after Olesen et al. (2007).

The word saprolite is derived from the Ancient Greek word “sapos” and literally means “rotten rock” or “decomposed rock”. As indicated in Fig. 4, saprolites develop when upper parts of basement rock are affected by extensive chemical weathering without subsequent erosion. Saprolites can be seen as disintegrated, decomposed bedrock at its original position (autochthon), forming a smooth transition zone between solid rock and soil (see Fig. 4). Especially in this transition zone (zone III and IV in Fig. 4), between the yet solid rock and the loose material lying on top of it, corestones can develop. Corestones are the result of spheroidal or concentric weathering and are commonly found in saprolitic profiles (see Fig. 6).

As in Sweden, deeply weathered basement in Norway is predominantly preserved along faulted and fractured zones where confined subsurface structures lead to concentrated per-

colation of acid rainwater (Olesen et al., 2012). In deep fractured zones surrounded by crystalline basement, weathered material is more likely to be preserved for a long period of time. A prerequisite for the development of saprolites is therefore persistent tectonic stability.

There is much evidence that deep weathering has a strong influence on the shape of bedrock (see Lidmar-Bergström, 1995, and references therein). The differences in relief remaining when the saprolites are removed depend on bedrock properties (erodibility), course and spacing of joints, and the overall weathering history (Lidmar-Bergström, 1995).

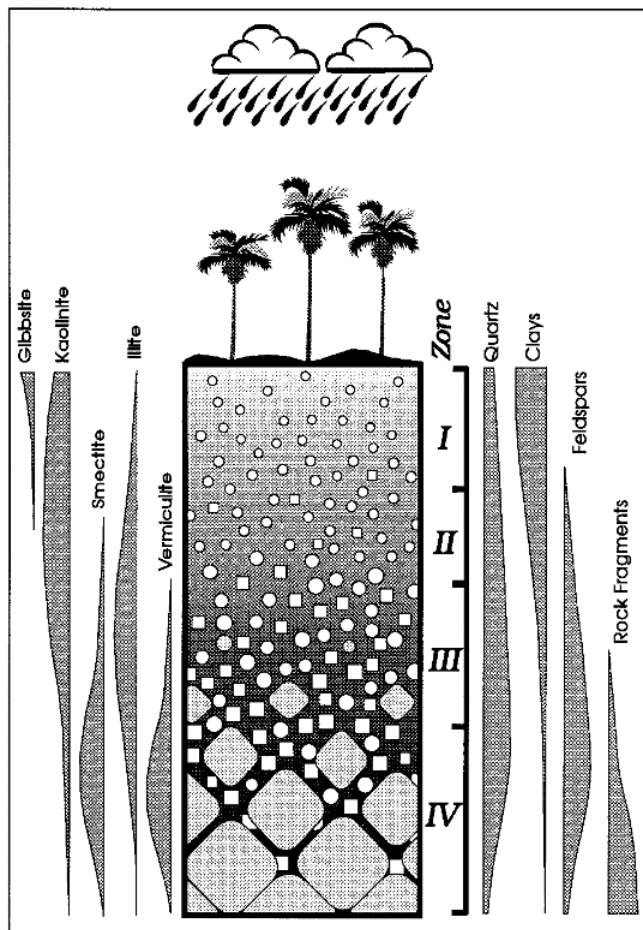


Figure 4: Idealized undisturbed weathering profile of granitic bedrock under tropical climate conditions. The four zones indicate successive grades of weathering starting from bedrock with joints and corestone development (IV) to clay-rich soil devoid of original rock texture (I). The columns on the left and right show the relative increase and decrease of clay types and residual weathering products. Source: Nesbitt (1997).



Figure 5: Saprolitic profile in Brennvinsaugen on Hadseløya, south-west Vesterålen. The scarp is approximately 18 m high. Details are given in Fig. 6 below.

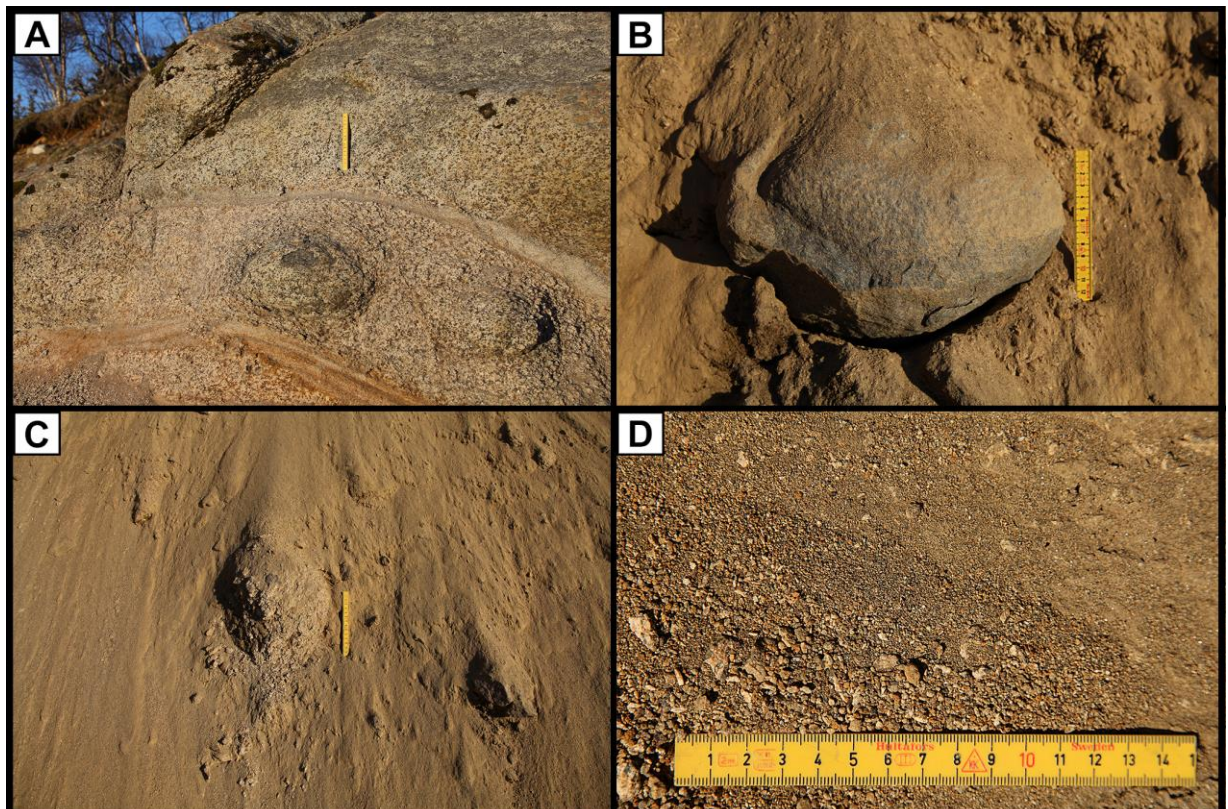


Figure 6: Weathered basement and corestone development on Hadseløya, south-west Vesterålen. **A:** Corestone development in an outcrop representing zone IV (see Fig. 4). The preserved crystalline fabric is evidence for the *in situ* state of the weathering. **B:** Solid corestone in loose weathered material. **C:** Strongly weathered remains of a corestone. **D:** Grus of different grain sizes at the foot of an open profile (Fig. 5). Scale bar in all four images: 15 cm.

The known sites with saprolites in Scandinavia are interpreted to represent remnants of layers once having much greater horizontal and vertical extend (Olesen et al., 2012). According to this assumption, most of the material was eroded, transported, and deposited on the shelf and adjacent areas. The yet remaining saprolites on the mainland somehow have survived glacial erosion, given they are of pre-glacial age. This allows to consult the material as reference for provenance studies of sand deposited on the proximal shelf. The former extent of the saprolite layers remains unknown, as does the present location of the eroded material. The term saprolite does not imply any specific composition. However, the global prevalence of the mineral quartz in basement rocks makes saprolites and saprolitic sand suitable for provenance studies based on quartz.

Saprolitic layers feature a higher porosity and permeability than the basement below and can principally serve as hydrocarbon or groundwater reservoir or migration path for hydrocarbons of economic interest. In addition, deeply weathered rock formations are potentially hazardous for constructions as for example tunnels or foundations and can possess a danger of rock avalanches and slides (Olesen et al., 2012). Their extent in both horizontal and vertical direction is therefore of great interest not only for geologists.

1.4 Properties and applicability of quartz

Since this study is exclusively based on quartz, some general information and properties of the mineral are given first. Quartz is a mineral composed of silicon dioxide, also called silica, a chemical compound of one silicon and two oxygen atoms (SiO_2). It is the most common silica modification. Quartz exists in nature in many varieties in both colour and microstructure and is a major constituent of numerous rock types. Quartz is considered one of the most pure minerals in the Earth's crust that in its purest form contains only small amounts of trace elements (Götze, 2009; 2012; Müller et al., 2012). Quartz is particularly applicable for provenance studies due to a variety of unique properties.

1.4.1 Physical and chemical properties

Quartz has a white streak, vitreous luster, and a hardness of 7 on the Mohs scale of mineral hardness which basically refers to scratch resistance. The room-temperature form of quartz (α -quartz) turns into the high-temperature β -quartz at 573°C under atmospheric pressure as it undergoes crystal structure change. This implicates that a very high temperature is necessary to change the intrinsic properties of a quartz grain once it is crystallised (e.g. Müller et al., 2002). Size and shape and corresponding roundness and sphericity change as the grains undergo physical contact with other solid matter on the sedimentary transport path. However, the overall inner structure stays the same which was repetitively shown by quartz-based provenance studies (e.g. Bernet & Bassett, 2005; Seyedolali et al., 1997). Nevertheless, once a quartz grain enters the geologic rock cycle again by increasing metamorphism and possibly melts, its geological history is erased. It remains unknown whether or not and how often a mineral has already been part of that cycle.

From a chemical point of view, quartz also comprises an exceptional stability. Experiments have shown that dissolution of quartz does not occur in most natural environments since solutions are easily saturated in the mineral (Nesbitt et al., 1997, and references therein). The weathering of feldspars in rocks also containing quartz releases SiO_2 to solution, which readily leads to quartz saturation and a stop of further dissolution (Nesbitt et al., 1997).

1.4.2 General applications

Quartz has become an important natural source for silicon used in semiconductor industry and for mono- and polycrystalline silicon in the photovoltaic industry. It also finds versatile applications as glasses or component of glasses in its amorphous state. Furthermore, quartz is used as a raw material for gemstones and decorations due to its colourful varieties (e.g. amethyst, rose quartz, tiger's eye, or the hydrated opal).

1.4.3 Occurrence of quartz

The Earth's solid crust is predominantly made of silicates resulting in silicon being the second most abundant element in the crust after oxygen. Quartz is therefore one of the most common minerals found within and on the continental crust and is a substantial constituent of all granitoids. With 20 % of all minerals, quartz is the second most abundant mineral in the upper continental crust after plagioclase (Nesbitt & Young, 1984). Quartz crystallizes from magma or precipitates hydrothermally. As a rock-forming mineral it occurs in sedimentary, metamorphic, as well as in plutonic rocks. An overview of estimates of the quartz distribution in different rock types is given by Wedepohl (1995). Whitish quartz is referred to as milky quartz when it is characterized by frequent fluid inclusions that are caused by fluids present during crystallisation and is commonly found precipitated in hydrothermal quartz veins. Hydrothermal fluids can provide suitable pressure and temperature conditions for quartz formation that are usually found in greater depths only. Hydrothermal quartz therefore forms in a wide range of pressure and temperature conditions (Rusk, 2012). Igneous quartz includes volcanic and plutonic quartz. Volcanic quartz is derived from volcanic eruptions and lava outflow. The grains usually undergo rapid cooling and hence crystallization. Textures, as for example growth zoning, are therefore commonly well preserved (Rusk, 2012). Plutonic quartz crystallizes more slowly in plutons deep within the continental crust, which is a common process in subduction zones. Quartz of any origin that underwent strong metamorphism is referred to as metamorphic quartz. It can be differentiated between low-grade, medium-grade and high-grade metamorphic quartz (according to today's concept of the metamorphic facies, based on early work by Eskola, 1920) (see Fig. 7). This differentiation is a representation of how strongly the minerals, or the rock containing the minerals, has been deformed. Quartz formed in situ by recrystallization or precipitation from fluids is referred to as authigenic quartz. This can principally occur with any type of quartz if the required diagenetic or metamorphic conditions are given. A single detrital grain with authigenic quartz overgrowth can hence consist of parts or zones that formed far apart from each other.

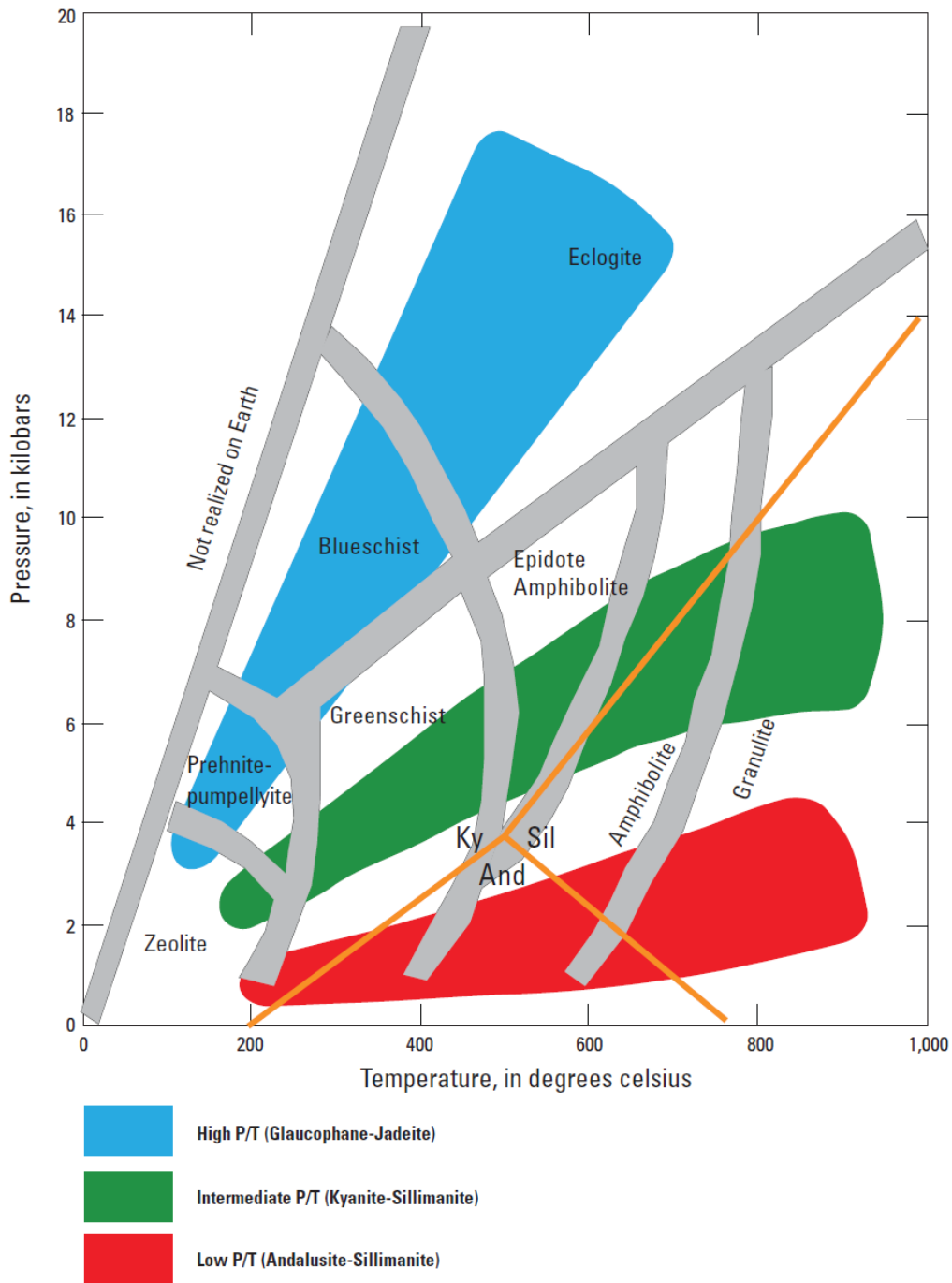


Figure 7: Pressure-temperature diagram showing the 8 principle metamorphic facies. The grey lines indicate that boundaries between the facies are gradational and have to be seen as proximate values. Source: Dusel-Bacon (2012). Based on data by Holdaway (1971) and Spear (1993).

All these types of quartz are subject to the same physical processes after their formation and quartz sand is one of the most common clastic sediments. Clastic sediments (as opposed to biogenic sediments) are particles derived from larger rock material broken down by weathering and erosion. Particles of disintegrated parental rock are usually carried by wind and water

(and, to a lesser extent, by ice) away from their original source. Transport predominantly follows the gravitational pull towards a depositional sink. On the way from the source to the sink, grains are shaped by abrasion and as a general rule, roundness increases and grain size decreases with increasing distance.

Sand particles usually slow down and deposit at coast when transport agents like water of narrow rivers lose energy by entering larger bodies of water. Due to its relatively high hardness and hence resistance to abrasion and dissolution, quartz sand is highly abundant in many mature depositional areas and generally seen as a residual mineral (e.g. Nesbitt et al., 1997; Nesbitt, 2003).

Considered, for example, the common plutonic parental rock granite, the less stable feldspar and mica minerals erode earlier (Grant, 1963; Nesbitt & Young, 1984), disintegrate into smaller particles and are subsequently transported further away. This leaves the amount of quartz relatively increased in both its source and sink area (e.g. Nesbitt et al., 1996; Nesbitt et al., 1997).

1.4.4 Trace elements in quartz

Trace elements in minerals are conventionally defined as being less abundant than 0.1 weight percentage (< 1000 ppm). Even though quartz is one of the most pure minerals in the world, it may always contain quantifiable amounts of trace elements (Fig. 8). The amount of such elements in quartz is highly confined due to several reasons. There is only a limited number of ions that can substitute for the silicon ion Si^{4+} in the crystal lattice, mainly due to its small size (Götze et al., 2004; Götze, 2009). Possible substitutional ions include Al^{3+} , Fe^{3+} , B^{3+} , Ti^{4+} , Ge^{4+} , and P^{5+} (Müller et al., 2012). Other ions such as Li^+ , K^+ , Na^+ , H^+ , and Fe^{2+} occur at interstitial positions in the lattice. In addition, the strong atomic configuration of the SiO_2 bonds prevents most other elements from being incorporated into the atomic structure (Flem et al., 2002). The incorporation of single external ions into the crystal lattice leads to so called point defects (e.g. Götze, 2012a) (Fig. 9). Impurities of quartz also occur as larger defects within the crystal lattice (interstitial) or as mineral or fluid inclusions. Lattice defects can generally occur in different types and frequencies, depending on the conditions that prevailed during mineralization (Götze, 2009). Mineral and fluid inclusions are not considered to be trace elements in a strict sense since they are generally seen as remnants of other, not specifically quartz-

related materials, which were present during the crystallisation of the quartz mineral. Therefore, they are excluded from this study and only used quantitatively for classification purposes. The most common structurally bound trace element in quartz is aluminium, followed by titanium (Götze, 2009; Müller et al., 2012) (Fig. 8). Aluminium is the third most common element in the continental crust (see e.g. review in Taylor, 1964). In addition to the global prevalence of the element, the cations Si^{4+} and Al^{3+} feature similar ionic radii, which favours substitution (Götze, 2009). Several studies attempted to distinguish between structurally bound, “true” trace elements and those concentrated in inclusions (e.g. Blankenburg et al., 1994; Gerler, 1990; Götze et al., 2004). Figure 8 illustrates amounts and type of the most common structurally bound trace elements in natural quartz. This thesis concentrates on the elements Al, Ti, Li, and Ge that are known to be mainly structurally bound. In addition, these four elements occur at elevated concentrations in quartz and are genetically indicative of magmatic rocks (e.g. Müller et al., 2015). Other analysed elements, such as Na, K, and Mg are known for commonly being hosted by fluid inclusions (Müller et al., 2003; Götze et al., 2004) and are therefore used to verify the data obtained by LA-ICP-MS (see below). Unusually high amounts of Fe, for example, indicate mineral inclusions involved in the data.

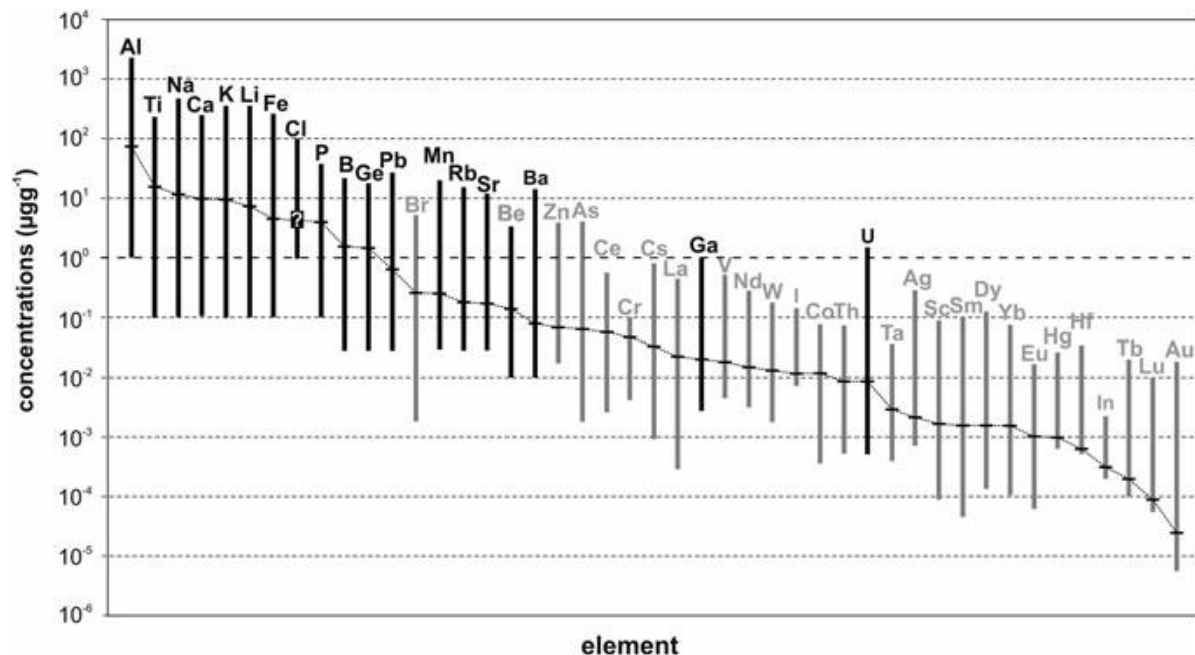


Figure 8: Compiled average concentration and variations of lattice-bound trace elements in natural quartz. Data is based on an average of 2500 LA-ICP-MS analyses. Data shown in black: 2117 LA-ICP-MS analyses carried out at NGU in Trondheim (Müller et al., 2012). Data shown in grey: Gerler (1990), Blankenburg et al. (1994), and Götze (2009). Chlorine concentrations are uncertain due to the very high detection limit of approximately 100 ppm. Source: Müller et al. (2012).

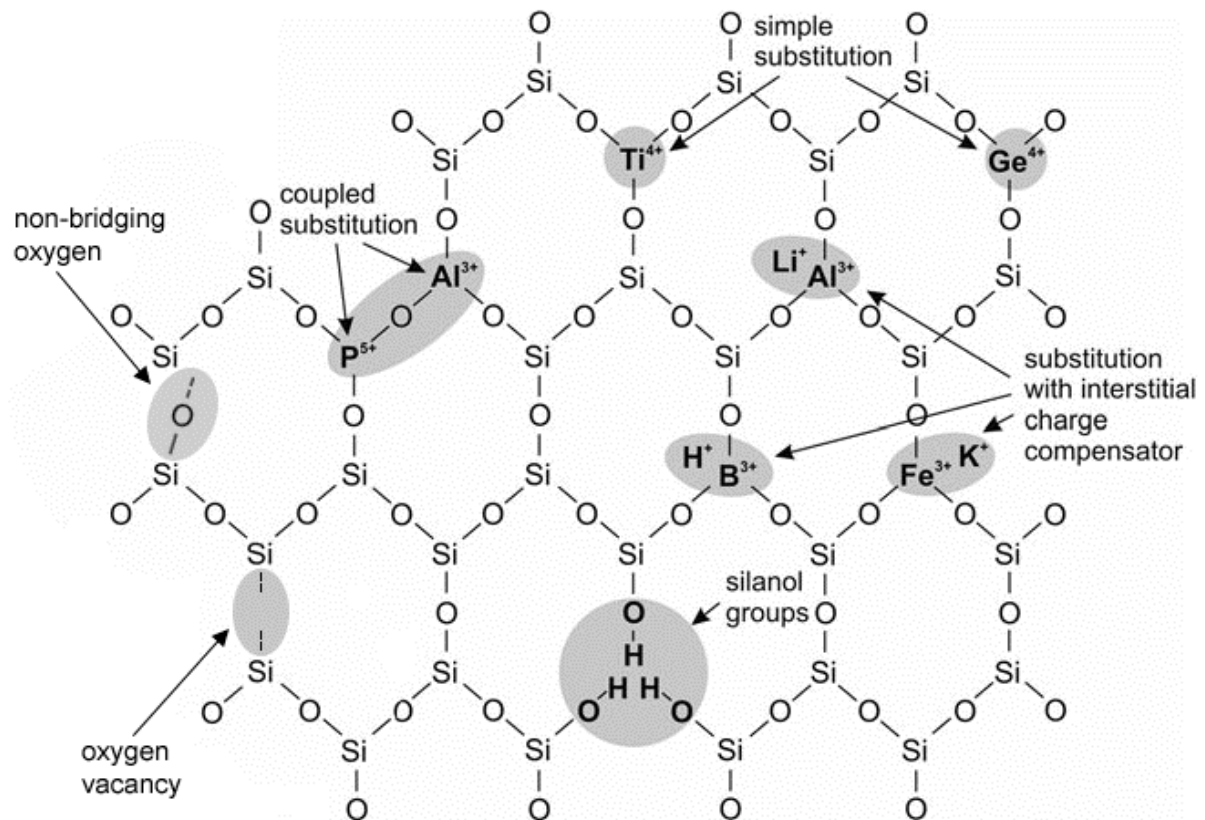


Figure 9: Schematic quartz structure indicating the configuration of the most common possible lattice defect types. Modified from Müller et al. (2012) and Götze (2009).

1.4.5 Laser ablation and trace element analysis

The general usefulness of trace elements in quartz as indicators for provenance has long been recognized (see Dennen, 1967, and references therein). Dennen (1967) already states that quartz derived from different granites can be distinguished by different trace element proportions. The achievable resolution and speed for trace element analyses increased dramatically within the last decades with the development of LA-ICP-MS (Flem et al., 2002; Müller et al., 2003; Flem & Müller, 2012). Laser ablation is a process in which a highly focused laser beam removes material from a sample. The vaporized matter can then be analysed by an inductively coupled plasma mass spectrometer, which reveals the concentration of elements selected prior to the analytical process. Highly sophisticated calibration is necessary especially for quartz analyses since trace element contents are close to the detection limits (LOD) of the equipment. Nevertheless, LA-ICP-MS allows the detection of trace elements even in high-pu-

quartz (Müller et al., 2012). Chemical cleaning in order to remove mineral and fluid inclusions is not necessary since the method allows optical control and manual determination of ablation paths around visible impurities. The employed application and more specific details are described in chapter 3: *Materials and Methods*.

1.4.6 Cathodoluminescence properties of quartz

This subchapter provides a short introduction to cathodoluminescence (CL) as used in mineralogy with emphasis on the CL properties of quartz. More details and the specific application of the method are given in chapter 3. Since the study at hand uses panchromatic CL micrographs only, terms such as black and white or dark and bright referring to CL contrasts are to be seen relatively. Different contrasts represent different colours that were used in several, especially early optical CL studies but neglected here.

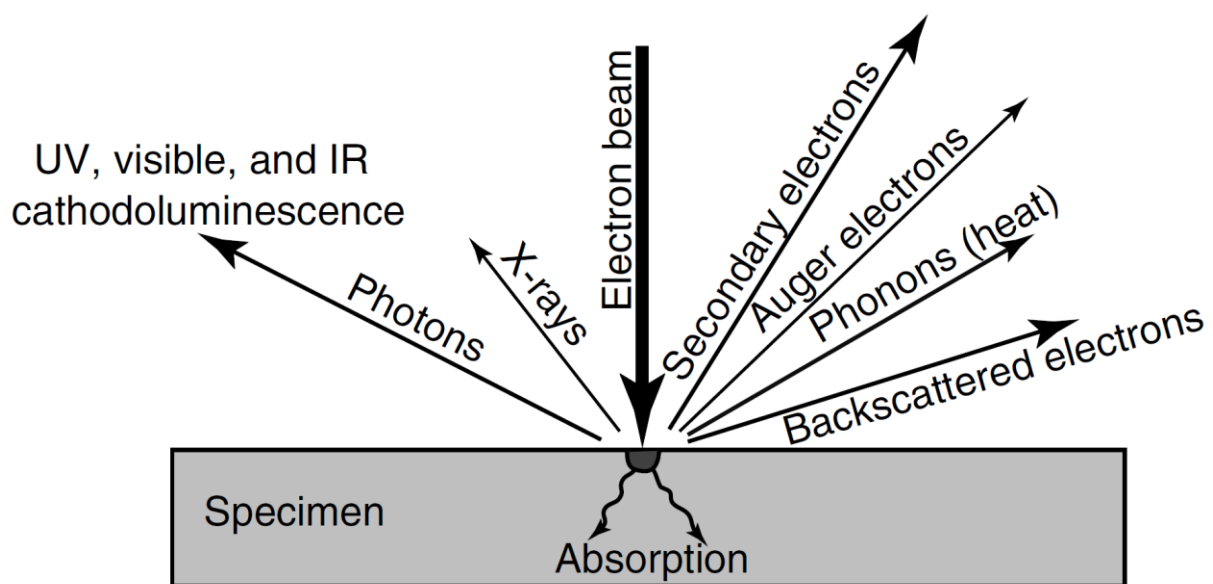


Figure 10: Schematic representation of electron-beam response and interaction with a specimen. The signals are measurable with different detectors that can be attached to a scanning electron microscope. The respective emissions originate from different depths of the sample, e.g. cathodoluminescence from deeper than backscattered electrons. Source: Boggs & Krinsley (2006), based on Walker & Burley (1991).

Cathodoluminescence is a type of luminescence generated by high-energy electron irradiation (see Fig. 10). The energy is transmitted via a cathode, which gives the type of luminescence its name. The CL characteristics of a sample can be investigated with a SEM equipped with a

CL detector. The technique is used in mineralogy as a high-resolution analytical method capable of visualising internal structures of merely weak-luminous minerals such as quartz. By this means, features are revealed that are indiscernible with SEM in backscattered electron mode or optical microscopy (see Fig. 11) (Seyedolali et al., 1997). For example, sand that consists only of high-purity quartz appears whitish when viewed with the naked eye under visible light. A closer look at natural sand grains deposited at the coast usually reveals some variation in colour ranging from glassy-transparent to black (see Fig. 26). CL visualizes colours and contrasts that emerge as response to intrinsic properties of the crystal that are still not fully understood (Seyedolali et al., 1997; Bernet & Bassett, 2005; Müller et al., 2012). Structures and features revealed by CL include growth zoning, traces of cracking, fracturing and shearing on a micro-scale, different quartz generations within single grains, and fluid migration-induced alterations along fractures (Müller et al., 2012). Consequently, the CL signal can hold information on the crystallization and deformation history of quartz. The distribution, variation, and concentration of trace elements within the crystal lattice are known to be the main cause for the diverse CL contrasts (Bernet & Bassett, 2005; Müller et al., 2012). Deformation, including fluid migration along micro-fractures, leads to redistribution of trace elements in the quartz lattice (Müller et al., 2002). Studies by Sippel (1968) and Smith & Stenstrom (1965) already described the possibility to differentiate between primary (i.e. unaltered, original) and secondary (altered) quartz by different CL contrasts. The dark appearance of secondary quartz in contrast to primary quartz was repeatedly demonstrated by several studies (Seyedolali et al., 1997; Müller et al., 2002; Müller et al., 2003; Bernet & Bassett, 2005; Müller et al., 2012; Götze, 2012b). The majority of these studies confirmed that the low CL signal in secondary quartz is due to low defect concentrations in the crystal lattice. The different CL contrasts were hence proven to be influenced by the trace element distribution, although the overall CL signal might be influenced by other features, like for example lattice defects that are not trace element-related. Figure 11 below provides a comparison of two types of scanned images (micrographs) obtained with SEM applying different types of detectors.

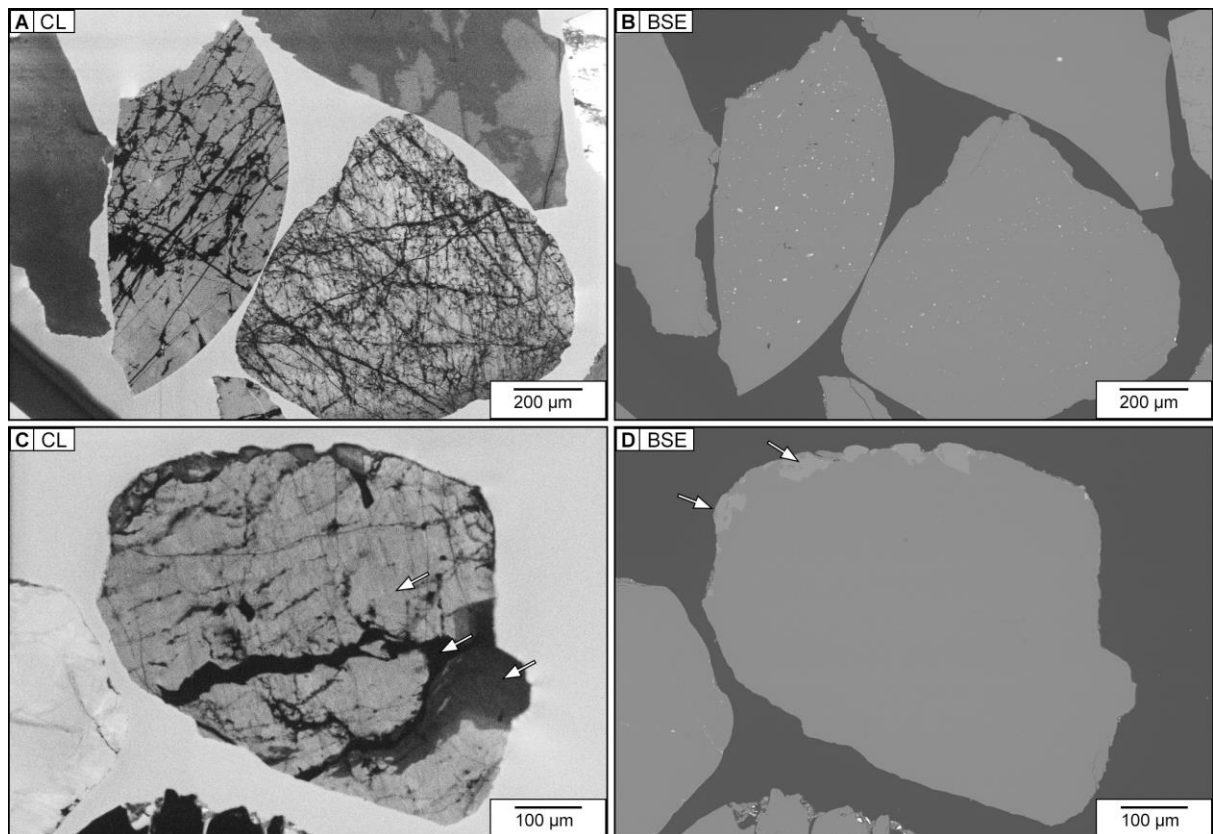


Figure 11: Cathodoluminescence (CL) micrographs in comparison with Backscatter electron (BSE) micrographs. **A:** CL revealing frequent secondary structures in the quartz grain but no distinct micro-inclusions are visible. **B:** The same location on the sample scanned with BSE revealing frequent micro-inclusions (white dots) but no secondary structures. **C:** CL scan revealing three different mineral alterations of the grain (arrows). **D:** BSE scan of the same location revealing that all three alterations consist of the same mineral, but traces of a different mineral phase become visible at the grain margin (compare arrows).

The use of CL properties of sediment particles for provenance studies has long been established in sedimentology (see Götze & Zimmerle, 2000; and Götze et al., 2001 for a review). The same applies to the use of trace element signatures. The multi-methodological approach for provenance studies that combines both techniques was recently introduced to the scientific community (Müller & Knies, 2013). The CL signal in combination with data obtained by LA-ICP-MS provides a unique technique to reveal characteristic properties of sediment grains that together can be seen as a fingerprint or a “mineralogical DNA sequence”. This fingerprint represents the chemical conditions of the mineral during the time of its formation (Götze, 2009).

The advantages of quartz for provenance studies can be summarized as follows:

- Quartz is a substantial constituent of most continental rocks including the granitic/gneissic basement in the study area.
- Because of the high abundance of quartz, the presented approach allows the application for provenance studies with comparability across the globe.
- Quartz grains are exceptionally resistant to both physical and chemical weathering.
- Quartz has exceptionally stable SiO₂ bonds that allow only limited incorporation of other (foreign) elements into its crystal lattice. Once the foreign elements are incorporated during crystal growth, they can only hardly be removed or redistributed by weathering, erosion, and diagenesis.
- The high purity of the mineral allows a relatively fast and accurate analysis with laser ablation and inductively plasma mass spectrometry without sophisticated specimen preparation.
- The cathodoluminescence signal as a result of the trace element content and the distribution of lattice defects does not change on the way to the depositional sink given that no metamorphic processes are involved.

2. PHYSIOGEOGRAPHIC AND GEOLOGICAL SETTING

This study focuses on the Norwegian Sea continental shelf (NCS) and coastal area of north-western Norway (Fig. 12). The Norwegian Sea lies between the North Sea in the south and the Barents Sea in the north and borders on the Greenland Sea towards the west. The study area includes the inner shelf, an island of the Lofoten-Vesterålen archipelago (Hadseløya), as well as adjacent peninsulas on the mainland south of that island (Hamarøy, Hundholmen) (Fig. 13). It stretches across the Arctic Circle from 64° N to 69° N. The whole study area thereby extends over a distance of approximately 560 kilometres along the shelf and coast. This chapter presents a general geological and geomorphological background and elucidates the concept of mountainous uplift.

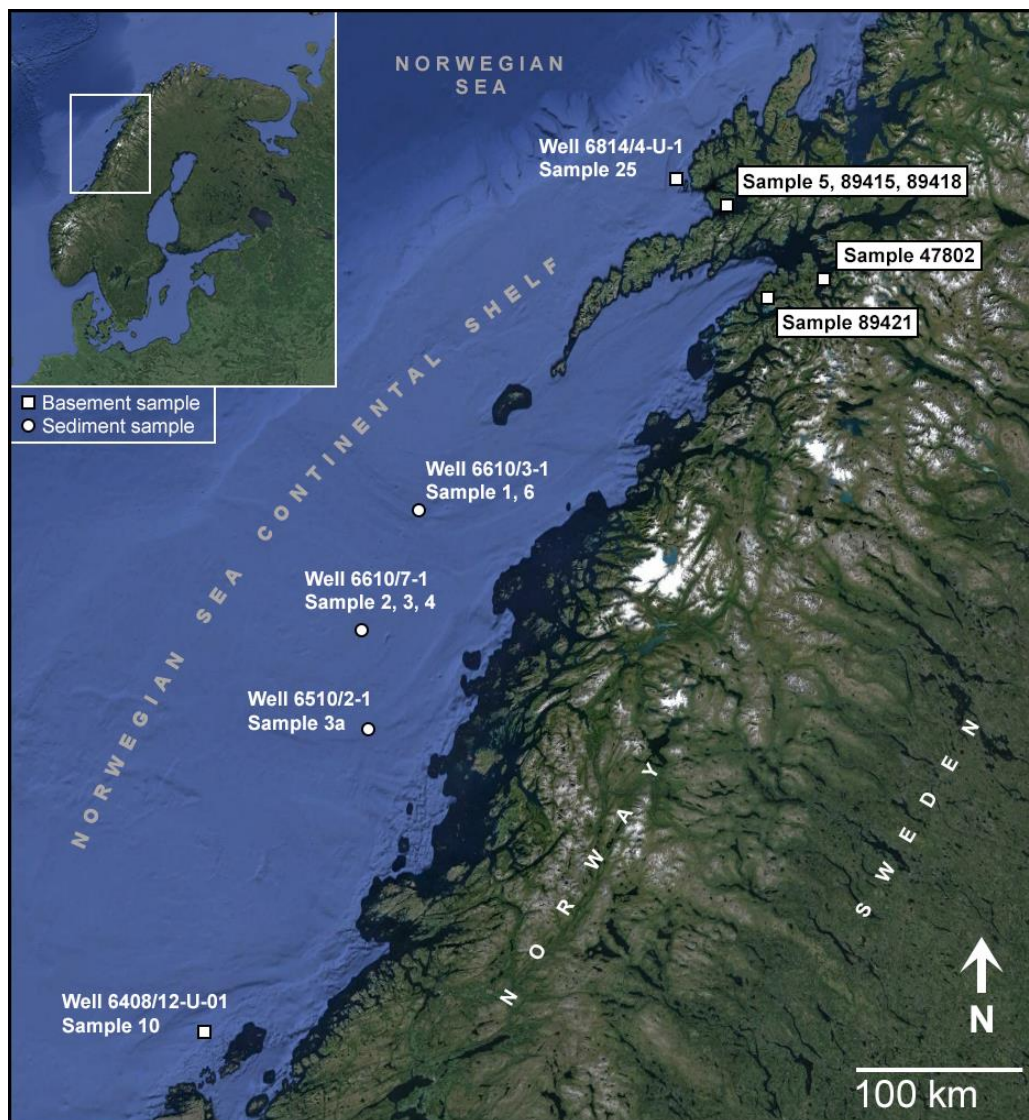


Figure 12: Overview map of the study area with indicated sample sites. For the Lofoten-Vesterålen area in more detail, see Fig. 13 below. Background images: Google Earth, 2013.

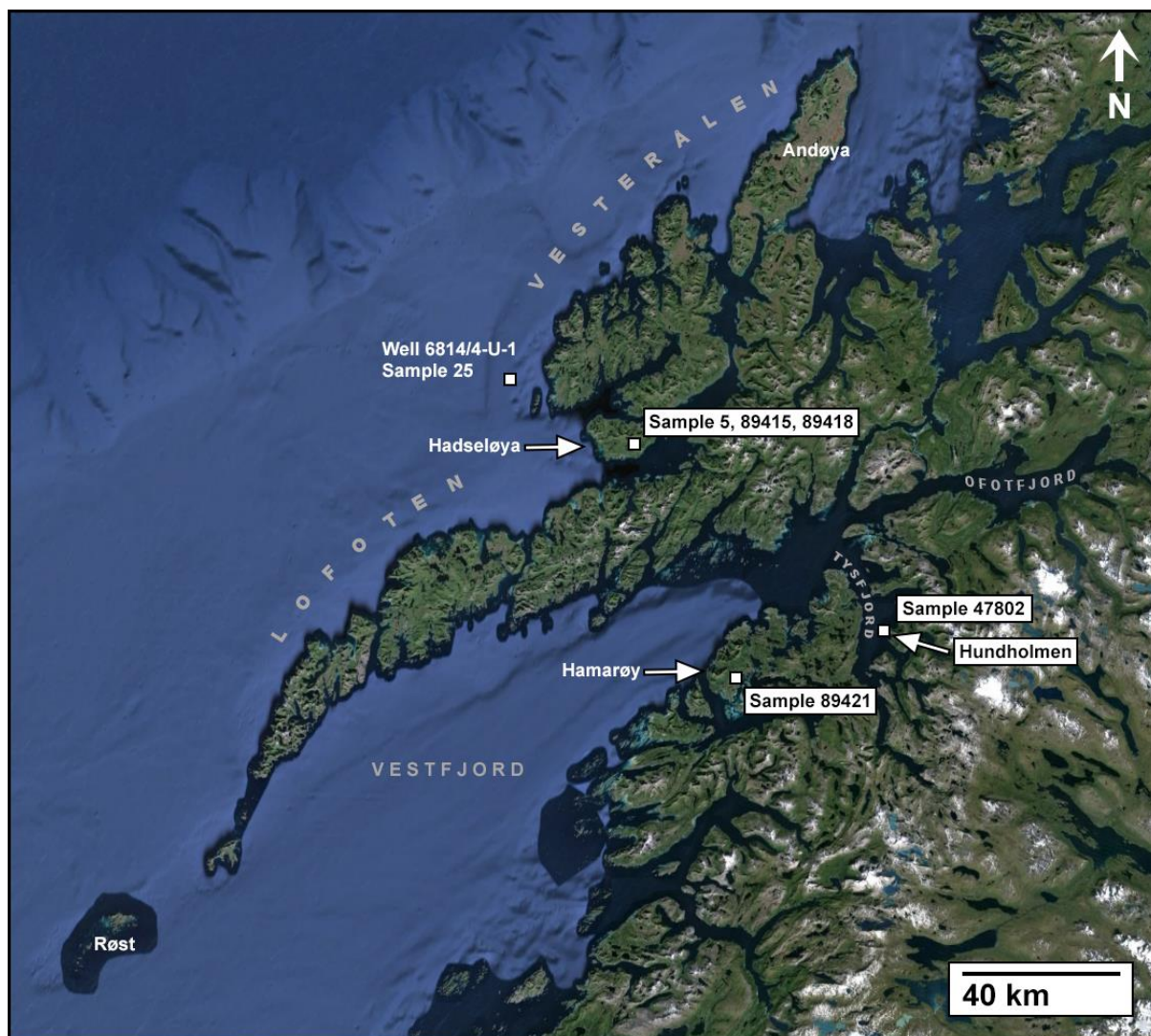


Figure 13: Overview map of the Lofoten-Vesterålen area that indicates the northern basement sample sites. Background image: Google Earth, 2013.

2.1 Hinterland and Oceanography

The Norwegian Sea is the easternmost part of the open North Atlantic Ocean and is influenced by the northward moving Norwegian Current, a warm coastal current that forms a branch of the North Atlantic Drift, which in turn is a continuation of the Gulf Stream (see Krauss, 1986; Rossby, 1996; Hansen & Østerhus, 2000) (Fig. 14). The Norwegian Sea is ice-free throughout the year. An ice cover only develops in small fjords in the interior of the country during winter. Compared to other areas west of the North Atlantic that lie at the same latitude, Norway features a relatively mild climate. This is mainly due to the warm ocean current and the influence of the South Westerlies (see Seager et al., 2002; Meteorologisk institutt, 2016).

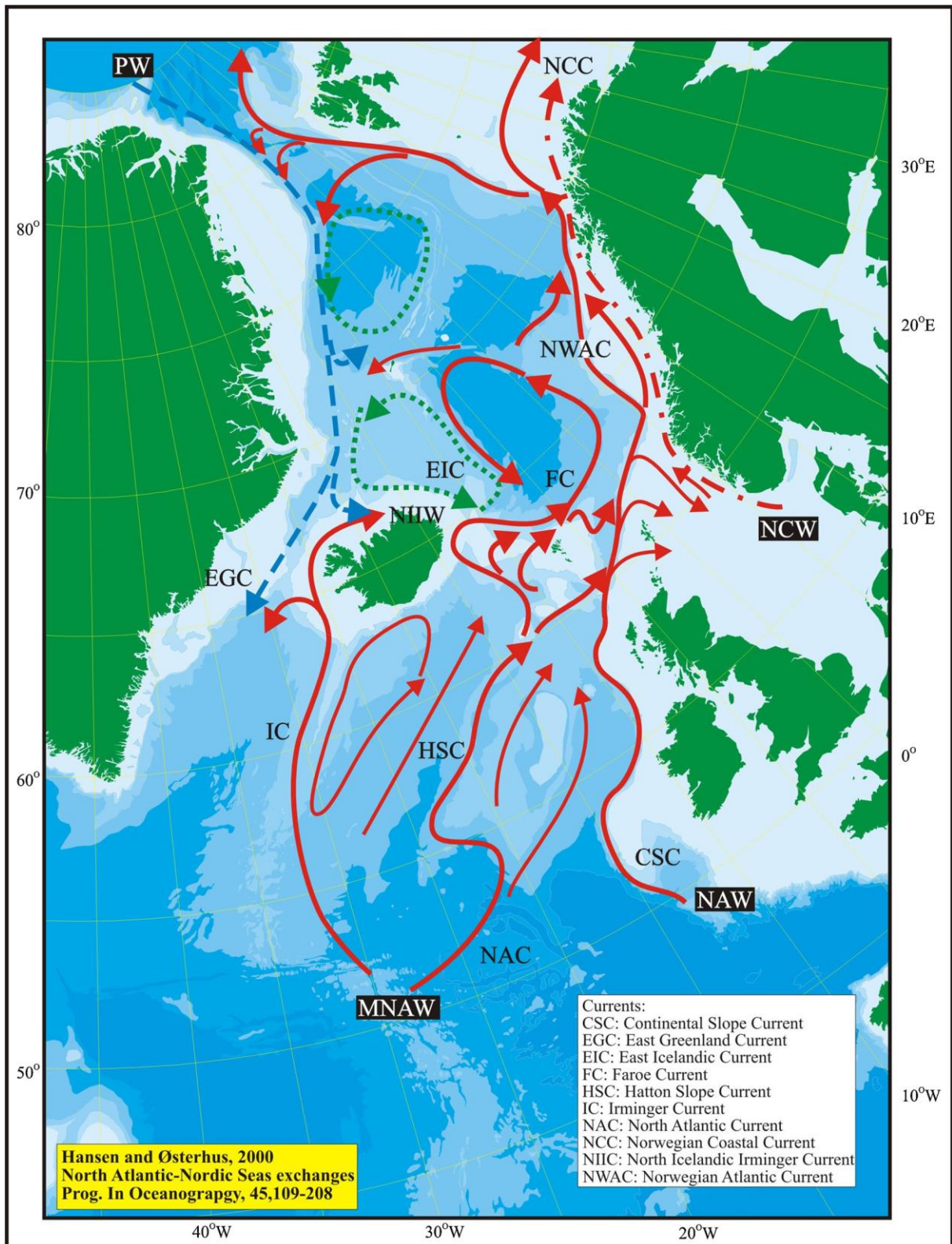
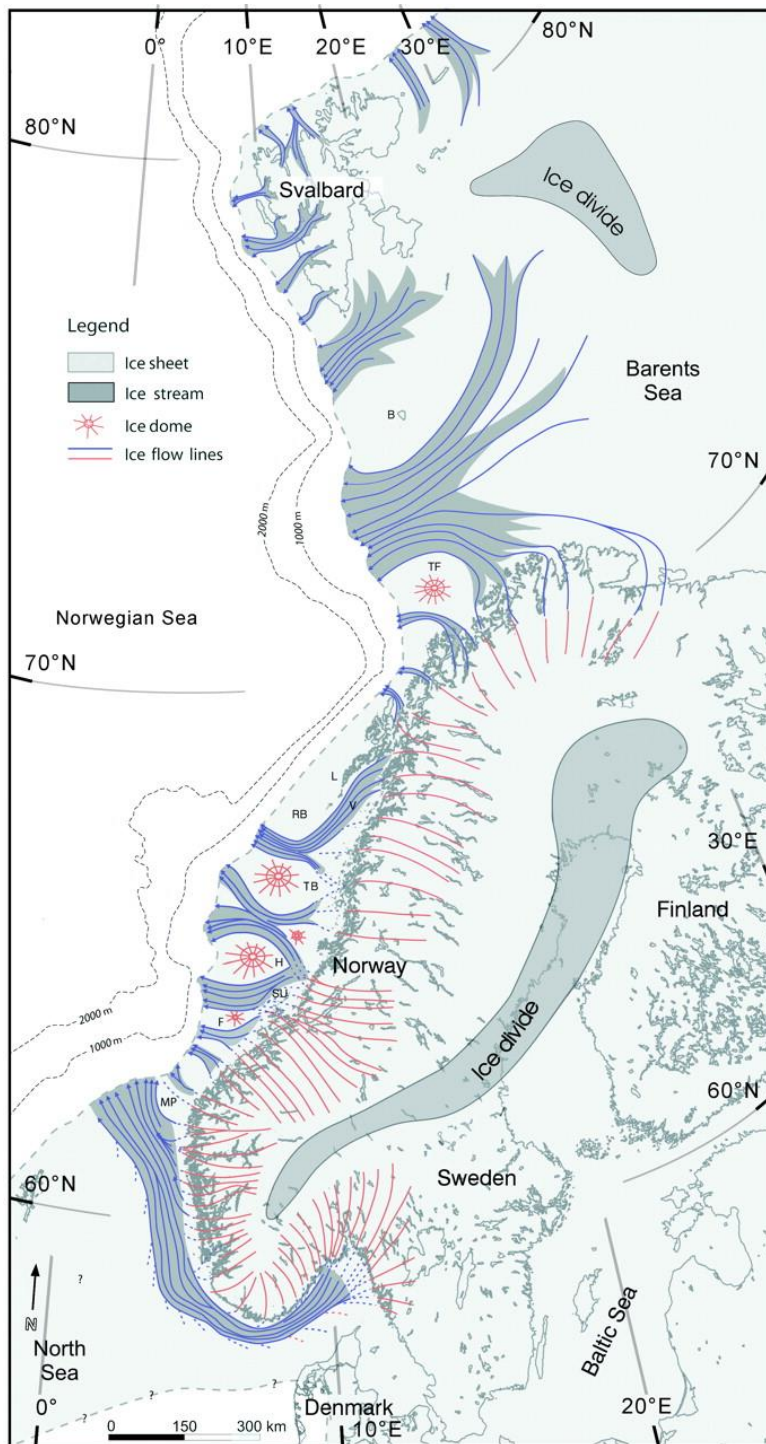


Figure 14: Near-surface Ocean currents of the North Atlantic. Continuous red arrows: Warm Atlantic water flow. Green dotted arrows: Cold water currents. Blue dashed arrows: Cold, low salinity current. Broken red arrow: Norwegian Coastal Current, featuring lower temperatures and salinity than the North Atlantic Current. From Lorentzen (2015), original source: Hansen & Østerhus (2000).

The mid-Norwegian continental margin, i.e. the transition zone between the continental and the oceanic crust that also includes the shelf, is commonly subdivided into three main segments based on structural elements: Møre, Vøring, and Lofoten-Vesterålen (Faleide et al., 2008; see Fig. 20). The Vøring Margin comprises the Trøndelag Platform that also includes the Træna Bank with the Helgeland Basin, with one of the drilling sites (6610/7-1). Water depths in this area range from 50 to 300 m at elevated banks and from 150 to 550 m at troughs (Ottesen et al., 2009).

The bathymetry, the present relief of the NCS, is characterized by topographic highs and lows traversed by traces of ice streams that moved from the glaciated mainland towards the outer shelf during the last glacial periods (Fig. 15) (Vorren et al., 1998; Ottesen et al., 2005a,b; Rise et al., 2005; Laberg et al., 2009). Extensive ice streams especially in the Vestfjorden area (see Fig. 13 & 15) south-east of the Lofoten are believed to have contributed to the preservation of the surrounding rugged mountains by providing concentrated and fast drainage of ice-sheets during the Late Weichselian (Ottesen et al., 2005). Ice streams played a major role in shaping the shelf and hinterland: They transported the majority of both ice and (glacial) sediments to the margin (Dowdeswell & Siegert, 1999) and thereby contributed to thick layers of glacial till deposits on the shelf (Naust Formation, see 2.2.2 *Offshore geology*). The present shelf edge and continental rise was shaped by several submarine slides that took place in the late Quaternary (Vorren et al., 1998; Laberg & Vorren, 2000). The western Norwegian Sea features deep sea with depths exceeding 3000 m.

The Norwegian landscape in general is characterized by the Scandes, the Scandinavian mountains. The ancient mountain range extends along the mainland from south-west to the north and marks a major water divide. The mountains are elevated up to 2470 m a.s.l. in south-western parts of the country and to 1700 m a.s.l. east of the Vesterålen-Lofoten area. Summits of the Lofoten itself reach altitudes of approximately 1000 m a.s.l. The Scandinavian mountains have a major influence on the precipitation in Norway (orographic lift). Precipitation is highest at the south-western coast and roughly decreases landwards as well as northwards (Meteorologisk institutt, 2016).



The entire Norwegian coast is characterized by fjords and plenty of islands and skerries. Especially in mid Norway, the coastal area features a characteristic plane shape that has been subject to some controversy. This area was recognized as a distinct coastal component and initially named the “strandflat” by Reusch (1894), which literally means “flat beach”. The strandflat today is defined as a geomorphological element comprising the flat coast with beaches, small islands and skerries that lies partly below, partly above, but always close to sea level. It has a width of 50 – 60 km and an abrupt transition towards the coastal mountains and towards some protruding mountains within. This transition is referred to as knickpoint (Holstedahl, 1998).

Figure 15: Reconstruction of ice flow patterns and fast-flowing ice streams along the western margin of the late Weichselian ice sheets from 57° N to 80° N. TB: Trænabanken; RB: Røstbanken; V: Vestfjorden; T: Trænadjupe; L: Lofoten; H: Haltenbanken; B: Bear Island; TF: Tromsøflanket; F: Frøybanken; MP: Måløy. Source: Ottesen et al. (2005b).

The strandflat is present along the coast between Stavanger and Magerøya (59° N - 71° N) and most distinctively developed between Møre and the Lofoten including the study area (Larsen & Holstedahl, 1985; Holstedahl, 1998). Several formation mechanisms have been discussed,

amongst others by Nansen (1922), who considered frost weathering and planation by sea ice as important factors (Holtedahl, 1998). Larsen & Holtedahl (1985) suggested that sea-ice erosion and frost-shattering, influenced by marine abrasion and glacial erosion, were major processes formative for the strandflat. Even though it is undoubtedly modified by ice-sheet erosion, they considered it a non-glacial feature. Holtedahl (1998) later emphasised mainly glacial erosion, marine erosion, and subaerial weathering as main processes that most probably affected the coast in Late Pliocene to Pleistocene times. More recent work by Olesen et al. (2013) involves deep tropical weathering of Triassic to Early Jurassic age and suggests the bedrock platform to be an exhumed old weathering surface. According to Olesen et al. (2013), this surface was later levelled by Pliocene and Pleistocene erosion. Peneplanation was probably supported by frost weathering and ocean wave abrasion during periods where inland ice did not reach the coast (Olesen et al., 2013).

The most protruding islands along the Norwegian coast belong to the Lofoten and Vesterålen archipelagos. These islands, which lie between 67°25' N and 69°20' N, form a south-west running extension of the continent where the Norwegian shelf reaches its narrowest extent. Widespread plateaus exist on the mainland that are partly considerably traversed by major valleys and fjords towards the coast. Mountains with alpine character are only present in the main elevated regions north and south. The rivers that enter the sea in the study area are all relatively short. The rugged relief devoid of major basins, the elongated fjords, and the early descent of the mountains towards Sweden in the east and hence the Gulf of Bothnia prevents the formation of prolonged rivers in northern and central Norway. The river catchment areas along the shelf are accordingly small.

2.2 Geological background

2.2.1 Onshore geology

The Baltic Shield (or Fennoscandian Shield) is the widely exposed part of the East European Craton, the Precambrian core of the palaeocontinent Baltica (Fig. 16). It forms the geologic basement of Scandinavia with Norway being the north-westernmost limit of it (e.g. Gorbatshev & Bogdanova, 1993). The shield is composed of several presently deeply eroded orogens and microcontinents. It was subject to a diverse, mainly Paleoproterozoic continental growth history that involved accretion of terranes, continental collision, shearing and nappe

thrusting, faulting and folding and related metamorphism, as well as subduction with corresponding igneous activity (Gorbatshev & Bogdanova, 1993; Plant et al., 2005; Lahtinen et al., 2008; Bingen et al., 2008). The younger Caledonian Orogenesis significantly reworked the western margin of the shield after its formation.

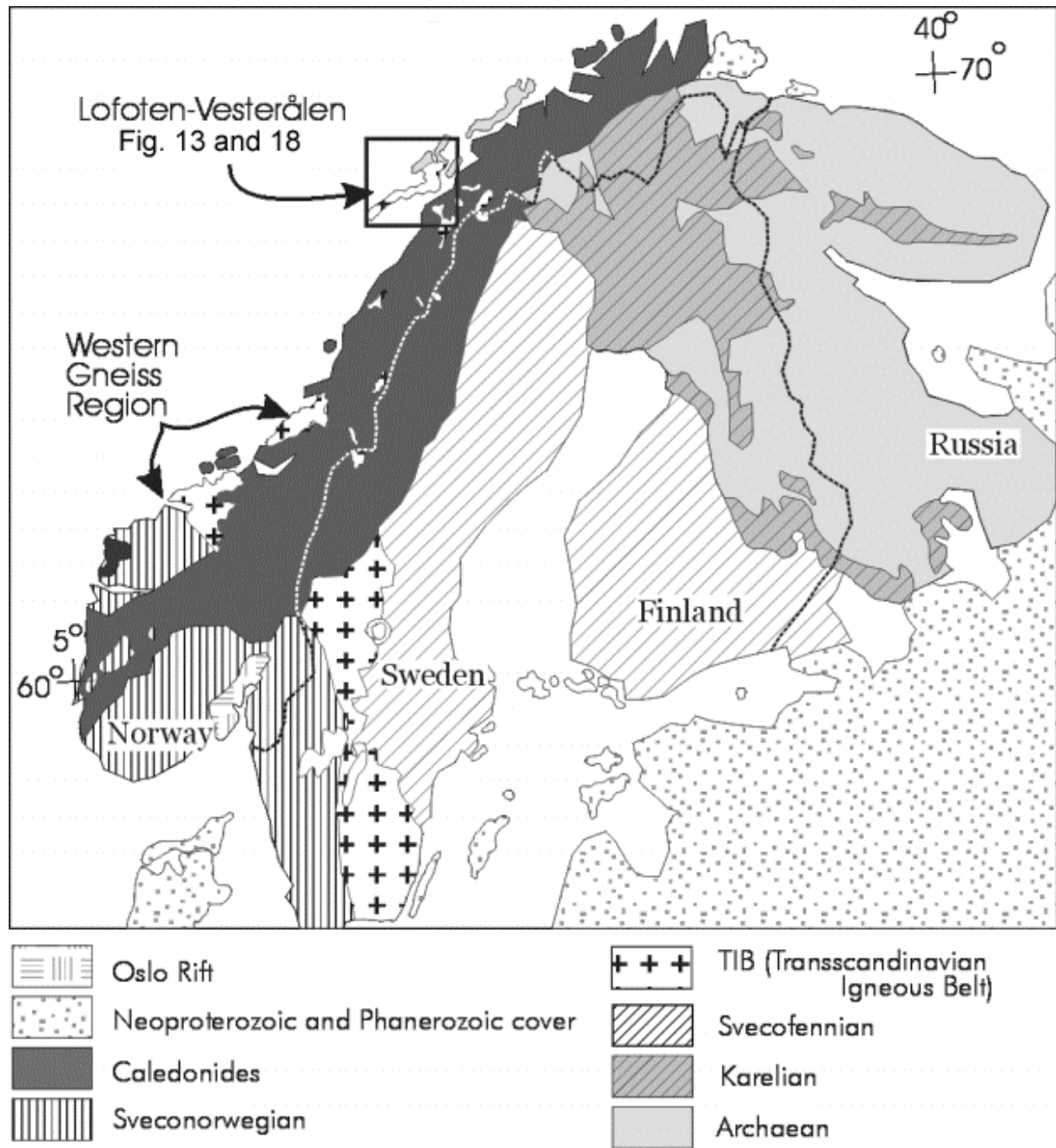


Figure 16: Overview map of the major geological subdivisions of the Baltic Shield. Source: Corfu (2004), after Weihed et al. (2002).

The present division of the Baltic Shield is based on the respective predominant rock ages and comprises several lithological units or tectonic blocks (Fig. 16): Archaean gneissic crust in the northeast, the Paleoproterozoic Svecofennian Orogen in the centre, and the Mesoproterozoic Sveconorwegian Orogen in the southwest (Lahtinen et al., 2008). Another important unit is the so-called Transscandinavian Igneous Belt (TIB) that also outcrops in the Lofoten area and south of the Vestfjord. The different lithological elements are briefly presented here with emphasis on the TIB.

The Svecofennian Orogen is a composite of microcontinents and juvenile island arcs that was attached to the Archaean (Karelian) craton (Plant et al., 2005; Lahtinen et al., 2009). It is the largest Paleoproterozoic lithological unit of the Baltic Shield and dominates the central part, especially in Sweden and Finland. The Sveconorwegian Orogen south-west of it is the well-exposed lithological unit that dominates southern and western Norway as well as the south-west of Sweden. The orogen includes the Western Gneiss Region (WGR, see below). The orogenic belt is composed of terranes and continents that collided in the Mesoproterozoic (Bingen et al., 2008).

The Transscandinavian Igneous Belt was formed continuously at the western edge of the Svecofennian Orogen and has a north-south extend of more than 1200 km from the Lofoten to south-western Sweden, where it primarily outcrops (Romer, 1992; Gorbatshev, 2004). The plutons and batholiths of the TIB predominantly consist of mafic intrusion and coarse to medium-grained granitoids with ages ranging between 1.85 and 1.67 Ga (Gorbatshev, 2004). The predominantly massive TIB is little deformed but reworking and metamorphism induced by the Sveconorwegian orogeny increases south and westward (Gorbatshev, 2004; Bingen et al., 2008). Pascal et al. (2007) point out that the granitoid intrusions that form parts of the TIB have a significant effect on the bulk density of the crust and therefore influence the uplift potential of the Baltic Shield. TIB granitoids have a relatively low density (Pascal et al., 2007).

In the late Proterozoic (Proterozoic: 2500 to 540 Ma, Cohen et al., 2013), most of the Baltic Shield was exposed, leading to a generally flat relief (Lidmar-Bergström, 1995). For this old plane in Scandinavia, Reusch (1901; 1903) introduced the term paleic surface. However, he also points out that the paleic surface was not a single peneplain. He attributed different elevational levels to peneplains of different ages. Peulvast (1985) later assigned the two main

penneplains to two major Cenozoic uplift events (see below). Peneplains are idealized, low relief erosion surfaces, close to or at sea level. They are believed to have existed several times in Scandinavia over geological time, including following the Caledonian orogenesis (Ramberg et al., 2008).

The onshore bedrock and basement geology of Norway is widely uncovered by the erosional power of past ice sheets and glaciers that were also responsible for the formation of the deeply incised fjords along the coast. Glacial erosion has removed the bulk of former soils and sediments and with it the geological record that now has to be studied indirectly based on sediment deposits from the adjacent shelf (e.g. Riis & Fjeldskaar, 1992; Riis, 1996).

Norway's bedrock geology is characterised by the Caledonian Orogen overlying large parts of the Precambrian basement (see Fig. 17). The Caledonian orogeny, the continent-continent collision of the palaeocontinents Baltica and Laurentia that contributed to the formation of the Scandes Mountains, is of Silurian to Early Devonian age (see Gee & Sturt, 1985). However, the timing and delimitation of the collision is a complex issue. Gee et al. (2008) designate the beginning of the orogenesis to the early Ordovician (480 Ma) and McKerrow et al. (2000) suggest to include even early tectonics of Cambrian age into the overall Caledonian orogeny. A subduction zone was formed presumably in the Ordovician in which Baltica was subducted beneath Laurentia (Gee, 1975; Gee et al., 2010). The collision closed the Iapetus Ocean and left behind a suture providing a weak zone for future rifting. Ocean-derived allochthons, i.e. oceanic crust material that has been transported away from its place of formation, preserved in the Scandes, is evidence for the earlier closure of the paleo-ocean (Gee et al., 2008).

The breakup of the crust between Eurasia and Greenland, and hence the onset of the development of the Norwegian continental margin, occurred in the early Eocene under massive magmatic activity (Faleide et al., 2008). The Norwegian continental shelf is hence part of an ancient, volcanic active continental margin. The margin in mid-Norway became passive in mid-Eocene time (Faleide et al., 2008). This event marks the beginning of sea-floor spreading in the North Atlantic Ocean that continues to the present day (e.g. Mosar et al., 2002a).

The Caledonian Orogen, that is deeply eroded today, stretches in Scandinavia from south-western to northern Norway over a distance of approximately 1800 kilometres (Fig. 17 & 20). Its western equivalent on the other side of the North Atlantic Ocean is exposed at the eastern coast of Greenland (e.g. Gee et al., 2008). The Caledonides form distinctive thrust sheets (also

called nappes) that are vertically stacked onto the western margin of the Baltic Shield (see Fig. 17). This complex structure is the result of subduction, collision, and subsequent rifting. Parts where erosion has revealed the old basement below the thrust sheets are referred to as geologic windows (e.g. Smelror et al., 2007). The most prominent windows show plutons of the TIB and are indicated in Fig. 20 (see also Pascal et al., 2007). The Caledonian thrust sheets are subdivided into four major allochthons (compare with Fig. 17) (Solli & Nordgulen, 2008): 1) The Uppermost Allochthon (which is of Neoproterozoic to Ordovician age) constitutes almost the entire coastal area north and south of the Lofoten-Vesterålen, but occurs only occasionally on the islands itself. Predominant rock type is mica schist, a low to medium-grade metamorphic rock. 2) The Upper Allochthon (Neoproterozoic - Silurian) is the main exposed part of the Caledonides and is of much greater extent than the Uppermost Allochthon. It is mainly composed of mica schist and phyllites (lower-grade, foliated metamorphic rocks with smaller grains than mica schist). Major Proterozoic windows are present in this allochthon. 3) The Middle Allochthon (Mesoproterozoic - Cambrian) has the greatest south-north extent and is discontinuously exposed along the entire Scandes. It is composed mainly of sandstone, schist, quartzite, amphibolite, as well as gabbro, diorite and anorthosite in the more southerly regions of Norway. 4) The Lower Allochthon (Mesoproterozoic - Palaeozoic) is most dominant in central Norway and has almost no exposure in northern Norway around the Lofoten-Vesterålen area. It is predominantly composed of sandstone, schist, quartzite, conglomerates, and amphibolite (Solli & Nordgulen, 2008).

From an elevational point of view, the Scandes are composed of two domes, the Northern Scandes Dome and the Southern Scandes Dome. They are separated by topographically lower mountain ranges in between (Trøndelag region). Lidmar-Bergström (1999) describes a third appertaining dome in southern Sweden and emphasizes its significance for geomorphologic studies in Scandinavia since this dome is still partly covered by Mesozoic sediments (Lidmar-Bergström, 1999; Japsen et al., 2002). The dome otherwise exposes Precambrian basement. The Norwegian Scandes are, however, devoid of Mesozoic sediments or sedimentary rocks. The Northern Scandes Dome and its geology as well as its uplift history (see below) is of particular interest for the study at hand.

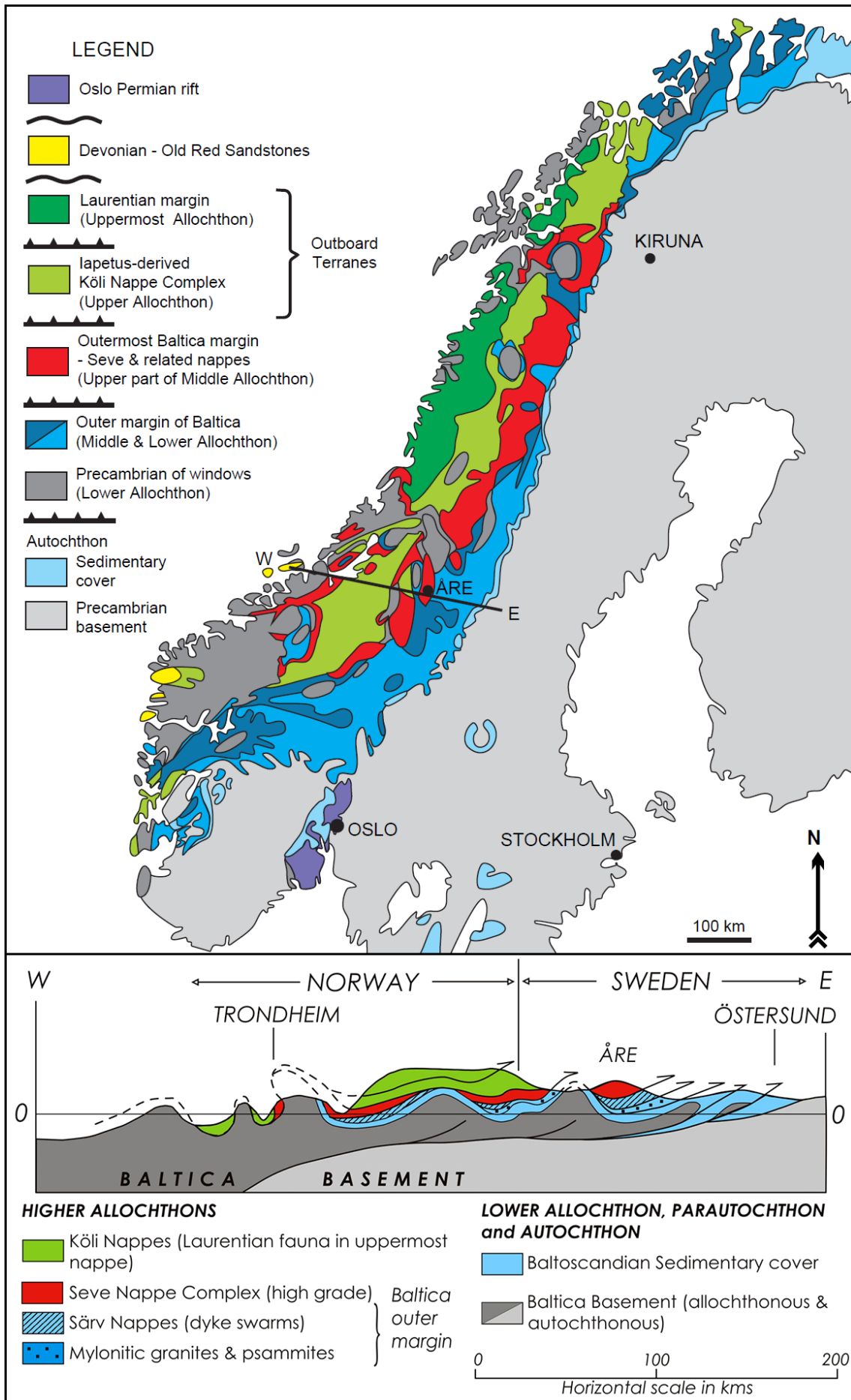


Figure 17 (previous page): Simplified tectonic map of the Scandinavian Caledonides. The lower subplot represents the schematic profile of the W-E line drawn in the upper section (vertical exaggeration x 5). Source: Gee et al. (2010), based on Gee et al. (1985).

In summary, the geology of mainland Norway at the Norwegian Sea exhibits predominantly metamorphic and magmatic Caledonian rocks. The basement is mainly composed of gneisses and granitic rocks (Smelror et al., 2007) and locally covered by glacial till or glaciofluvial deposits. Archaean and Proterozoic basement is mainly exposed in southern and northern Norway (Ramberg et al., 2008). The following section provides a more detailed presentation of the geology of the Lofoten-Vesterålen area including two peninsulas south of Vestfjorden.

2.2.1.1 Geology north and south of Vestfjorden/Ofotfjorden

2.2.1.1.1 Geology north of Vestfjorden/Ofotfjorden

The Lofoten-Vesterålen area possesses a prominent role in the on- and offshore geology of Norway as the islands form a basement high that exposes the most internal rocks in northern Norway (Åm, 1975; Klein & Steltenpohl, 1999). Both Precambrian basement and Caledonian allochthons are exposed (e.g. Steltenpohl et al., 2004). Exposed migmatitic gneisses that were formed ca. 2700 Ma ago are among the oldest discovered rocks in Norway (Griffin et al., 1978). The south-western end of the Lofoten represents the outermost occurrence of exposed Caledonian basement in northern Norway and the islands can be seen as a north Norwegian part or equivalent of the Western Gneiss Region (WGR) (Andersen & Jamtveit, 1990; Klein & Steltenpohl, 1999; Steltenpohl et al., 2004; Corfu, 2004). The WGR is the deepest exposed tectonic unit of the Scandinavian Caledonides and considered a major basement window (see Fig. 20). The Lofoten (Fig. 18) provide a similar deep insight into the geology of northern Norway, with its gneissic rocks that were subject to eclogite-facies metamorphism. This magnitude of metamorphism is marked by extremely high pressures and temperatures (> 400 °C and > 12 kbar, see Fig. 7). These conditions are known to occur in orogenic zones and existed during the Caledonian continent-continent collision when Baltica was subducted beneath Laurentia (Andersen & Jamtveit, 1990). Evidence is represented in exposed rocks showing high-grade metamorphism of Silurian to Devonian age (e.g. Griffin & Brueckner, 1980).

The rocks of the Lofoten-Vesterålen belong to the Anorthosite-Mangerite-Charnockite-Granite Suite (Corfu, 2004). The Suite is part of the TIB and is subdivided into several plutons. The island of Hadseløya, except for the very western part, belongs to the Raftsund pluton. The Raftsund mangerite is dated to be 1796 Ma old (Corfu, 2004). In the western part of the island, gneisses and migmatites of Archaean and Palaeoproterozoic age are present (Tveten, 1978) (Fig. 18).

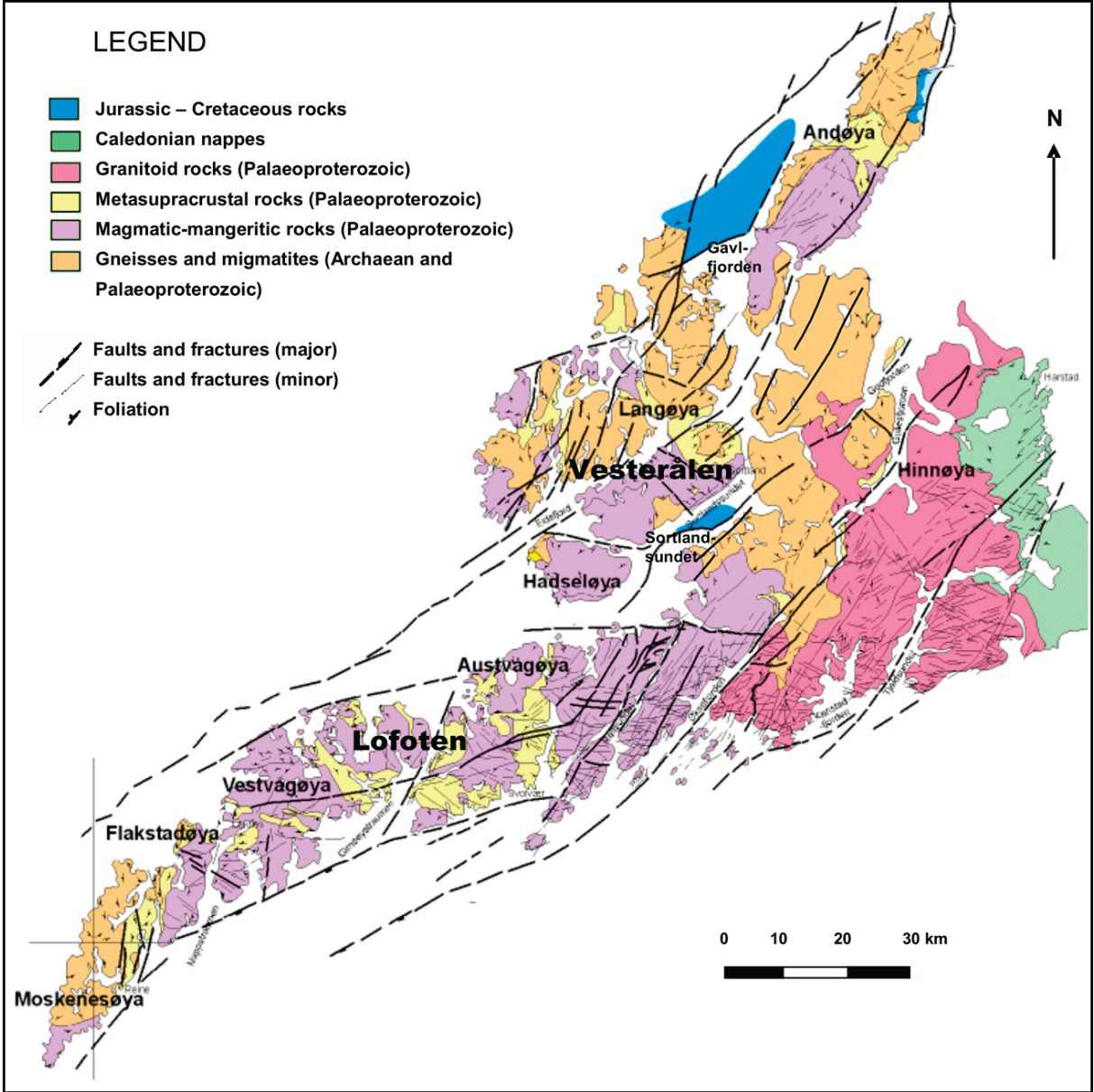


Figure 18: Bedrock geology map of the Lofoten-Vesterålen archipelago. Based on Tveten (1978). Source: Bergh et al. (2007).

Andøya, the northernmost island of the Vesterålen archipelago (see Fig. 18), is a unique and exclusive locality in Norway. Mesozoic sedimentary rocks of Jurassic and Lower Cretaceous age resting upon Precambrian basement have been preserved on its eastern coast (see e.g. Dalland, 1975; 1981). It is the only known locality where Mesozoic rocks are preserved on the mainland. The Jurassic layers consist of siltstone, sandstone, and shale (Solli & Nordgulen, 2008). The locality is stratigraphically comparable to the South Swedish Dome as the underlying basement is deeply weathered (Dalland, 1975). Andøya is part of a well-developed strandflat (Holtedahl, 1998; Olesen et al., 2013).

Exposed bedrock in the central archipelago including Hadseløya consists mainly of mangeritic plutonic rocks of Precambrian age (Paleoproterozoic) and migmatitic gneisses (Tveten, 1978; Bergh et al., 2007). Migmatitic gneisses are partially melted and recrystallized high-grade metamorphic rocks that often show distinct folding. Mangerite is the source material of the saprolitic sand sampled in the Lofoten-Vesterålen area and the parental rock of the sampled core stones. According to the QAPF diagram (Streckeisen, 1979), mangerites are defined as having a maximum of 20 % quartz. Mangerite is a plutonic rock type that occurs as intrusions within a basement predominantly characterized by polymetamorphic and migmatitic gneisses in that area (Olesen et al., 2013).

Extensive Caledonian nappes are prevalent only at the eastern side of Hinnøya towards the connection to the mainland (Tveten, 1987). The Caledonides seem to have had a minor deformation effect on the Lofoten and Vesterålen basement rocks (Steltenpohl & Hames, 2004, and references therein). During the Caledonian orogeny, the Lofoten and Vesterålen were probably a part of the Baltic plate (Griffin et al., 1978; Corfu, 2005). Their position at a high tectonic level and the prevalence of highly resistant granulite-facies rocks also contributed to the extensive preservation of the rugged mountains (Griffin et al., 1978).

2.2.1.1.2 Geology south of Vestfjorden/Ofotfjorden

The bedrock geology of the Hamarøy peninsula as well as Hundholmen at Tysfjorden south of Vestfjorden is characterized by granite, mangerite, and charnockite, all being quartz bearing rock types of Paleoproterozoic age (Solli & Nordgulen, 2008). The bedrock at Hundholmen is

slightly foliated and hence referred to as Tysfjord gneiss granite. Radiometric rubidium-strontium dating suggests the pluton to have an age of 1700 Ma (Statherian) and the foliation is interpreted to have been caused by plastic deformation during Caledonian Orogenesis (Andresen & Tull, 1986). The Tysfjord gneiss granite is also part of the TIB.

The TIB is grouped into three major groups according to its varying ages (TIB 1-3). U-Pb ages of the Tysfjord gneiss granite in the study area can be attributed to two of these groups: 1796 - 1770 Ma (TIB 1) and 1719 - 1703 Ma (TIB 2) (Romer et al., 1992).

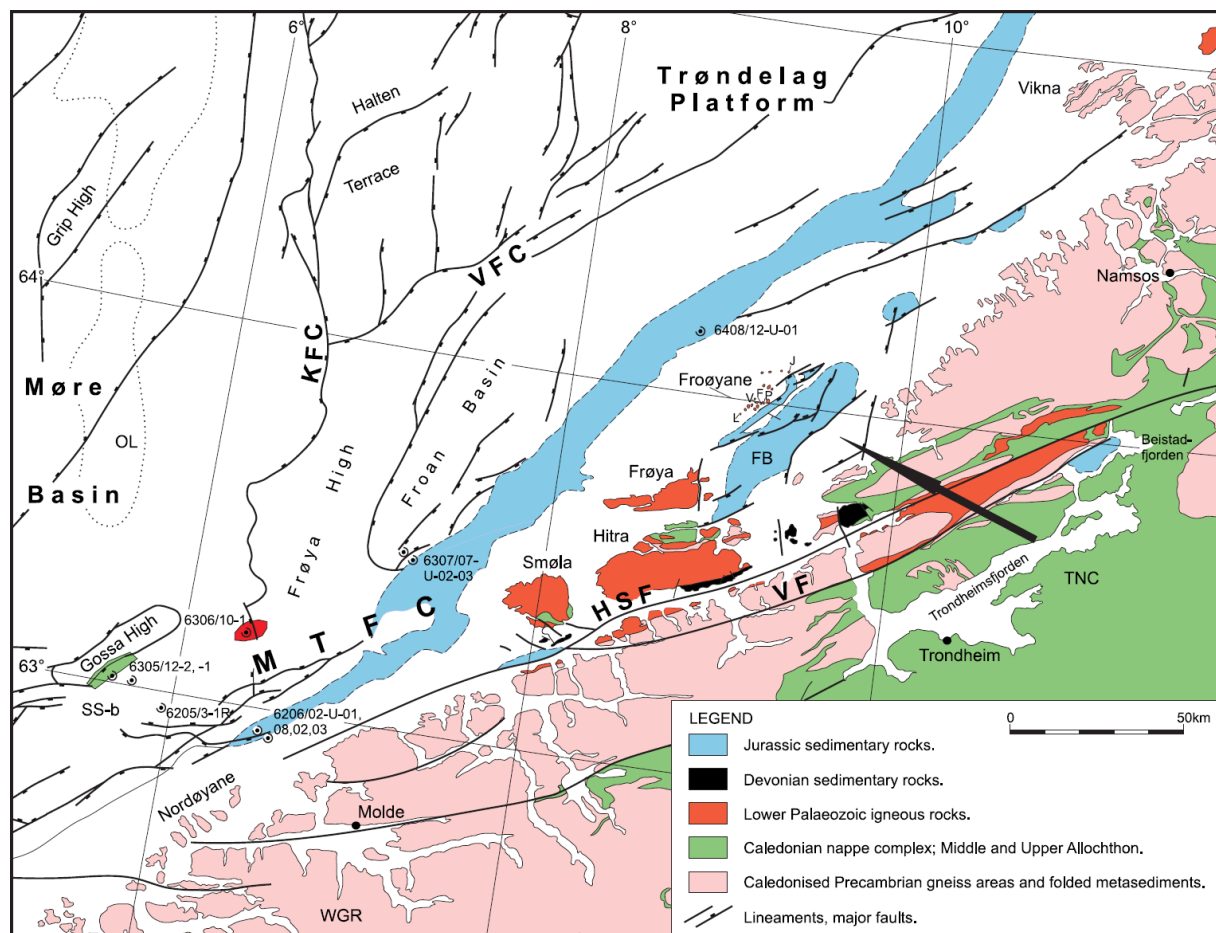


Figure 19: Main geological provinces around the Froan Basin. Drilling site 6408/12-U-01 is indicated in the area of Middle Jurassic sedimentary rock (coloured in blue). Sampling of the core for this study (sample 10) took place in a depth of the underlying granitic basement. MTFC = Møre-Trøndelag Fault Complex, FB = Frohavet Basin, WGR = Western Gneiss Region, KFC = Klakk Fault Complex, VFC = Vingleia Fault Complex, HSF = Hitra-Snåsa Fault, VF = Vingleia Fault, TNC = Trondheim Nappe Complex. The black arrow refers to the possible sediment transport direction into the Frohavet Basin in Mid Jurassic time (based on a sandstone provenance study by Mørk & Johnsen, 2005). Source: Mørk & Johnsen (2005), based on data by Blystad et al. (1995), Roberts (1998), and Lundqvist et al. (1996).

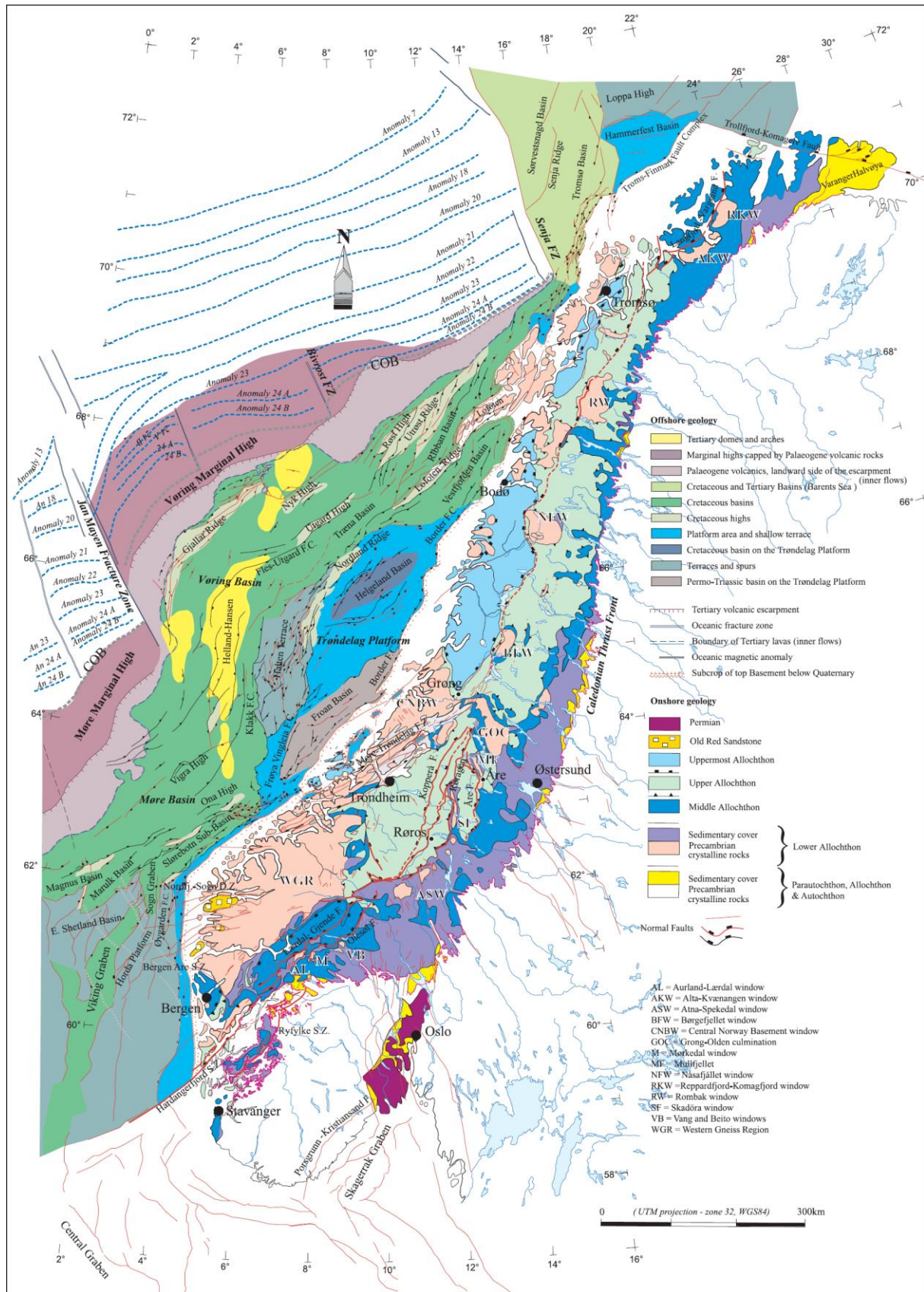


Figure 20: Tectonostratigraphic overview map of Norway and its passive continental margin. Source: Mosar et al. (2002b), based on various sources (see references in Mosar et al., 2002b).

2.2.2 Offshore geology

This section describes the stratigraphy of the Norwegian Sea continental shelf with emphasis on the Molo Formation (Fm), a depositional unit of supposedly Miocene age overlain by a thick package of Plio-Pleistocene glacial sediments.

The Norwegian continental shelf consists of different stratigraphic units composed of sediments lying upon crystalline basement rock belonging to the Baltic Shield. These layers are of post-Silurian age and record geological history until the present day. Drillings and aeromagnetic mapping have revealed sediments and sedimentary rocks with a thickness of more than 10 km deposited on the Baltic Shield (Åm, 1975). The stratigraphic units are usually referred to as formations and are distinguished from their vertical and lateral surroundings by unique seismic characteristics (compare A and B in Fig. 24). The borders are defined according to changes in seismic reflection (velocity and consequent density) which are interpreted to be caused by abrupt changes in sediment supply, sediment properties, or discontinuities as a result of erosion or time periods of non-deposition. This is supported by wells that can witness changing sediment properties at certain depths and confirm conjectures. Correlation of both seismic profiles and wells allows to interpolate data between actually investigated areas.

The offshore sediment samples analysed in this study were taken from exploration wells drilled into the Molo Fm, which is part of the Trøndelag Platform (see Fig. 20 & 22). The Molo Fm is a buried depositional unit that stretches over 500 kilometres along the inner shelf of the Norwegian Sea from Møre to the outermost islands of the Lofoten archipelago (Fig. 21 & 22). Its present distance from the coast varies between 90 and 50 km (see Fig. 21). Its east-west extension is usually less than 50 km in the southern and central parts and up to approximately 80 km in the north. Vertically the formation reaches a thickness of 100 - 200 m (Eidvin et al., 2007) and thins out towards the west where it is overlain by the much larger Naust Fm that also includes the westernmost extend of the shelf (see Fig. 23). At some localities, the Molo Fm is nearly exposed on today's seabed. Its high erosional resistance has led to the conclusion that the formation is most probably sand dominated (Eidvin et al., 2007). Deposition of the Molo Fm is estimated to be of Early Oligocene to Early Pliocene age and was presumably driven by coastal progradation in a wave-dominated environment influenced by long-shore (littoral) drift (Rokoengen et al., 1995; Eidvin et al., 2014).

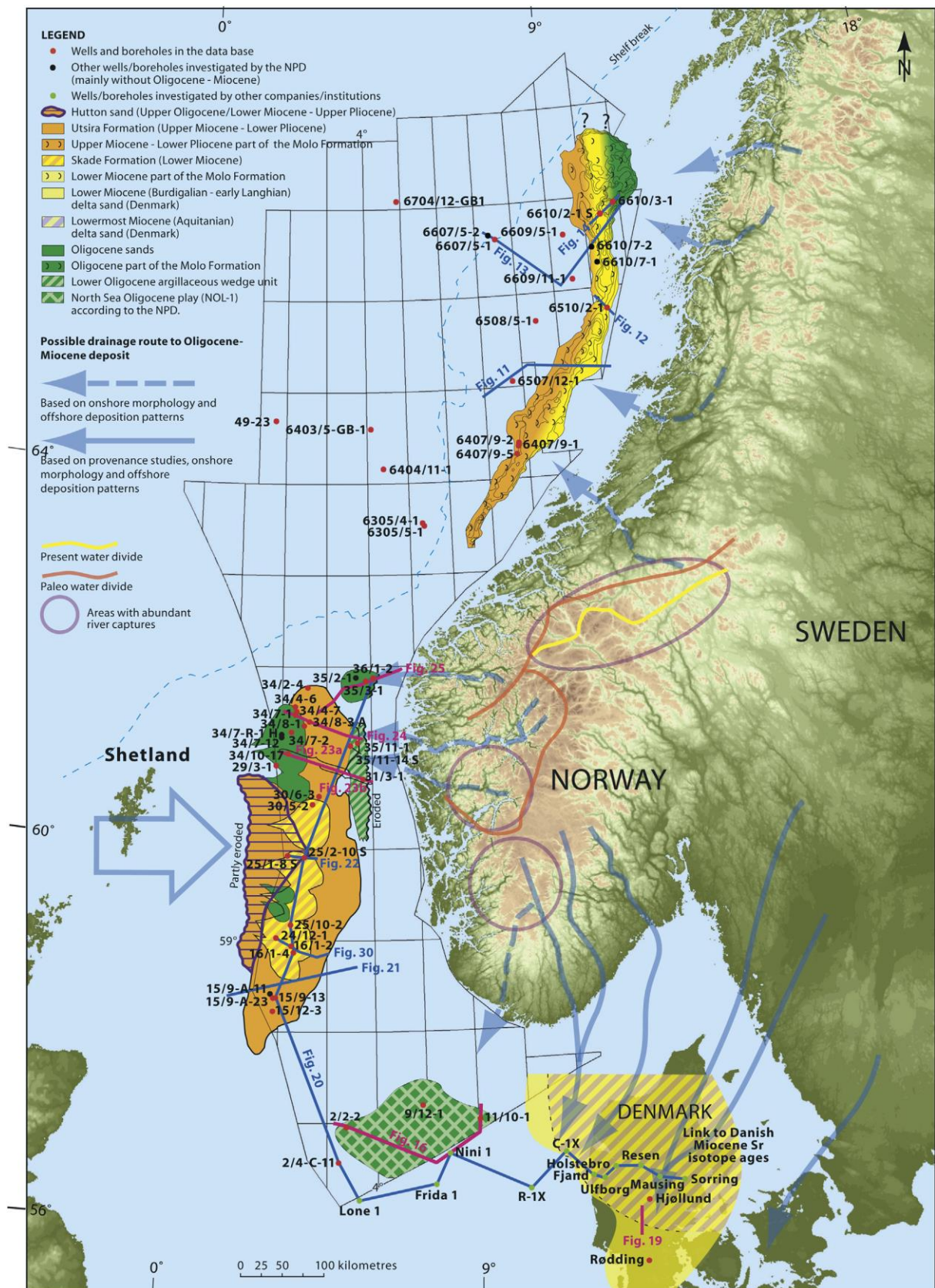


Figure 21: Overview map showing locations of Oligocene to Pliocene wells at the mid- and south Norwegian shelf area. The compilation is based on work by Bullimore et al. (2005), Rundberg & Eidvin (2005), Gregersen & Johannessen (2007), Olivarius (2009), and Olesen et al. (2010). Source: Eidvin et al. (2014).

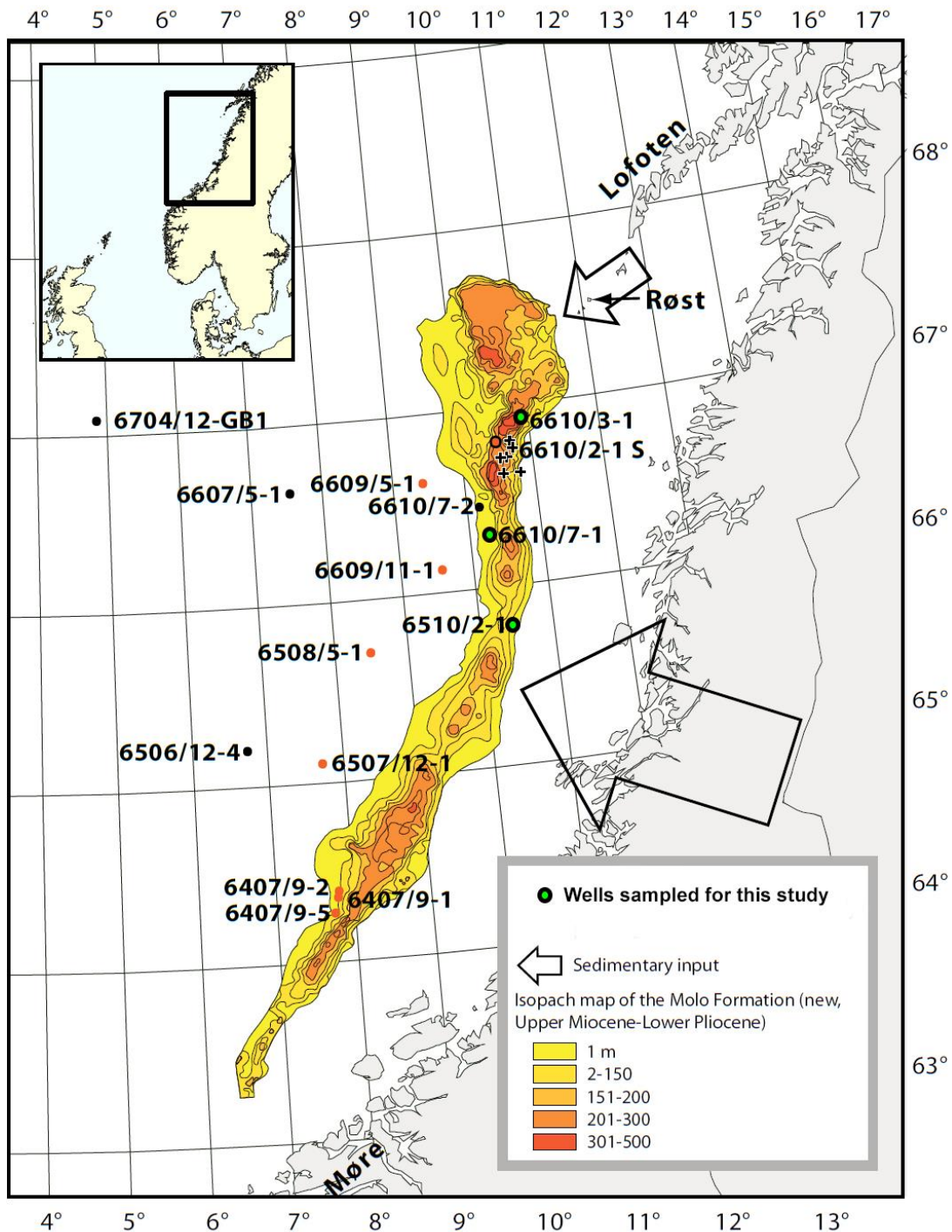


Figure 22: Isopach map of the Molo Formation with indicated well locations. Based on work by Bullimore et al. (2005) and Brekke (2000). Modified after Eidvin et al. (2007).

The depositional unit known today as the Molo Fm was first described by Eldholm & Nysæther in 1969. The formation was initially termed the “Delta” by Bugge et al. (1976) and finally named “Molo” by Gustavson & Bugge (1995) on a geological map. In 2007, it was formally defined as a stratigraphic unit by Eidvin et al. (2007). “Molo” is the Norwegian word for jetty or mole, an allusion to its location close to the seabed.

The age determination of the formation leaves some ambiguity. The Molo Fm was initially dated to be entirely of Early Oligocene age (Eidvin et al., 1998). It has later been re-dated by Eidvin et al. (2007) and assigned to Late Miocene - Early Pliocene age. Eidvin et al. (2013) then extended this age again to Early Oligocene - Early Pliocene based on new seismic data (Eidvin et al., 2014). The Molo Fm was identified on the basis of a series of westward-prograding steeply dipping seismic reflections (Clinofolds, see Fig. 24 C) and accordingly interpreted to be a sub-sedimental equivalent of a contemporary coastal delta (Smelror et al., 2007; Eidvin et al., 2007; Eidvin et al., 2013; Eidvin et al., 2014). This implies that the assumed delta front of the Molo Fm was the shelf break at the time when shelf glaciations and hence deposition of the now overlying Naust Fm commenced (Ottesen et al., 2009; see Fig. 23). The shelf break is the sudden increase in water depth between continental shelf and -slope and marks the maximum extent of ice sheet advance throughout its development towards the open sea.

West of the Molo Fm in deeper waters lies the Kai Formation, which is considered the proximal equivalent of the Molo Fm (Fig. 23 & 24) (Løseth & Henriksen, 2005; Eidvin et al., 2007). The two formations are not connected (anymore). In the North Sea to the south, the Utsira Formation forms the lateral equivalent. Both the Molo and Kai formations as well as Utsira Formation belong to the Nordland Group (Eidvin et al., 2007). The Brygge Fm lies below the Molo Fm and the proximal equivalent Kai formation and is accordingly older (Oligocene to Lower Miocene, Eidvin et al., 2014). The upper end of the Brygge Fm is an unconformity. The Molo Fm lies on top of this Mid-Miocene unconformity. Sediments that lie on top of the Molo and Kai Fm all belong to the Naust Fm, which consists of glacial sediments deposited during late Pliocene and Quaternary (Dahlgren et al., 2002). Deposition of the Naust Fm started in the Upper Pliocene with the onset of the first glaciations. Seismic profiles revealed sediment layers, increasingly dipping with burial depth within the formation (Fig. 24 A), which indicates that the rapidly increasing sediment load caused subsidence on the shelf in response (Dahlgren et al., 2002; Dowdeswell et al., 2010). Before the onset of the Pleistocene glaciations and the subsequent deposition of the Naust Fm, the Molo Fm was a prograding wedge-shaped deposit at the coast and the upper part of the formation was situated at sea level. The continental margin at the Norwegian Sea was subject to regional subsidence since the middle Eocene (Faleide et al., 2008). The Miocene is widely considered as the main phase of compressional deformation and the development of domes on the Vøring Margin (mid-Cenozoic compressional deformation) (Faleide et al., 2008).

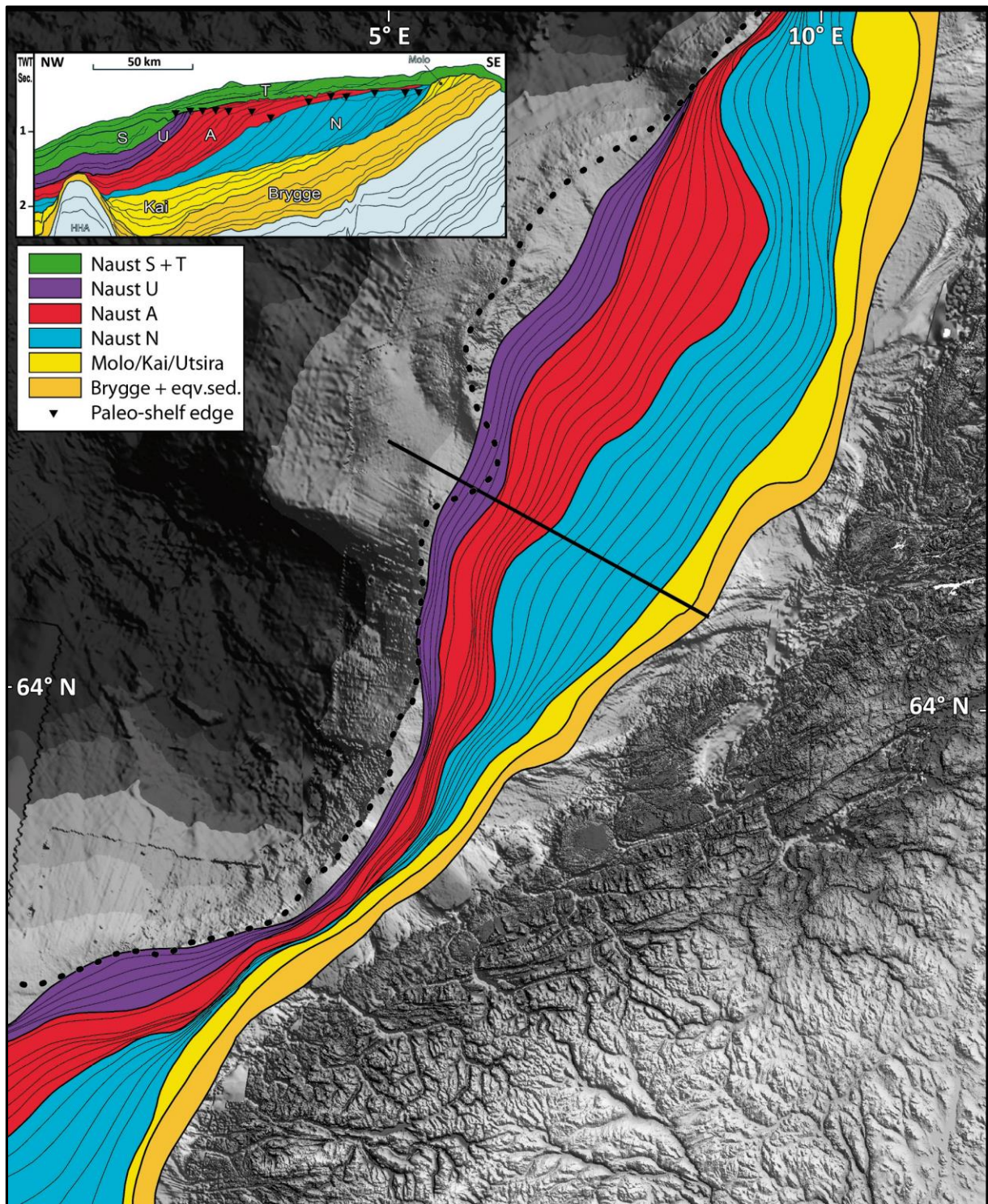


Figure 23: Seismic representation of the Naust Fm, Brygge Fm, and Molo Fm with its deep-water equivalent Kai Fm in the west and the horizontal equivalent Utsira Fm in the south. The black line indicates the location of the profile in the upper left corner. A high-resolution image of the profile is given in Fig. 24 below. The black dotted line indicates the position of the present shelf break. The progradational pattern of the palaeo-shelf break is marked in the profile. Source: Ottesen et al. (2009).

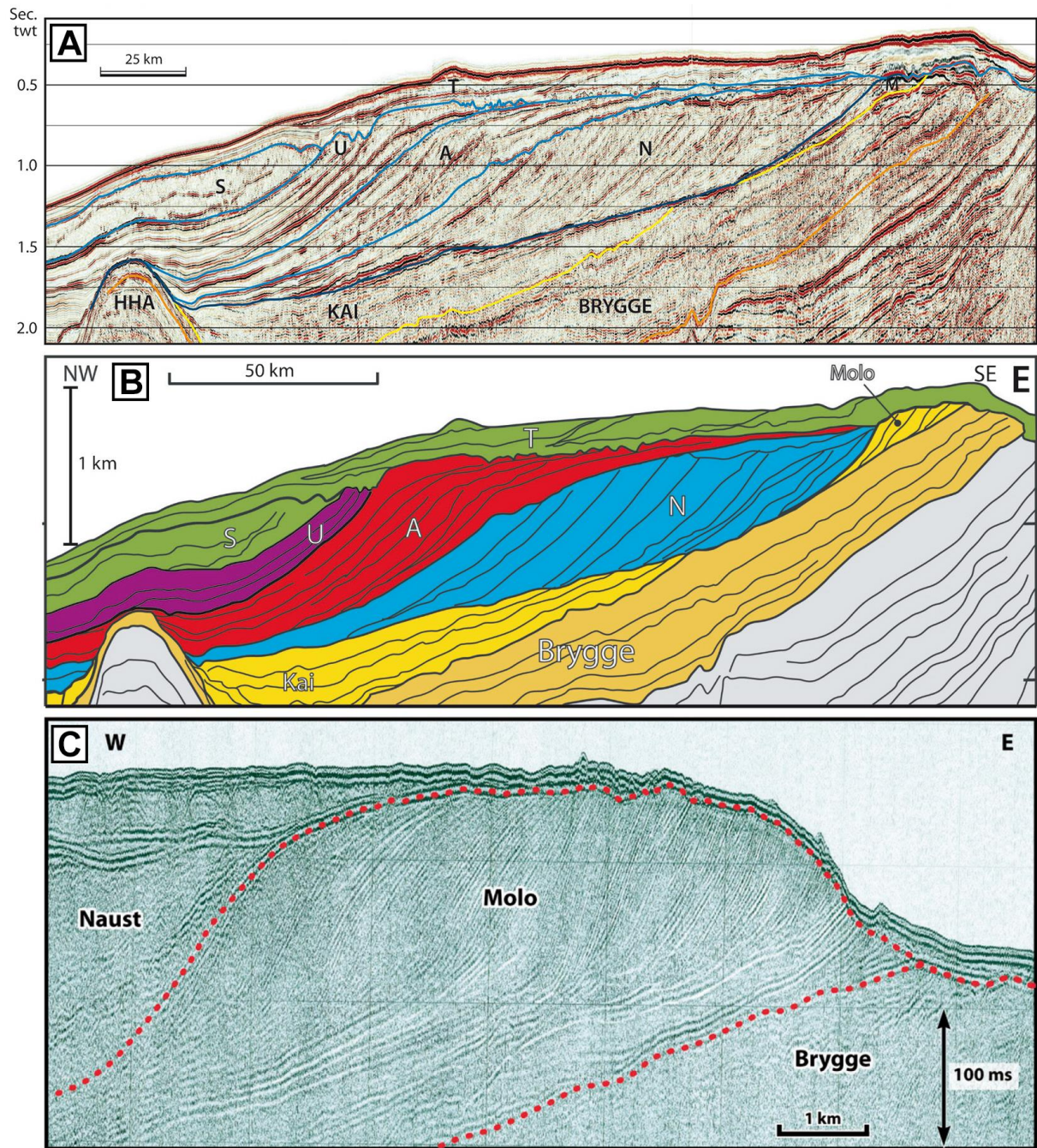


Figure 24: Seismic profiles across the mid-Norwegian shelf. **A:** Seismic profile GMNR-94-310. The location is indicated in Fig. 23 (black line). **B:** Schematic representation derived from the seismic profile in A, providing a simplified overview of the depositional units. **C:** High-resolution seismic profile of the Molo Formation. HHA: Helland-Hansen Arch. M: Molo Formation. N, A, U, S, T: Sequences of the Naust Formation. Figures from Ottesen et al. (2009).

According to Eidvin et al. (2007), the Norwegian coast turned into a prograding coast in mid Miocene time when compression and uplift of mainland Norway commenced. Since the beginning of the Quaternary period, the Norwegian continental shelf has increased in lateral

extend up to 150 km westward west of the Molo Fm as a result of coastal progradation (Ottesen et al., 2009). Today, the Norwegian shelf reaches its maximum horizontal extent at 65°45' N, becomes very narrow north of the Lofoten and Vesterålen and covers almost the entire Barents Sea between and around Svalbard and the Norwegian mainland.

Most of the Naust sediments on the mid-Norwegian shelf were deposited within the last 3 million years and are mainly the result of glacial erosion during the Pleistocene glaciations (Jansen & Sjøholm, 1991; Rise et al., 2005; Ottesen et al., 2009). More than 400 m of sediment layers are attributed to the Weichselian (Rise et al., 2005). The Late Weichselian glaciation was also the last major event that shaped the present topography of the shelf. The ice released the shelf 13,000 years ago and since then glacial erosion is restricted to the mainland (Ottesen et al., 2009).

The Trøndelag Platform (see Fig. 20) with its deep basins has been stable since the Jurassic (Faleide et al., 2008). Eidvin et al. (2014) state tectonic stability since the Triassic. Sedimentation was therefore not disturbed by major tectonic events. Initial sedimentation started with the opening of the Norwegian-Greenland Sea (Ottesen et al., 2009). Since then, bottom currents may have influenced deposition on the continental margin. First evidence for bottom currents circulation is discovered in late Eocene layers (Laberg et al., 2005).

In conclusion, the offshore sediment samples are taken from the inner Norwegian continental shelf at different depths that are all assigned to the coast-parallel Molo Fm, dated to be of Early Oligocene to Early Pliocene age (Eidvin et al., 2013). The Miocene is the first epoch of the period Neogene and lasted from 23.03 to 5.333 Ma (Cohen et al., 2013). The epoch is followed by the Pleistocene that is characterised by several glacial periods. The Weichselian glaciation is only the last of a period with several glacial cycles within the last 2.58 million years.

The prevailing climate at the time of deposition is crucial for the understanding and interpretation of sediment transport processes. In the Miocene, a short global warming event known as the Miocene Climatic Optimum interrupted the trend of long-term Cenozoic cooling (Pound et al., 2012; Holbourn et al., 2015). Climate at the end of the Miocene was globally decreasing but in general still warmer and more humid than today. Glacial erosion and influence of an ice sheet on sedimentation processes can therefore be excluded for the Molo Fm. Crustal uplift has most probably a stronger influence of the sedimentation history on the NCS than climate.

2.2.3 Uplift of Fennoscandia

Uplift is an important factor to be considered for the reconstruction of sedimentary transport. It is an upward directed, vertical crustal motion that can be triggered by a variety of different processes. As a general rule, uplifted land features a higher relief energy than lowlands and is hence more prone to erosion. Uplift of a contemporary peneplain marks the onset of sedimentation of the eroded material and creates new accommodation space. The magnitude of uplift influences speed and strength of sediment transport. Depending on the erodibility of the prevalent source material, uplift can change the course of rivers or even the position of entire drainage basins (Riis & Fjeldskaar, 1992; Løseth & Henriksen, 2005; Eidvin et al., 2013; Eidvin et al., 2014). The uplift history of Scandinavia is therefore directly related to the sedimentation history of the surrounding shelf areas and especially important when saprolitic layers with a low erosional resistance are considered. Reusch (1903) already noticed that the formation of the present Scandinavian relief required uplift in some way. Elevated even plateaus and later progradational sediment wedges visualised by seismic studies have been subject of suspicion concerning uplift. Extensive sedimentary wedges were interpreted to reflect sudden influx of sediments into basins at the coast as response to uplift (e.g. Riis, 1996). For example, the increase in lateral extent of the inner Norwegian shelf in the late Miocene is seen as the result of regional uplift (Faleide et al., 2008).

Since the melt of the continental glaciers and ice sheets that covered Scandinavia during the last glacial period (the Weichselian glaciation in the Pleistocene), the continental mass is subject to uplift as response to the loss of weight that previously depressed the rigid lithosphere down into the viscous asthenosphere (see Fjeldskaar et al., 2000 for a review). This process is known as post-glacial rebound or isostatic adjustment and aims isostatic equilibrium, occasionally leading to small earthquakes (e.g. Walström, 1993; Fjeldskaar et al., 2000). However, Scandinavia was subject of a much more complex uplift history, which predates the last glacial period. There is a general acceptance of this uplift theory for Scandinavia in academia (early studies include Gutenberg, 1941), but its cause, influence, extent, and timescale are still disputed (e.g. Stuevold & Eldholm, 1996; Japsen & Chalmers, 2000; Anell et al., 2009; Nielsen et al., 2002; Nielsen et al., 2009; Gregersen & Voss, 2010). Magnitsky (1967) already noted difficulties in disentangling isostatic and tectonic processes causing uplift in Scandinavia. Bungun et al. (2010) suggest that isostatic adjustment plays a minor role and seismic activity is rather

caused by ridge-push processes as a result of sea-floor spreading at the North Atlantic ridge. Many authors suggest ridge-push rather than post-glacial rebound as dominant mechanism for seismicity recorded in Norway today (Smelror et al., 2007). Stuevold & Eldhom (1996) state that the Plio-Pleistocene uplift was mainly caused by tectonics, and, instead of being its main cause, were only amplified by the post-glacial rebound. In addition, the magnitude of both tectonic and isostatic components seems to vary along the uplift axis (Stuevold & Eldholm, 1996).

The uplift history of Fennoscandia appears to be an interplay of different processes that are difficult to distinguish and many studies are based on single techniques applied in limited areas (Japsen & Chalmers, 2000). Anell et al. (2009) provide a comprehensive and critical review, summarizing the strong probability that uplift is caused by a number of geodynamic mechanisms superimposing each other. Nielsen et al. (2009), however, suggest to simplify the theory. Although they exclude several mechanisms, their model still explains uplift solely on the basis of climate, erosion, and the corresponding isostatic corrections.

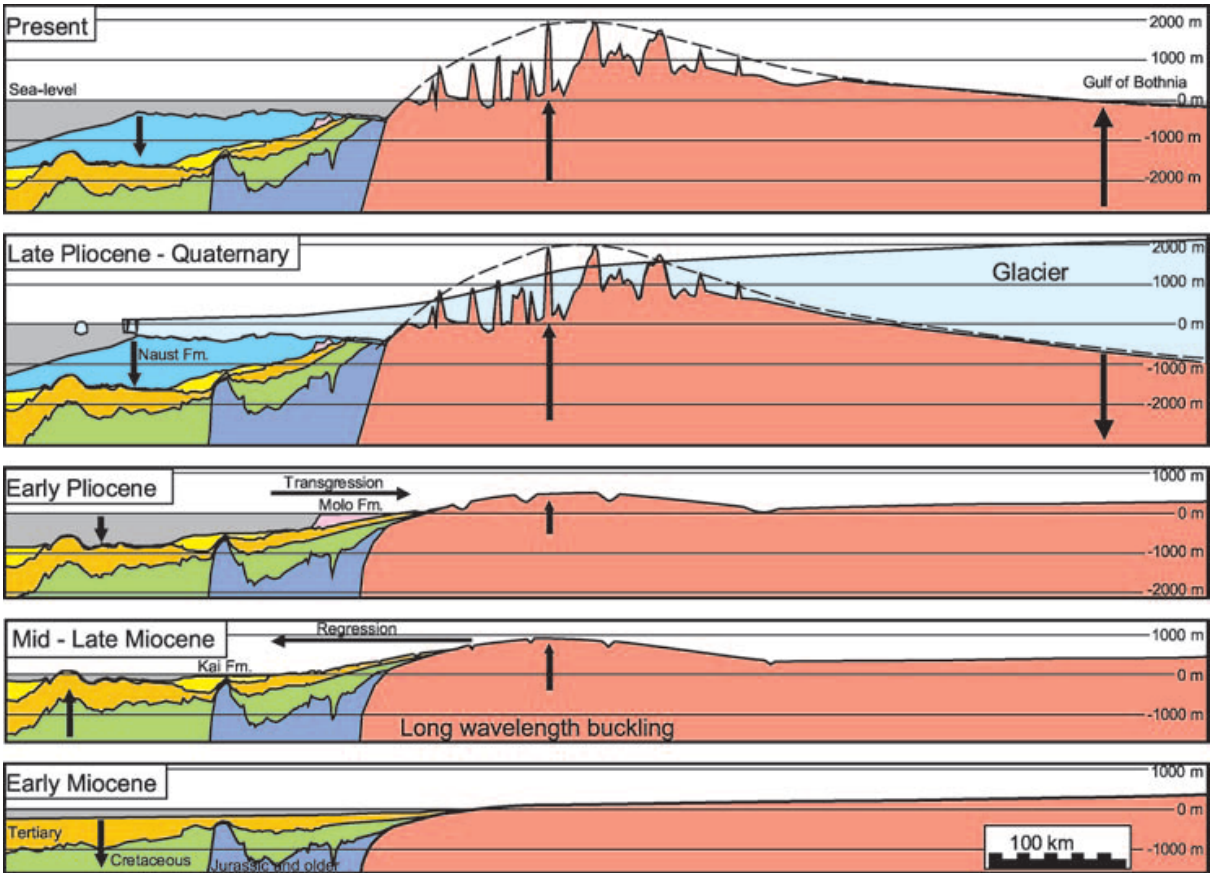


Figure 25: Idealized sketch illustrating possible uplift and subsidence mechanisms of the Baltic Shield and the corresponding sedimentation history on the mid-Norwegian Shelf. The profile is situated at approximately 66° N. Source: Løseth & Henriksen (2005).

Uplift can be associated with exogene and endogene processes. Both are subject to interdependency. Any significant change in load on the continental crust as a response to exogene processes causes uplift or subsidence. Uplift events are usually associated with corresponding subsidence adjacent to and erosion at the uplift centres (Japsen & Chalmers, 2000). Even increased precipitation can initiate uplift as amplified erosion removes higher amounts of material and therefore weight from the crust (Stuevold & Eldholm, 1996). On the other hand, internal (endogene) changes within the asthenosphere or the lower lithosphere that effect movements of hot mantle material (for example as induced by the emplacement of a mantle plume) cause vertical movements of the overlying crust. Magmatic underplating, for example, which refers to an entrapment of rising magma below the lithosphere without the development of a volcano, has been proposed to contribute (see Anell et al., 2009, and references therein). The need for uplift mechanisms other than postglacial isostasy was raised (e.g. Riis & Fjeldskaar, 1992; Riis, 1996) because the estimated uplift in several models was larger than the calculated erosion, and unloading alone could not explain the difference. In the following, the trend that has emerged in academia is presented.

Two episodes of significant uplift around the northern Atlantic have been recognized that took place in the Cenozoic Era (e.g. Riis, 1996). They most probably affected all surrounding continental margins including the study area (Japsen & Chalmers, 2000). However, the two episodes cannot be clearly separated in all areas (Japsen & Chalmers, 2000) and the mechanisms primarily responsible for the vertical movements remain uncertain because the proposed mechanisms do not seem to be valid for all uplifted areas (Riis, 1996). The first uplift episode in the Palaeogene is generally associated with the formation of the Iceland plume and the opening of the North Atlantic in the Paleocene and Eocene epochs (Riis, 1996; Stuevold & Eldholm, 1996; Japsen et al., 2002). This time marks the onset of sea-floor spreading and formation of the Mid-Atlantic Ridge. The second episode is assigned to the late Neogene and Quaternary and also includes the isostatic rebound caused by the removal of the ice and related glacial erosion, as described above. Riis (1996) estimated a maximum of 1000 m of erosion as response to uplift along the Norwegian coast. Several studies suppose different uplift mechanisms for the two uplift centres (domes) in southern and northern Norway (e.g. Riis, 1996). The areas of maximum uplift and hence maximum erosion were in the southern and northern Scandes in the Lofoten area (Riis, 1996). According to Japsen & Chalmers (2000) and Japsen et al. (2002), all three Scandinavian domes are the result of Neogene uplift.

The asymmetric shape of the Scandes favours the idea of an uplift related to rifting (rift-flank uplift, comparable to the contemporary Red Sea). Steep towards the coast and slowly flattening towards the inland is a pattern frequently observed at mountain ranges around the North Atlantic (Anell et al., 2009). Moreover, modelling performed by Burov & Poliakov (2001) indicates that rift shoulders can remain uplifted for up to 50 Ma due to mass flow in the lower crust. While there is great consensus that uplift in the Paleogene and Eocene was related to the continental break-up between Laurentia and Baltica, the effect and even the existence of the Iceland plume is questioned (see Anell et al., 2009; Nielsen et al., 2002).

As mentioned above, studies on the uplift history of Norway depend on the adjacent sedimentological record, as no continuous record is present on the mainland. Age and extent of the sediments serve as a signature in response to uplift and the inclination of the layers revealed by seismic studies can serve as indicator for the direction and magnitude. The offshore stratigraphy on the Norwegian shelf implies at least one major pre-glacial uplift component (Stuevold & Eldholm, 1996) but the thermal component has been questioned by Nielsen et al., (2009). Nielsen et al. (2009) explain the present Scandinavian topography entirely by climate, erosion, and corresponding isostasy.

A common method to quantify uplift based on the sedimentary record is mass balance calculation. This method includes modelled comparisons of the eroded volume with the deposited volume and was among others performed by Riis & Fjeldskaar (1992) and Riis (1996). These studies assume that the compared sediments indeed originate from the uplifted land. An approach that requires certainty that can be given by sediment provenance studies.

In summary, the uplift history of Norway and the development of the continental shelf are closely connected. The shelf basically consists of the material eroded from the mainland. The timing and the extent of the source material from the mainland can be studied on the basis of the sediments on the shelf. The identification and classification of sediments sampled from the Molo Fm can therefore shed light on the question to what extent saprolites have existed on the mainland and to when they were eroded.

3. MATERIALS AND METHODS

3.1 Materials

This study is based on a systematic comparison of onshore and offshore samples of different types. The main part of the material represents loose siliciclastic sand samples of the grain size fraction > 0.5 mm, on slides embedded in epoxy resin. The remaining samples are thin sections of basement rock and basement derived saprolitic corestones with a thickness of 250 μm . For investigation, all material was mounted on standard glass slides. The main subject of investigation were digital panchromatic images of the samples obtained by BSE and CL scanning. In addition, trace element contents of the grains were compiled by means of LA-ICP-MS. The object of interest was the mineral phase quartz. Altogether 13 samples were analysed, six of which were offshore (sediment) and seven were onshore (basement) samples.

Integration of the samples into stratigraphic contexts was based on information drawn from the literature. Data on the individual boreholes were mainly collected from the *Factpages* of the *Norwegian Petroleum Directorate* (NPD).

3.1.1 Image data

All images were taken with an SEM equipped with a CL detector, located at the NGU in Trondheim. The original scans were grey scale images (256 grey levels) with a resolution of 1024 x 768 pixels and a bit depth of 24, scanned in November 2014, May and November 2015. Additional image adjustments were carried out with *Adobe Photoshop CS6* ver. 13.0.1.

Of the 13 samples, CL micrographs were compiled for a total of 400 grains. Additionally, BSE scans were prepared for 11 samples, including 106 grains and thin section details. All images provided a scale (μm) and information on magnification, working distance (WD), stage at Z (distance to the detector), and the scanning date.

Deployed spatial magnification ranged from 125 - 500 X for detrital grains and to a maximum of 1000 X for thin section details. Average magnification applied was approximately 300 X for grains and 445 X for thin section details. Several images of larger quartz grains were composed of two or more scans in order to provide a reasonable magnification.

3.1.2 Offshore samples

An overview of all samples with corresponding wellbore-names and coordinates is given in Tab. 1. The six offshore samples (sample no. 2, 3, 4, 3a, 1, 6) were taken from three different cores drilled on the Norwegian Sea continental shelf off the coast of central and northern Norway (wells 6610/7-1, 6510/2-1, and 6610/3-1; see Fig. 12 & 22). The drilling sites are situated between 65°45' N and 68°45' N latitude and are at the maximum 90 km away from the present coastline. The cores reach a total depth of more than 4700 m (well 6510/2-1). However, sampling of the cores for this study was done in the range from 441 m to a maximum of 940 m depth. The depths for all well are given in metres below rig floor. Three samples (no. 2, 3, and 4) were taken from the same well (6610/7-1) but at different depths (20 m intervals). Samples 1 and 6 were also taken from one well (6610/3-1) with a 20 m interval. The wells were all drilled by different gas and oil companies in 1983, 1992, and 1997, mainly for exploration purposes in the search for hydrocarbons (wildcat wells). The drillings were operated by *Den norske stats oljeselskap A/S*, today known as *Statoil ASA* except for well 6510/2-1 (*A/S Norske Shell*). All offshore samples consist of clastic sediments (sand, > 0.5 mm) (see Fig. 26). Altogether 339 CL scans and 62 BSE scans have been prepared.

3.1.3 Offshore samples in detail

Well 6610/7-1: Sample 2, 3, 4

Offshore samples no. 2, 3, and 4 were taken from well 6610/7-1 (66°17'32.82" N, 10°16'52.92" E) drilled at the Træna Bank, Helgeland Basin, which is part of the extensive Trøndelag Platform. All sampled depths (900, 920, and 940 m) lie within the range of the Molo Fm (Eidvin et al., 2013; Eidvin et al., 2014). The well reached a total depth of 3333 m (Late Jurassic) (NPD, 2016). The sample site is situated approximately 90 km away from the present coastline and 110 km from the shelf break. The following quantity of CL and BSE scans was prepared: Sample 2 (900 m): 77 grains with CL, 12 of them with BSE parallels. Sample 3: (920 m): 73 CL scans, 17 BSE scans. Sample 4 (940 m): 51 CL scans.



Figure 26: Exemplary true-colour scan of an offshore sample (well 6610/7-1, 920 m) with siliciclastic sand of the grain size fraction > 0.5 mm embedded in epoxy resin. Inlet in bottom right-hand corner displays the actual size of the slide.

Well 6510/2-1: Sample 3a

For sample 3a, taken from well 6510/2-1 ($65^{\circ}47'15.60''$ N, $10^{\circ}25'51.33''$ E) at a depth of 441 m, 52 CL scans of grains were prepared as well as one BSE scan. The drilling site is situated south east of the Helgeland Basin on the Vega High, Trøndelag Platform, within the Ylvingen Fault Zone (Blystad et al., 1995). At this latitude ($65^{\circ}45'$ N) the continental shelf of the Norwegian Sea reaches its largest horizontal extend. The well was drilled in 1997 at a water depth of 325 m and reached a total depth of 4707 m (Early Triassic).

Well 6610/3-1: Sample 6 and 1

The samples 6 and 1 were taken from well 6610/3-1 (66°55'29.70" N, 10°54'6.28" E) at 480 m depth (sample 6) and 460 m (sample 1). The site is situated approximately 80 km southwest of Røst, the furthest island of the Lofoten archipelago at the Lofoten Ridge/Vestfjorden Basin (see Fig. 20). The well reached Late Cretaceous sediments at a total depth of 3126 m (NPD, 2016). Scanned images available: CL: 31 grains, BSE: 26 grains.

3.1.4. Onshore/basement samples

The seven basement samples (samples no. 5, 89415, 89418, 89421, 47802, 10, and 25) were taken from potential sediment source areas on a Norwegian island (Hadseløya) and the mainland of Norway between 64°10' N and 68°33' N latitude. They included two sand samples (> 0.5 mm) derived from weathered saprolitic profiles (samples no. 89415 and 89421), two thin sections (250 µm) of mangerite corestones (samples no. 5 and 89418) and a thin section of a gneissic granite (sample 47802). Furthermore, two thin sections from cores that were actually drilled offshore, but close to the coast into basement rock were included (well 6814/4-U-1: sample 25, and well 6408/12-U-01: sample 10). These two cores were drilled as part of the *IKU Shallow Drilling Program*. All onshore/basement samples except for the latter two were taken from surface outcrops.

Three samples (no. 5, 89418, and 89415) were taken from the same locality, called Brennvinsaugen, on the island of Hadseløya, which is one of the southernmost islands of the Vesterålen archipelago (Fig. 13). The island has a west-east expansion of 16 km and a north-south expansion of approximately 10 km. The sample site is situated 3 km away from the present-day coastline at an elevation of 145 m a.s.l.

3.1.5 Onshore samples in detail

Hadseløya: Sample 5, 89415, 89418

Samples no. 5, 89415, and 89418 were all taken from the same quarry at Brennvinsaugen on Hadseløya (68°31'58" N, 14°52'57" E). Brennvinsaugen is situated in the eastern centre of the island in the upper Husbydalen between the mountains Husbykollen (513 m a.s.l.) and Storheia (504 m a.s.l.). Sample 5 is a thin section of a mangerite corestone. Six scans were prepared for both CL and BSE, including an overview scan covering 1690 X 1265 µm. For the thin section no. 89418, nine CL and BSE scans were prepared. Sample 89415 consists of sand grains derived from saprolitic mangerite basement. It was the same but slightly more weathered/eroded material sampled at the close vicinity of the thin section sample spot. Ten CL and BSE scans were prepared.

Hamarøy: Sample 89421

Sample 89421 consists of sand derived from a saprolitic mangerite but was taken from a sample site situated about 60 km southeast of Brennvinsaugen. The sample was taken from an outcrop at Stotland on the Hamarøy peninsula approximately 1 km away from the present coastline at an elevation of 77 m a.s.l. (68°03'17" N, 15°26'50" E, see Fig. 13). Ten CL scans with ten corresponding BSE scans were prepared.

Tysfjord, Hundholmen: Sample 47802

Sample 47802 is a thin section (250 µm) of a coarse grained gneissic granite sampled at almost sea level on the Hundholmen peninsula, Tysfjord (68°08'50.34" N, 16°16'00.10" E, see Fig. 13). Eight CL scans of the thin section were prepared.

Well 6408/12-U-01 (32.42 m): Sample 10

Sample 10 (well (6408/12-U-01) was drilled offshore into granitic/gneissic basement rock between Frøya and Suladjupet, in the Froan Basin, north-west of Trondheim (64°10'13.29" N 8°44'53.49" E). The drilling site is situated close to the Møre-Trøndelag Fault Complex (see Fig. 19). The basement is kaolinite-weathered (Mørk & Johnsen, 2005; Müller, 2015). The core was

drilled in 1988 and sampled for this study at a depth of 32.42 m. Eleven CL scans and five BSE scans were prepared.

Well 6814/4-U-1 (174.48 m): Sample 25

Sample 25 was taken from well 6814/4-U-1 off the western coast of Langøya, Vesterålen (68°39'10.90" N, 14°11'8.90" E). The drilling site is about 8 km off the coast and 7 km away from the island Gaukværøy in the south-east at the edge area of the Ribban Basin (Blystad et al, 1995). The sample was taken from a depth of 174.48 m which is below the sediment cover in the crystalline basement rock. Therefore it is considered an onshore/basement sample



here. Drilling took place in 1991 for scientific purposes (by *IKU Petroleumsforskning SINTEF Gruppen*) at a water depth of 241 m. The thin section consists of monzogranite rock. Seven CL scans and four BSE scans were prepared.

Figure 27: Exemplary true-colour scan of a basement sample drilled offshore (6814/4-U-1, 174.48 m)

Table 1: Synoptic table summarizing the data used in this study.

	Sample no.	Well/ Location	Altitude	Area	Latitude	Longitude	Drilled/ sampled	Source material	Grain-size/thickness	CL - Scans	BSE - Scans	LA-ICP-MS-data
Basement samples	Sample 5	Brennvins-haugen	145 m a.s.l.	Hadseløya	68°31'58"	14°52'57"	2014	Mangerite corestone	Thin section 250 µm	6	6	
	Sample 89415	Brennvins-haugen	145 m a.s.l.	Hadseløya	68°31'58"	14°52'57"	2014	Sand/Saprolite, Mangerite	> 0.5 mm	10	10	5
	Sample 89418	Brennvins-haugen	145 m a.s.l.	Hadseløya	68°31'58"	14°52'57"	2014	Mangerite corestone	Thin section 250 µm	9	9	
	Sample 89421	Stotland	77 m a.s.l.	Hamarøy	68°03'17"	15°26'50"	2014	Sand/Saprolite, Mangerite	> 0.5 mm	10	10	5
	Sample 47802	Hundholmen	1 m a.s.l.	Tysfjord	68°08'50.34"	16°16'00.10"	2008	Gneissic granite	Thin section 250 µm	8	0	2
	Sample 10 01	6408/12-U-01	32.42 mRKB	Froan Basin	64° 10' 13.29"	8° 44' 53.49"	1988	Granitic basement	Thin section 250 µm	11	5	4
	Sample 25	6814/4-U-1	174.48 mRKB	Ribban Basin	68°39'10.90"	14°11'8.90"	1991	Monzogranite basement	Thin section 250 µm	7	4	4
	Sample 2	6610/7-1	900 mRKB	Træna Bank	66°17'32.82"	10°16'52.92"	1983	?	> 0.5 mm	77	12	43
	Sample 3	6610/7-1	920 mRKB	Træna Bank	66°17'32.82"	10°16'52.92"	1983		> 0.5 mm	73	16	
	Sample 4	6610/7-1	940 mRKB	Træna Bank	66°17'32.82"	10°16'52.92"	1983		> 0.5 mm	50	2	
Sample 3a	6510/2-1	441 mRKB	Vega high	65°47'15.60"	10°25'51.33"	1997	> 0.5 mm		52	1		
Sample 1	6610/3-1	460 mRKB	Vestfjorden basin	66°55'29.70"	10°54'6.28"	1992	> 0.5 mm		56	5	41	
Sample 6	6610/3-1	480 mRKB	Vestfjorden basin	66°55'29.70"	10°54'6.28"	1992	> 0.5 mm		31	26		

3.2 Methods

This chapter describes the multi-methodological approach implemented to track the sources of 6 samples of continental shelf sediments. Two different analytical methods were used to identify characterising features of the individual quartz grains of both offshore and onshore samples. The methods include imaging with SEM using BSE modus, CL scanning, and LA-ICP-MS. The SEM equipped with the CL detector allows comparative CL and BSE scanning of the exact same sample section.

The results for the different samples were compared with each other with special attention to the comparison between offshore and onshore samples. By this means classes and groups were compiled and possible connections, i.e. potential common source areas of the sediment, were examined. For scanning, all material was mounted on glass slides. The specimen were prepared for analysis in a conventional manner as described below.

3.2.1 Specimen preparation

Specimen preparation was performed in Trondheim (NGU). After sampling of the original drill cores the grain size fraction (> 0.5 mm) was achieved by wet sieving with deionised water. The grain size was chosen for practical reasons (image resolution and material availability for subsequent laser ablation). After drying a first selection was done by manually picking grains under a binocular microscope. Grains that were obviously not composed of quartz were disregarded. Grains consisting of other minerals, mainly feldspar, that could not be differentiated and were picked unintentionally were later identified by a brighter BSE signal and omitted. The grains were picked randomly in order to provide a representative selection for each sample but with concentration on larger grains. The grains were then embedded in epoxide resin on standard glass slides (2.8 x 4.8 cm). The hardened samples could then be polished down to approximately half the size of the grains and were again cleaned with deionised water for subsequent scanning. The grains were polished until a thickness of approximately 250 μm was reached in order to allow maximal comparability with the thin sections, which have the same thickness.

Grain selection of the loose sand samples for CL scanning was based on BSE contrasts. For that purpose, BSE overview images of the samples were prepared first. Each grain was given an

individual fixed number. The numbers were also included on an overview image for orientation during laser ablation.

The mineral quartz is a weak electrical conductor. In order to prevent a build-up of electric charge on the sample during scanning with high-energy electron bombardment, the surface needs to be conductive to allow the discharge of excess electrons. Carbon coating was therefore first applied to each sample in a vacuum chamber by vaporizing a graphite wire (standard grade carbon fibre cord, type C5421, *Quorum Technologies Ltd*). By this means, a very thin layer of carbon, only a few nm, precipitated on the sample surface. Equipment (carbon evaporator) used for this process was a *Thermo VG Scientific Polaron CC7650 Carbon Coater* combined with a vacuum pump (*Edwards 12* model RV12, a rotary vane pump provided by *Ideal Vacuum Products, LLC*). The entire process took approximately 1 hour, mainly due to the time needed to create the vacuum. After the necessary pre-heating of the wire the vacuum was stabilised again. The actual coating process (using 8-9 volts) took only ca. 2 seconds.

Even though carbon is a non-metal it is a good electric conductor. In addition to the coating the sample was provided with conductive tape on two sides in order to further improve electrical discharge.

3.2.2 Scanning electron microscope: Backscattered electron

A scanning electron microscope operates with a highly focused electron beam that bombards the surface of a sample. The recorded signal represents the surface topography of the sample and/or gives indication of the sample composition (depending on the detector used) as electrons interact differently with various atoms. The application principle of BSE scanning in mineralogy is based on the fact that electrons tend to be scattered back stronger when heavier elements are irradiated. The higher the atomic number of an element, the brighter the BSE signal. E.g. a pure quartz molecule consists of only SiO_2 . With one silicon atom ($Z=14$) and two oxygen atoms ($Z=8$) it consists to more than 50 wt. % of the light element O. The mica biotite, for example, contains also heavier elements such as potassium and iron and hence appears brighter under electron radiation. However, since minerals in pure form are relatively rare and are not essential for this work, the BSE contrasts here express different mean atomic numbers of the respective mineral phases. BSE scanning is therefore a convenient tool to detect different mineral phases and was mainly used to differentiate between quartz and feldspar as well as to detect micro-inclusions. The scans were also used comparatively to the CL scans to study

noticeable features (e.g. healed fractures, see below). The used SEM (*1450VP, LEO Electron Microscopy Ltd*) has a stage with space for two thin sections/probes. Since the sample must be investigated under thermal and chemical stability, the microscope was provided with a high vacuum chamber. The BSE detector used was a four *Quadrant fixed Backscattered electron Detector Type 601 (K.E. Developments LTD., Cambridge, England)*. The system was operated using *Zeiss SmartSEM V05.04* software (*Carl Zeiss SMT Ltd*).

An advantage of the technique is the high depth of focus and the high resolution that can be obtained. A major disadvantage is the high expenditure of time due to the necessary specimen preparation as described above.

3.2.3 Cathodoluminescence imaging

Since quartz of different origin or different quartz generations all have the same mean atomic number (molecular weight), BSE scanning easily reaches its limit when only one mineral phase is investigated. CL is a type of luminescence caused by excitation of matter through electron irradiation released by a cathode. It is used in mineralogy as an analytical method that is capable of visualising inner structures of luminescent minerals that are indiscernible with BSE or pure optical microscopy (see Fig. 11). The size of the electron beam that reaches the sample surface determines the highest resolution that can be obtained. The scanning produces a very high resolution digital image which represents the luminescence activity of the sample's surface upper few micrometres. The instrument used for this study is a *Centaurus BS bialkali*-type CL detector attached to the SEM described above. It operates with a hot-cathode using a tungsten filament as electron source. The electron bombardment causes the irradiated sample to emit photons with wavelengths from UV to IR that includes visible light. The method is especially applicable for material with weak CL response such as quartz (Bernet & Bassett, 2005). The weak CL signal is due to the extremely high purity of quartz. A working distance of 20 mm was used.

The grains and thin section details were scanned one by one. Scanning contrast was adjusted for grains with a very strong CL signal in order to allow the visualisation of internal structures of otherwise just white appearing areas. Some grains were therefore scanned twice in order to provide a scan with different brightness and contrasts. Those grains were only counted once. Contrast and brightness adjustments after scanning were only performed for scans with

a (too) dark CL signal. Problems occurring during CL scanning include difficulties with occasionally emerging very high brightness. Grains with a very bright CL signal (e.g. feldspar, but also some quartz grains) can outshine other grains or lead to partial illumination of them resulting in distorted CL contrasts (see Fig.31 A). This effect was avoided by placing the requested grain as close as possible to the scan field margin and hence placing the bright shining grain outside of it. The sample boundary, or, by using high contrasts, even the sample matrix (resin) can outshine the information bar (including the spatial scale) at the lower image boundary. In addition, already scanned areas show slightly changed luminescence that can influence further scanning contrasts in the proximity of the sample area. For practical reasons (further image processing) the grain were not placed behind the information bar. Since the CL signal is the result of interaction between different factors that are still not all fully understood, a further method is needed to unambiguously characterize the mineral grains.

3.2.4 Laser Ablation Inductively Coupled Plasma Mass Spectrometry

Inductively coupled plasma mass spectrometry (ICP-MS) is an analytical method that allows highly detailed determination of element contents of gaseous sample material. All samples investigated here were initially solid. The word “laser” is an acronym for *light amplification by stimulated emission of radiation*. Laser ablation (LA) is the method used to selectively vaporize certain areas of the quartz grains in order to transform the solid matter into a state measurable by mass spectrometry. The combination of these methods (LA-ICP-MS) was used to determine the trace element content of quartz.

The analysis was performed on selected grains and thin sections with an *ELEMENT XR* type double-focusing sector field inductively coupled plasma mass spectrometer from *Thermo Scientific*. The laser probe used was a *New Wave UP193 FX ESI* excimer laser operating a 193 nm beam, which lies within the UVC spectrum. The instrument was equipped with a CCD camera (charge coupled device) that allowed full optical control of the ablation process (see Fig. 28 & 29).

Selection of the grains for LA-ICP-MS analysis was mainly based on the BSE scans. Grains with a high abundance of visible microinclusions were omitted from the outset. Larger grains were chosen preferably in order to provide enough material for ablation. A number of international reference material was used as standards for external calibration of the instruments prior and

in between the measurements. These include NIST SRM 610, 612, 614, 616 (synthetic silicate glasses), and 1830 (soda-lime float glass), produced by the *National Institute of Standards and Technology* (NIST), USA. Further used standards were BAM No. 1 SiO₂ glass as well as a Qz-Tu synthetic quartz monocrystal from the *Federal Institute for Materials Research and Testing* (BAM) in Germany. Specimen preparation after SEM-CL scanning only included cleaning and removing of the conductive carbon coating (using deionised water) in order to allow an easier recognition of inner structures and possible micro fluid- and mineral inclusions that need to be avoided. The following elements were measured: Li, Be, B, Mn, Ge, Rb, Sr, Sb, U, Na, Al, P, K, Ca, Ti, Fe, Zn, and Ga. The area for ablation was selected by manually drawing a path (ablation raster, see Fig. 28 & 29). Since this optical control allows ablation around or between visible microinclusions, no dressing techniques were needed to remove inclusions before the analysis.

A total of 164 grains (including thin sections) were ablated, each in a continuous raster of approximately 130 X 400 µm and a depth of 20 to 30 µm. The following settings were used: Laser repetition (pulse) rate: 20 Hz. Irradiance (power density): 0.90 GW/cm². Energy density (fluence): 4.60 J/cm². Laser beam diameter used for ablation was 50 µm. The length of the necessary ablation path depends on the number of elements to be measured in the ICP-MS. With the given parameters (including the skipping of the first few seconds of ablation, see below) an average path length of about 800 µm was ablated in order to erode enough material for element composition measurement in the MS. The ablation path was, when possible, always set parallel to the grain boundaries and parallel to inner structures. Processing close to or towards the grain boundaries in a perpendicular angle was avoided as it increases the chance that the grain breaks. A grain once cracked easily continues cracking. However, larger particles that might break apart during ablation are not carried to the ICP-MS and hence not included in the calculation. Between every ablation process, a background measurement was performed that was later subtracted from the actual measured values (from the following analysis). In addition, after every 10th ablation process, a standard was measured in order to avoid memory effects (NIST 612). The ablated material was transported to the MS by a high-purity carrier gas mixture of argon and helium and then ionised by the inductively coupled plasma. This charging makes the atoms susceptible to an electromagnetic field and allows mass spectrometry. The final output is a spreadsheet with all preselected element concentrations given in parts per million (ppm) (see *Appendix*).

3.2.4.1 The ablation process in detail

After insertion of the sample into the specimen chamber of the LA instrument the requested grain (and standards) were focused on the screen. The operating software used was *New Wave Research – Laser Ablation System* (version 1.14.3.3). The software interface offers an overview window of approximately 1000 x 750 μm with a μm scale (see Fig. 28). There is no zoom available. Optical focus on the grain is also the focus for the laser beam. Two optical views on the specimen can be selected: top view (“coax”) and transmitted light (“ring”) (see Fig. 29 C and D). Top view corresponds more to the BSE image and was preferably used for navigation and search for the grains. Transmitted light reveals larger inclusions and was mainly applied to determine the ablation pattern. Grain boundaries were often indistinct and some grains partly continued below the glue (Fig. 29 C, D). Blurred structures do not lie within the focus and are hence not on the sample surface.

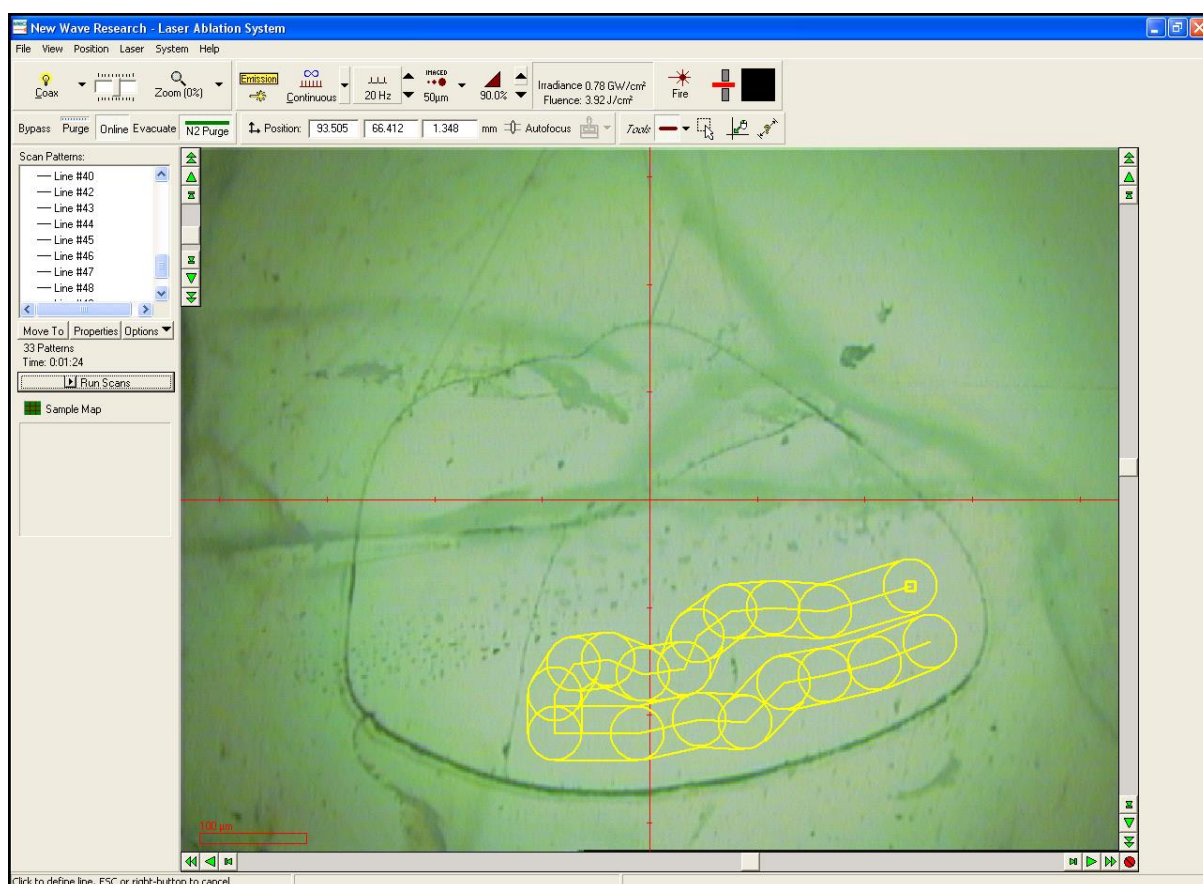


Figure 28: Software interface of *New Wave Research – Laser Ablation System*. Screenshot taken in top view light between ablation raster determination and ablation process. A belt of inclusions is visible that traverses the grain diagonally (greenish dots). The ablation raster is set below these impurities (yellow pattern).

The ablation process was started after the raster was defined (and the MS finished processing of previous measurements). LA and ICP-MS instruments worked independently and were controlled via separate computers. Since the carrier gas containing the ablated material needs time to reach the MS, the element measurements were started after some seconds. The signal must stabilize first. In addition, the first few seconds (the first ablated material) is more likely to be contaminated and was avoided. Time resolved LA-ICP-MS measurements performed by Müller (2000), showed that best results are achieved when the first 8 seconds of ablation are omitted.

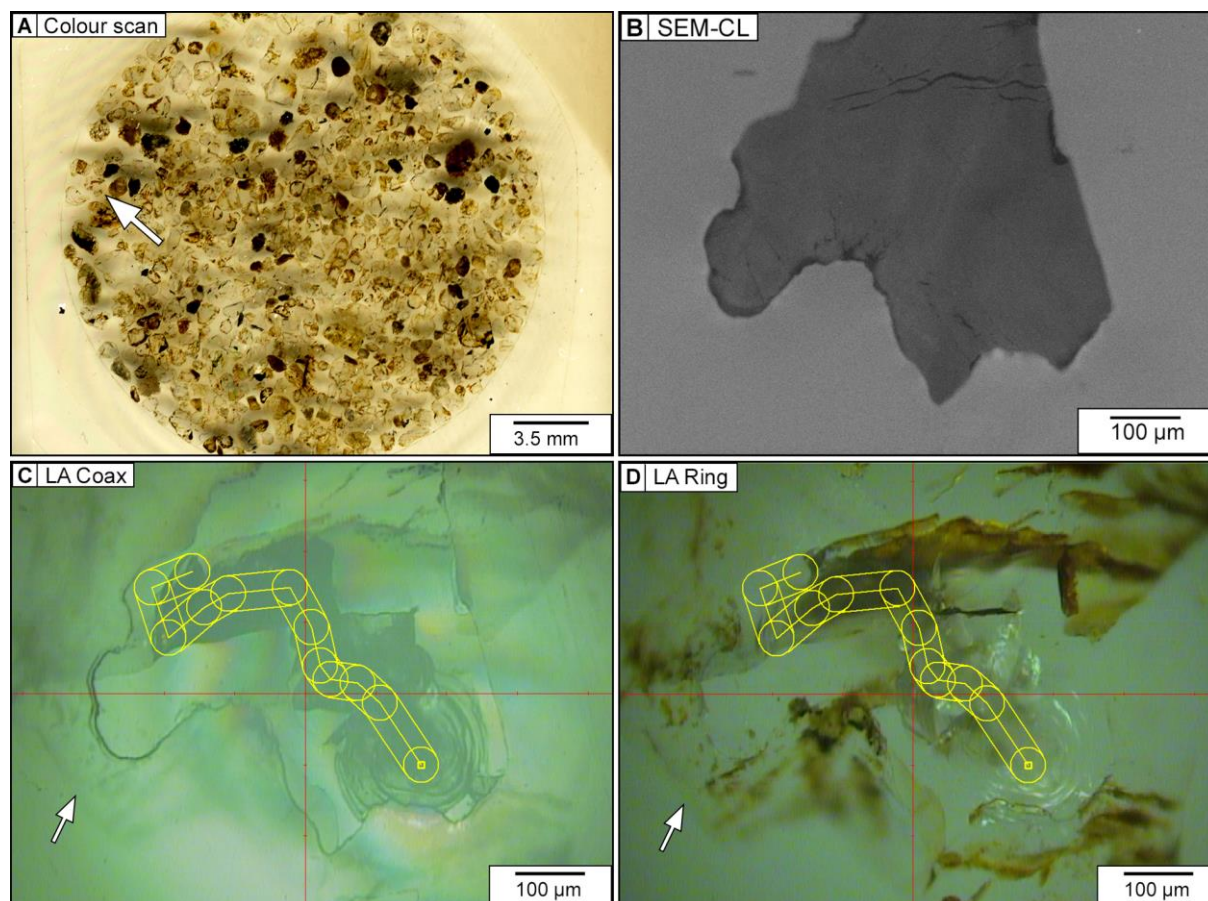


Figure 29: Scans prepared by using different methods demonstrating the ablation procedure (compare with Fig. 28). **A:** True-colour scan of a siliciclastic sediment sample (> 0.5 mm). The arrow indicates one selected grain for the LA-ICP-MS analysis. **B:** SEM-CL micrograph of the grain selected from the slide in A before ablation. **C:** Ablated grain in top-view mode. **D:** Ablated grain in transmitted light mode. The images C and D exemplify the conchoidal fracture of quartz. The arrows indicate the actual grain boundary.

As soon as the selection of elements was processed by the MS, ablation was stopped even if the selected ablation raster was not fully used. The MS computer then needed some seconds for calculation. During the MS calculation in the background, the next grain was selected on the screen. The signal levels off slowly and therefore a pause of 30 seconds was taken before

the next analysis. After the ablation process the grains were irreversibly damaged (see Fig. 29 C). Larger splinters that broke away during ablation found spread over the sample were neglected. They were blown away during the next process. Since they have not been sucked in by the carrier gas initially the splinters were apparently too large to be processed and do not further influence the measurements.

In general, a “cleaner” grain can be expected to give better results. However, since the laser energy is transmitted along (invisible) lattice-bound impurities (A. Müller, 2015, personal communication), ablation works better the higher the impurity of the quartz is. The ablation behaviour can therefore give a first rough hint concerning the purity of the quartz.

3.2.4.2 LA-ICP-MS analysis and trace element evaluation

Trace elements in quartz are extant in a range close to the detection limits of today’s analytical equipment. The detection limits (LOD) are values empirically developed for each element and separately for each sample (see tables 4, 5, 6, appendix). Values below the LOD cannot be distinguished from the background noise and are, if available, only plotted to provide an overview but excluded from further considerations.

Of the 13 samples, seven were analysed with LA-ICP-MS (2 sediment, 5 basement samples). Of the 164 analyses performed, data of 102 were usable (62 %). The remaining analyses were excluded from further considerations because values of Fe, K, Ca, Na, and P exceed 10-20 ppm. These high values indicate that the measured elements were not all structurally bonded in the crystal lattice but also part of fluid or mineral inclusions (Müller et al., 2012). Selected trace element concentrations that are most relevant for classification (Li, Al, Ti, Ge) were plotted against each other using *Microsoft Excel* 2013. These elements are among the most common structurally bound trace elements in quartz and are indicative for their crystallization environment (e.g. Müller et al., 2012). Plotting of more than two elements is necessary in order to identify and approve distinct patterns and trace element concentration ranges of the respective samples. The ablated material of a single quartz analysis performed on one grain gives insufficient data to use for a numerical evaluation since the identification of outliers requires a certain amount of analyses.

3.2.5 Classification and grouping of individual quartz grains

Seven onshore samples were investigated for comparison with offshore samples in order to verify or falsify the locations as potential source areas of the sediment. All grains of both offshore and onshore samples were first grouped according to their CL intensity, contrasts, and overall similarity. The classes and groups were then compared with each other. Besides the overall CL intensity, the classification was also based on visible primary and secondary structures as well as roughly the roundness of the grains. Quartz classes were divided into plutonic, low-grade metamorphic, and medium-grade metamorphic. These were further subdivided into several groups (presented in *Results*).

The classification of the CL scanned grains was mainly based on work by Seyedolali et al. (1997), Bernet & Bassett (2005), Boggs & Krinsley (2006), Müller & Knies (2013), and supported by A. Müller (personal communication). Remaining grains were subdivided into grains with frequent secondary structures and grains with little secondary structures. The yet remaining plutonic grains were simply grouped as “plutonic” and represent exotic grains that are either unique within one sample or even in all samples.

The following two plates (Fig. 30 and 31) illustrate structures and artefacts that occur during specimen preparation and scanning. These are important to recognise and to differentiate from actual features of the grains and are therefore illustrated in detail. All illustrated features were then neglected and not used for classification purposes. Cracks that occurred in grains or at grain margins that had the same CL intensity as the epoxy resin are not considered. Identical CL contrast is an indication that the crack occurred during specimen preparation and was subsequently filled with the glue. This was also evidenced by some obviously displaced parts of grains as shown in Fig. 30 C. In some cases this gave the impression of apparent porosity. Many scans showed straight whitish scratches aligned randomly and in some cases beyond single grains across adjacent grains (see Fig. 31 C-D). These strokes originate from the specimen preparation and were caused by polishing. These structures occurred in all offshore samples with varying frequency and were disregarded, too. Also negligible artefacts occurred in a few scans in the form of black streaks at scattered inclusions. They were most probably caused by CL signals that were too bright for the detector to be recorded properly (Fig. 31 B). The most common artefacts are summarized in Fig. 30 and 31.

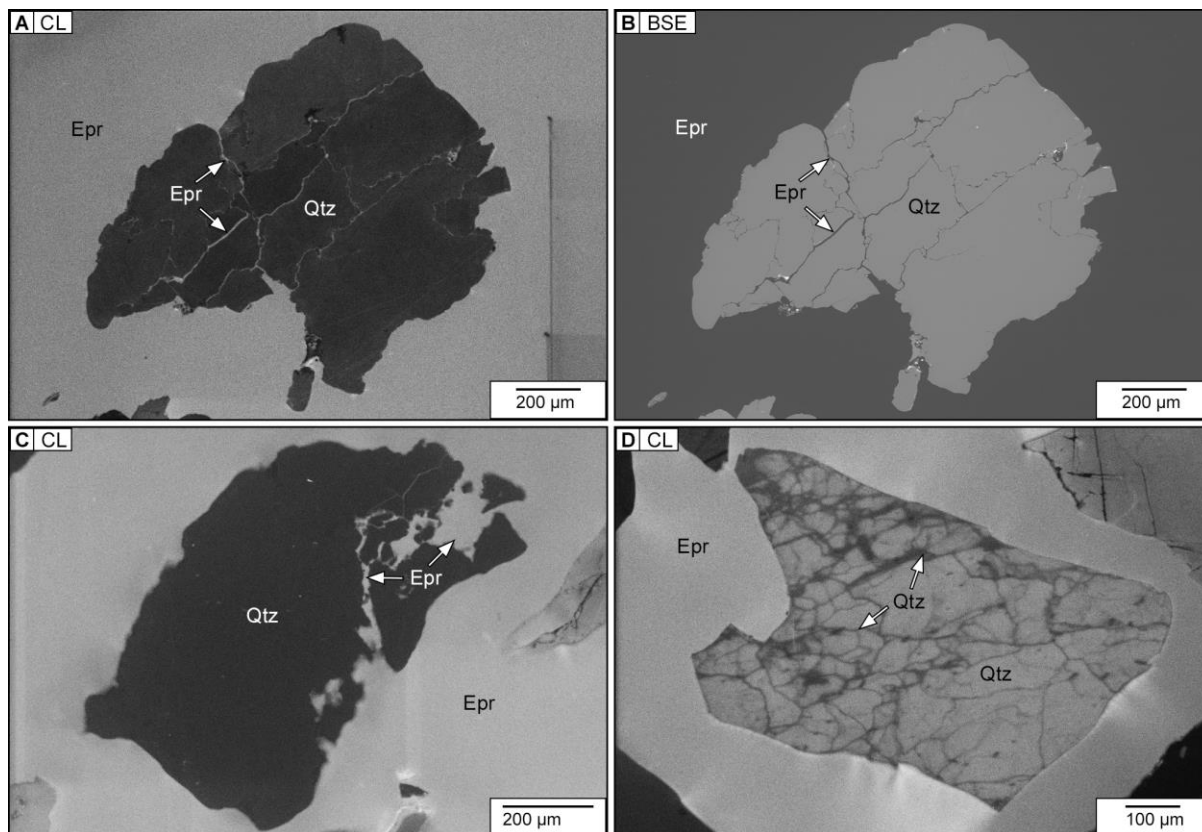


Figure 30: Micrographs showing specimen preparation-induced cracks that do not belong to the grain properties. **A - B:** CL - BSE comparison of the same grain showing cracks filled with epoxy resin (arrows). **C:** Grain cracked during specimen preparation: cracks and area between displaced parts filled with epoxy resin (arrow). **D:** Comparison with recrystallized healed cracks (arrows) that constitute secondary quartz (actual features of the grain). Epr = epoxy resin, Qtz = quartz.

Plutonic quartz was mainly grouped according to primary quartz characteristics and secondary quartz characteristics (Bernet & Bassett, 2005). Primary characteristics include original features as for example growth zoning that developed during crystallization and cooling of the grain. Features that developed subsequently are referred to as secondary characteristics (or structures). These include healed cracks and micro-cracks that developed during cooling (thermal stress), deformation lamellae, or recrystallization. Micro-cracks or healed cracks of random orientation are considered primary structures whereas preferred orientation indicates subsequent (secondary) deformation (Bernet & Bassett, 2005). Metamorphic quartz grains usually do not feature any primary quartz structures, depending on the grade of metamorphism that affected the grains. Figure 32 illustrates primary and secondary structures on two examples. Figure 33 and 34 then shows features that were used for classification.

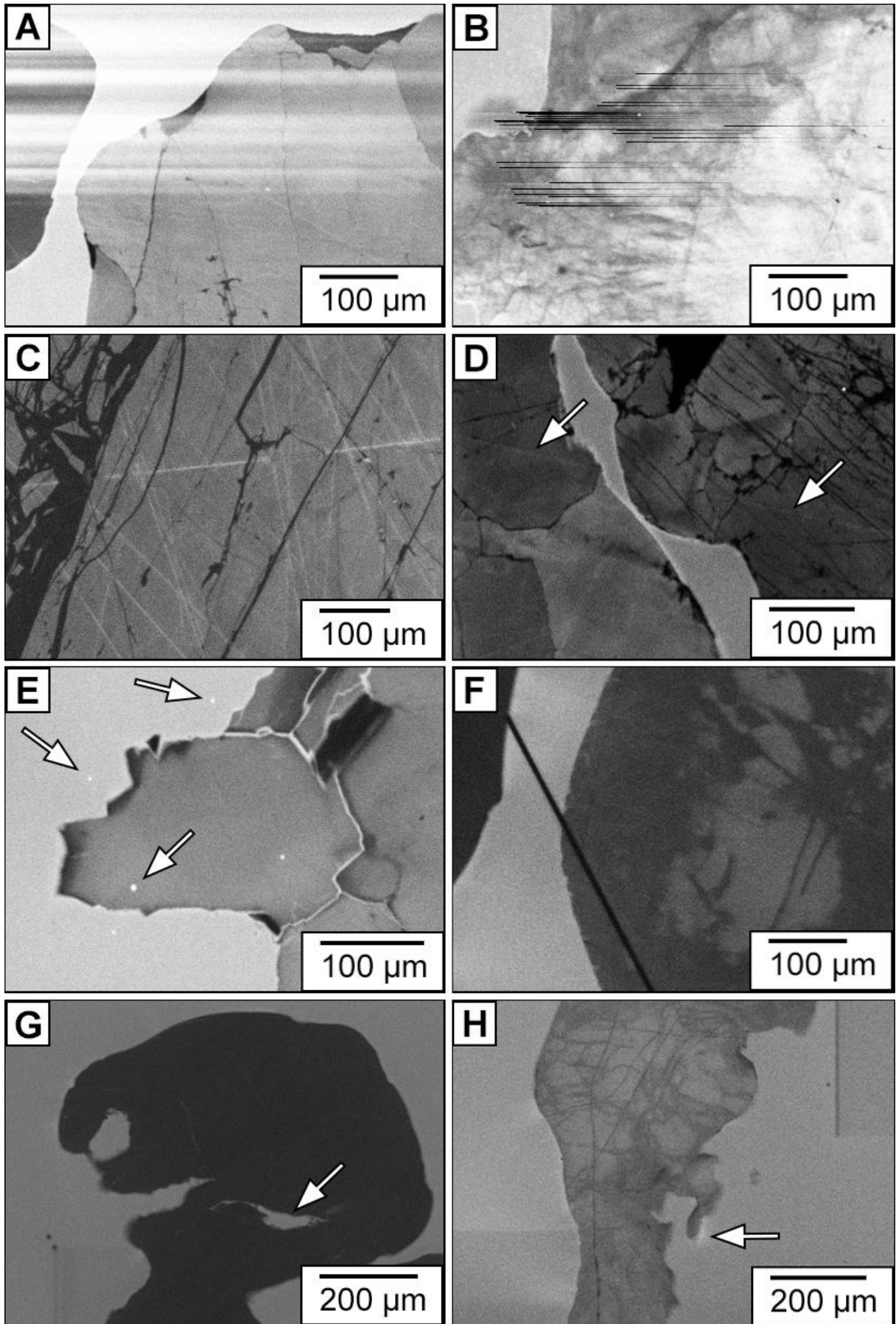


Figure 31 (previous page): Most common artefacts that occur in CL scanning of polished epoxy-mounted siliciclastic sand samples that also include other minerals. **A:** Outshining due to adjacent minerals with stronger CL signal. This effect can also occur at bright inclusions within grains (see Fig. 68 A and B). **B:** CL signal distortion. **C - D:** Scratches that occurred during polishing that traverse secondary intrinsic structures (C) and continue towards grains initially randomly combined (D). **E:** White spotty impurities that resemble inclusions but also occur beside the grain in the epoxy resin. **F:** Hair-like impurity. **G - H:** Epoxy-embedded grains in samples that were not properly polished down to half size of the grains produce unusual grain-boundaries in CL (H) or even parts with epoxy resin in the middle of the grain (G). All features presented in the figures do not belong to the actual properties of the grains and were therefore not used for classification purposes.

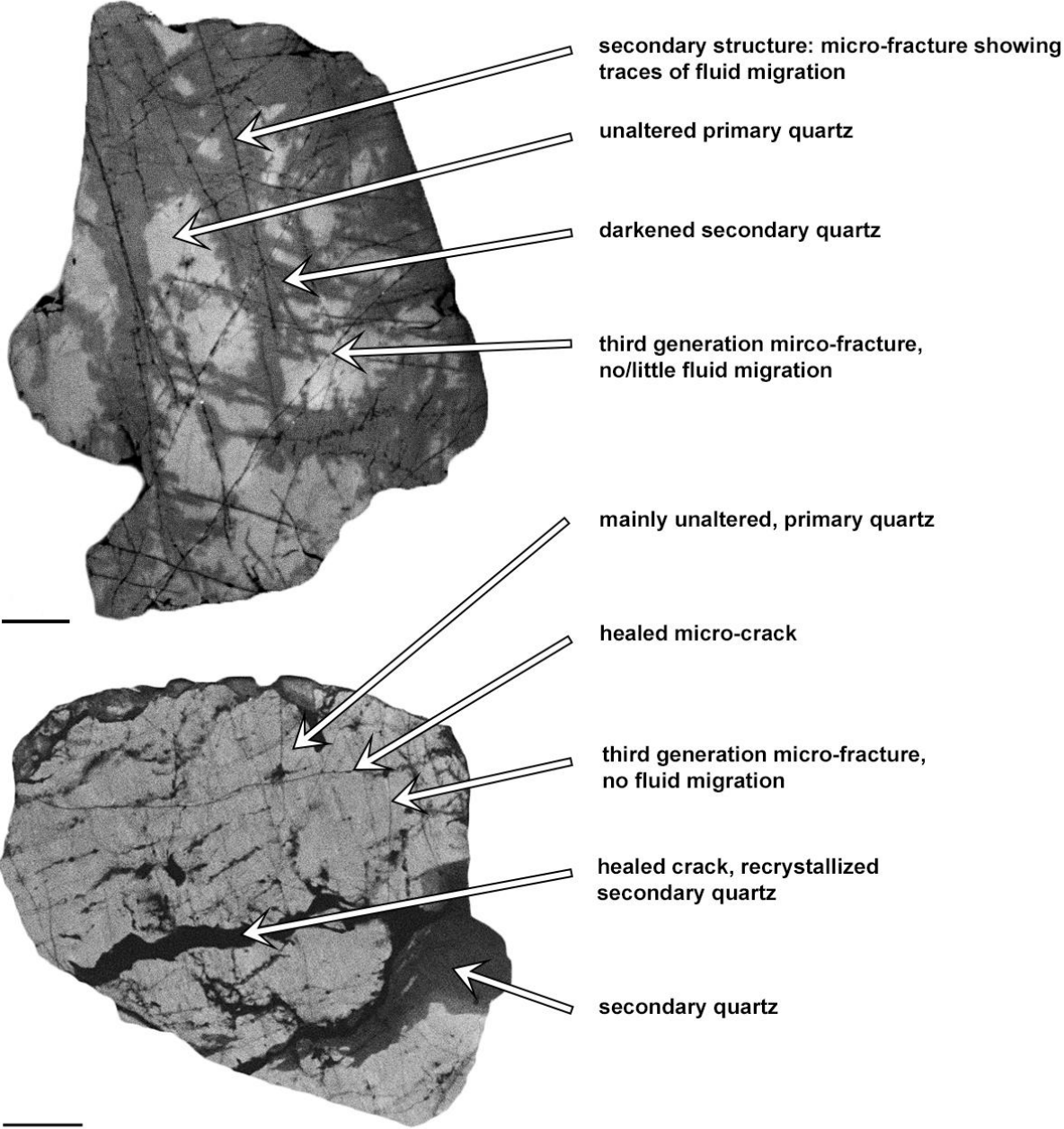


Figure 32: Quartz grains scanned with CL with indicated primary and frequent secondary features used for classification and grouping. Scale bar lengths correspond to 100 μm.

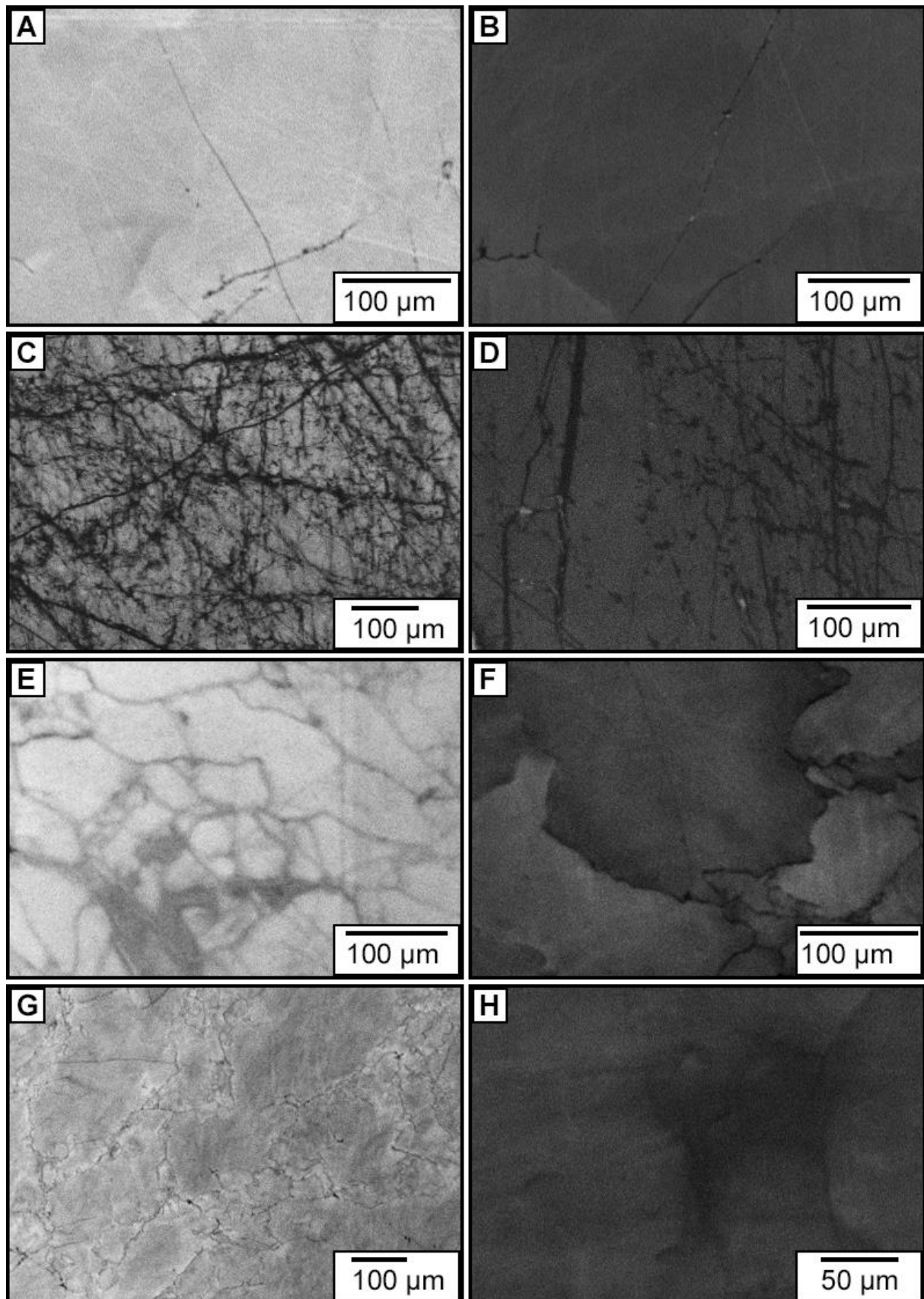


Figure 33: CL micrographs showing contrast features used for classification and grouping of the quartz grains. **A:** Few secondary structures, intermediate CL. **B:** Same type as in A, but with dull CL. **C:** Frequent secondary structures (cracks and fractures) in a primary quartz matrix. **D:** Frequent secondary structures (cracks and fractures) in secondary quartz with dull CL. **E:** Weak recrystallization with sub-grain formation, bright CL. **F:** Weak recrystallization with sub-grain formation, dull CL. **G:** strong recrystallization with sub-grain formation. **H:** Strongly altered quartz showing no distinct sub-grain formation.

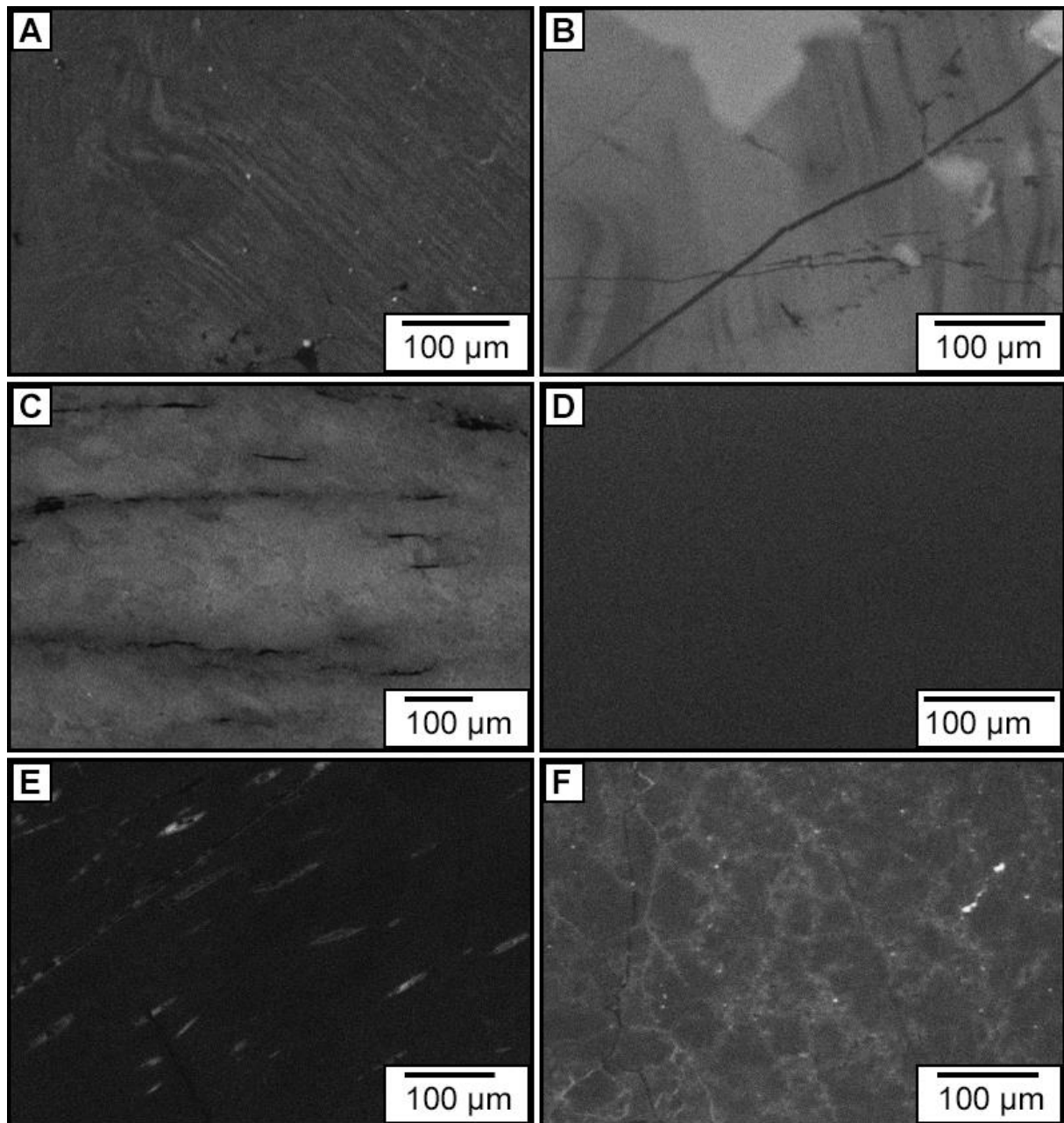


Figure 34: CL micrographs showing features used for classification and grouping. **A:** Deformation lamellae. **B:** Growth zoning. **C:** Strong shearing. **D:** Non-differential, homogeneous and dull CL. **E:** Micro-inclusions with preferred orientation, dark CL. **F:** Heterogeneous, dull CL with micro-inclusions of random orientation.

As an additional feature to characterize the sand grains, the roundness was considered. The roundness was determined by means of the silhouettes of the half grains according to the six classes as proposed by Powers' (1953) "Roundness scale".

4. RESULTS

All results presented here were based on BSE and CL images as well as trace element data obtained by LA-ICP-MS. Micrographs of 400 sediment grains and thin section details from 13 samples were studied in terms of luminescence characteristics and similarities. The optical comparison was supplemented with geochemical data for seven of the samples. The most distinct quartz grain classes and groups of each offshore sample are illustrated in this chapter and trace element contents are given. This provides an overview of the grains present and allows the determination of common or less common quartz types and narrows down potential connections between basement and sediment samples. The results of onshore and offshore samples are presented descriptively and separately first. The findings will then be put into context and discussed in the next chapter *Discussion*.

4.1 General cathodoluminescence observations

Except for some well-rounded grains with weak or even absent CL signal all investigated quartz grains of both onshore and offshore samples were distinctive. The grains were clearly distinguishable in terms of shape, CL contrasts and intra-granular structure distribution. At the same time, in all offshore samples several groups of grains with obvious similar to very similar CL properties were present (see Fig. 47 and following compilations). The similarities in the CL signal intensity together with primary and secondary intra-granular structures such as recrystallization with sub-grain formation and healed micro-cracks were used to develop groups of quartz grains that were further tested with LA-ICP-MS data. The developed groups are interpreted to represent groups of grains that crystallized under similar conditions and/or underwent a similar metamorphic history (see *Discussion*). The main classes developed include plutonic and metamorphic quartz. Metamorphic quartz were classified into low-grade and medium-grade metamorphic quartz. Within the classes, several subgroups could be established which are presented below. The subgroups were mainly based on CL contrasts, however, the grain roundness was taken into account as well. Seven generic types of offshore quartz grains were distinguished. The grains and thin section details from the basement samples were considered single quartz types each, since they were sampled at single designated localities and not the result of mixing and accumulation as was the case with the offshore sand samples.

Most of the investigated offshore sand grains were sub-angular (41 %). Only 4 % were well rounded, 4 % were very angular. An overview of the grain roundness distribution is given in Fig. 35. Some obviously well rounded grains were subsequently broken and some broken surfaces showed anew rounded edges to different degrees.

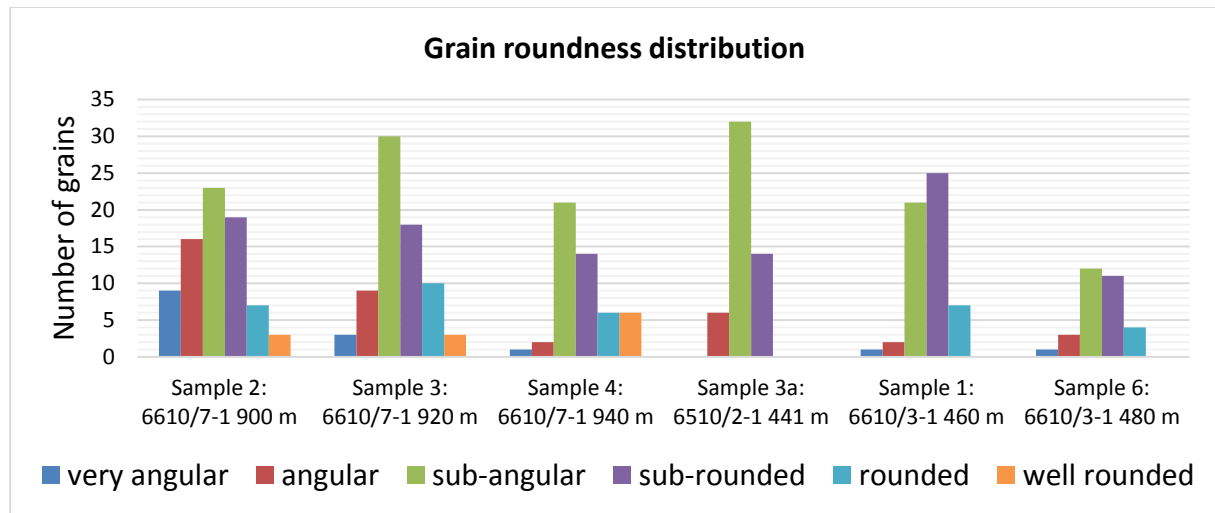


Figure 35: Grain roundness distribution of all six offshore sediment samples with sub-angular (columns in green) being the most common roundness observed (41 %). The data is based on 339 grains in total with an average of 56.5 grains per sample.

4.2 LA-ICP-MS analysis: Trace element content

Results of the LA-ICP-MS analyses reflect the CL contrast diversity with a generally wide range of concentrations for most trace elements (see Fig. 36 and tables in *Appendix*). The most common element detected in offshore quartz grains was Al with an average amount of 30.25 ppm and a maximum value of 109.64 ppm. This is followed by Ti with an average of 20.43 ppm (maximum 71.44 ppm). Figure 36 combines all obtained LA-ICP-MS data and gives an overview of the average trace element concentration for all seven analysed samples (including onshore samples). Aluminium was the most common trace element in all quartz samples except for sample 25, in which Ti dominated and in sample 47802, in which Ca dominated.

The trace element concentration ranges given in Fig. 36 are based on the average values for each sample. The widest range was recorded for iron with average values ranging from 0.48 ppm (sample 89421) to 62.04 ppm (sample 25). This was followed by Ti with values ranging from 4.12 ppm (sample 47802) to 162.28 ppm (sample 25). Not all elements included in the analytical protocol were considered for further inspection. However, the smallest range of the

most important elements was recorded for Ge with values ranging from 0.57 ppm (sample 25) to 0.85 ppm (sample 2). In the following, trace element data are incorporated in the respective results and not considered separately.

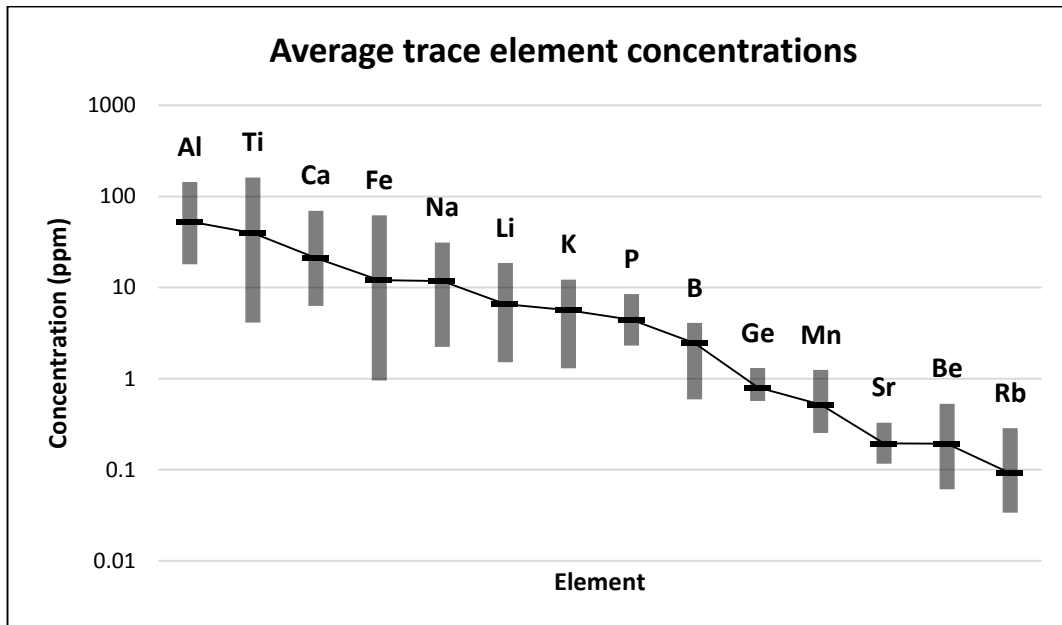


Figure 36: Average lattice-bound trace element concentrations of all LA-ICP-MS analyses combined. The grey columns represent the recorded ranges of average values, the black bars represent the total average values. Data based on 98 analyses: 5 basement samples, 2 sediment samples). Carried out at NGU, Trondheim.

4. 3. Offshore samples

4.3.1 Cathodoluminescence properties of the offshore quartz grains

The 339 CL- scanned offshore quartz grains exhibited an enormous variety of CL signal intensities ranging from completely black (no luminescence) to highly bright in a way that contrast and brightness adjustment were necessary prior to the scanning in order to visualize inner structures. The samples contained grains with heterogeneous as well as featureless, homogeneous CL contrasts (nondifferential). Features visualized include fluid and/or mineral inclusions, healed (recrystallized) fractures and micro-cracks of preferred or random orientation, authigenic quartz overgrowths, strong and weak recrystallization with sub-grain formation of entire grains and, to a very small amount, growth zoning (one grain from well 6610/3-1, 460 m depth, sample 1). Further features detected are deformation lamellae on plutonic as well

as metamorphic grains, dark staining along fissures of different extents, and distinct CL contrast concentrated at the grain margins with or without smooth transition towards the centre of the grains. Comparative BSE images confirmed that darker parts of the grains along fissures consist of quartz as the signal intensity showed identical contrasts (see Fig. 11).

Polycrystallinity (i.e. grains containing several different minerals or minerals differently aligned) was recorded in all samples except for sample 6 (6610/3-1, 480 m). Most grains were monocrystalline. The degree of metamorphism visualized in metamorphic grains varied from slightly to fully recrystallized. However, most recrystallized grains were classified as plutonic. No glass was found in the samples. Single grains with unique CL appearance that do not correspond to any other grain of the other samples were present in all samples. In general, grains showing a dark CL signal were more common than very bright appearing grains.

81 % of all offshore quartz grains were classified as plutonic. Of the remaining 19 % metamorphic grains, 83 % were classified as low-grade metamorphic and 17 % as medium-grade metamorphic. Of the low-grade metamorphic grains 57 % featured homogeneous, featureless CL contrasts. The 43 % with heterogeneous CL contrasts mainly showed frequent micro-inclusions. Low-grade metamorphic grains with a dull and featureless CL signal were present in all 6 samples but with different grades of roundness. 19 % of the plutonic grains showed recrystallization with sub-grain formation. The recrystallized grains were subdivided into weakly recrystallized (58 %) and strongly recrystallized (42 %). 15 % of the plutonic grains were strongly altered (other than clear sub-grain formation). All remaining plutonic grains were grouped into grains with frequent secondary structures (7 %), grains with few or no secondary structures (24 %) and the yet remaining 34 % plutonic grains show no clear affiliation to any of the other groups.

Based on their CL properties, the grains were classified into seven major groups, termed Type A to Type G. These quartz grain types were defined in the following way:

Type A: Plutonic recrystallized with sub-grain formation

Type B: Plutonic strongly altered

Type C: Plutonic with few or no secondary structures

Type D: Plutonic with frequent secondary structures

Type E: Low-grade metamorphic heterogeneous

Type F: Low-grade metamorphic homogeneous

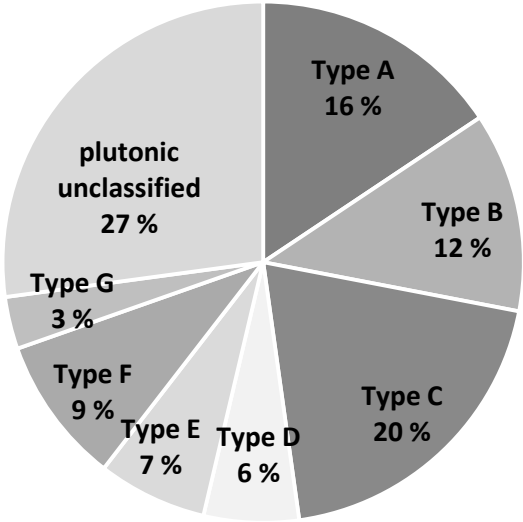
Type G: Medium-grade metamorphic

The types are described and illustrated in more detail below.

Table 2: Number of grains per type listed for each offshore sediment sample. The 92 uncategorized plutonic grains were excluded from the count but were included in the percentage numbers (Fig. 37).

Number of grains per type	Sample 2: 6610/7-1 900 m	Sample 3: 6610/7-1 920 m	Sample 4: 6610/7-1 940 m	Sample 3a: 6510/2-1 441 m	Sample 1: 6610/3-1 460 m	Sample 6: 6610/3-1 480 m	Total (grains)
Plutonic	54	61	38	49	45	27	274
Type A	8	13	10	9	10	3	53
Type B	6	5	14	9	6	2	42
Type C	9	18	4	13	13	10	67
Type D	8	6	0	1	2	3	20
Metamorphic	23	12	12	3	11	4	65
Type E	13	3	2	2	3	0	23
Type F	6	5	10	1	5	4	31
Type G	4	4	0	0	3	0	11
In total	77	73	50	52	56	31	339

Figure 37: Percentages of the quartz grain types listed above, including the unclassified plutonic grains.



4.3.2 The seven quartz grain types in detail

Type A: Grains classified as Type A were polycrystalline plutonic grains and showed different degrees of deformation recognized as recrystallization with sub-grain formation. More grains with bright CL signal were among the more strongly recrystallized grains. Strongly recrystallized grains show smaller sub-grains and the majority featured further secondary structures, mainly micro-fractures. The weakly recrystallized grains had larger sub-grains, often embedded in a matrix of secondary quartz. Type A grains had an average Al content of 34.27 ppm ranging from 17.58 to 95.40 ppm. Average Ti content was 22.29 ppm, ranging from 8.35 to 38.99 ppm. Further



Figure 38: Example of a Type A grain.

trace elements concentrations include Li with an average of 5.39 ppm, ranging from 1.15 to 9.23 ppm and Ge with an average of 0.81 ppm ranging from 0.47 to 1.05 ppm.

Type B: Type B grains were strongly altered plutonic grains that did not show sub-grain formation. Very heterogeneous, medium grey to dark CL signals characterized the group. Only few remains of primary quartz were indicated by small areas of brighter CL contrasts. In many grains mineral inclusions were visible. Due to these frequent inclusions, the trace element data are based on only 5 measurements: Al: average: 32.34 ppm, range from < 5.28 to 62.81. Ti: average: 8.96 ppm, range from < 0.92 to 13.24. Li: average: 3.69 ppm, range from 0.34 to 11.56 ppm. Ge: average: 0.75 ppm, range from 0.49 to 0.95 ppm.



Figure 39: Example of a Type B grain.

Type C: Grains categorized as Type C were a large collective group of plutonic quartz grains that show no or only few secondary structures such as fractures and cracks. Medium grey to white CL signals were most common. Al: average: 31.86 ppm, ranging from < 5.28 to 71.84 ppm. Ti: average: 26.52 ppm, range from < 0.92 to 56.81 ppm. Li average 6.32, range from < 0.14 to 16.89. Ge: average: 0.86 ppm from 0.35 to max. 1.56 ppm.

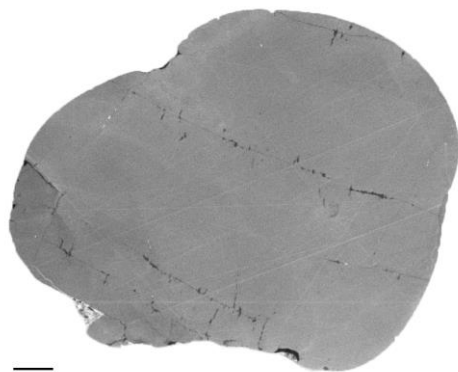


Figure 40: Example of a Type C grain.

Type D: Type D grains were plutonic and showed frequent to very frequent secondary structures, mainly fractures and cracks. Healed fractures and cracks of up to 60 μm wide were recorded. Deformation lamellae occurred on one grain. Most grains of this type consisted of primary quartz apart from



Figure 41: Example of a Type D grain.

the secondary structures. Trace element concentrations: Al: average: 48.65 ppm, ranging from 6.92 to 80.51 ppm. Ti: average: 29.27 ppm, ranging from 5.71 to 71.44 ppm. Li: average: 1.30 ppm, ranging from < 0.14 to 4.30 ppm. Ge: average: 0.65 ppm, ranging from 0.50 to 0.75 ppm.

Type E - G were classified as metamorphic and the classes generally contained lower concentrations and smaller ranges of trace elements. This becomes most distinctively visible if Ti is plotted against Al (Fig. 46).

Type E: Grains categorized as Type E were classified as low-grade metamorphic quartz with a heterogeneous CL signal, which was mainly due to scattered mineral inclusions and traces of slight shearing. All grains feature a dark CL signal. Trace element concentration: Al: average: 30.45 ppm, ranging from 10.42 to 65.76 ppm. Titanium concentrations were very low and lay, except for one grain (3.36 ppm), below the detection limit of 0.92 ppm. Three out of 7 Li values were below the LOD (0.14 ppm). Average of Li: 0.82 ppm, range: < 0.14 to 2.75 ppm. Ge: average: 0.92 ppm, range from 0.36 to 1.49 ppm.

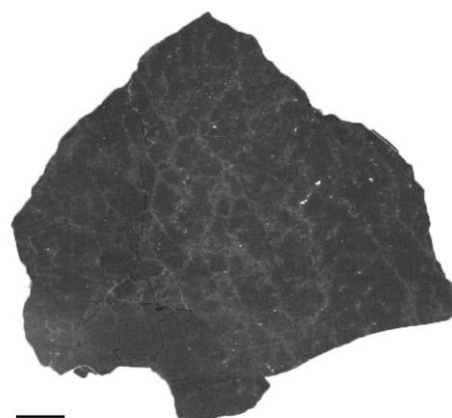


Figure 42: Example of a Type E grain.

Type F: Type F low-metamorphic grains were similar to Type E grains but showed featureless, homogeneous CL signals without inclusions. Well-rounded grains were common, some with “tattered” margins. All grains were monocrystalline. Titanium content for all grains lay below 5.54 ppm. Trace element concentrations in detail: Al: average: 12.79 ppm, ranging from < 5.28 to 22.19 ppm. Ti: average: 4.08 ppm (3 values below LOD), range from < 0.92 to 5.54 ppm. Li: aver-

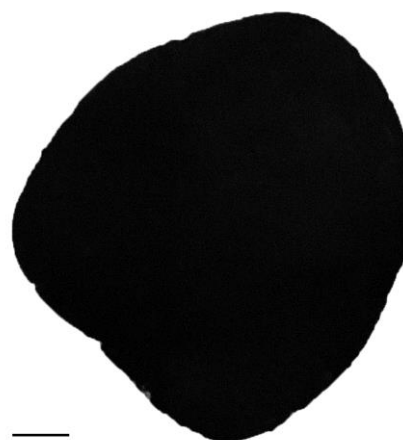


Figure 43: Example of a Type F grain.

age: 1 ppm, range from < 0.14 to 1.88 ppm. Ge: average: 0.92 ppm, ranging from < 0.32 ppm to of 1.36 ppm. Type F grains were present in all samples but occurred frequently only in sample 4 (well 6610/7-1, 940 m).

Type G: Grains categorized as Type G were classified as medium-grade metamorphic, meaning that they had been subject to higher temperature and pressure metamorphism than Type E and F grains. The group was very small. Deformation lamellae occurred on 27 % of the grains. Due to the rare occurrence of Type G grains, the LA-ICP-MS analysis was based on only 4 measurements. Average concentration of Ti: 6.78 ppm, ranging from 5.67 to 8.65 ppm. Al: average: 12.59 ppm, ranging from 6.36 to 20.61 ppm. Values for lithium lay below LOD except for one grain (3.13 ppm). Ge: average: 0.96 ppm, ranging from 0.69 to 1.26 ppm. Trace element concentrations of all the types are plotted in Fig. 45 & 46.

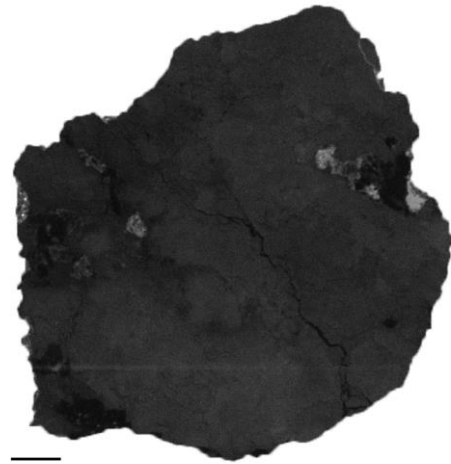


Figure 44: Example of a Type G grain.

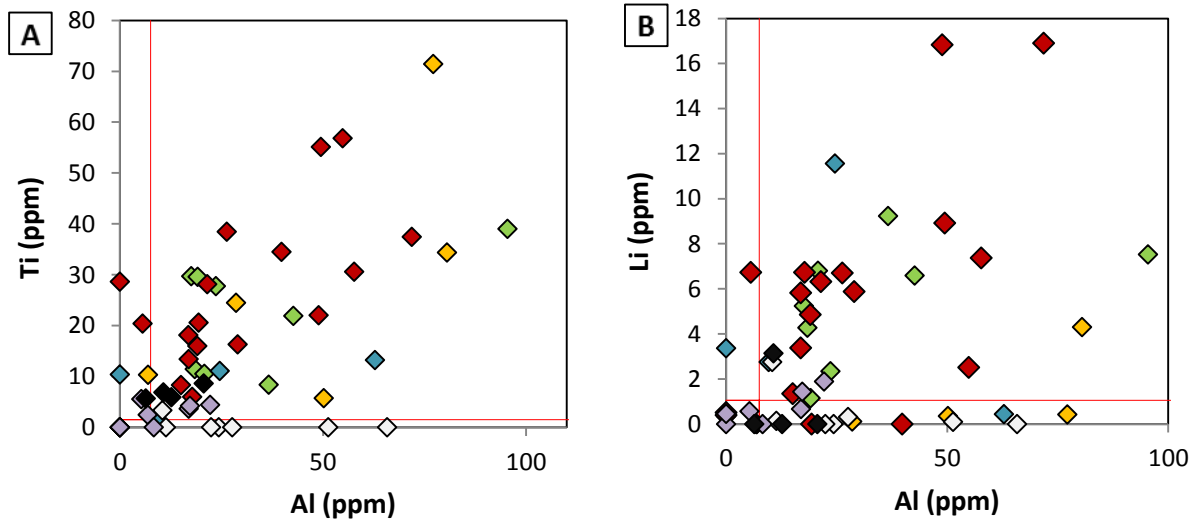
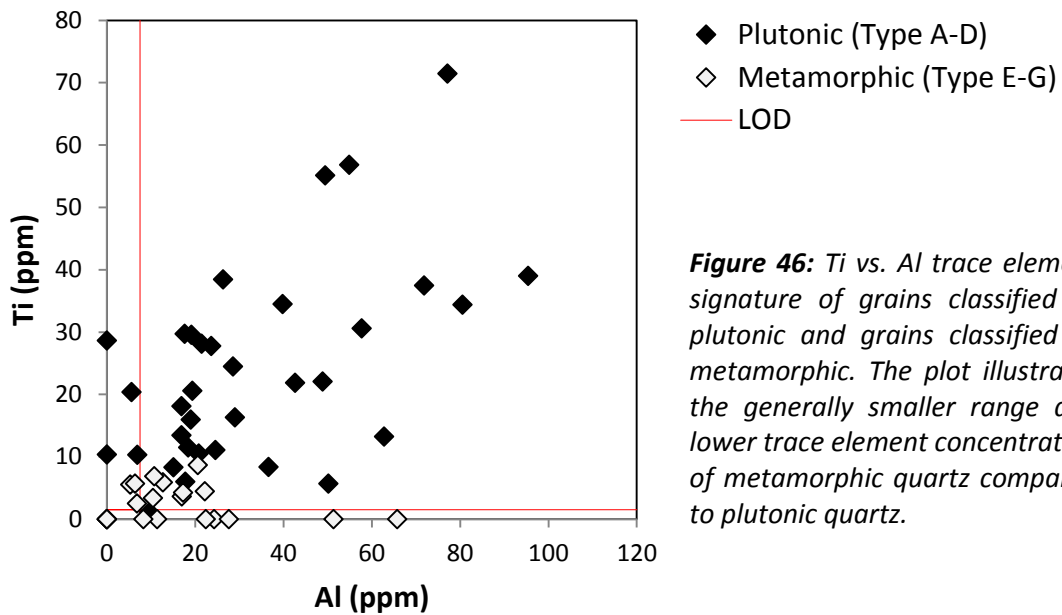


Figure 45: Trace element concentrations plotted with respect to quartz type. Included are all classified grains found in well 6610/3-1 (460 m) and well 6610/7-1 (900 m) (sample 1 and 2). **A:** Ti vs. Al. **B:** Li vs. Al.

- ◆ Type A
- ◆ Type B
- ◆ Type C
- ◆ Type D
- ◇ Type E
- ◇ Type F
- ◆ Type G
- LOD



4.3.4 The offshore samples in detail

Well 6610/7-1 (900 m): Sample 2

Sample 2 featured 70 % plutonic and 30 % metamorphic quartz grains of which the majority was low-grade metamorphic (83 %). Four grains were medium-grade metamorphic. Type E was most dominant in the sample. The second most common group was an uncategorized plutonic quartz with micro-fractures along which primary quartz has altered to darker secondary quartz. This group is presented in Fig. 50. Most of the grains in sample 2 were sub-angular (30 %), only three grains were well rounded. Sample 2 showed very diverse ablation behaviour during LA-ICP-MS analysis: partly big rupture (resulting in craters of up to > 200 μm in diameter) and partly very good ablation behaviour with only minor cracking of the grains. Average trace element concentration: Al 30.20 ppm, Ti 20.43 ppm, Li 3.44 ppm, Ge 0.85 ppm. Highest value for Al was 80.51 ppm. There was a tendency for grains with a bright CL signal to have high Ti content as well. Fig. 51 exemplifies the range and diversity of the trace elements measured in the sample by using the four elements Al, Ti, Li, and Ge. The full numerical outcomes are given in Tab. 4 (appendix). In the following, the groups that have been distinguished are presented and assigned to specific types, if possible.

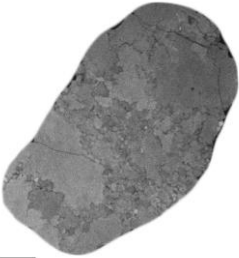
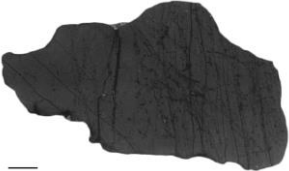
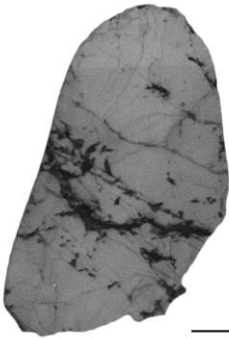
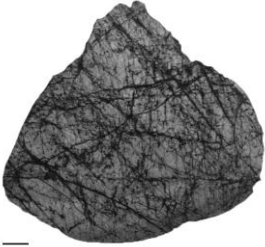
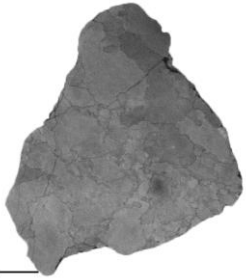
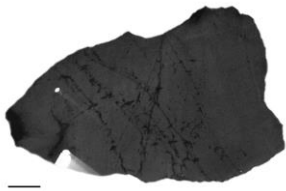
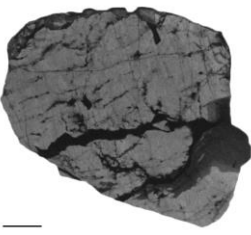
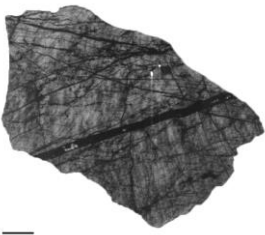
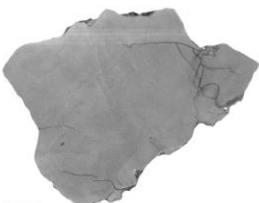
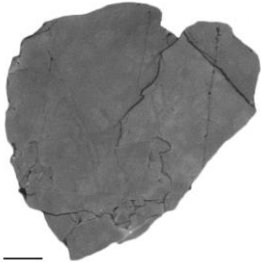
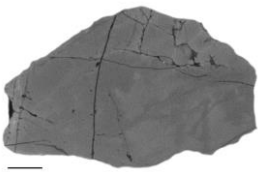

Well 6610/7-1 (900 m depth): Sample 2 – Plutonic quartz grains			
Type A	Type D		
Strongly recrystallized	Dull CL	Intermediate CL	
			
			
Type C			
			

Figure 47: Different types of quartz grains found in sample 2, classified as plutonic. The selection is based on CL similarities. Scale bar lengths correspond to 100 μm .


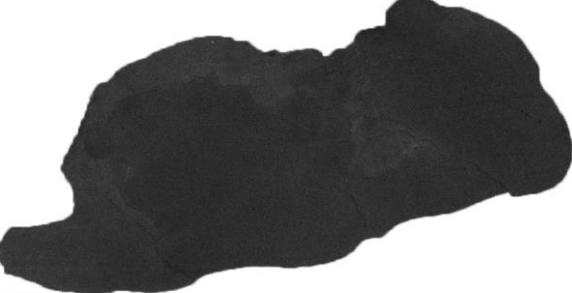
Well 6610/7-1 (900 m depth): Sample 2 – Medium-grade metamorphic quartz grains – Type G	
	

Figure 48: Medium-grade metamorphic quartz grains found sample 2. Scale bar lengths correspond to 100 μm .



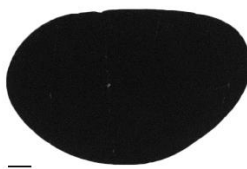



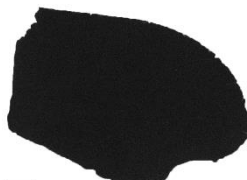



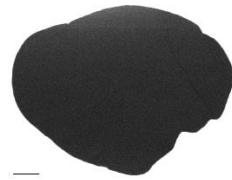



Well 6610/7-1 (900 m depth): Sample 2 – Low-grade metamorphic quartz grains			
Type E		Type F	
(sub) angular, randomly oriented inclusions		(well) rounded	Sub-angular
			
			
	Preferred orientation		
			
			
			

Figure 49: Different types of low-grade metamorphic quartz grains found in sample 2. Scale bar lengths correspond to 100 μm .

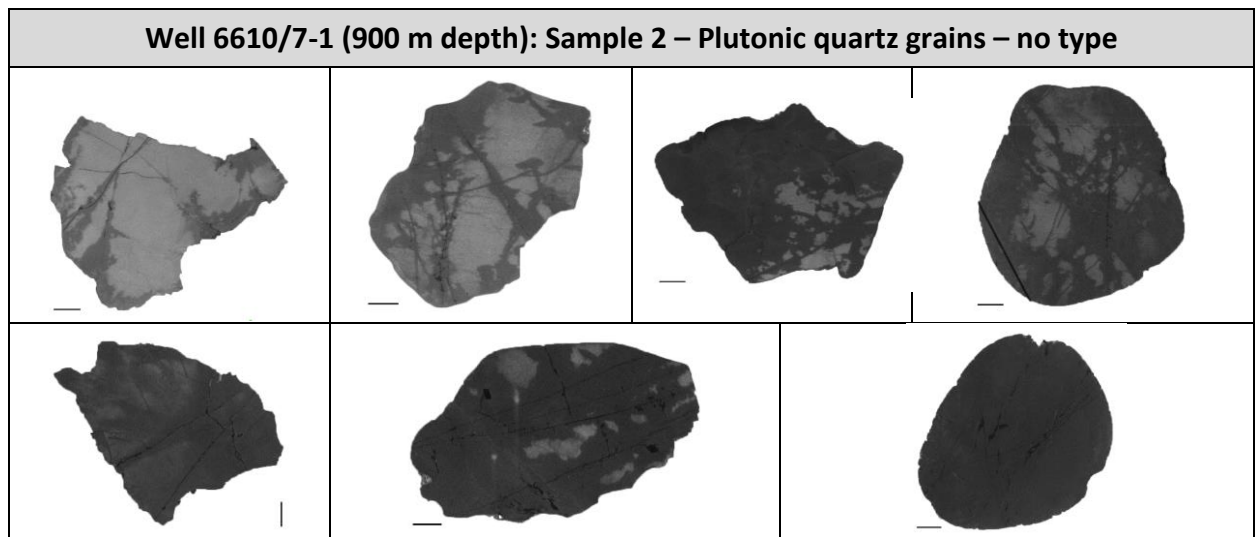


Figure 50: Plutonic quartz grains of sample 2 showing different degrees of alterations along fractures. Affiliation of the grains among one another was tested with trace element data and confirmed by similar ranges. Scale bar lengths correspond to 100 μm .

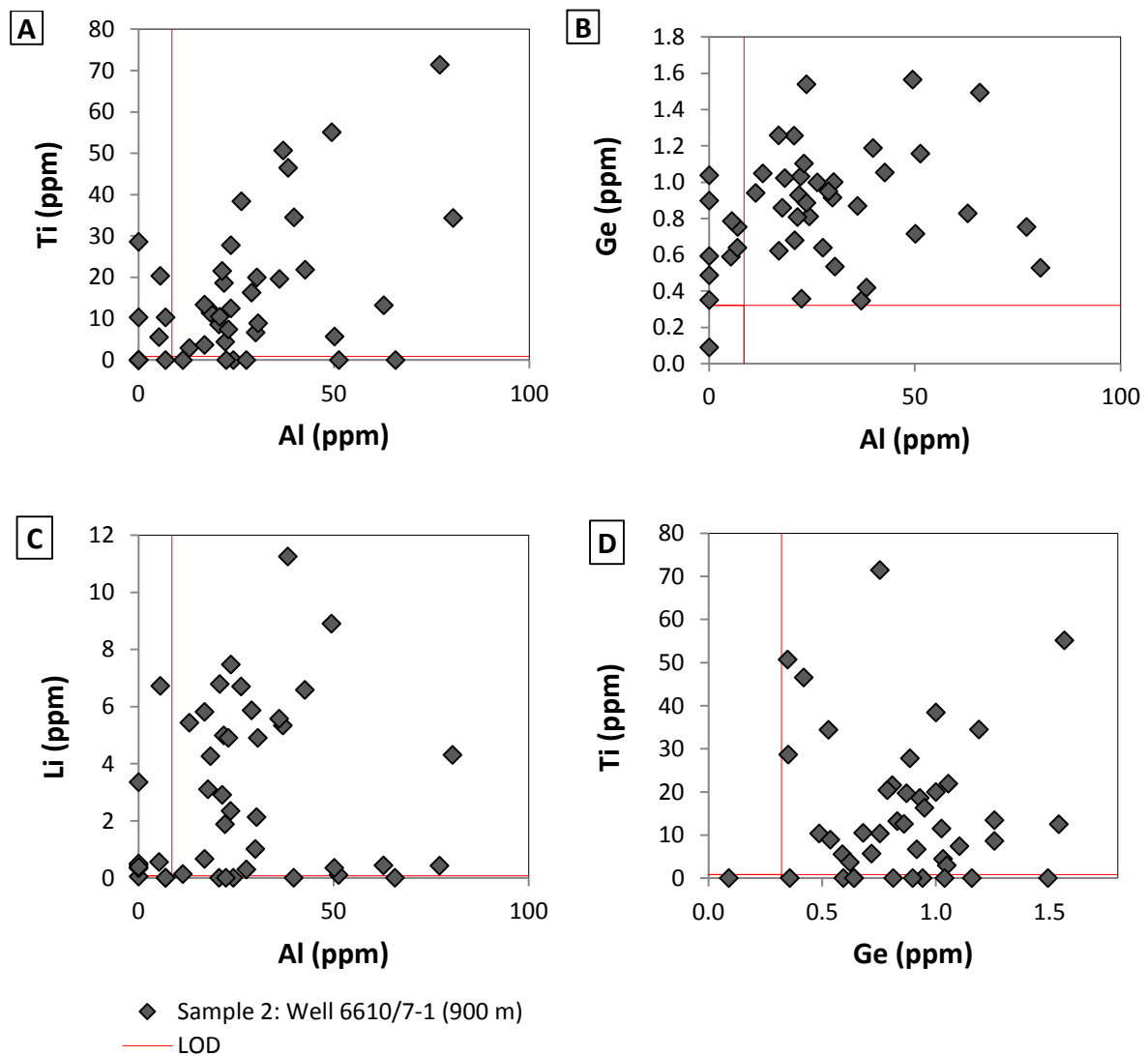


Figure 51: Trace element variation of offshore sample 2 (well 6610/7-1, 900 m), Molo Formation. Analysed with LA-ICP-MS. **A:** Ti vs. Al, **B:** Ge vs. Al, **C:** Li vs. Al, **D:** Ti vs. Ge. LOD: Limit of detection.

Well 6610/7-1 (920 m): Sample 3

Sample 3 contained 84 % plutonic and 16 % metamorphic quartz (low-grade metamorphic: 67 %, medium-grade: 33 %). The most dominant type was Type C, followed by Type A. In general, the sample contained equal proportions of bright and dark CL contrasts. The majority (41 %) of the grains was sub-angular.

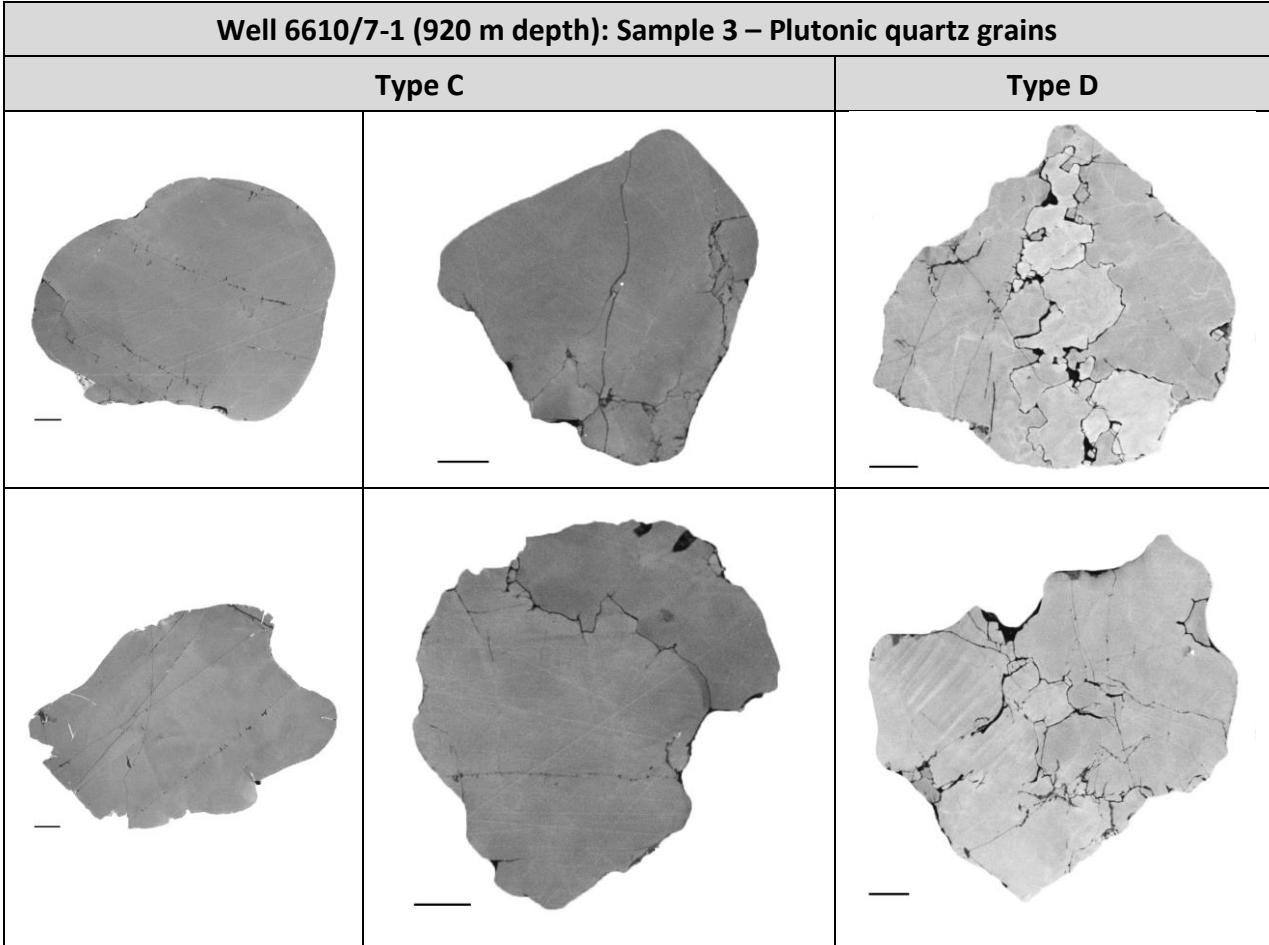


Figure 52: Different types of plutonic quartz grains found sample 3. Scale bar lengths correspond to 100 μm.

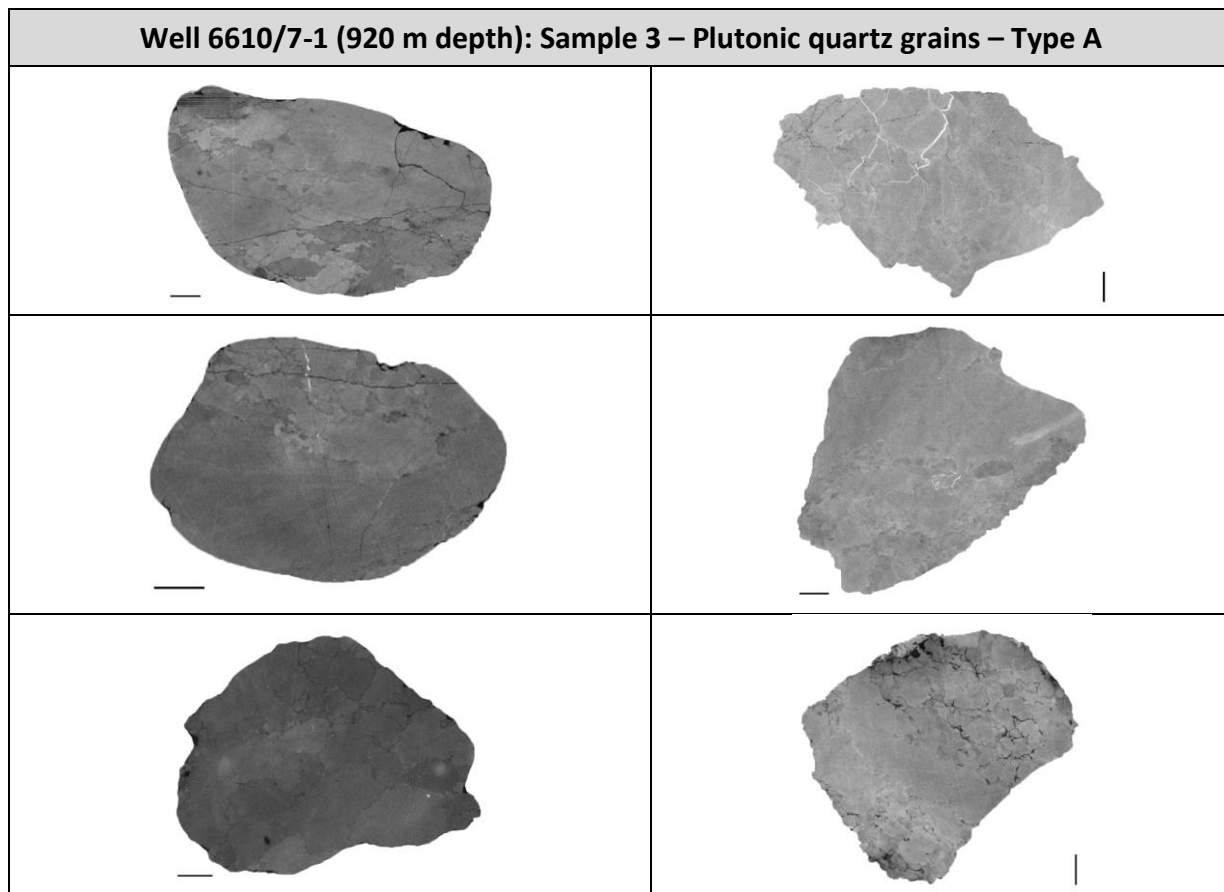


Figure 53: Examples of plutonic grains attributed to Type A, found in sample 3. Scale bar lengths corresponds to 100 μm .

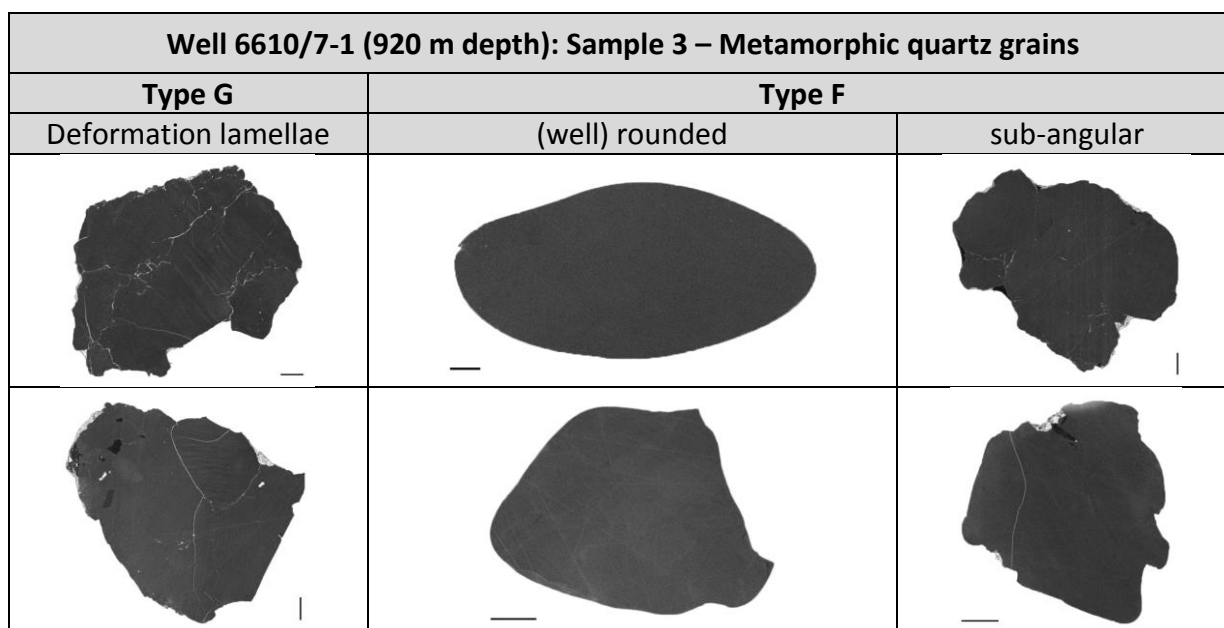


Figure 54: Examples of metamorphic quartz grains of sample 3. Scale bar lengths correspond to 100 μm .

Well 6610/7-1 (940 m): Sample 4

Approximately 65 % of the grains in sample 4 showed dark CL, 35 % showed a bright signal. 76 % of the grains were classified as plutonic, the remaining 24 % as low-grade metamorphic. The most dominant group was plutonic quartz categorized as strongly altered (Type B). The second most common type in the sample was low-grade metamorphic quartz showing homogeneous CL signals (Type F).

The majority of the grains was sub-angular (42 %) or sub-rounded (28 %). The sample showed the highest number of well-rounded grains (6), which corresponded to 12 % of all grains.

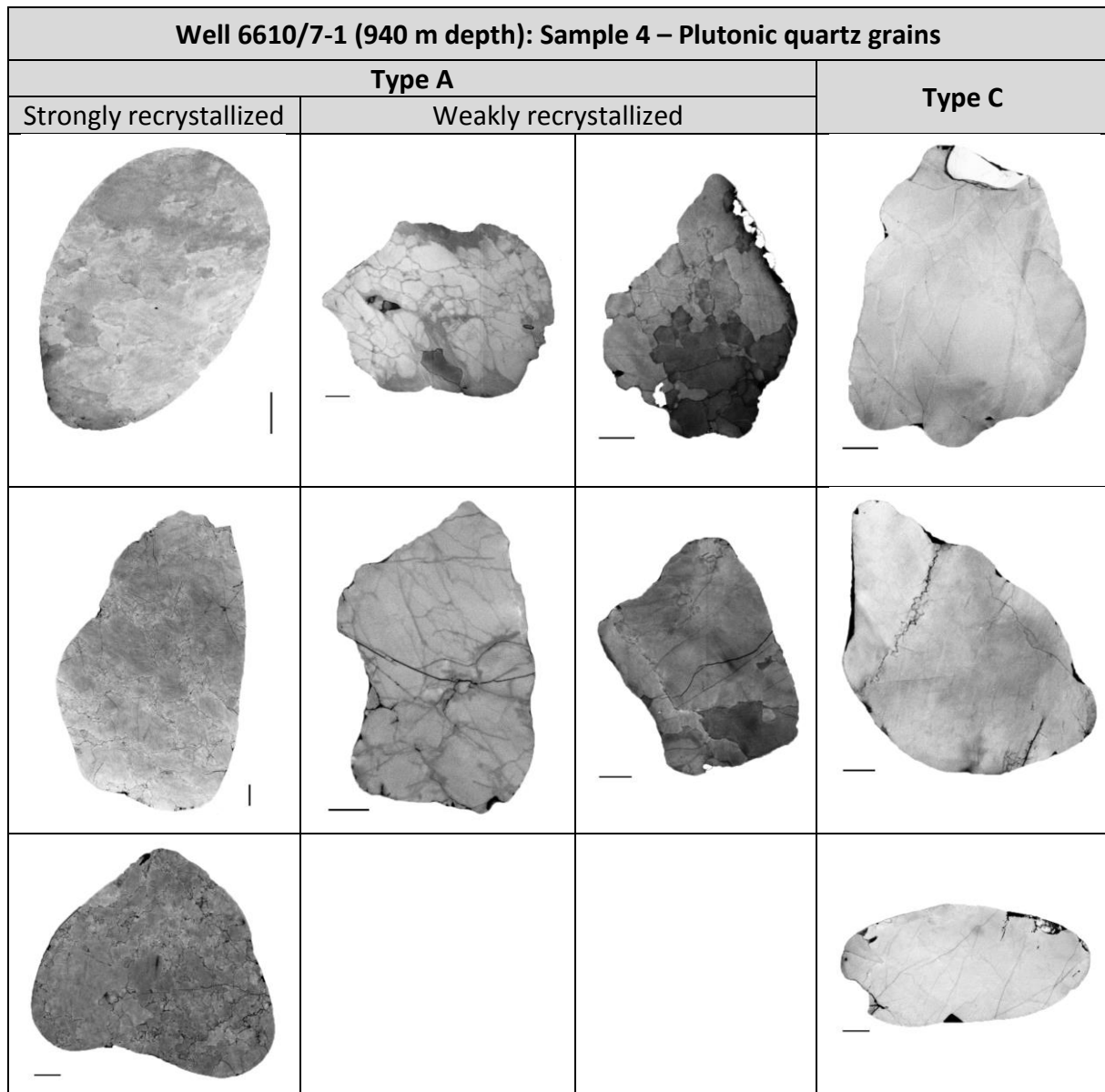


Figure 55: Examples of plutonic quartz grains from sample 4. Scale bar lengths correspond to 100 μm .

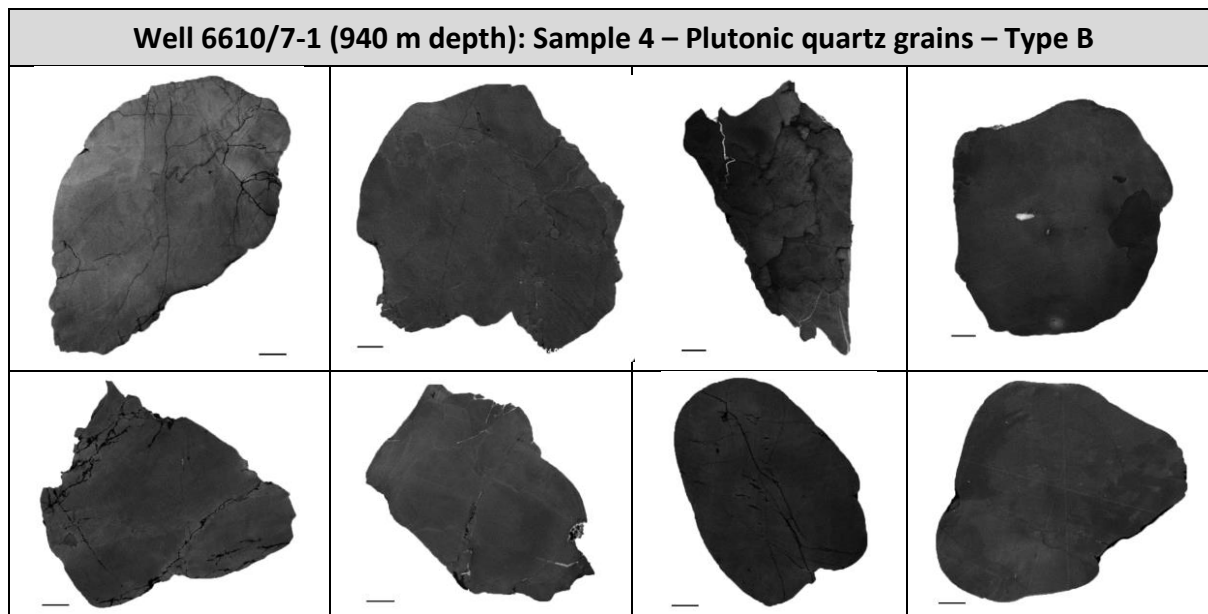


Figure 56: Different types of plutonic quartz grains found sample 4. Scale bar lengths correspond to 100 μm .

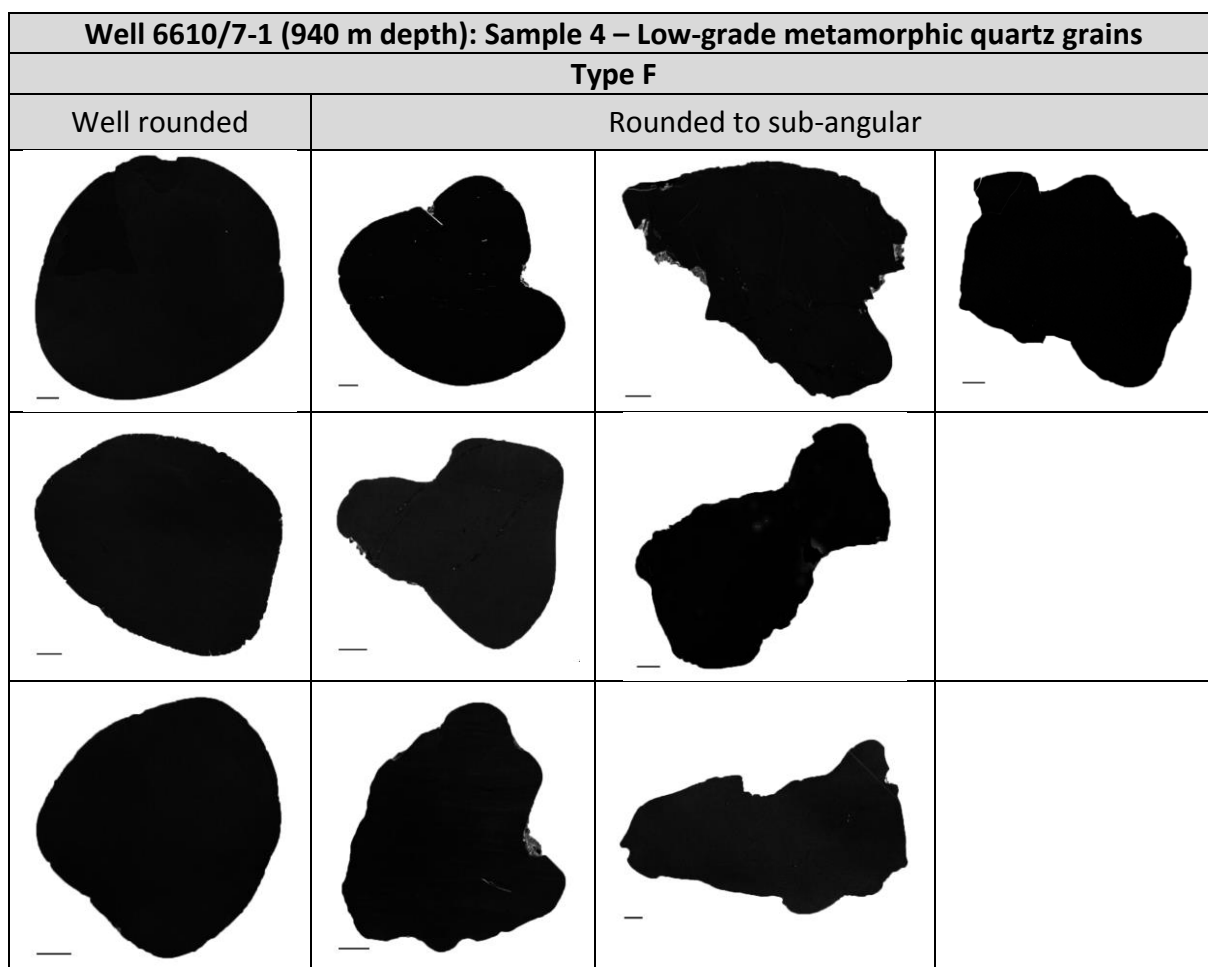


Figure 57: Low-grade metamorphic quartz grains found in sample 4. Scale bar lengths correspond to 100 μm .

Well 6610/3-1 (460 m): Sample 1

In sample 1, 60 % of the grains had darker CL signals, 40 % had bright signals. The most dominant type was Type C: plutonic grains with few or no secondary structures. The second most abundant grains belonged to Type B. The most common lattice-bound trace element in sample 1 was Al with an average concentration of 30.32 ppm. Values for Al ranged from 6.36 to 109.64 ppm. The second most trace element was Ti with an average of 20.44 ppm, ranging from < 0.92 to 56.81 ppm. Li: average 6.50 ppm, ranging from < 0.14 to 17.25 ppm. Ge: average: 0.76 ppm, ranging from 0.37 to 1.36 ppm. Fig. 59 exemplifies range and diversity of the analysed trace elements distributed in the sample.

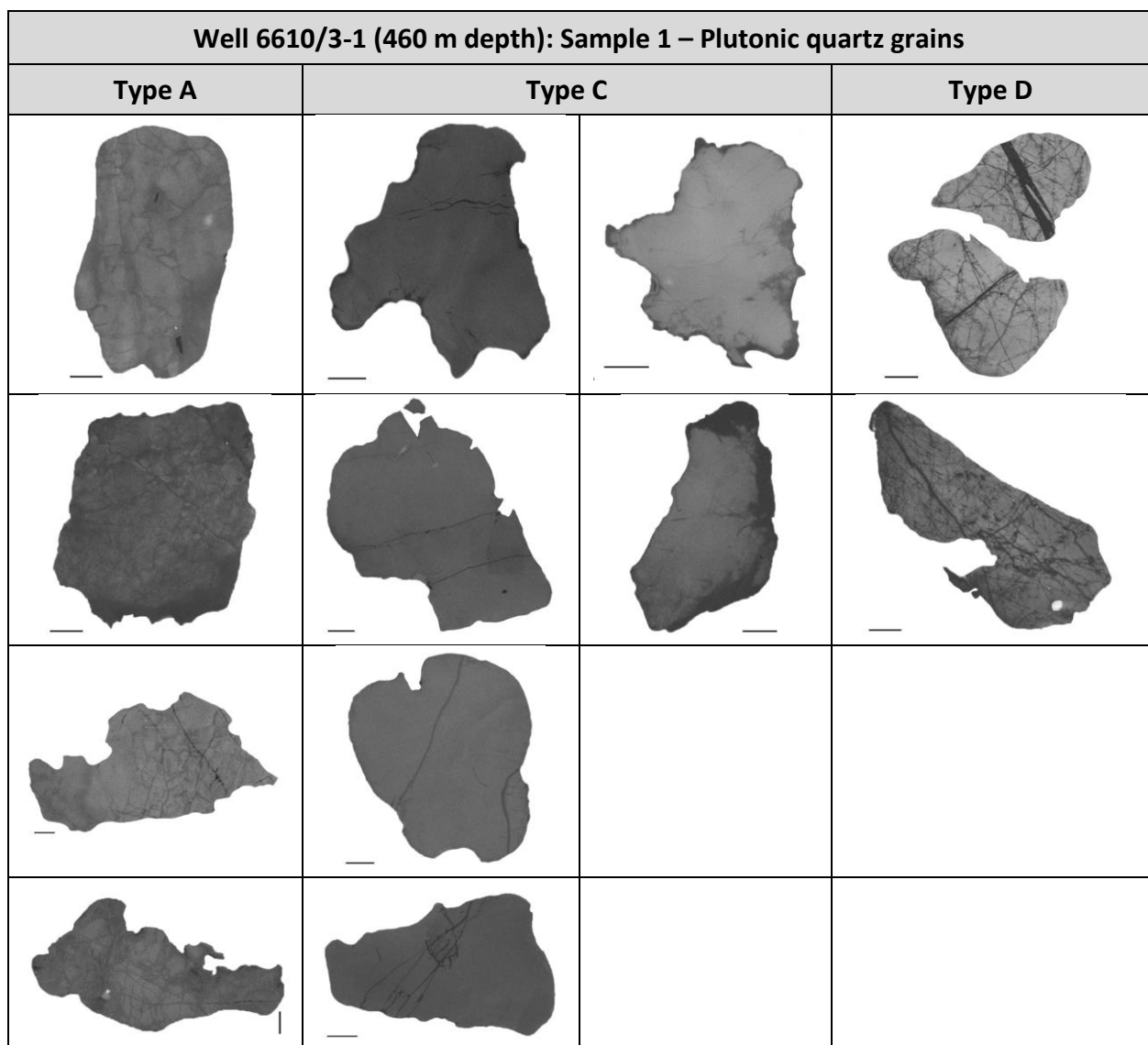


Figure 58: Different plutonic quartz grain types found in sample 1. Scale bar lengths correspond to 100 μm .

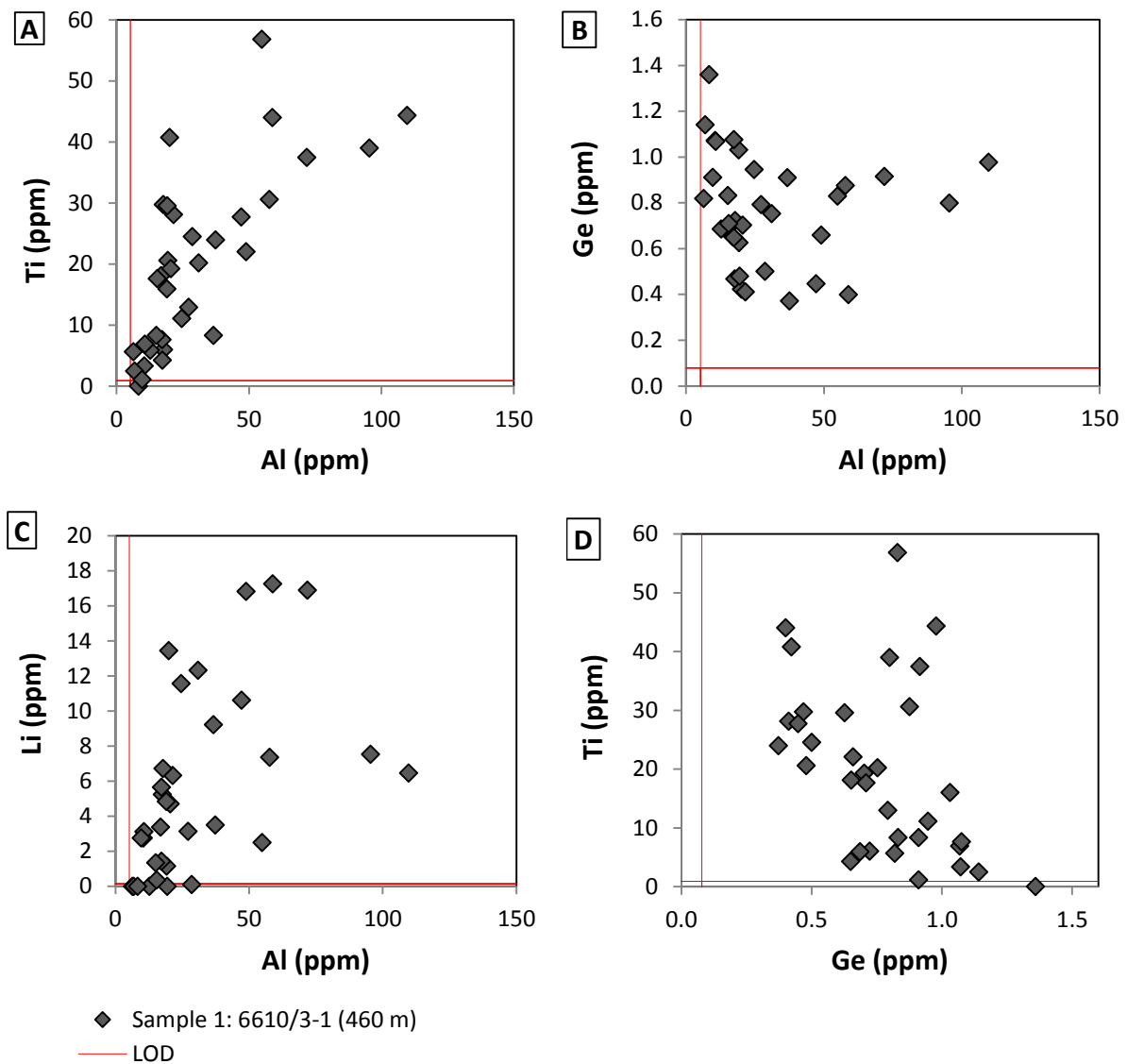


Figure 59: Plotted trace element concentrations of sample 1 (6610/3-1, 460 m depth). **A:** Ti vs. Al, **B:** Ge vs. Al, **C:** Li vs. Al, **D:** Ti vs. Ge.

Well 6610/3-1 (480 m): Sample 6

No clearly polycrystalline grains were present in sample 6. Slightly more very dark grains than bright grains were identified by CL. 87 % of the grains were classified as plutonic, 13 % as low-grade metamorphic (all Type F). Most grains in sample 6 belonged to Type C.

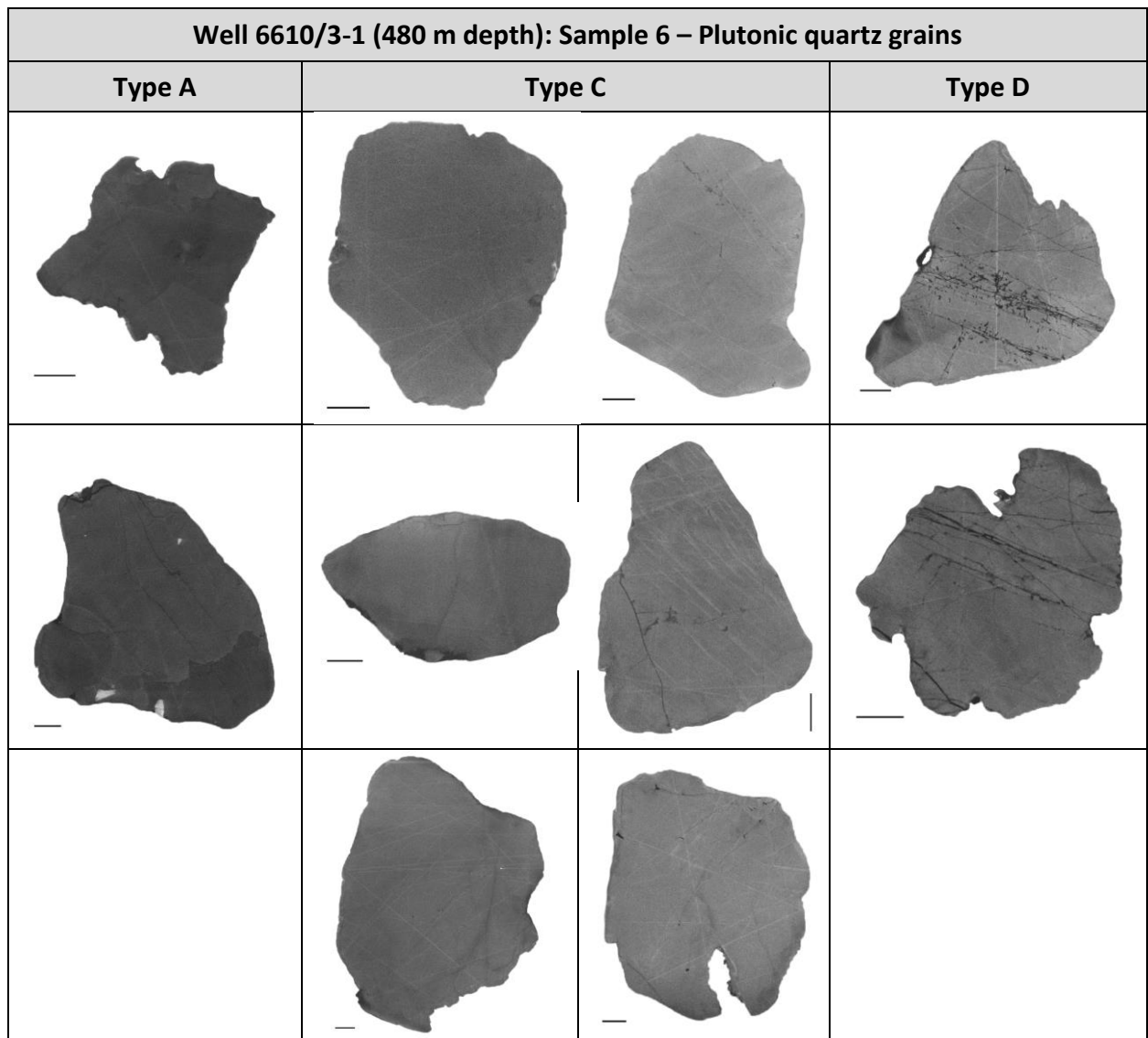


Figure 60: Different plutonic quartz grain types found in sample 6. Scale bar lengths correspond to 100 μm .

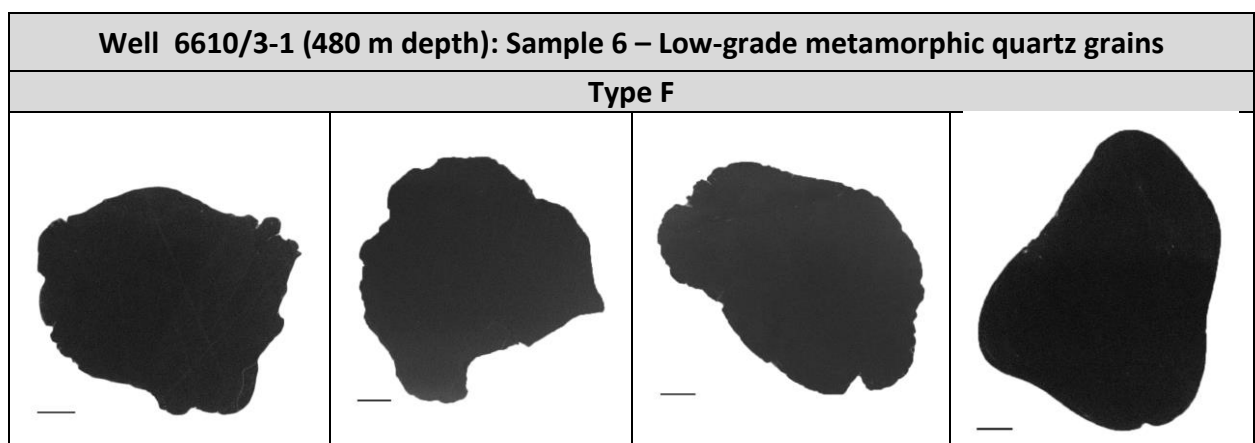


Figure 61: Different metamorphic quartz grain types found in sample 6. Scale bar lengths correspond to 100 μm .

Well 6510/2-1 (441 m): Sample 3a

Sample 3a contained no grains with homogeneous, featureless CL properties. In general the sample contained slightly more grains showing a distinctively bright CL than a dark signal. The vast majority of the grains was classified as plutonic (94 %), only 3 grains were low-grade metamorphic (two grains Type E, one grain Type F). The sample comprised a distinct group of grains with patchy CL signal and varying lightness ranging from light grey to dark grey. The grains within this group were arranged according to their degree of deformation (see Fig. 63). The the sample contains no rounded or well-rounded grains. The majority was sub-angular (62 %), the remaining were sub-rounded (27 %) or angular (11 %).

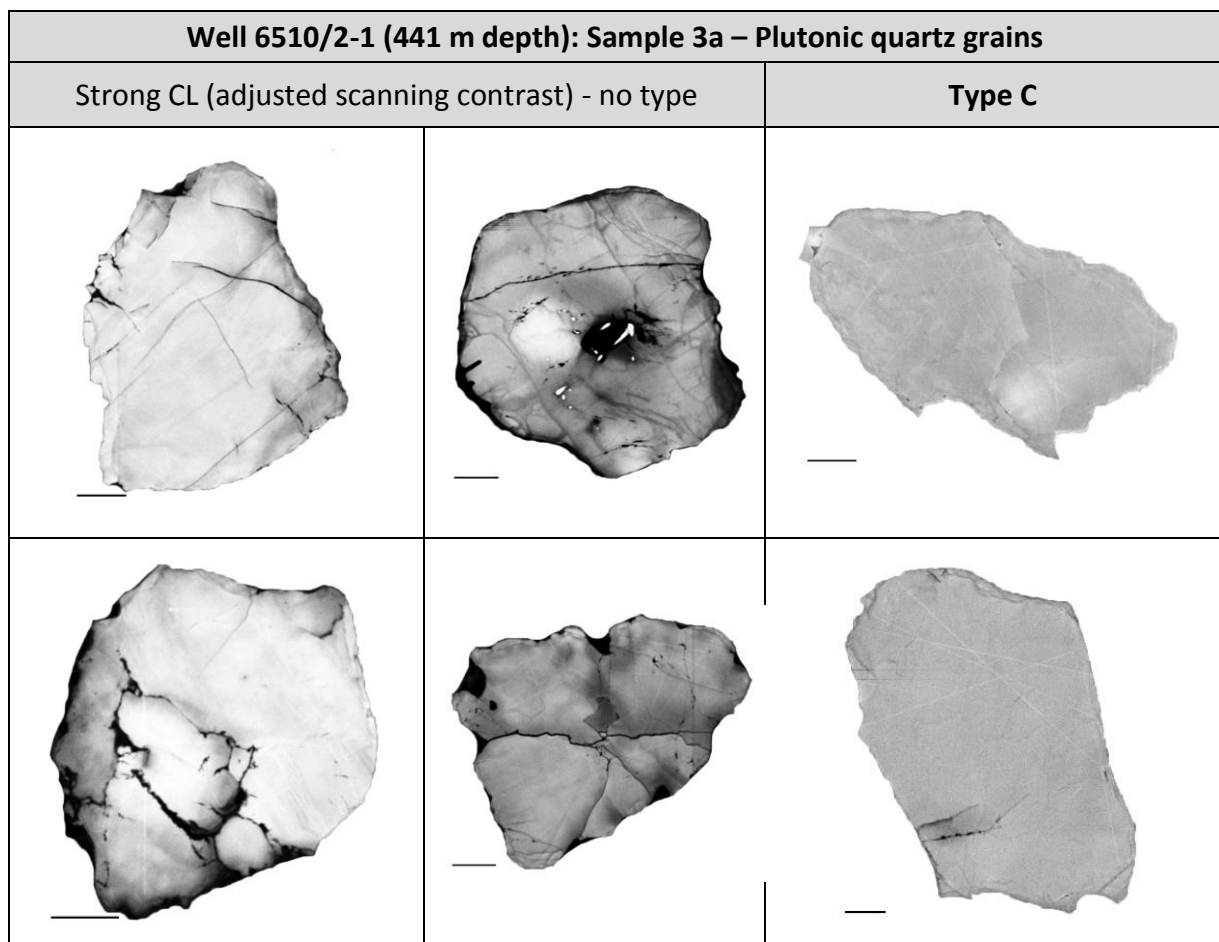


Figure 62: Different plutonic quartz grain types found in sample 3a. Scale bar lengths correspond to 100 μm .

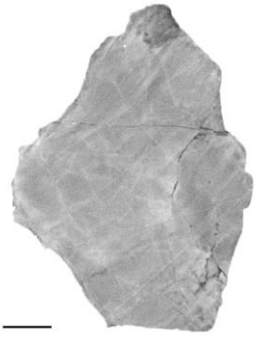
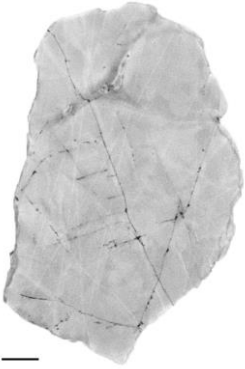

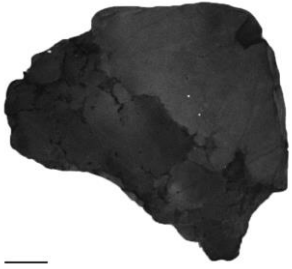
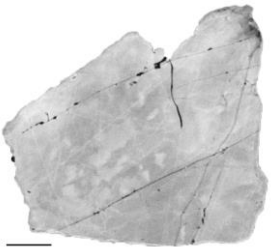
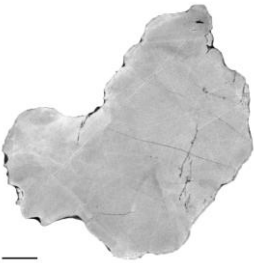
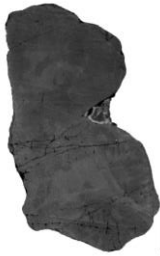

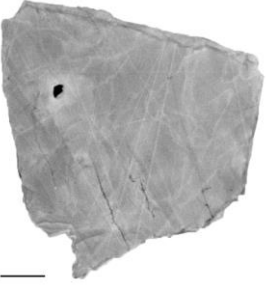
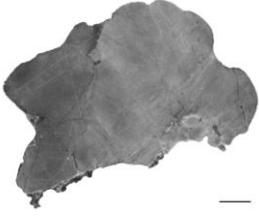
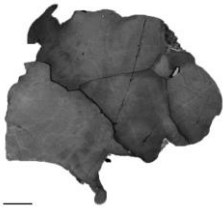
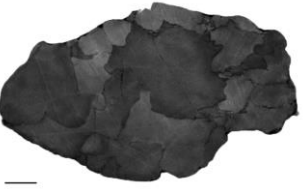

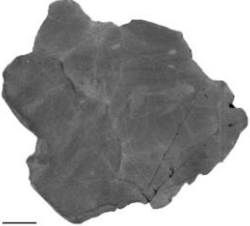
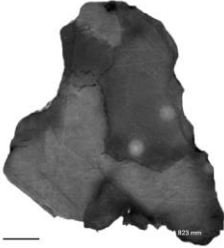
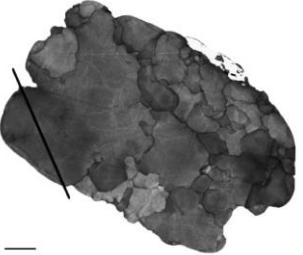
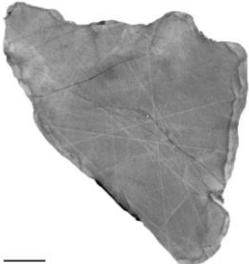
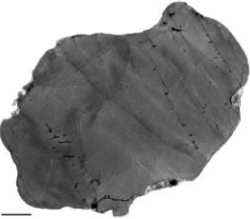
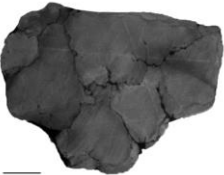
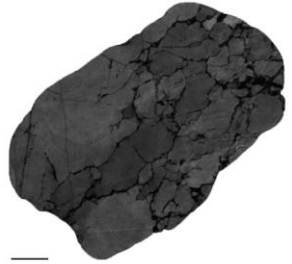
Well 6510/2-1 (411 m depth): Sample 3a – Plutonic quartz grains			
Type D		Type A	
		Weakly recrystallized	Strongly recrystallized
			
			
			
			
			

Figure 63: Different plutonic quartz grain types found in sample 3a. Scale bar lengths correspond to 100 μm .

4.4 Onshore/basement samples

4.4.1 Cathodoluminescence properties of the onshore/basement samples

The investigated onshore (basement) samples represent single classes of quartz each, as all grains of the particular samples were taken from single, definite locations with preserved crystalline fabric. The in situ weathered loose saprolitic sand (of samples no. 89415 and 89421) is directly derived from the basement and was sampled before sediment transport commenced. All these loose basement-derived grains were very angular to sub-angular. The sample locations are indicated in Fig. 13.

4.4.2 The onshore/basement samples in detail

Hadseløya: Sample 5

Sample 5 (Brennvinshaugen, Hadseløya, 145 m a.s.l.) showed very heterogeneous SEM signals in both CL and BSE images. BSE contrasts indicated at least four different mineral phases. Frequent mineral inclusions were visible and the quartz showed intergrowth with other mineral phases as for example K-feldspar. Recrystallization with sub-grain formation was observed to some extent.

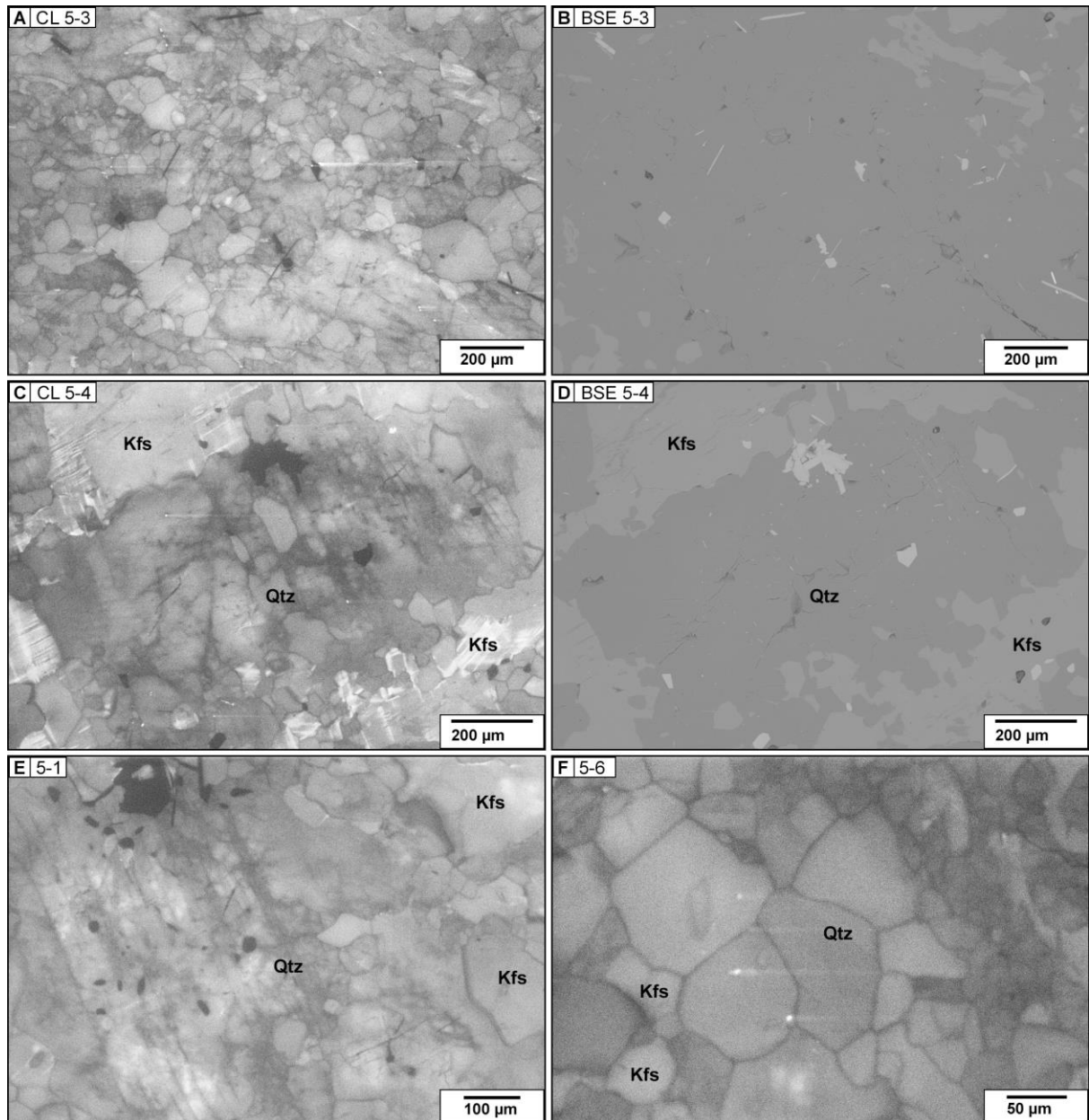


Figure 64: SEM-CL and corresponding BSE micrographs of sample 5, a thin section (250 µm) taken from a mangerite corestone found in a saprolite weathering profile on Hadseløya, Vesterålen. **A - B** and **C - D:** CL - BSE comparisons of the same areas on the thin section. **E - F:** Representative CL micrographs of the sample. Most important mineral phases are indicated as follows: Kfs = K-feldspar, Qtz = quartz.

Hadseløya: Sample 89415

Scanning of sample 89415 (Brennvinshaugen) revealed quartz grains with mineral inclusions such as K-feldspar and mica (Fig. 65). Bigger grains broke during specimen preparation. Some thin micro-fractures occurred. CL signals are predominantly dull.

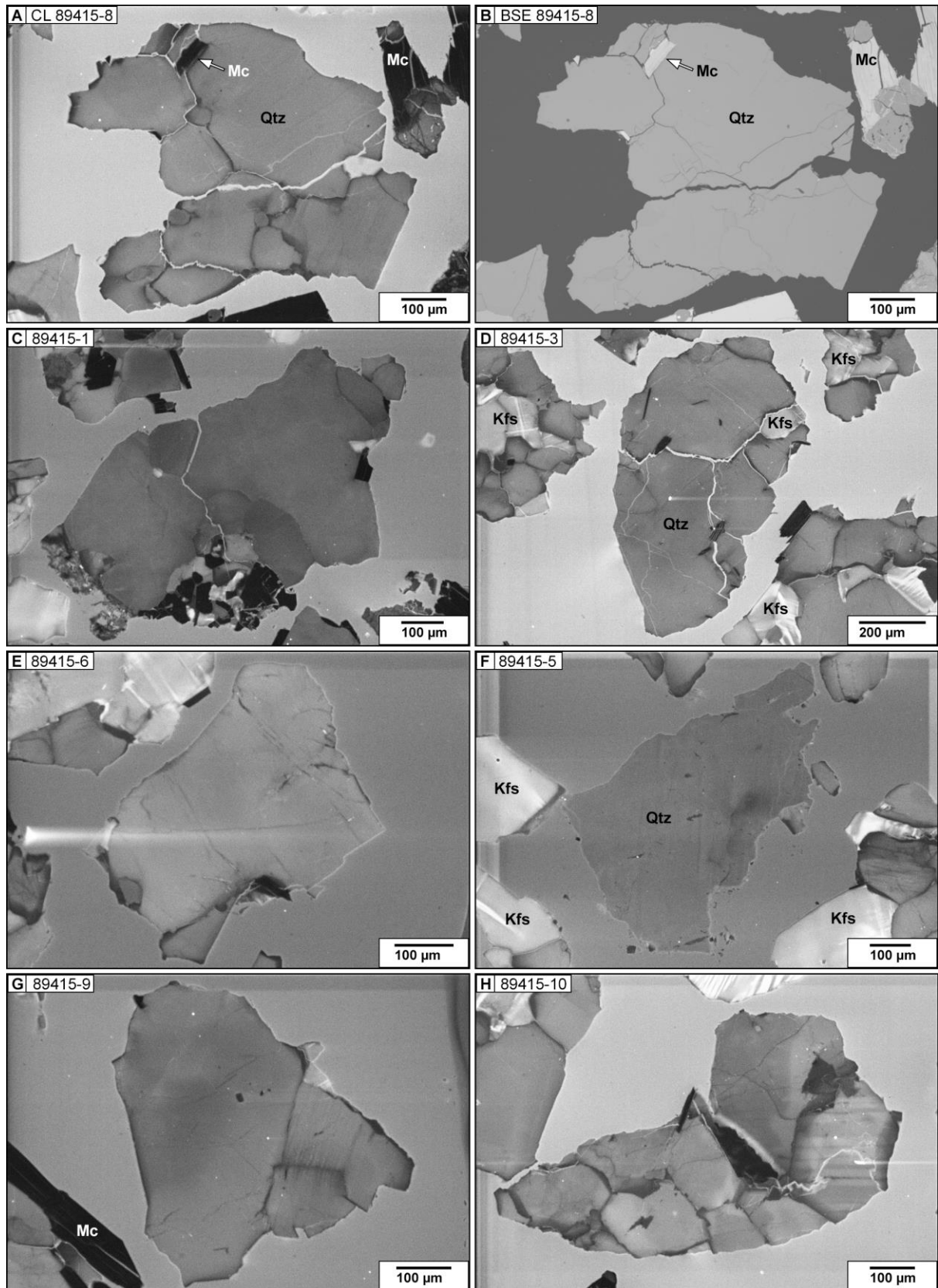
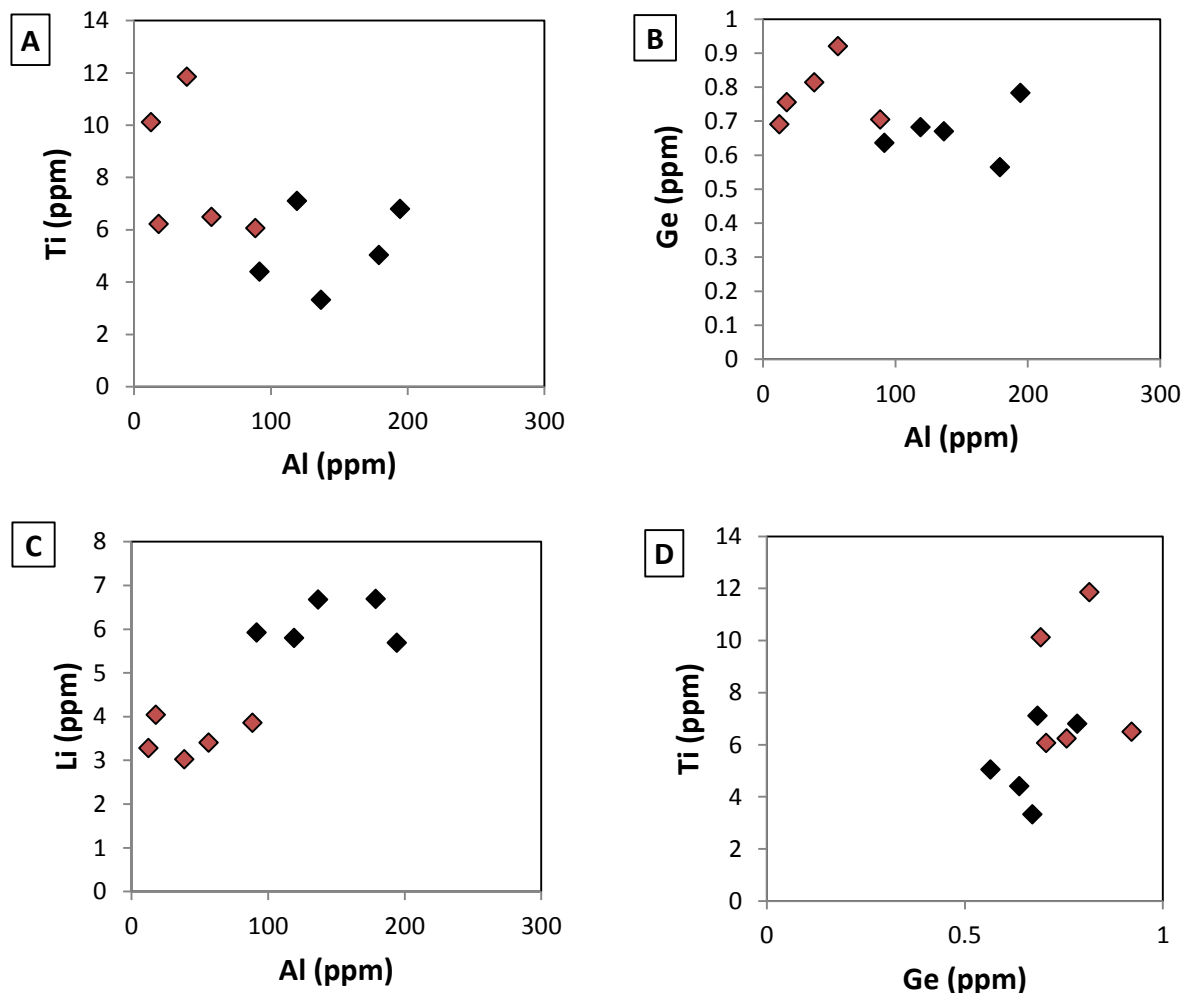


Figure 65: SEM-CL and BSE micrographs of sample 89415. The sampled sand (grain size fraction > 0.5 mm) was weathered in situ on saprolitic mangerite bedrock. The fissility of mica is visible in G. **A - B:** CL - BSE comparison indicating mica inclusions. **C - H:** Representative CL micrographs. Mc = mica, Qtz = quartz, Kfs = K-feldspar.

LA-ICP-MS analysis revealed high trace element concentrations of Al (average: 144.10 ppm, ranging from 91.66 to 194.35 ppm). The second most common trace element was Ca with an average of 6.31 ppm, ranging from 2.50 to 8.92 ppm. This was followed by Li, with an average value of 6.16 ppm, ranging from 5.69 to 6.69 ppm and K: average: 6.08 ppm, ranging from 1.44 to 9.74 ppm. Further values: Ti: average: 5.34 ppm, range from 3.33 to 7.11 ppm. Ge: average: 0.67 ppm, from 0.56 to 0.78 ppm.

The grains were very angular to sub-angular. White dots appeared throughout the sample that gave the impression of fluid/mineral inclusions (see Fig. 65, e.g. A and G). They also appeared in the epoxy resin (see Fig. 31 E). Figure 66 illustrates the different ranges of the trace element concentrations in sample 89415 in comparison with sample 89421 (Hamarøy, see below). Only minor overlapping occurs in plots A, B and C, values show more overlap in plot D. (Fig. 66).



- ◆ Hadseløya (sample 89415)
- ◆ Hamarøy (sample 89421)

Figure 66: Plotted trace element concentrations of sample 89415 (black) and sample 89421 (red) (see below). The sample sites were 58 km apart from each other. **A:** Ti vs. Al, **B:** Ge vs. Al, **C:** Li vs. Al, **D:** Ti vs. Ge.

Hadseløya: Sample 89418

The grain margins of the quartz crystals in sample 89418 had distinct dark CL contrast alterations that were unique for the sample (Fig. 67). Mica mineral inclusions were common within both K-feldspar and quartz grains. Micro-fractures were uncommon. Most of the cracks visible in the micrographs ran alongside grain-boundaries and were filled with epoxy resin.

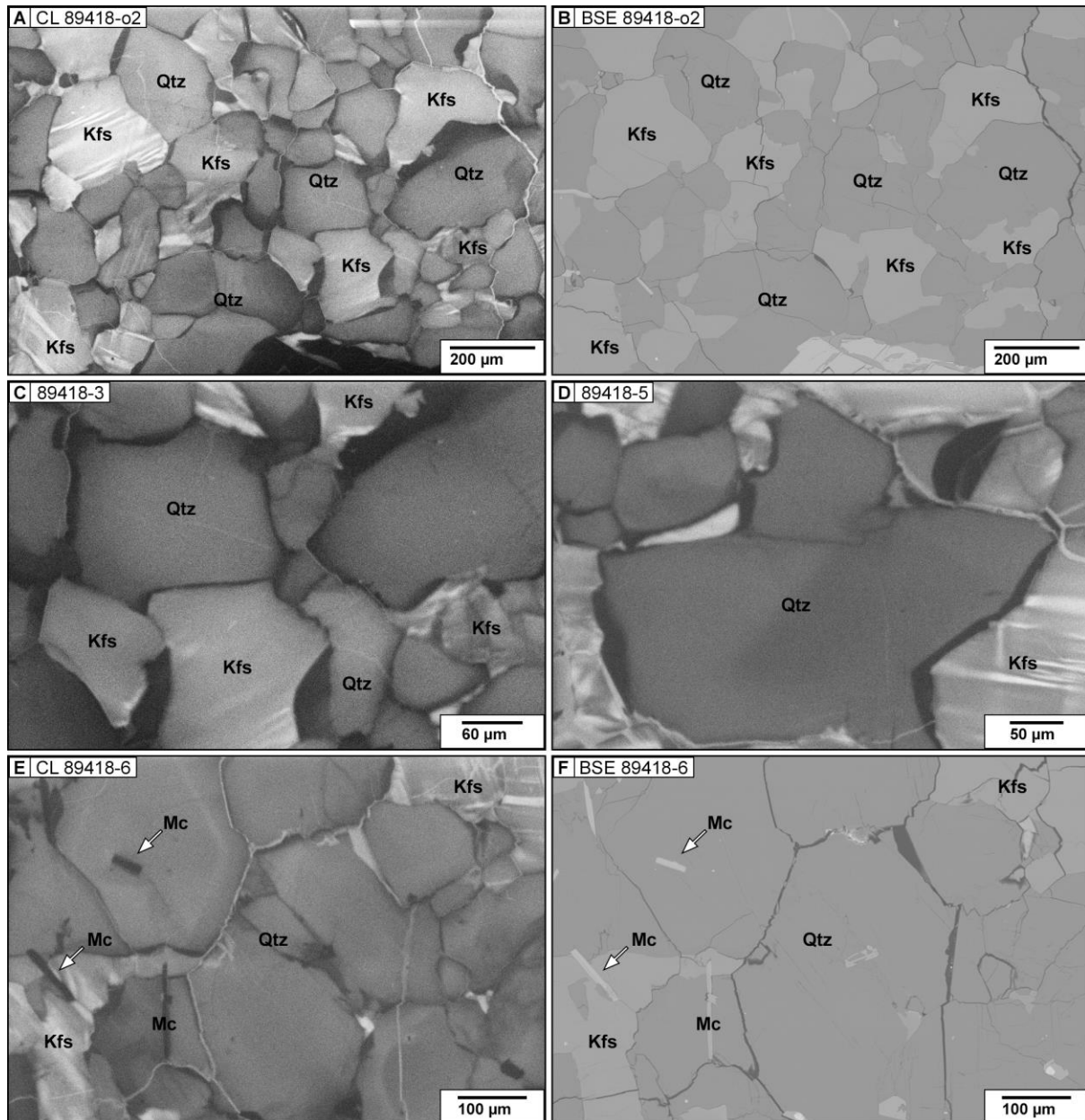


Figure 67: CL and BSE micrographs of a mangerite corestone representative for sample 89418. Sample site: Brennvinsaugen on Hadseløya, south-west Vesterålen, 145 m a.s.l. **A - B:** CL - BSE comparison showing frequent feldspar minerals between the quartz crystals. **C - D:** High-resolution CL micrographs showing quartz grains with black margins. **E - F:** CL - BSE comparison showing scattered mica minerals. Qtz = quartz, Kfs = K-feldspar, Mc = mica.

Hamarøy: Sample 89421

Sample 89421 from Hamarøy, south of Vestfjorden/Ofofjorden, contained grains with heterogeneous to very heterogeneous CL contrasts. Frequent mineral inclusions were visualized, including small needle-shaped mica minerals (see Fig. 68, A and B). Especially in parts with more bright CL contrasts, a feature emerged in the quartz phase that resembled hatching (Fig. 68, A and F). The selected grains were predominantly very angular.

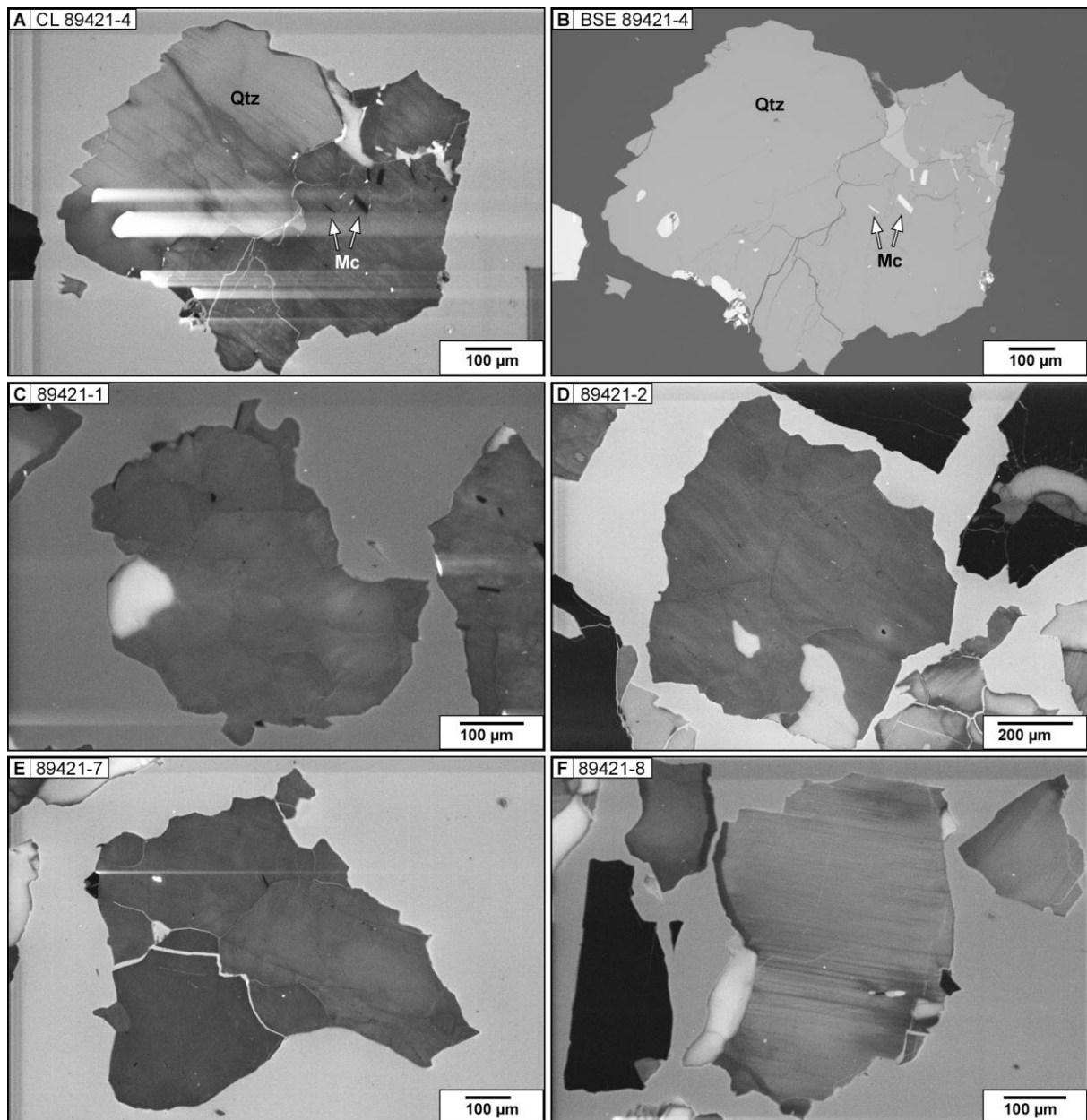


Figure 68: Representative quartz grains found in Sample 89421 taken from Hamarøy, Stotland, 77 m a.s.l. **A - B:** CL - BSE comparison of the same grain, showing three different mineral phases. **C - E:** CL micrographs with dull CL. **F:** Intermediate CL with "hatching". Qtz = quartz, Mc = mica.

Tysfjord, Hundholmen: Sample 47802

The Tysfjord gneiss granite sampled at Hundholmen was the only bedrock sample investigated that was not subject to strong weathering. Two mineral phases were identified: Quartz and feldspar. CL contrasts were homogeneous with only few secondary structures and predominantly dull.

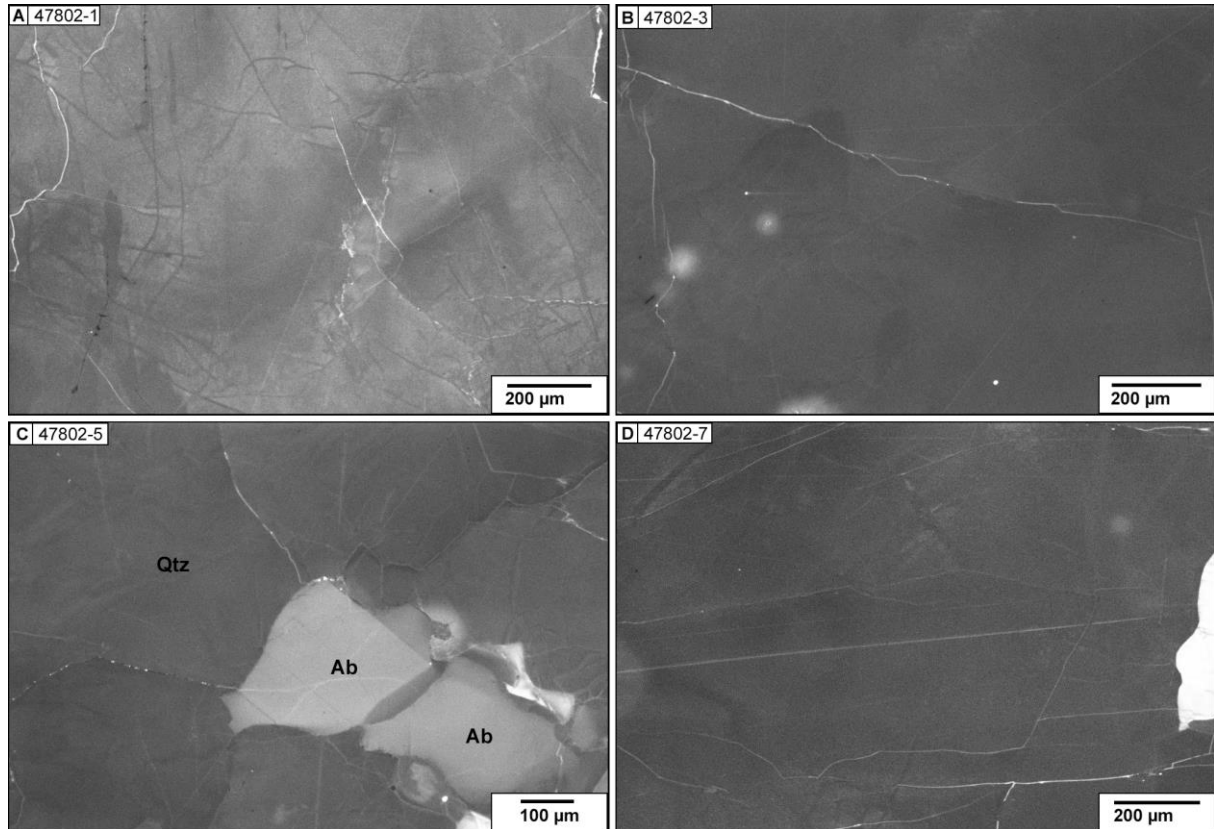


Figure 69: Representative thin section details of sample 47802, Tysfjord granite, Hundholmen. **A:** CL micrograph showing dark strokes. **B - D:** Micrographs showing predominantly dull, homogeneous CL of the quartz. Feldspar was identified in C. Qtz = quartz, Ab = albite.

Trace element concentration of sample 47802 was measured in two analyses and is given in Tab. 6 (Appendix).

Well 6408/12-U-01 (32.42 m): Sample 10

Sample 10 was a strongly kaolinized granitic rock with coarse grained crystals. It contained intensively cracked/fractured and healed quartz grains within a predominantly dark matrix. Micro-fractures of different extent and orientation were visualized. Some parts were characterized by very frequent, densely occurring fractures of preferred orientation (Fig. 70, F).

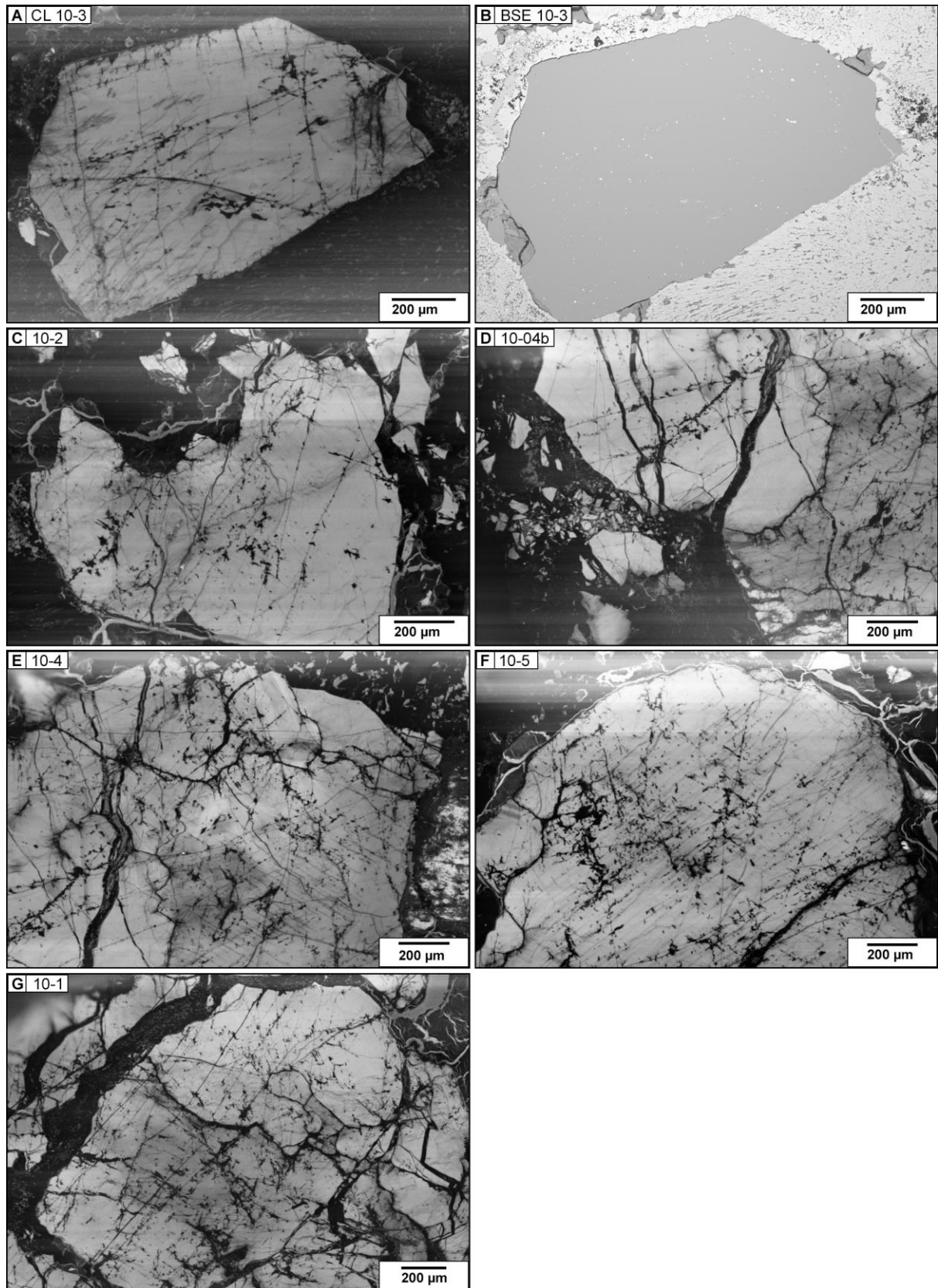


Figure 70: SEM-CL and BSE micrographs of deformed quartz crystals in sample 10, (well 6408/12-U-01, 32.42 m depth). **A - B:** CL-BSE comparison indicating differences in mineral phases. **C - G:** CL micrographs showing randomly distributed healed cracks and micro-cracks (e.g. D and E) and micro-fractures of preferred orientation (F).

Well 6814/4-U-1 (174.48 m): Sample 25

Basement sample 25 consisted of a medium-grained, kaolinized, K-feldspar-rich granite that contained deformed quartz grains embedded in a matrix of darker mineral phases other than quartz (as revealed by CL-BSE comparison, Fig. 71, A-B). Fractures were only partly healed with secondary quartz. The grains were characterized by very frequent micro-fractures and sub-grain formation.

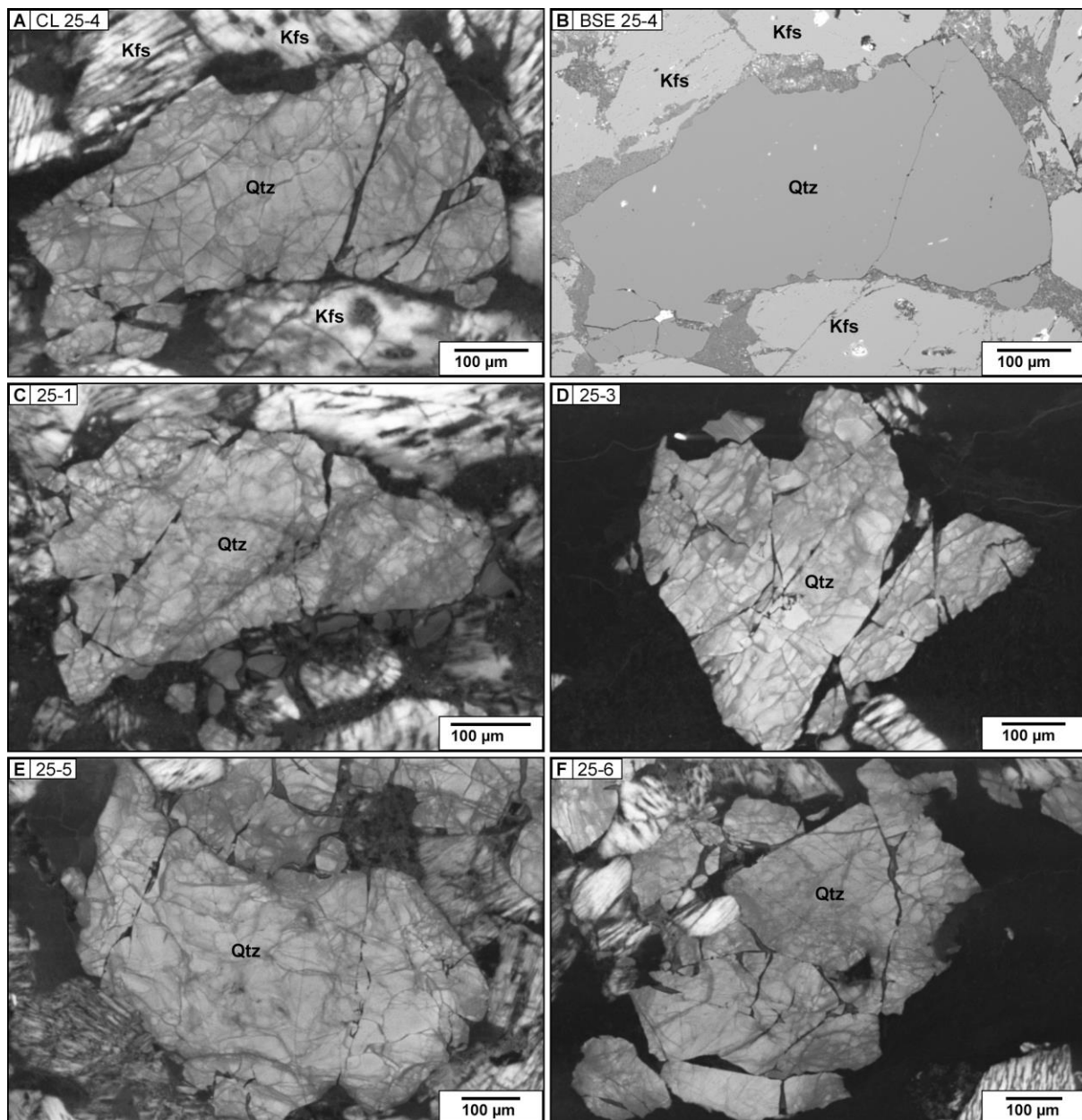
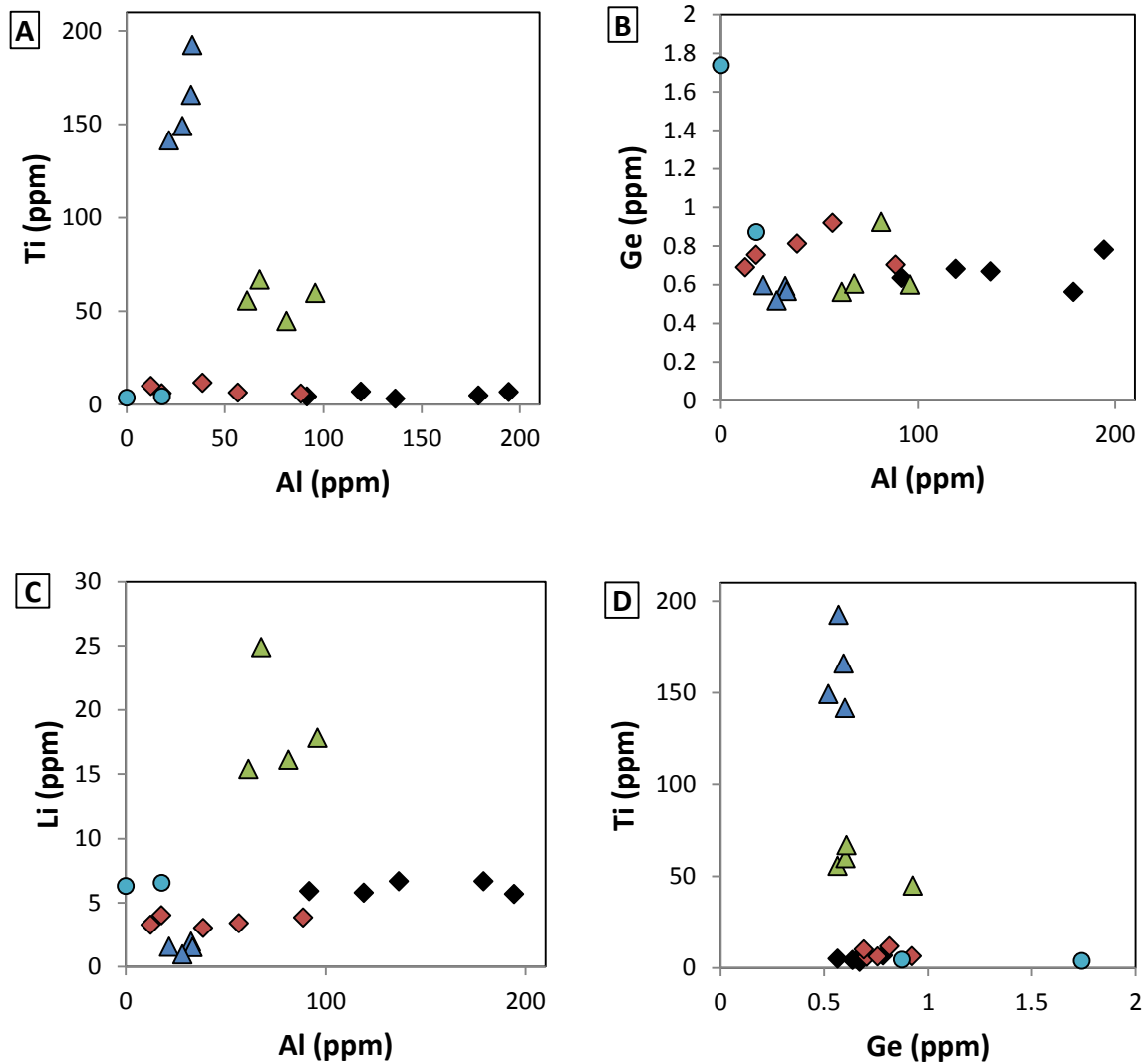


Figure 71: SEM-CL micrographs of deformed quartz crystals in sample 25 (well 6814/4-U-1, 174.48 m depth). **A - B:** CL - BSE comparison indicating differences in mineral phases. **C - F:** CL micrographs representative for the sample, showing cracking and displacement of parts of the grains. Kfs= K-feldspar, Qtz = quartz.

In the following, available trace element concentrations of the onshore/basement samples illustrated above are plotted (Fig. 72).



- ◆ Hadseløya (sample 89415)
- ◆ Hamarøy (sample 89421)
- ▲ 6408/12-U-01, 32.42 m (sample 10)
- ▲ 6814/4-U-1, 174.48 m (sample 25)
- Tysfjord, Hundholmen (sample 47802)

Figure 72: Plotted trace element concentrations of all 5 onshore/basement samples that were analysed with LA-ICP-MS. **A:** Ti vs. Al, **B:** Ge vs. Al, **C:** Li vs. Al, **D:** Ti vs. Ge.

In the following chapter (*Discussion*), the offshore sediment samples and onshore/basement samples are juxtaposed and possible connections discussed. The distances between all sample sites are compiled in Tab. 3 below. Largest distance and hence possible sediment transport way between offshore depositional area and the potential sediment source area is approximately 360 km (the outcrop on Hadseløya and the southernmost offshore drilling site 6510/2-1).

Table 3: Compiled distances between all sample sites.

Distance between sample sites in km	Brennvinsaugen	Stotland	Hundholmen	6814/4-U-1	6408/12-U-01	6610/3-1	6610/7-1	6510/2-1
Brennvinsaugen		58	70	30	560	245	320	360
Stotland	58		35	85	530	230	300	335
Hundholmen	70	35		100	555	265	330	365
6814/4-U-1	30	85	100		555	235	310	360
6408/12-U-01	560	530	555	555		320	250	200
6610/3-1	245	230	265	235	320		75	130
6610/7-1	320	300	330	310	250	75		56
6510/2-1	360	335	365	360	200	130	56	

5. DISCUSSION

Sediment transport by itself follows simple physical rules. It is a major task for geologists to reconstruct the complex setting for those rules that have prevailed millions of years ago. This setting is far from being understood wholly for various regions including the Norwegian Sea continental shelf. Provenance research depends on indirect signs and indications. However, the simplicity of the physical rules allows the incorporation of observations from unrelated study areas. With an interdisciplinary approach adequate conclusions can be drawn and used for further improvements of the applied methods. This Master thesis contributes to this process by showing potentials and difficulties of a new combination of two established methods.

Glacial erosion has eminently incised the crystalline basement rock along the Norwegian coast and resulted in plenty of fjords and scattered islands (e.g. Fredin et al., 2013). Despite strong evidence for the influence of deep tropical weathering on the Baltic Shield (e.g. Lidmar-Bergström, 1995; Lidmar-Bergström et al., 1999), which has been underestimated until recently (Olesen et al., 2013), the most distinct geomorphological features on the Norwegian coast are still attributed to past (and active) glacial activity (e.g. Fredin et al., 2013; Hall et al., 2013). All eroded areas on the western side of the paleo-ice divide that has developed during the Weichselian glaciation (see Fig. 15 in chapter 2) are potential source areas for recent sediments deposited on the Norwegian shelf. The ice divide was situated far east from the present water divide (Ottesen et al., 2005) and the catchment area for glacial sediments was accordingly larger than the present catchment area for fluvial activity. The deposition of sediments on the shelf is potentially influenced by the Norwegian Coastal Current that runs along the coast from southern to northern Norway (Hansen & Østerhus, 2000). Mixing, erosion, and redistribution of sediments are possible consequences. The influence of ocean currents on sediment layers, which are currently deeply buried, can be estimated based on the interpretation of seismic profiles (e.g. Laberg et al., 2005a).

This chapter intends to discuss the sedimentological setting of the mid-Norwegian shelf with respect to the samples investigated. Special attention is paid to the genesis of weathered basement rock. A combined overview of the detected offshore quartz grain groups is presented and discussed with respect to the applicability of the quartz types for provenance studies and their geologic significance. The comparability of the offshore sediment grain groups

with onshore quartz grains will be presented and discussed. Centrepiece of the discussion is the classification of the offshore quartz grains and the resulting comparison with onshore samples. A link between most of the offshore and onshore samples is questioned and thus alternative sediment sources as well as transport routes and mechanisms are suggested.

5.1 General CL and LA-ICP-MS findings

Both CL and LA-ICP-MS analyses revealed a marked variety in composition of the sediment of the sampled Molo Fm as a whole, as well as in the composition of the sediment samples themselves. The internal diversity of grains revealed by CL signals reflects the complexity of the geological history of the quartz grains. The highly diverse optical, luminescence, and geochemical properties of the quartz grains indicate that the sediments deposited on the Norwegian shelf are a mixture of broken rock particles originating from various different sources. The presence of grains showing all grades of roundness ranging from very angular to well-rounded also indicates that the shelf is composed of sediments that travelled dissimilar distances and are most probably reworked to a high degree. Despite this high diversity, several distinct groups with similar quartz grains could be established in all offshore samples. The different quartz grain groups are interpreted to reflect sources with a similar magmatic and metamorphic history and the grains might thus have been transported along the same routes within the same geological time. Some of these groups overlap in different wells and different depths (see Fig. 73 & 74). The overlap in groups of quartz grains showing similar CL characteristics both vertically and horizontally indicates that the three investigated offshore sediment wells indeed represent the area and the sand of the Molo Fm. Within an area spanning 130 km and a total sampled range of 499 m (between 940 and 441 m depth), the accumulated grains show several distinct groups. The fact that sediment grains of different types were present in single samples is also an indication that drilling cores contain sediments of varying age at given depths, and that these depths can therefore not be attributed to specific ages determined for basement rocks onshore. The depositional age of sediments differs from both crystallisation age and weathering/erosion age. Due to the high number of single exotic grains that display no similarities with grains in the rest of the samples, it is expected that much more groups would emerge if the number of samples was increased. Remaining grains that are still unique after the data base is increased would then be interpreted to be “true” exotics that are either

transported from much farther away or represent, for example, smaller intrusions that underwent local changes. The compiled data shows, however, no connection between uniqueness in CL signal and roundness. The presence of grains with similar CL contrasts in different depths within the same core also indicates that sediment supply to the shelf was stable over a long period of time, heading more or less in the same direction. The results obtained by LA-ICP-MS are in concert with the results compiled by Götze (2009) and Müller et al. (2012): Aluminium and Ti are the most common structurally bound trace elements in natural quartz (see Fig. 8 and 36). The prevalence of Al reflects that the element is very common in the Earth’s crust and in addition is prone to substitution due to the similar ionic radius with Si (Götze, 2009).

5.2 The quartz grain classification

In a similar study performed at and around Svalbard, Müller & Knies (2013) developed quartz grain classes. They stated that their classification only applies to the investigated area. Consequently, the categories for this study are new. A high number of comparable studies that used the same methods is necessary to recognize classes that can be seen as generally validated. In the following, a combined classification of the investigated quartz grains is presented.





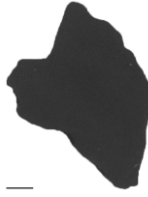
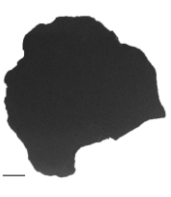


		Classification - Low-grade metamorphic quartz grains - Molo Formation					
		6610/3-1		6610/7-1			6510/2-1
		460 m	480 m	900 m	920 m	940 m	411 m
Type F							
							

Figure 73: Summarized classification of metamorphic quartz grains (> 0.5 mm) found at six different depths in tree wells in the Molo Formation (6610/3-1, 6610/7-1, 6510/2-1). The selection is based on CL characteristics. The distances between the wells are given in Tab. 3. Scale bar lengths correspond to 100 µm.

		Classification - Plutonic quartz grains - Molo Formation					
		6610/3-1		6610/7-1			6510/2-1
		460 m	480 m	900 m	920 m	940 m	441 m
Type A							
Type B							
no type							
Type C							

Figure 74: Summarized classification of plutonic quartz grains (> 0.5 mm) found at six different depths in tree wells in the Molo Formation (6610/3-1, 6610/7-1, 6510/2-1). The selection is based on CL characteristics. The distances between the wells are given in Tab. 3. Scale bar lengths correspond to 100 μm .

5.2.1 Features used for classification

The groups within the two main classes (plutonic and metamorphic) are based on the most common features revealed by CL and the overall CL contrasts. Healed cracks and micro-cracks, fractures as well as trails of fluid inclusions (most common in Type D) are typical for plutonic quartz (Seyedolali et al., 1997; Bernet & Bassett, 2005). Micro-fractures are caused by deformation and are often directionally aligned, whereas micro-cracks are effected by cooling induced contraction of plutonic quartz (Bernet & Bassett, 2005). Healed fractures are uncommon in metamorphic quartz (Seyedolali et al., 1997). Since quartz has generally no cleavage but conchoidal fracture (see example in Fig. 29), fine parallel fractures visible within the grains are always due to deformation processes. A contrasting example of (flaky) fracture in mica is shown in Fig. 65 (G). Healed cracks are most probably filled with secondary, non-luminescing quartz by precipitation (Seyedolali et al., 1997). BSE scanning was applied to confirm that grains clearly showing different CL contrasts entirely consist of quartz. A homogeneous BSE signal indicates that both bright (primary quartz) and darker (secondary quartz) still have the same mean average atomic number which would be clearly different if another mineral phase, such as biotite, was scanned.

Weak polycrystallinity (Type A) is an indicator for deformation processes in plutonic quartz. Very strong recrystallization changes the texture of the minerals and is an indication for metamorphism. According to Bernet & Bassett (2005), low metamorphic conditions can cause micro-fractures but do not change the original CL characteristics of the grains. Authigenic quartz forms out of solution during diagenesis. Grains featuring this sort of secondary overgrowth represent a transition between unaltered and low-grade metamorphic quartz.

5.2.2 Interpretation of features used for classification

Water that is present during cooling and solidification of a pluton can move along fissures and cracks that develop when the pluton contracts. These fluids react with minerals and recrystallization leads to healing of the cracks with secondary quartz. According to Götze (2000), the distinct, dark CL signal at micro-cracks is probably caused by high densities of lattice defects such as non-bridging atoms and vacancy defects in the crystal lattice (see Fig. 9).

The distribution pattern of dark staining along micro-fissures (see Fig. 50 and 76) indicates that the alteration is most probably caused by fluids that moved along the fissures. The darker quartz is then referred to as secondary quartz. The changed CL contrasts suggest a redistribution of defect structures in the crystal lattice (Müller, 2000). All stages of fluid advance through the grains could be observed and fully stained grains cannot be differentiated from grains showing the same contrast caused by other means as long as no statistically significant comparisons with LA-ICP-MS are incorporated. Since this staining along fissures is not visible in BSE images, they are not fluid-inclusion trails as described by Bernet & Bassett (2005).

Black margins at grain boundaries could be post-magmatic hydrothermal overprints. The “tattered” margins visible at some of the well-rounded grains classified as Type F (Fig. 57) can be interpreted as dissolution or rupture caused by removal of the grain out of a sandstone matrix. If this is the case, the grains are probably derived from a secondary source. Source rocks for low-grade metamorphic (Type E and F) grains can be low-grade metamorphic quartzites.

CL intensity seems to be a function of Ti content (e.g. Wark & Spear, 2005; Müller et al., 2002). This was confirmed by this study. Grains with bright CL signal have higher Ti concentrations. The substitution of Ti into the lattice of quartz is proportional to pressure and temperature which allows the development of a crystallisation thermometer (Wark & Watson, 2006) or even a thermobarometer (Thomas et al., 2010). Low Ti concentrations indicate low crystallization temperatures within the range of low-grade metamorphism (quartz grain Type E and F) because the Ti^{4+} can only substitute for Si at high temperatures (Müller et al., 2002). The correlation between temperature and Ti concentration seems straight forward, whereas considerations with pressure are intricate and the applicability of a thermobarometer for natural quartz is questioned (Wilson et al., 2012).

5.2.3 Quartz type comparison with Svalbard

Low-grade metamorphic grains with dull, featureless CL signals and high proportions of well-rounded grains but distinctly different trace element concentrations have been found on the mid-Norwegian shelf (this study) and at Svalbard (Müller & Knies, 2013).

The Al and Li concentrations in Type F grains from this study were extremely low compared to those values detected by Müller & Knies (2013) for their type A grains with otherwise similar

characteristics. Müller & Knies (2013) interpreted the high Al and Li values to indicate hydrothermal quartz (based on Jourdan et al., 2009), which consequently is not the case for the investigated grains in this study.

This comparison has several implications: 1. Grains with similar or even identical CL can have different trace element signatures. 2. Grains with similar or identical CL contrasts can be used for provenance studies if an additional analytical method is applied. 3. The CL signal alone cannot be used as a reliable provenance indicator. 4. The grains found at Svalbard and the grains from the mid-Norwegian Shelf are derived from different, regional sources.

A more comprehensive database could shed light on the differences and similarities (see *Outlook* in chapter 6). The similarities further imply that difficulties are likely to emerge when sink areas with several, large potential catchment areas are investigated where mixing and reworking of sediments is extensive. A possible overlap of trace element data plotted in diagrams cannot be differentiated based on CL structures alone. The incorporation of more data can at some point make a differentiation impossible. To establish low-metamorphic grains with dull, homogeneous CL (Type F here, type A in Müller & Knies, 2013) as a general type is intricate and requires, if still applied, consequent validation with additional analytical methods.

5.3 Cathodoluminescence properties of the offshore samples

The investigations of the three offshore wells revealed sediments derived from metamorphic rocks as well as plutonic rocks. This indicates that both eroded Paleozoic Caledonian thrust sheet as well as Precambrian basement might be incorporated in the Molo Fm. The presence of hydrothermal quartz among the metamorphic grains cannot be excluded. Since hydrothermal quartz is predominantly derived from hydrothermal veins that usually occur in metamorphic quartz (Bernet & Bassett, 2005), a possible attribution to metamorphic quartz is, however, reasonable.

The results of the offshore classification indicate that the analysed samples mainly contain plutonic quartz grains. It is therefore assumed that sources from Caledonian rocks play a minor role. Low-grade metamorphic grains (Type F), especially the well and very well rounded, may be derived from the Caledonides, most probably from the Neoproterozoic to Ordovician Uppermost Allochthon. The grains could be originated from slates or greenschist. The extreme

low number of quartz grains showing growth zoning is interpreted to represent the relatively rare occurrence of hydrothermal quartz in basement rock compared to plutonic quartz. The absence of high-grade metamorphic grains suggests to exclude any source that contains ultra-high pressure (UHP) minerals. This includes the UHP domains of the Western Gneiss Region (WGR) that outcrop in a major basement window in western Norway south-west of the well 6408/12-U-01 (sample 10) location. Grains interpreted to be derived from Precambrian crystalline rocks are most dominant in all samples.

A high number of distinguished quartz grain groups only consists of two grains. Some have different grades of roundness must have travelled different distances since the time they were separated from the original bedrock. The possibility that they belong to the same pluton is highly unlikely. It is therefore interpreted that similar CL structures can develop in different plutons which calls for a supplementary analytical method.

The absence of glass grains within the samples indicates that no volcanic quartz is contained in the Molo sediments. This suggest that no volcanic activity was present at the time of erosion and deposition of Molo sediments and that no layers of ancient volcanic deposits were eroded. The near absence of quartz showing growth zoning is a further indicator since zoning is a common feature in volcanic quartz (Seyedolali et al., 1997; Boggs & Krinsley, 2006; Rusk, 2012). Albeit unzoned volcanic quartz is common in some areas as reported by Bernet & Bassett (2005). Homogeneous, non-differential CL is rare in volcanic but common in metamorphic quartz (Seyedolali et al., 1997).

5.3.1 Classification difficulties

The contrast of CL images was generally used as a feature for classification but entails some difficulties including both homogeneously and heterogeneously contrasted images. Black colour or no luminescence visualised in panchromatic CL images of quartz grains does not necessarily indicate absence of CL, as they can appear in a dark red when colour CL is applied (Bernet & Bassett, 2005). A major problem in categorizing quartz grains based on CL micrographs is the fact that there are no clear borders between the different processes that form and characterize the grains. The transition between diagenetic and metamorphic processes can be conventionally defined by numbers in terms of pressure and temperature. However, a clear

allocation afterwards when the grains have been deformed and removed from these conditions is not straight forward. All grains, unless they are derived from volcanic, plutonic, metamorphic, or sedimentary rocks, are initially of igneous origin and crystallized from magma or lava. Generally, metamorphic grains are believed to have preserved the maximum metamorphic grade they were subjected to. High-grade metamorphism can erase growth zoning originally present in the grain (Bernet & Bassett, 2005). It cannot be reconstructed what kind of features have been erased by metamorphism. The use of grains with featureless homogeneous CL contrasts for provenance studies is therefore intricate. Grains classified as low-grade metamorphic quartz can also be hydrothermal without growth-zoning. Bernet & Bassett (2005) found that plutonic quartz characteristics such as microcracks and healed fractures can partly be preserved when the grains are subject to metamorphism. CL colour and hence grey-scale contrast of quartz changes with increasing degree of metamorphism (Sprunt et al., 1978, Bernet & Bassett, 2005). The distinction between low-grade, medium-grade, and high-grade metamorphic quartz grains is difficult because the characteristic features can overlap (Bernet & Bassett, 2005). There is a smooth transition of the metamorphic facies between zeolite (low) and eclogite (high) (see Fig. 7).

It is important to remember that sedimentary mineral grains always represent only small parts of the initial rock (or of the thin section investigated). Therefore, not only the grains need to be compared in their entirety but also just parts of both grains and thin section details. Quartz grains that break along fractures might leave smaller grains behind that do not show fractures (anymore) and are hence classified differently. It is therefore recommended to use large grains not only accounted for by material availability for laser ablation, but also in order to keep this effect low. Figure 75 shows examples of grains with domains that would lead to different interpretations if considered separately.

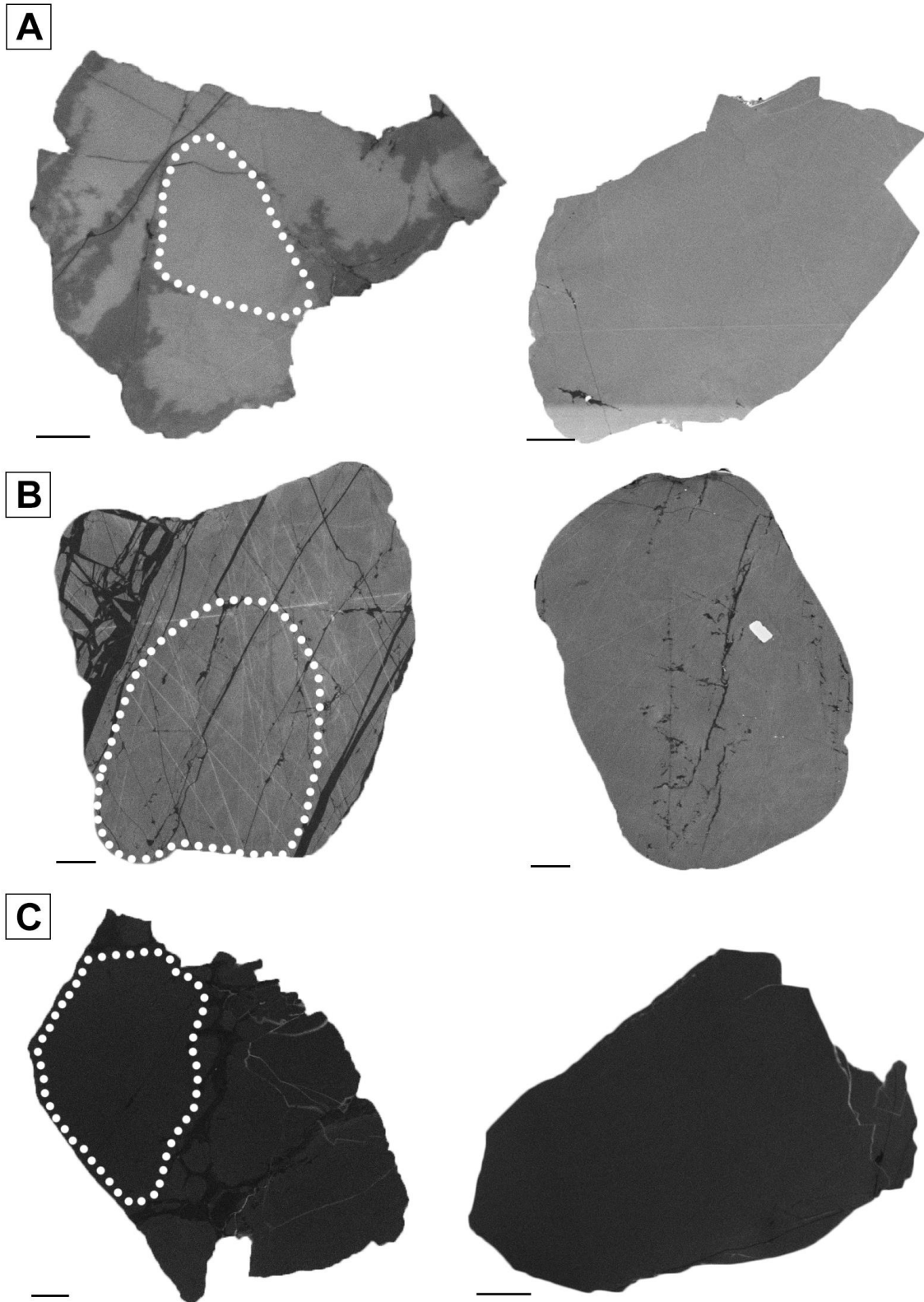


Figure 75: Examples of grains with domains that potentially can represent other grains with different overall CL properties. This effect is most confounding if smaller, homogenously contrasted grains are compared. **A:** Plutonic quartz grain that shows alterations along fissures of different extents. **B:** Plutonic quartz grain with frequent healed cracks at the grain margin, having parts with few healed cracks in the centre of the grain. **C:** Strongly altered plutonic quartz grain with healed cracks but also larger domains with nondifferential CL without cracks. Scale bar lengths correspond to 100 μm .

This effect is further illustrated in Fig. 76. Alterations along micro-fractures can eventually homogenize the CL contrasts.

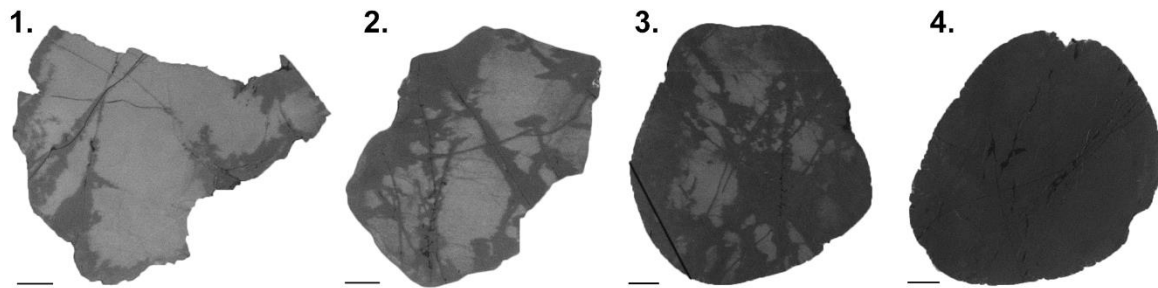


Figure 76: Representative grain selection showing dark staining along micro-fractures observed at different stages. **1:** Primary quartz, initial alteration along fractures to **4:** Grain entirely changed to secondary quartz. The affiliation of the four grains is confirmed by trace element data. However, the apparent increase in roundness from 1. to 4. cannot be correlated with the CL contrasts because the CL properties persist sediment transport. Scale bar lengths correspond to 100 μm .

A further difficulty bears the scanning with a CL detector itself. Irradiation of samples causes contrast differences. A colour change due to heating during CL scanning was first observed by Sprunt et al. (1978). The CL signal changes slightly during irradiation of the sample as shown by Müller (2000) and Müller et al. (2002). Müller (2000) investigated irradiation time versus sample temperature and CL intensity change in detail. The effect was also observed during scanning for the study at hand. Other possible scanning artefacts are compiled in Fig. 31. One of the most common artefacts were bright scratches on the samples (Fig. 31 C). Since deep scratches that affect the actual sample surface would be visible in BSE images, which was not observed, the white scratches present on multiple grains are most probably located only on the surface in the carbon coating. Even though epoxy resin filled cracks were not considered for classification (see Fig. 30), it is likely that the grains cracked along weak structures that have already existed prior to the specimen preparation. Those features can therefore be used as a rough indicator for the physical stability of the grain.

5.3.1.1 Fluid and mineral inclusions versus structurally bound trace elements

Inclusions in quartz can generally have an influence on the trace element composition present within the crystal lattice (Götze, 2012a). The presence of both inclusions and substitutional lattice defects entails major problems for the analysis of true trace element concentrations. Fluid inclusions are normally water bubbles that can contain salt (NaCl). Fluids circulate during

solidification of magma and get trapped in the mineral structure under high pressure (Müller et al., 2012). The high amounts of Na, K, and Ca in the samples are problematic because these elements commonly occur as trace elements in fluid inclusions (Müller et al., 2012). An over-estimation of the content of these elements can therefore not be excluded. There is no known minimum size for fluid inclusions – no boundary can be drawn between very small fluid inclusions and parts with a high amount of structurally bound trace elements. Therefore, the elements Na, K, and Ca were excluded from plotting even though they partly occurred in higher concentrations than for example Ge. Consequently, the applied methods could not differentiate between lattice bound trace elements and fluid inclusions only containing a minor amount of elements. In addition, Müller et al. (2002) reported redistribution and accumulation of the trace elements Al and K in sub-microscopic inclusions as a result of deformation of the quartz.

5.4. Cathodoluminescence properties of the onshore/basement samples

CL scanning of the basement samples confirmed that the method provides a means to distinguish quartz from different sources. The investigation revealed several features that were not observed among the offshore grains. The angularity of the in situ weathered sand grains is in accordance with the concept of particle rounding through abrasion (transport via saltation, reptation, and creep).

The variety in CL properties of sample 5 and sample 89418 that were both sampled from mangerite corestones at the same locality shows that general CL property variations can be expected in plutons on very small spatial scales. Thin sections are an extremely small representation of rocks compared to sand samples. In order to cogently characterize a basement rock, several thin sections are necessary. In addition, background-based CL contrast corrections are not possible in thin section which makes it even more important to use the same settings when comparing thin sections with loose grain samples.

In the following, the onshore basement samples are presented together with offshore grains with similar CL characteristics that have been selected out of 339 grains of from samples.

5.5 Onshore - offshore comparison

Hadseløya: Sample 5

The mineral texture of the investigated thin section details in sample 5 is similar to some of those offshore sediment grains of Type A (strongly recrystallized with sub-grain formation). The two most similar Type A grains (found in two different offshore samples) were selected and are juxtaposed in opposition below (Fig. 77).

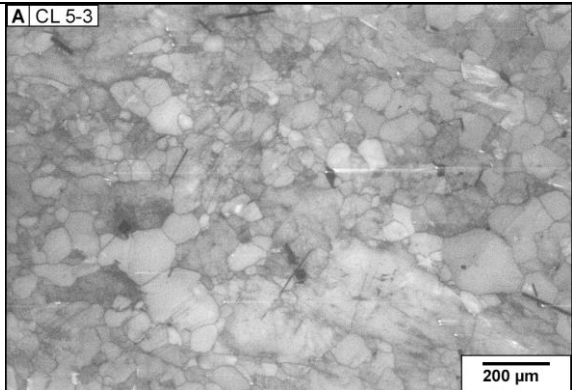
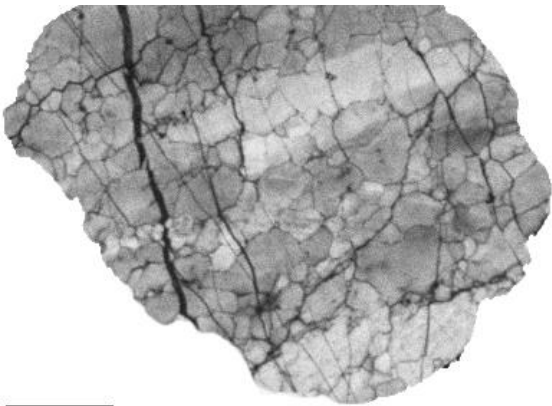
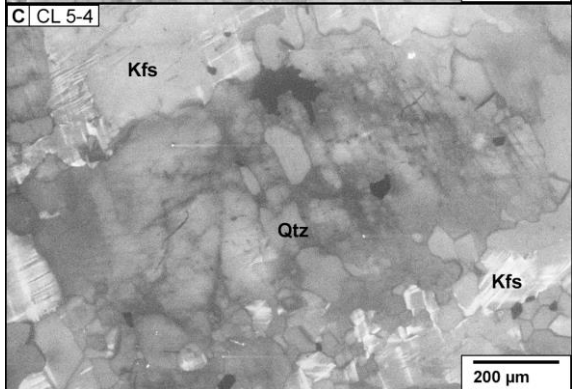
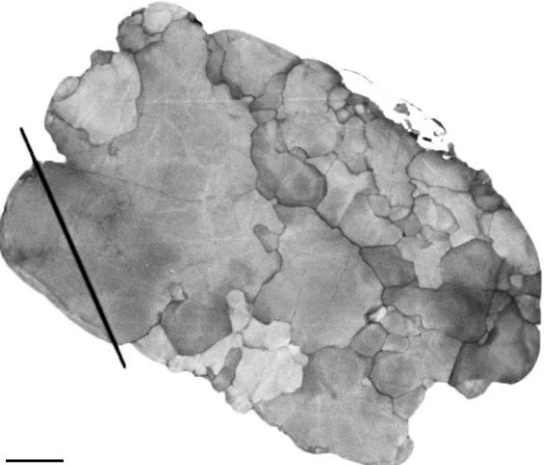
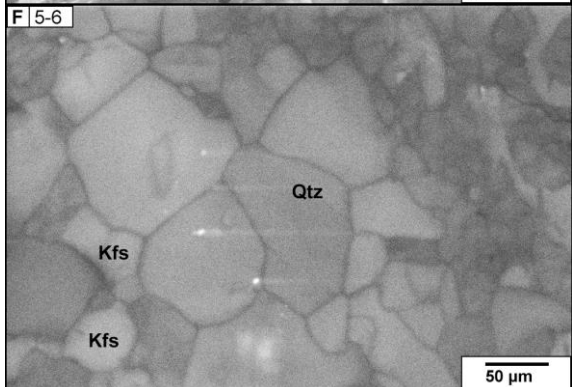
Onshore - offshore comparison	
basement	sediment
<p>Sample 5: Thin section, Hadseløya, 145 m a.s.l. Saprolitic, mangerite corestone</p>	<p>Quartz grains > 0.5 mm Molo Formation Potentially matching grain selection</p>
<p>A CL 5-3</p> 	<p>Sample 3: 6610/7-1, 920m depth Distance: 320 km</p> 
<p>C CL 5-4</p> 	<p>Sample 3a: 6510/2-1, 441m depth Distance: 360 km</p> 
<p>F 5-6</p> 	

Figure 77 (previous page): Closest matches of the onshore - offshore comparison of sample 5, Hadseløya. Kfs = K-feldspar, Qtz = quartz. The black line on the second grain (right column) is an impurity on the sample. Scale bar lengths in right column correspond to 100 μm .

The CL signal shows similarities in terms of state and strength of recrystallization and in overall contrast. However, the high amount of mineral inclusions on the thin sections (black areas on CL images that appear bright in the comparative BSE images) excludes the possibility for a link of the samples since these inclusions are not present in the sediment grains.

Hadseløya: Sample 89415

The in situ weathered grains from Sample 89415 are derived from the same locality and rock type as the thin section from sample 5. Sampling for sample 89415 preferably concentrated on bigger grains. The possibility to choose larger grains from sample 5 was restricted due to the given size of the thin section. It is important to pay attention to the spatial scale when both are compared.

The CL signals of the grains in sample 89415 show most similarities with offshore grains Type F, which are classified as low-grade metamorphic quartz with dull, homogeneous CL signals. The plutonic mangerites on Hadseløya are locally retrograded (Griffin et al., 1978; Andersen & Tull, 1983). Retrograde metamorphism can be seen as an adjustment of rocks to atmospheric pressure-temperature conditions when they are uplifted from their original place of formation. As already indicated, metamorphism can erase structures originally present in the grain (Bernet & Bassett, 2005). The use of homogeneous grains without any visible structural features is therefore intricate. The range of possible primary structures is vast. The use of this type of grains for provenance studies therefore strongly depends on comprehensive additional data.

In the following, two offshore grains with the most similar CL signals (Type F) are juxtaposed (Fig. 78). They can represent only parts of the grains in sample 89415 (see also Fig. 75 A). Further disintegration of the saprolitic sand grains is expected when they are affected by erosion.

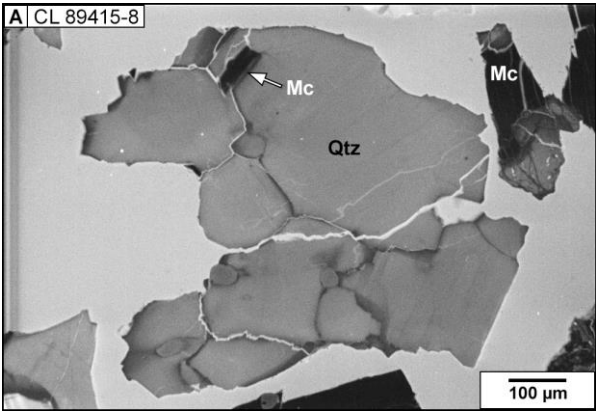
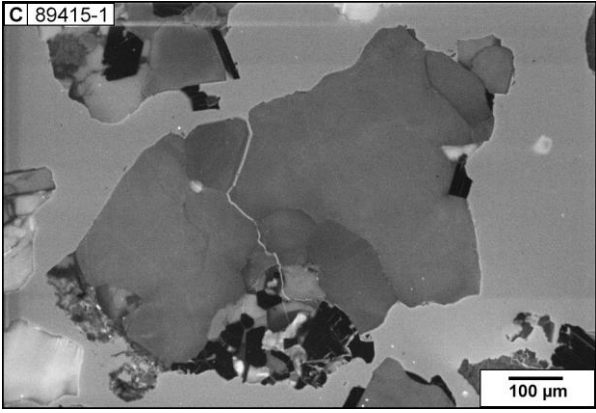
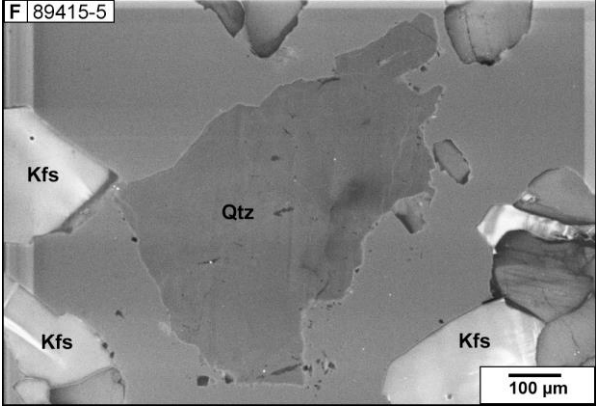
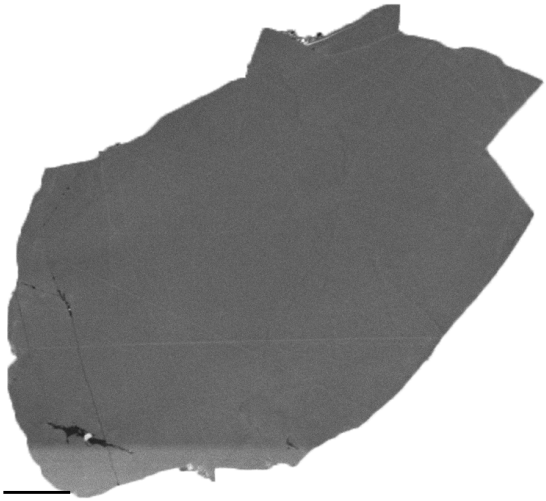
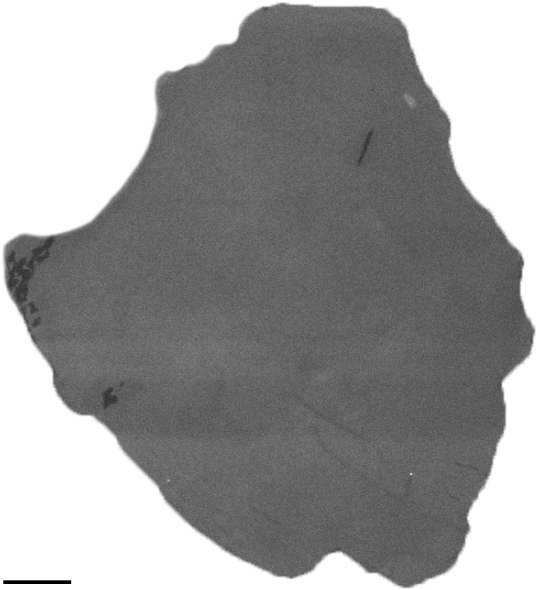
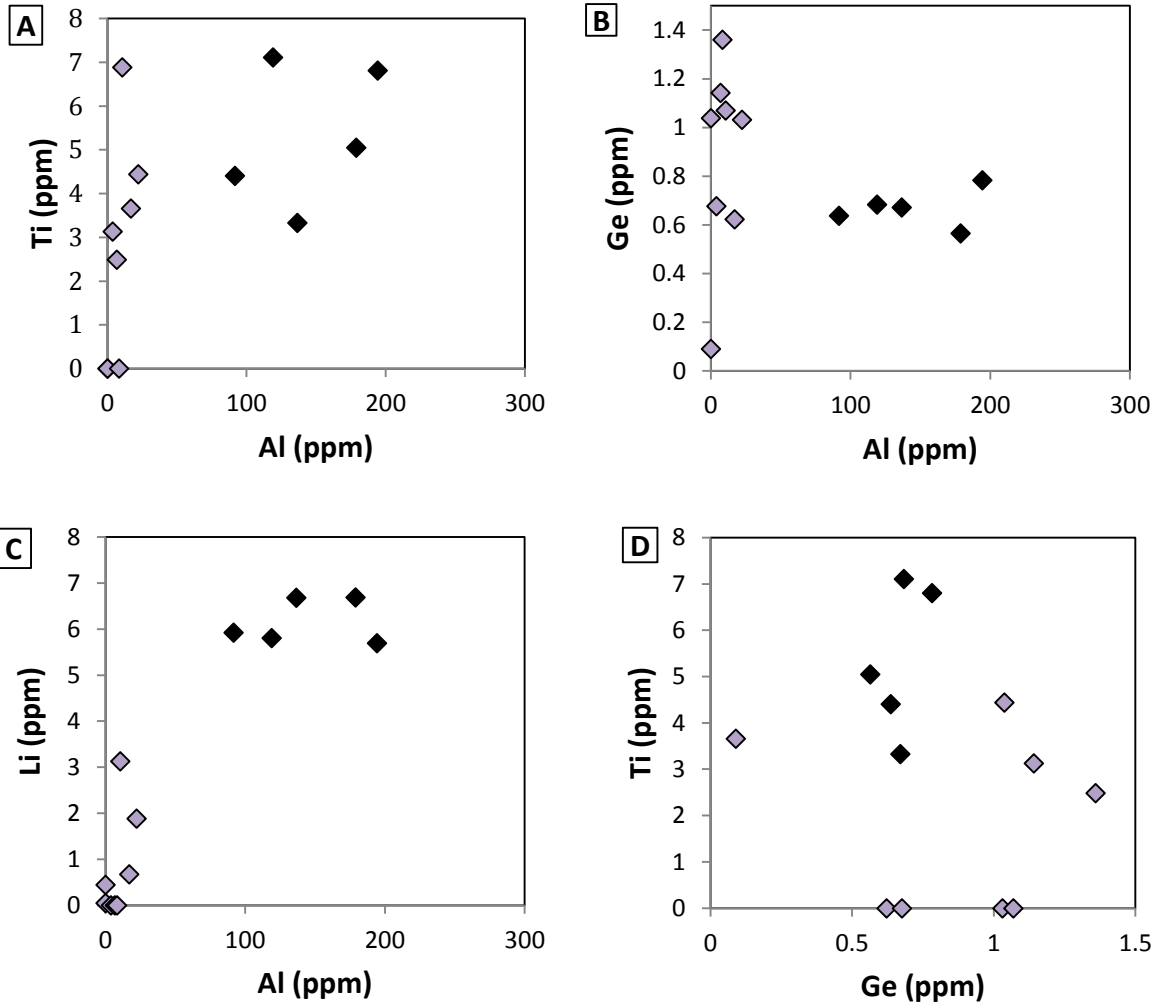
Onshore - offshore comparison	
basement	sediment
<p>Sample 89415: Saprolite sand (> 0.5 mm) derived from mangerite, Hadseløya, 145 m a.s.l.</p>	<p>Quartz grains > 0.5 mm Molo Formation Potentially matching grain selection</p>
<p>A CL 89415-8</p>  <p>C 89415-1</p>  <p>F 89415-5</p> 	<p>Sample 2: 6610/7-1, 920 m depth Distance: 320 km</p>  <p>Sample 1: 6610/3-1, 460 m depth Distance: 245 km</p> 

Figure 78: Closest matches of the onshore - offshore comparison of sample 89415, Brenvninshaugen, Hadseløya. Mc = mica, Qtz = quartz, Kfs = K-feldspar. Scale bar lengths in right column correspond to 100 µm.

Trace element concentrations (especially Al) of sample 89415 are, however, much higher than those values of the grains with similar CL (see Fig. 79). The validation of the similarity with Type F grains shows cluster clearly plotting in different ranges, almost without overlap (except for Ti vs. Ge, Fig. 79 D). The difference clearly negates a possible connection between grains of Type F (including the selection above) with the in situ weathered sand grains sampled on Hadseløya. The difference further indicates that Type F grains were properly classified as metamorphic and the sampled grains on Hadseløya preserved their plutonic character.



- ◆ Hadseløya (sample 89415)
- ◇ Type F grains (6610/3-1, 460 m and 6610/7-1, 900 m)

Figure 79: Trace element concentrations of sample 89415 compared with Type F offshore grains. The plots show that both plot in different ranges. This indicates that Type F grains are not derived from the saprolite locality on Hadseløya. **A:** Ti vs. Al, **B:** Ge vs. Al, **C:** Li vs. Al, **D:** Ti vs. Ge.

Hadseløya: Sample 89418 and Hamarøy: Sample 89421

Sample 89418 is the third sample taken from Brennvinsaugen on Hadseløya. The characteristic black margins discovered in this sample (Fig. 67) have not been discovered in any offshore sample. This is in agreement with the findings of the two previous comparisons. It is therefore interpreted that no link exists between the onshore location on Hadseløya and the sands sampled offshore.

In sample 89421 south of Vestfjorden on Hamarøy, also no distinct match with offshore sampled grains was identified. It is therefore assumed that the saprolites are not the source for the sediments deposited in the Molo Fm. This conclusion obviously applies only to the sampled range both horizontally and vertically.

Tysfjord, Hundholmen: Sample 47802

The granitic basement investigated in sample 47802 shows most similarities with grains categorized as Type C (plutonic with frequent secondary structures) (Fig. 80). Since Type F grains were confirmed to be low-grade metamorphic (Fig. 79), they are not expected to be derived from the Tysfjord gneiss granite, even though general CL similarities exist.

Due to the predominantly nondifferential CL and the few LA-ICP-MS data, the same problem occurs as in the onshore - offshore comparison with sample 89415 (Fig. 78): Similarities with only featureless offshore grains do not allow much interpretation. Best matches are found in sample 3, 4, and 6 (See Fig. 80), but for none of these samples trace element data exist.

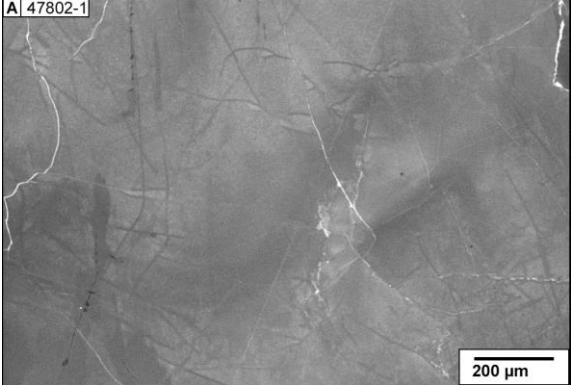
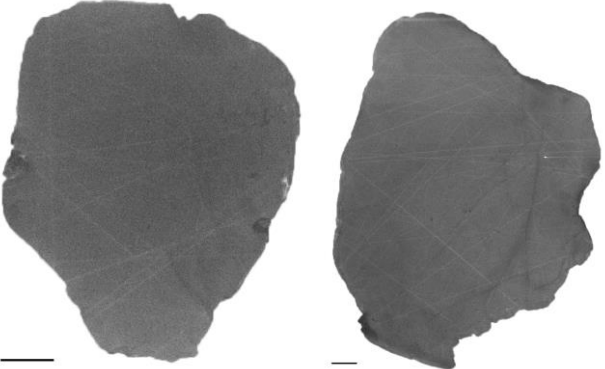
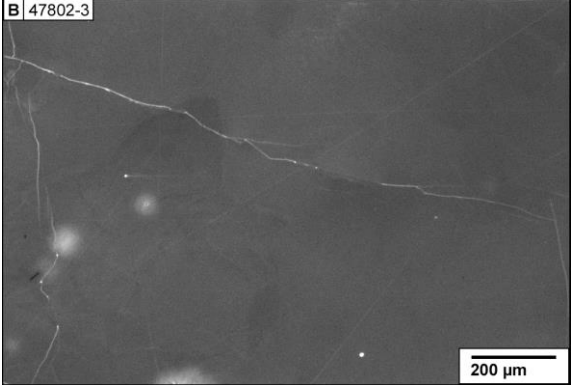
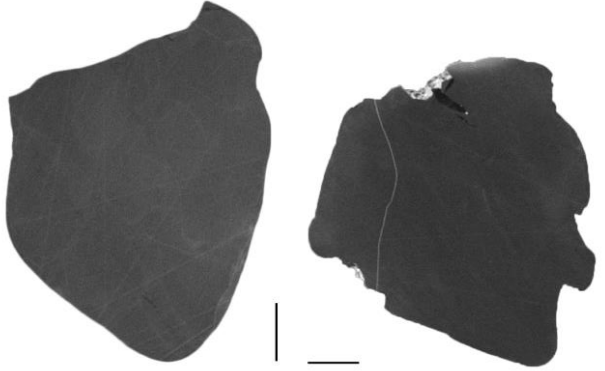
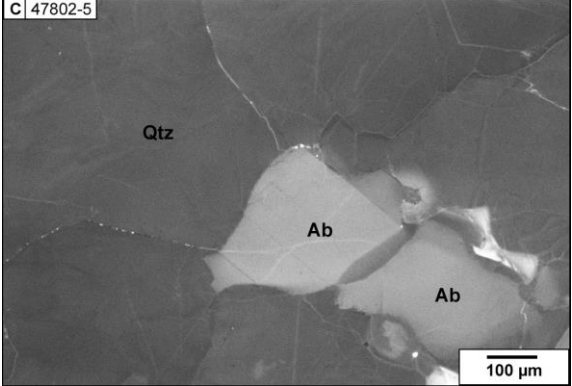
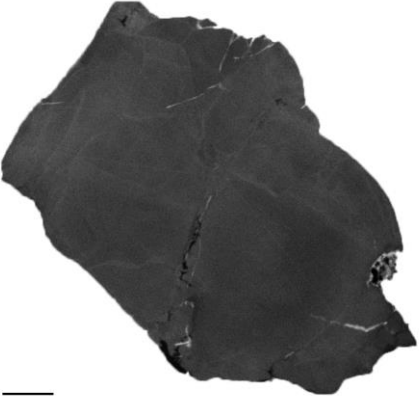
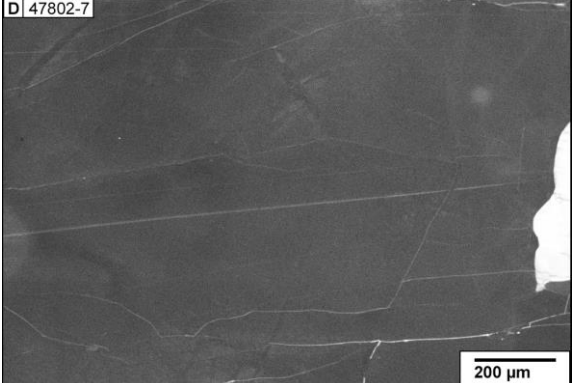
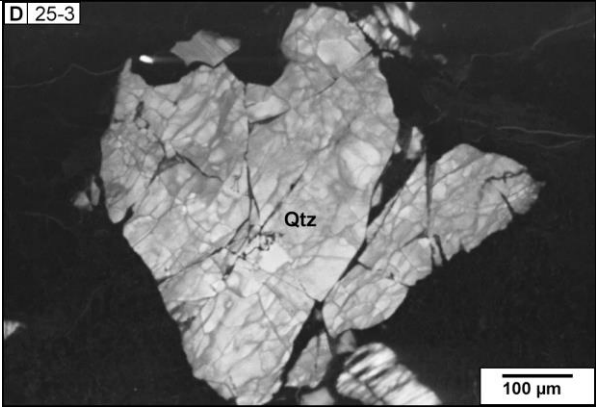
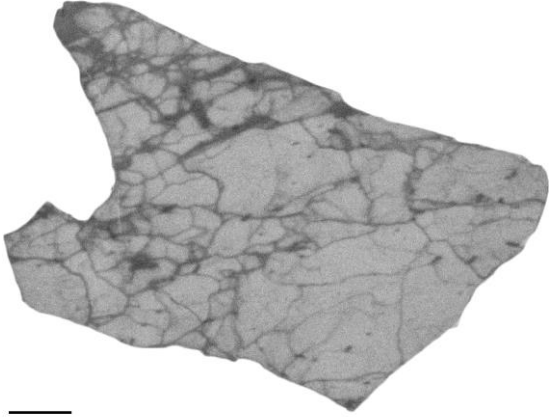
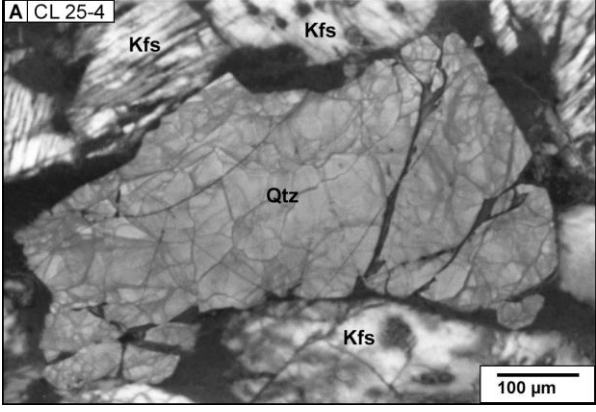
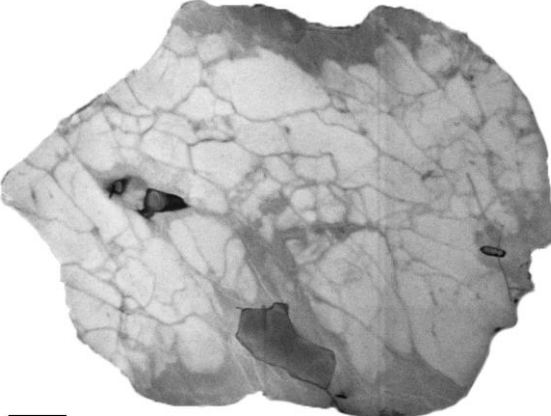
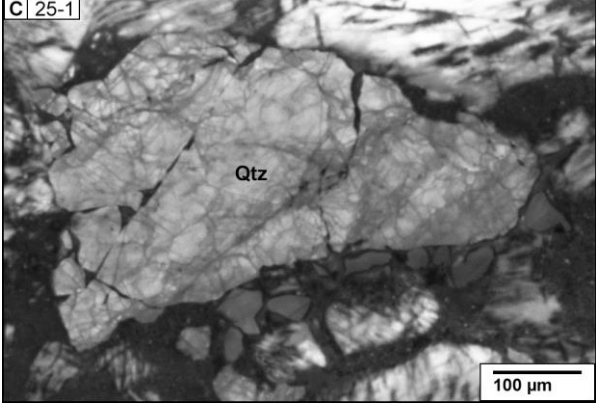
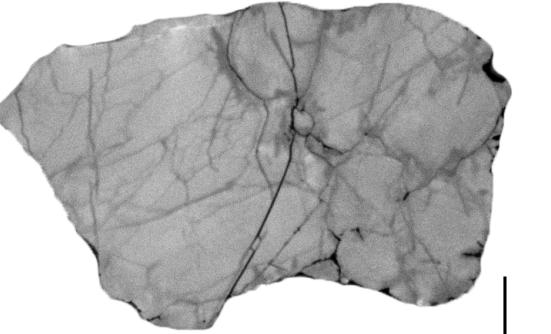
Onshore- offshore comparison	
Basement	sediment
<p>Sample 47802: Thin section, Hundholmen Tysfjord gneiss granite</p>	<p>Quartz grains > 0.5 mm Molo Formation Potentially matching grain selection</p>
<p>A 47802-1</p>  <p>200 μm</p>	<p>Sample 6: 6610/3-1, 480 m depth Distance: 265 km</p> 
<p>B 47802-3</p>  <p>200 μm</p>	<p>Sample 3: 6610/7-1, 920 m depth Distance: 330 km</p> 
<p>C 47802-5</p>  <p>100 μm</p>	<p>Sample 4: 6610/7-1, 940 m depth Distance: 330 km</p> 
<p>D 47802-7</p>  <p>200 μm</p>	

Figure 80: Closest matches of the onshore - offshore comparison of basement sample 47802, Hundholmen, Tysfjord. Qtz = quartz, Ab = albite. Scale bar lengths in right column correspond to 100 μm.

Well 6814/4-U-1 (174.48 m): Sample 25

Onshore- offshore comparison	
basement	sediment
<p>Sample 25: Thin section, south-west Vesterålen well 6814/4-U-1, 174.48 m depth Monzogranite</p>	<p>Quartz grains > 0.5 mm Molo Formation Potentially matching grain selection</p>
<p>D 25-3</p> 	<p>Sample 2: 6610/7-1, 900 m depth Distance: 310 km</p> 
<p>A CL 25-4</p> 	<p>Sample 4: 6610/7-1, 940 m depth Distance: 310 km</p> 
<p>C 25-1</p> 	

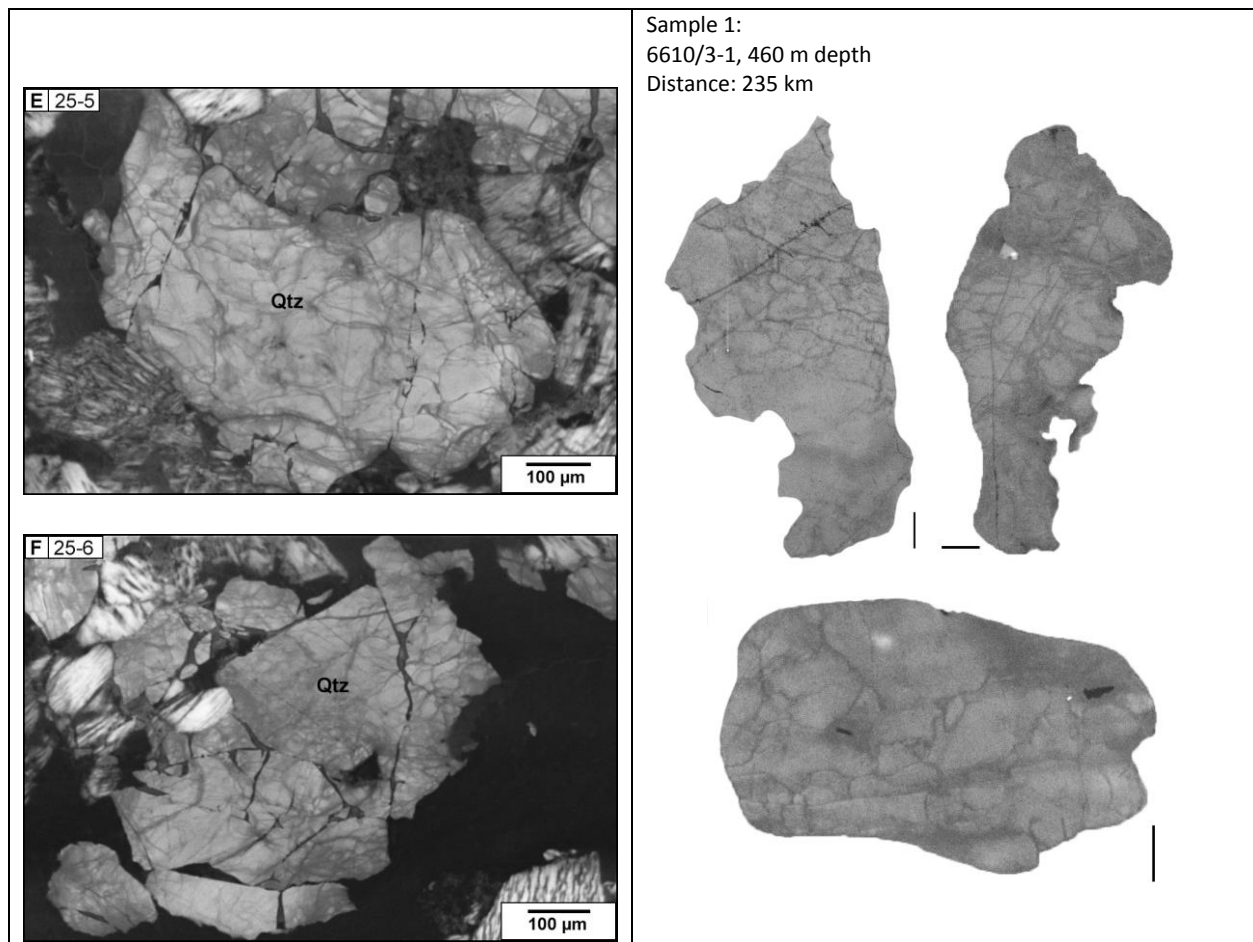


Figure 81: Closest matches of the onshore - offshore comparison of sample 25, south-west Vesterålen. Qtz = quartz, Kfs = K-feldspar. Scale bar lengths in right column correspond to 100 µm.

Figure 81 above compiles the best matches between selected offshore grains and sample 25. The best fit of the comparison was discovered with Type A grains. Of the 58 Type A grains counted in all offshore samples, 31 % were grouped as weakly recrystallized and hence show the most similarities with the weathered basement of sample 25. Potential of four of the grains was tested with LA-ICP-MS and is presented in Fig. 82.

The deformation (recrystallization) in sample 25 most probably occurred during syn- or post-magmatic deformation (Müller, 2015).

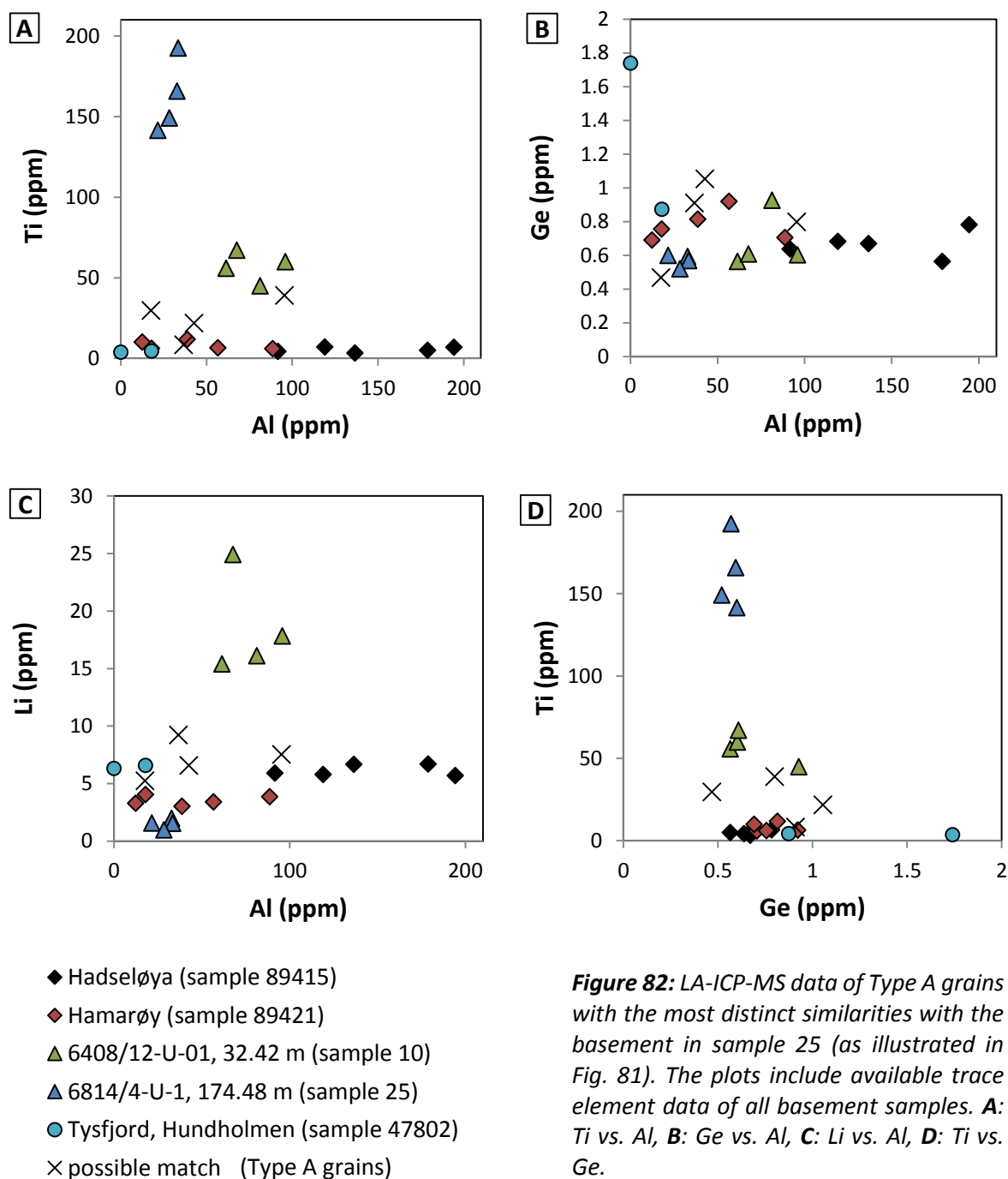
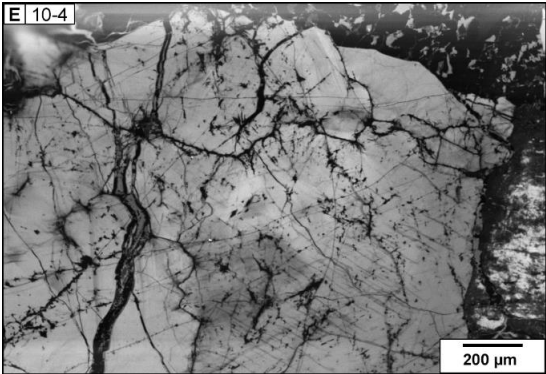
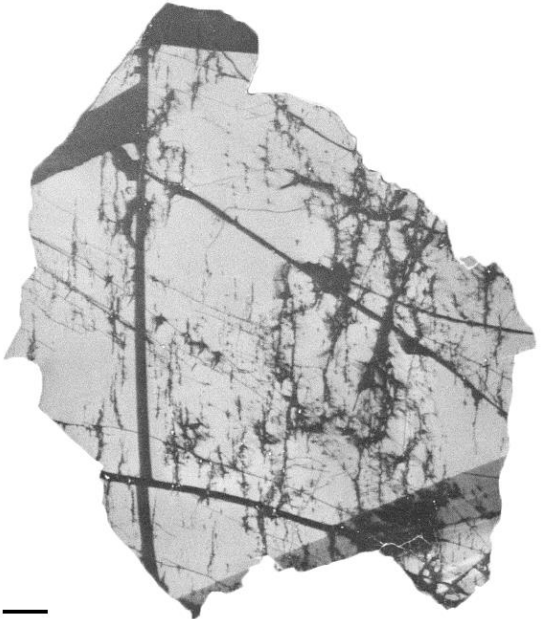
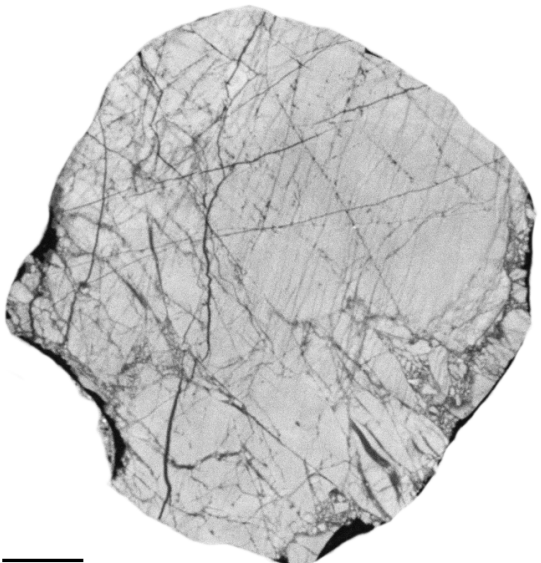
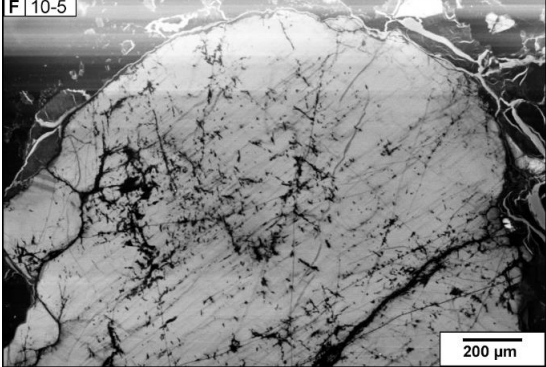
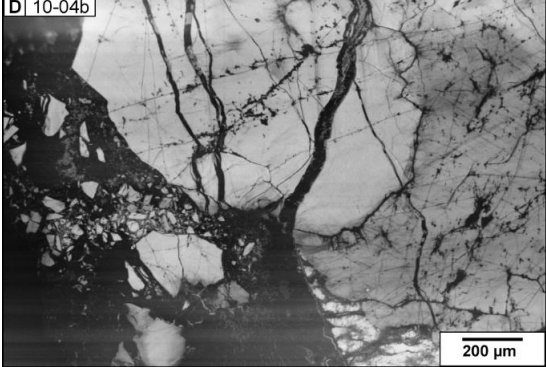
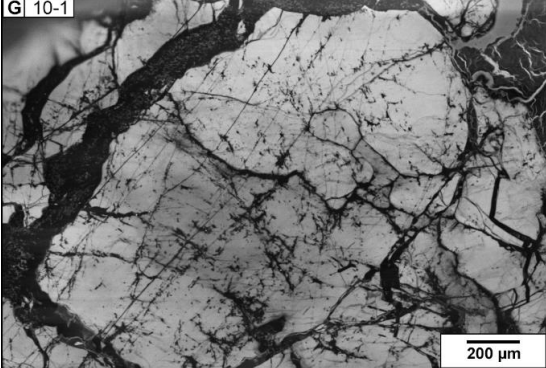


Figure 82: LA-ICP-MS data of Type A grains with the most distinct similarities with the basement in sample 25 (as illustrated in Fig. 81). The plots include available trace element data of all basement samples. **A:** Ti vs. Al, **B:** Ge vs. Al, **C:** Li vs. Al, **D:** Ti vs. Ge.

Figure 82 illustrates that the four potentially matching grains (belonging to Type A from wells 6610/7-1, 900 m and 6610/3-1, 460 m) are clearly distinguished from sample 25 especially by much lower Ti concentrations (Fig. 82, A & B). They are further distinguished from sample 10 by their much lower Li concentrations (C). Best match would be with sample 89421 from Hamarøy, but visual CL comparison revealed no similarities with the selected grains. Despite the differences in trace element concentrations, basement sample 25 shows much more similarities with grains sampled offshore than the saprolites and is therefore interpreted to be closer linked.

Well 6408/12-U-01 (32.42 m): Sample 10

Onshore - offshore comparison	
basement	sediment
<p>Sample 10: Thin section 6408/12-U-01, 32.42 m depth</p>	<p>Quartz grains > 0.5 mm Molo Formation Potentially matching grain selection</p>
 <p>E 10-4</p> <p>200 μm</p>	<p>Sample 3: 6610/7-1, 920m depth Distance: 250 km</p>  
 <p>F 10-5</p> <p>200 μm</p>	
 <p>D 10-04b</p> <p>200 μm</p>	
 <p>G 10-1</p> <p>200 μm</p>	

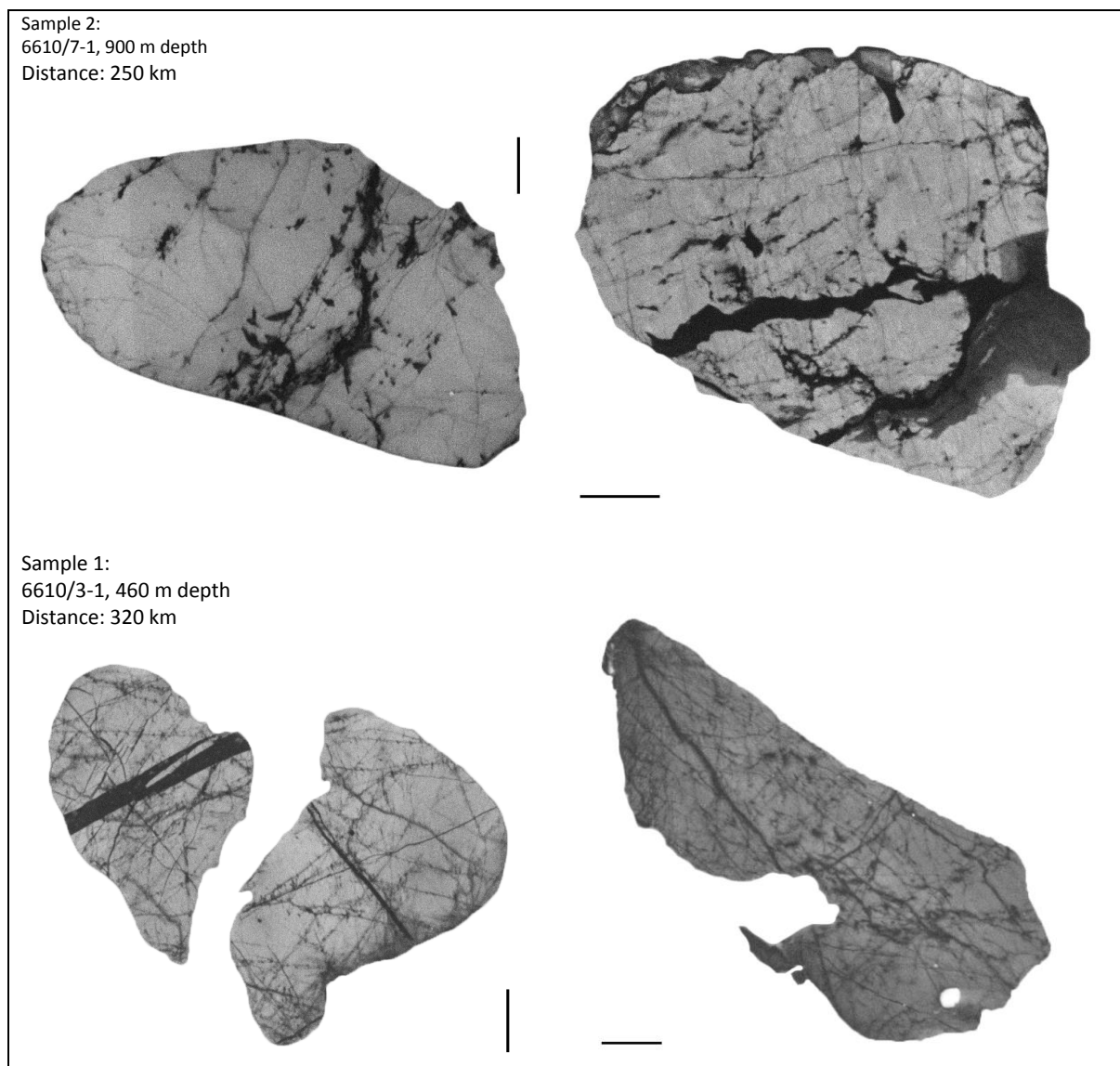
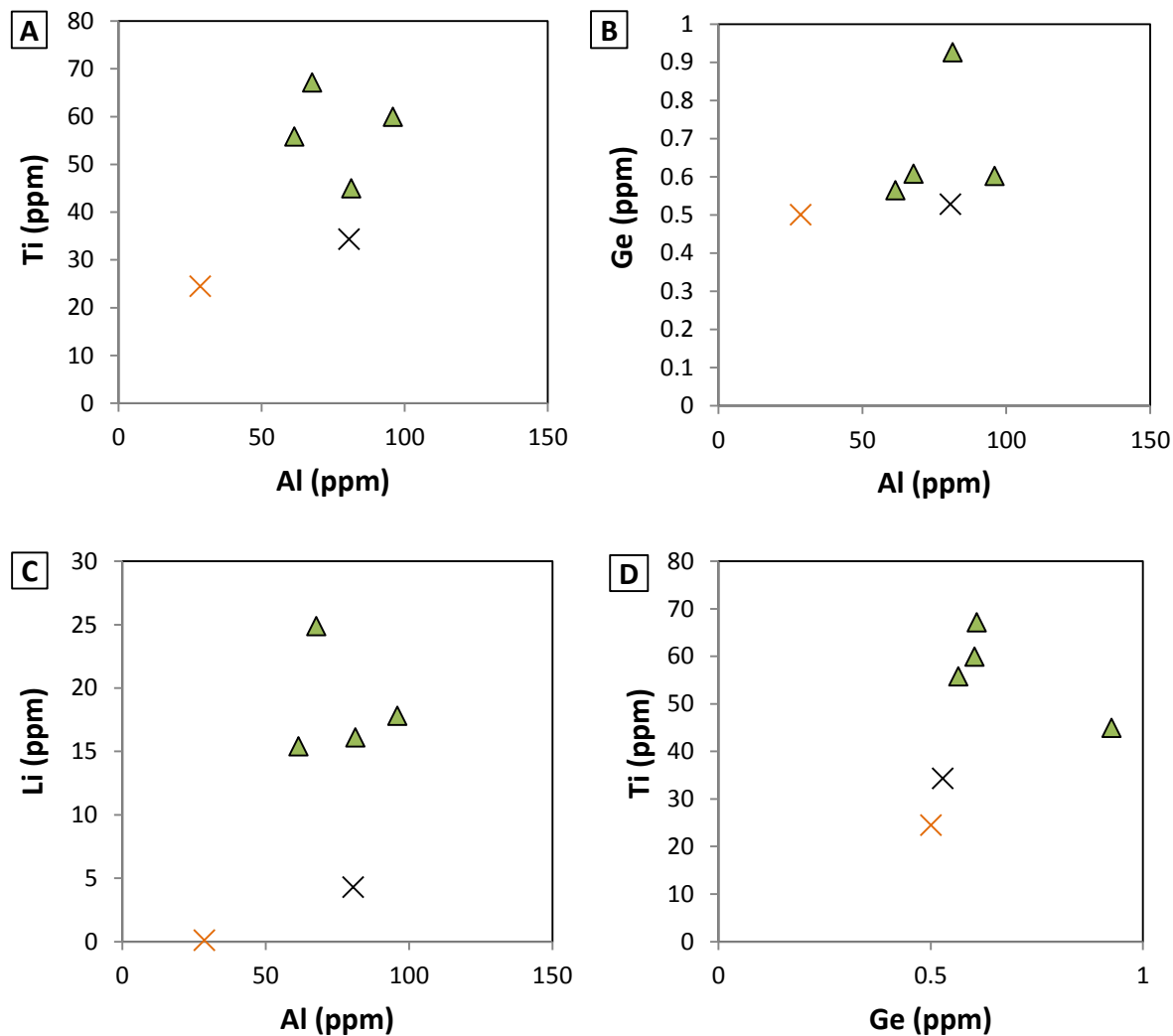


Figure 83: Closest matches of the onshore - offshore comparison of basement sample 10. Scale bar lengths in right column and section on second page correspond to 100 μm .

As illustrated in Fig. 83 above, the basement sample 10 from well 6408/12-U-01 at 32.42 m depth features the most distinct CL resemblances with grains from the Molo Fm among all investigated comparisons. The best matching grains belong to Type D. It is therefore concluded that Type D grains are closely related to the basement at the Froan Basin. The bedrock at and around the Froan Basin is hence a likely source of sediments for the Molo Fm deposited in the Miocene (see Fig. 88). However, trace element data available are limited and include only two grains (see Fig. 84).



▲ 6408/12-U-01, 32.42 m (sample 10)

× possible match in well 6610/3-1, 460 m (sample 1)

× possible match in well 6610/7-1, 900 m (sample 2)

Figure 84: Trace element concentrations of sample 10 in comparison with two grains found in samples 2 and 1 that showed the most distinct CL similarities (illustrated in Fig. 83). The grain from sample 2 shows stronger affiliation than the grain from sample 1. **A:** Ti vs. Al, **B:** Ge vs. Al, **C:** Li vs. Al, **D:** Ti vs. Ge.

The combined plots of all five basement samples (Fig. 72 & 82) clearly show at least four distinct clusters of trace element data. These clusters represent different trace element signatures, representative for the respective plutons they were sampled from. The diagrams can be used to plot grain groups with similar CL characteristics (as performed in Fig. 82). Plotting of grain types or groups in the diagram reveals to which cluster the grains are more related. The range in trace element concentration revealed by plotting of the basement sample values provides an important implication for the range of trace element concentrations that can be expected to occur in single plutons.

In the following, all available offshore trace element data are plotted in order to evaluate the mismatch of the sand in the Molo Fm and the saprolites preserved on the mainland (Fig. 85).

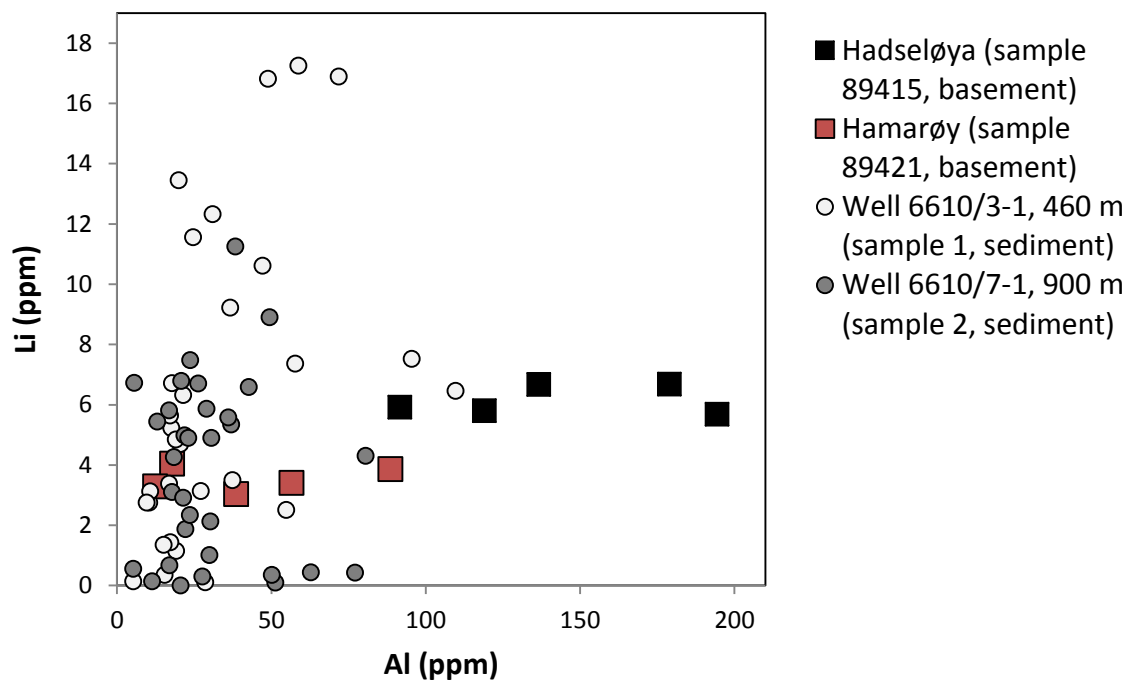


Figure 85: Available trace element data of Li and Al for all offshore grains plotted in comparison to the saprolite trace element concentrations of sample 89415 (Hadseløya) and sample 89421 (Hamarøy).

Fig. 84 shows that sample 89415 (Hadseløya) can be excluded as a source area for sediments found in well 6610/7-1 at 900 m depth (sample 2). Li as well as Al values of sample 89415 lie entirely outside the trace element concentration range of sample 2 and almost entirely outside the concentration range of sample 1. Values of sample 89421 (Hamarøy) lie, however, within the range of Li and Al but the grains plotting close to the range of sample 89421 do not show CL similarities.

The investigated saprolitic profiles on Hadseløya and Hamarøy are representative for saprolite occurrences found along the coast of northern and south-western Norway in terms of intensity of weathering (Olesen et al., 2012). On Hamarøy, a presumably deeper section of weathered bedrock is exposed compared to Hadseløya (Olesen et al., 2012). As already indicated, saprolitic profiles develop independently of bedrock type. Geochemical data of both localities show that distinct differences in trace element concentrations occur (Fig. 66). Al and especially Li concentrations are much higher in mangerite quartz sampled on Hadseløya (Fig. 66, A & C). Ti values are slightly lower but the ranges show some overlap (A). The comparison with Ge values (B & D) is delicate due to the generally small concentration range of the element. However, if the data of both localities are plotted together with all other basement data (Fig. 72), it becomes obvious that the exposed saprolites are closer related to each other than to the basement samples from the Froan and Ribban basins.

The following two figures (Fig. 86 & 87) emphasize the results of the onshore - offshore comparison obtained for samples 25 and 10. Trace element data reveal that the basement from sample 10 is much closer related to the grains of the Molo Fm than those of sample 25.

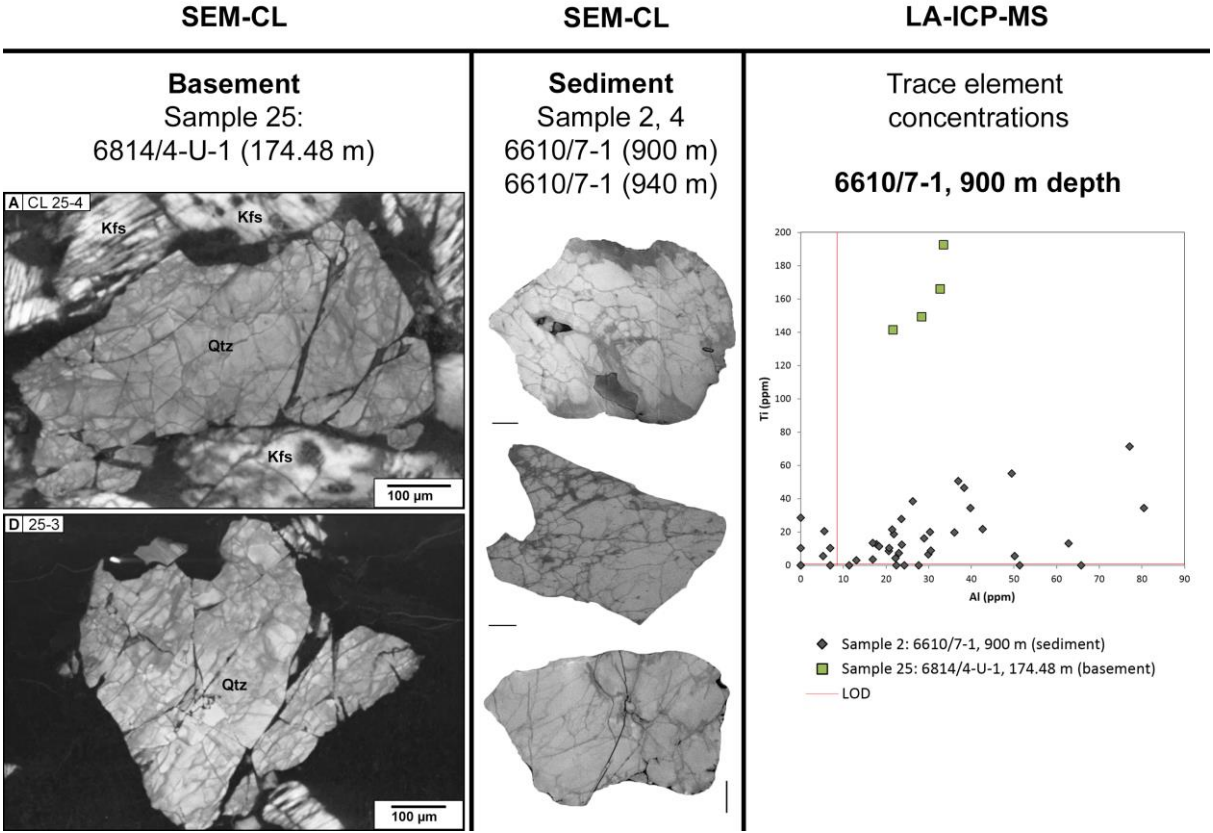


Figure 86: Summarized results of the onshore - offshore comparison from sample 25.

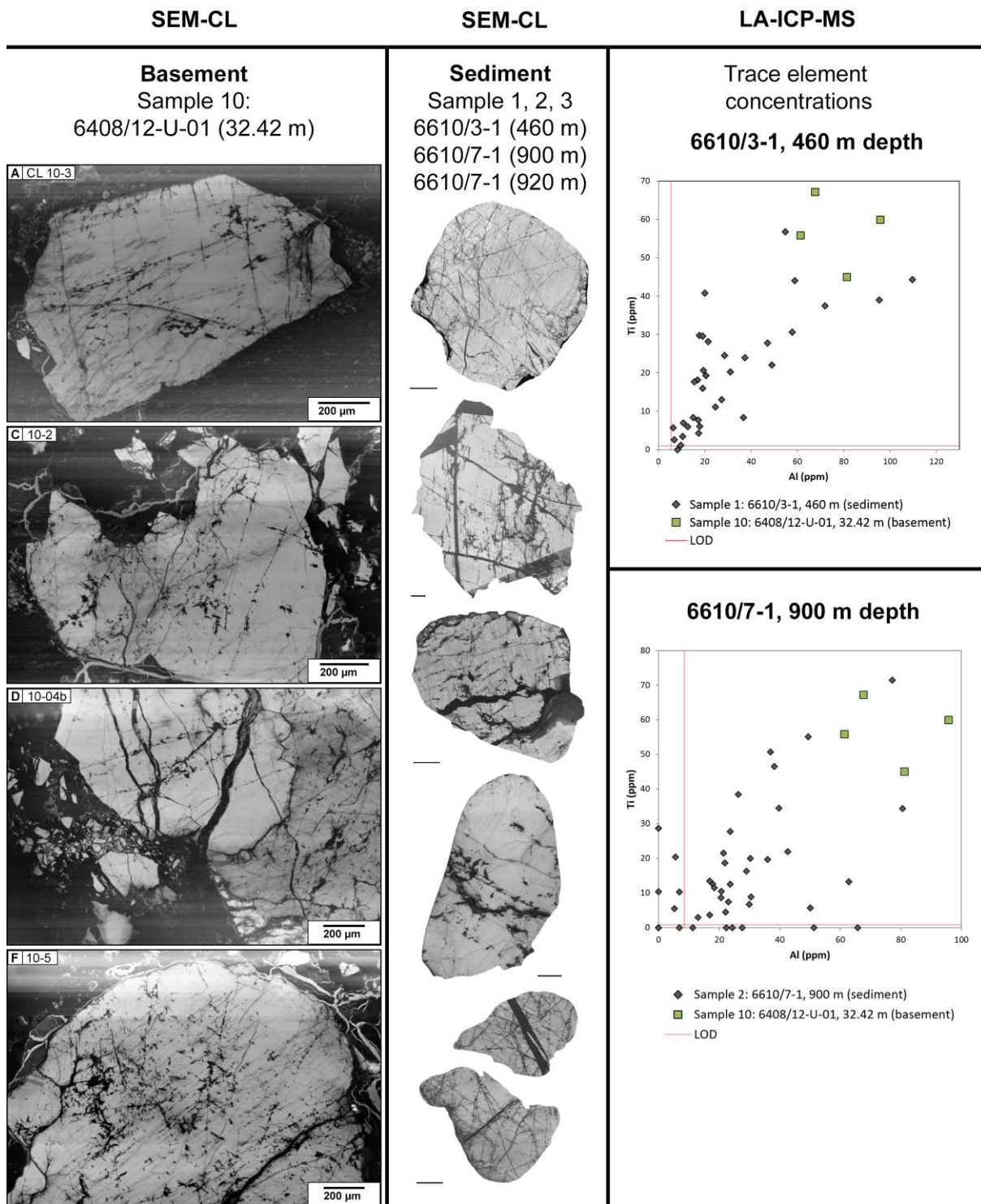


Figure 87: Summarized results of the onshore - offshore comparison from sample 10.

5.6 Discussion of the Onshore - offshore comparison

Results of the onshore - offshore comparison imply that the strongly weathered basement in mid- and northern Norway was not the main source for the sediments that comprise the Early Oligocene - Early Pliocene Molo Fm.

No unequivocal match between source and sink quartz that could be confirmed with trace element data was detected among the studied samples. However, higher amounts of grains with decent CL similarities were found when the non-saprolitic basement samples from the cores north (Ribban Basin, 6814/4-U-1) and south (Froan Basin, 6409/12-U-01) were compared with grains deposited in Molo Fm (see Fig. 81 & 83 and Fig. 68 & 67). Among these two, the basement sampled in well 6408/12-U-01 shows the strongest affiliation with the offshore grains (see Fig. 87). This generally implies a more south-north directed sediment supply responsible for the Molo Fm, which is in agreement with the prevailing ocean current direction observed today (Hansen & Østerhus, 2000), that might have been established already in the Miocene (Bryn et al., 2005). This conclusion is also in agreement with the predominant bedrock types in that region. The Uppermost Allochthon of the Caledonides dominates the mainland east of the Molo Fm. A predominantly westward sediment transport direction would most probably have deposited much more metamorphic quartz grains. South of the Molo Fm, the Central Norway Basement window and the WGR primarily outcrop and are therefore more likely to be major sediment sources for the Molo Fm.

Based on the onshore morphology and offshore deposition patterns, Eidvin et al. (2014) suggest a westward directed sediment supply from the proximal mainland as main source for the Molo Fm. The deltaic shape of the Molo Fm revealed by seismic profiling (westward dipping Clinofolds, see Fig. 24 C) indicates a direct connection to the coast and it seems reasonable to conclude that the Molo sediments are derived from the nearest coast. According to Stuevold & Eldholm (1996), the Fennoscandian landmass and the inner shelf served as the main sediment source for sediments deposited west of the shelf edge since the Oligocene (see also Eidvin 2014). Based on the presented data, it cannot be excluded that sand derived from the saprolites preserved on the mainland of northern Norway is deposited in the Molo Fm because (1) the high diversity of grains is not exhaustively sampled and (2) given the vertical thickness of the Molo Fm of up to 200 metres of the Molo Fm (Eidvin et al., 2007), the sampling at 6 different depths is very random. The proposed sediment supply routes by Eidvin et al.

(2014) are, however, not necessarily connected to the presence or absence of saprolitic sand since these could also have been deposited later in the overlying Naust Fm.

5.7 Absence of saprolitic sand in the Molo Formation

The assumed absence of saprolitic sand in the Molo Fm gives some implications concerning the preservation and erosion history of the weathered basement in Norway. The simplest explanation is that no saprolites were eroded at the time the Molo Fm was deposited. There is, however, strong evidence that the former extent and the erosion of the saprolites was extensive, hence the main amount of saprolites is probably deposited somewhere else. This implies that something else, supposedly deposited on top of the saprolites was eroded and deposited as Molo Fm. In order to discuss the indications of saprolites for the Molo Fm, the preservation of saprolites on land needs to be considered in greater detail first.

5.8 Preservation of saprolites in Norway

The occurrence of weathered bedrock on the mainland of Norway can be taken as indicator for inefficient or absent glacial erosion. However, the possibility that extensive layers of unrelated sediments lay on top of the saprolites and were eroded first, perhaps by glaciers, needs to be taken into account.

In order for saprolites to still be present on the mainland, several possible processes and factors need to be considered: 1. The saprolites have not been totally eroded by glaciers during the last glacial periods. 2. The same is true for the erosional power of rivers before the glaciations and in interstadials, including strong meltwater rivers at the transition from cool to warmer periods. 3. Uplift has placed parts of the saprolites in a position sufficiently high to be protected from strong glacial erosion. 4. An elevated position also prevents saprolites from being positioned within floodplains. 5. Ice streams have concentrated ice drainage, leading to less erosional influence in adjacent areas, including the present saprolite sites (e.g. Ottesen et al., 2005). 6. The saprolites developed in the Holocene and have never been subject to glacial erosion (e.g. Peulvast, 1985). 7. Deep marine burial of the weathered basement in the Cretaceous protected the saprolites from being eroded subsequently (e.g. Lidmar-Bergström, 1995; Riis, 1996).

Several landforms in Scandinavia are known to have survived glacial erosion throughout the last glacial periods (Kleman, 1994; Kleman & Stroeven, 1997). Kleman & Stroeven (1997) came to the conclusion that pre-glacial landforms in glaciated areas have mostly been preserved at intermediate elevations between the common altitude of cirque glaciers and the altitude of the glacier bed where glacial erosion is high. Saprolitic profiles have been discovered at up to an altitude of 500 m a.s.l. in the Lofoten-Vesterålen area (Peulvast, 1985). In addition, Andøya, an island also featuring saprolites, most probably provided a refugium for pine tree species during the last glaciation which excludes the assumption that the entire mainland was covered by a vast ice sheet (e.g. Parducci et al., 2012). All this indicates that glacial erosion in northern Norway has been overestimated.

Recent studies favour the idea that a protective cover of marine sediments was deposited on the weathered bedrock when the Baltic Shield was largely transgressed (e.g. Olesen et al., 2013; Lidmar-Bergström et al., 2013). According to Riis (1996), the Scandinavian peneplain was probably transgressed in the Cretaceous, providing burial with marine sediments necessary for preservation of Jurassic sediments and sedimentary rocks below (see Fig. 3). Lidmar-Bergström (1995) states that the Baltic Shield was mostly covered by shallow seas already during the Paleozoic.

This preservation mechanism requires that the relative rise in sea level did not subsequently erode all saprolites. It further suggests that the marine sediment deposited on the weathered basement (shales and carbonates, Olesen et al., 2012) developed layers that were highly resistant to erosion. Olesen et al. (2013) suggest that the deep weathering in the study area was preserved due to the Late Pleistocene uplift and erosion.

An extensive protective cover would have been necessary to provide a shelter against the erosional power of the ice that eroded Norway during the Plio-Pleistocene glaciations. Without such a cover, probably no saprolites would be preserved today. According to this approach, the glaciers subsequently eroded the protective cover entirely from the mainland with the exception of a small area on Andøya, Vesterålen. If glaciers first had to erode all protective layers lying on top of the saprolites, erosion and deposition of saprolites would have started later and the products are expected to be found in the Naust Fm or in upper parts of the Molo Fm.

5.9 Sedimentation of the Molo Formation

The sediments of the Molo Fm were most likely eroded from the mainland after they were exposed as the result of uplift and then redistributed by longshore drift to an unknown extent (e.g. Eidvin et al., 2014). Bottom-current activity has influenced sedimentation along the Mid-Norwegian margin since the mid-Miocene (Bryn et al., 2005).

Stuevold & Eldholm (1996) suppose that Miocene sediment wedges were strongly eroded during the Miocene-Pliocene transition when sea level decreased. North of 66° N, Miocene sediments are locally absent (Stuevold & Eldholm, 1996). Deposition of Molo sediments was most probably influenced by longshore currents that led to redeposition and redistribution (Eidvin et al., 2007). Especially in the outer parts of the Vøring Plateau, contouritic currents are known to have rearranged sediments (Laberg et al., 2005b). Seismic reflections at the Kai Fm have also been interpreted as contourites (Løseth & Henriksen, 2005). Contourites indicate redistribution of sediments in deep water, however, the Molo Fm was interpreted to have been deposited in shallow, coastal water (Eidvin et al., 2014). Redistribution of Molo sediments by contouritic drifts is believed to have minor influence on the deposition as compared to coastal currents.

Since the Miocene was an epoch with higher temperatures than during the glacial periods and today (e.g. Pound et al., 2012; Holbourn et al., 2015), glaciers or sea ice are unlikely sediment transport agents. The sands of the Molo Fm are marked out in contrast to the overlying Naust Fm and do not show influence of glacial erosion and deposition (see Fig. 24 C). However, Dowdeswell et al. (2007) point out that sedimentary products derived from glacial and non-glacial processes can be similar. According to Eidvin et al. (2007), significant increase of Ice rafted debris (IRD) supply to the deep ocean was related to climate deterioration in the latest Miocene. No fjords have existed at the time the Molo Fm was deposited. Since rivers and glaciers usually follow pre-existing weak structures like faults or otherwise fractured zones, it is reasonable to assume that the main pattern for the sediment transport of rivers and hence the river catchment areas did not change fundamentally since the Miocene.

Saprolites are the result of weathering in warmer climate and extensively weathered saprolites progressively transition to laterites. Eidvin et al. (2007) reported dark yellow, probably lateritic sand in the Molo Fm in the Nordland Ridge area that they interpreted as incorporation

of sediments originally deposited during periods with warmer climate. The Kai Fm is the deep water equivalent of the Molo Fm and known to be clay dominated (Eidvin et al., 2007; Eidvin et al., 2014). Since clay is a final product of weathering and the strong weathered saprolites on Hadseløya and Hamarøy have produced clay (Olesen et al., 2012), it is possible that these were partly deposited in the Kai Fm. Clay as the smallest possible grain size can be washed out of weathered rocks and transported far away before larger particles of the same parental rocks are eroded. Therefore, the presence of clay derived from the saprolites in the Kai Fm does not presume the presence of more coarse grained saprolitic sand in the Molo Fm.

The existence of still preserved saprolites on the mainland of Norway makes it unlikely that the derived sediments lie below the Molo Fm in the Brygge Fm. A break in deposition for the time it took to deposit the Molo Fm is highly improbable. In addition, the Molo Fm as well as the Kai Fm rest upon an unconformity that has been interpreted to have been caused by non-deposition rather than erosion (Eidvin et al., 2007; Eidvin et al., 2014). A possible direct connection between the outcrops and the saprolites exists today even though the saprolitic profiles do not lie in areas currently being significantly eroded. It is therefore again more likely that the saprolites were deposited in the more recent Naust Fm. Since the Naust Fm consists of glacial till that basically includes all eroded material, independent of type, the frequency of occurring saprolite derived sand grains is probably very low, depending on the former extent of the saprolitic layers.

There are no known localities where saprolites are currently being eroded by remaining glaciers on the mainland of Norway. Saprolitic sand is therefore not expected to be found in upper layers of the Naust Fm (Naust section T, see Fig. 23) or in recent Holocene sediments. There is probably a smooth transition from depositional units containing saprolites and those devoid of saprolites in both vertical directions. Dowdeswell et al. (2010) have calculated that the sedimentation rates of Naust sediments were not highest with the onset of the glacial periods. In theory (Andrews, 1979; 1982; Bell & Laine, 1985), with the onset of glacial erosion most of the material lying on top of the basement is easily eroded, leading to high sedimentation rates. As the glaciers “finish” the easily accessible material and start to erode more resistant bedrock, sedimentation rates offshore decrease. According to Dowdeswell et al. (2010), this was not the case on the mid-Norwegian shelf. It is therefore unlikely that vast amounts of weathered, saprolitic bedrock were eroded when glaciation started. This is again an indication that

a protective cover deposited on top of the saprolites would have to be removed prior to erosion of the saprolites. Alternatively, the former extend of saprolitic layers on the mainland is overestimated. If saprolites were first eroded with the onset of the glacial erosion, the first saprolites would have to be found in the lower Naust Fm (section N, see Fig. 23). If the bulk of the saprolites is expected to be deposited in the Naust Fm, especially more shallow depth (upper parts of the Molo Fm) have to be sampled in order to confirm the absence of saprolitic sand in the Molo Fm. The transition between upper Molo and lower Naust was most probably disturbed by reworking of Molo sediments into the base of the Naust Fm (Hall et al., 2013).

Well 6408/12-U-01 was drilled into the Froan Basin 20 km west of numerous scattered islands and lies approximately 60 km away from the main coastline (see Fig. 19). Sample 10 was taken from that well at 32.42 m depth. The sample presumably represents a depth that has already been eroded on the uplifted mainland. At the sample site offshore, the Mesozoic protective cover lying on the weathered basement is still intact (e.g. Mørk & Johnsen, 2005). The grains that show close matching characteristics with the Molo sediments (see Fig. 83) are hence not eroded

from the very area of the sample site but rather represent the state of weathering (depth) of the profile expected to have existed at the adjacent coastal area from which the grains are derived and deposited in the Molo Fm. The studied saprolites that remain on the mainland on Hadseløya and Hamarøy show less strong weathering and therefore represent a depth that

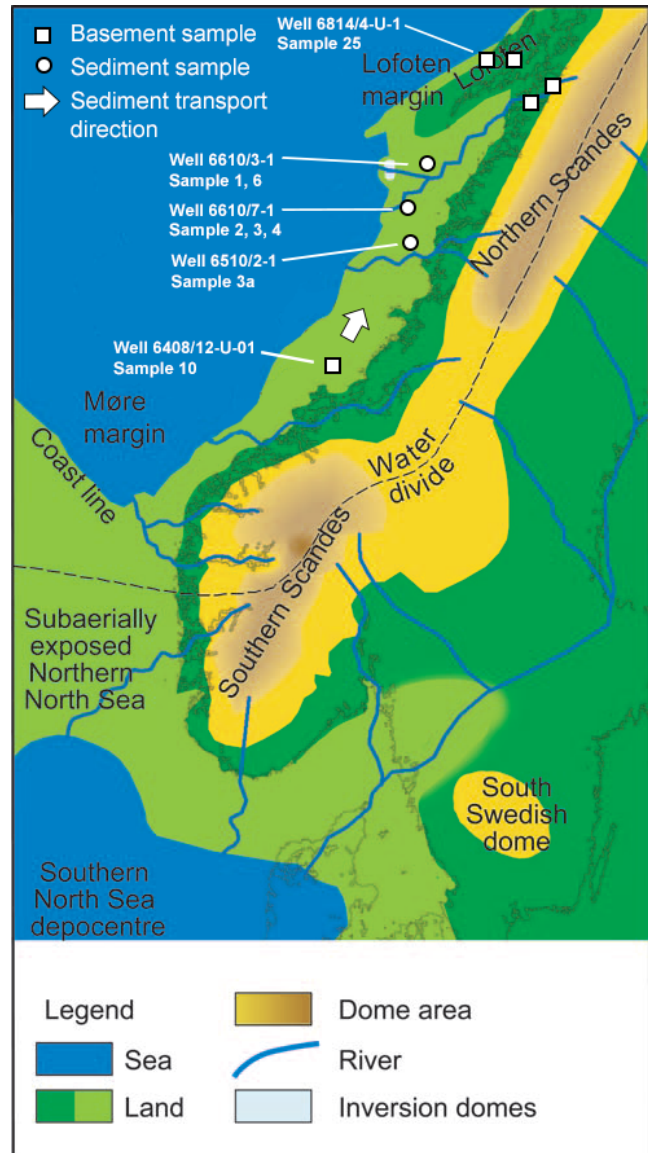


Figure 88: Palaeogeographical interpretation of the Late Miocene. The sample sites of this study are indicated and the potential sediment transport direction based on the results of the onshore - offshore comparison. Modified after Løseth & Henriksen

lies below the depth of sample 10. Following this approach, the Mesozoic protective cover was widely removed before the Plio-Pleistocene glaciations because weathered material that was lying below the cover has already been incorporated in the Molo Fm. Supposedly fluvial erosion has removed the majority of the Mesozoic cover and deposited the Molo Fm as response to uplift. Preferably easily erodible material of the saprolites that corresponds to the range of the sampled depth from well 6408/12-U-01 was incorporated. In the Pliocene glacial erosion then took over and eroded deeper and hence more resistant parts of the saprolites that were, consequently, then deposited in the Naust Fm. The onset of glacial erosion at a time when the most easily eroded material was already removed is in accordance with the observations of Dowdeswell et al. (2010). Consequently, saprolitic sand in the Molo Fm, if any, must be derived from the uppermost layers of the saprolitic basement that feature geochemical and luminous properties different from the less weathered deeper parts (represented by the samples from Hadseløya and Hamarøy). The uppermost layers of weathered basement correspond to zone I and II (after Nesbitt, 1997, see Fig. 4) that contain less quartz but increased amounts of clay. This approach implies that the clay was contemporaneously deposited in the Kai Fm.

5.10 Age of the saprolites

Evidence of Mesozoic sediments covering saprolites in Sweden (Lidmar-Bergström, 1995) and on Andøya in Norway (Olesen et al., 2012) suggests an age for the saprolites of at least late Jurassic/early Cretaceous. This assumption is supported by Riis (1996), who described the continuation of the characteristic weathered relief down under Mesozoic sediments offshore based on correlations of morphological surfaces with offshore data. The assumptions of Riis (1996) are confirmed by offshore exploration wells that penetrated through Mesozoic sedimentary rocks into coarse-grained weathered Late Silurian basement (Carstens, 2011). Furthermore, a continuation of weathered basement offshore under Mesozoic basement was revealed by seismic data (see e.g. Japsen et al., 2008).

Dating of the preserved remains of saprolites onshore would probably give very old ages relative to the range of age assumed by the former extent of the saprolite layers. The identification of sediments derived from saprolites in the upper Molo Fm or lower Naust Fm would exclude the possibility that the weathering is post-glacial, as was discussed by Peulvast (1985).

5.11 Critical consideration of the data

The distribution of well bore records that can be used for correlation and validation of interpretations is sparse at the Molo Fm compared to the extent of the mid-Norwegian shelf. Sampling of the offshore sand grains took place in a range of just a few centimetres at depths of several hundred metres. The probability to find a statistically significant amount of grains derived from the same source is low. What additionally constrained the development of different verified grain classes is the lack of LA-ICP-MS data complementary to the CL images. Due to the general small number of grains, several similar appearing grain groups could not be additionally tested for trace element contents. However, a complete LA-ICP-MS record is beyond the scope of this work. The quality of the existing LA-ICP-MS data depends on the quality of the standards used and hence relies on the certificates provided by the companies.

Despite all uncertainties, the results have shown that clear trends and patterns in depositional units can be revealed by the analytical methods applied. With the presented combination of methods it seems feasible to identify source and sink material that belongs together independently of time and travel distance.

6. SYNTHESIS AND OUTLOOK

6.1 Summary and conclusion

Geochemical properties of quartz grains reflect the plutonic and metamorphic history of the rocks from which they are derived. On a larger scale, changes in sedimentological deposits reflect changes of the geography in the source area. This Master thesis demonstrated and illustrated capabilities and difficulties of a multi-methodological analytical approach for qualitative sediment provenance studies. The combination of scanning by using a scanning electron microscope equipped with a CL detector as well as trace element analysis by means of LA-ICP-MS allows detailed characterisation of quartz grains within siliciclastic sediments. The characteristics were used to identify common and less common quartz grain types in 6 samples from 3 offshore exploration wells drilled into the Molo Fm on the mid-Norwegian shelf (6610/3-1, 6610/7-1, 6510/2-1). The obtained overview was further used for a systematic comparison with potential source material from the mainland of Norway, namely saprolitic bedrock samples from Hadseløya and Hamarøy, as well as weathered offshore bedrock samples from the Froan Basin (well 6408/12-U-01) and Ribban Basin (well 6814/4-U-1).

Despite all difficulties and controversies, both geologically as well as methodologically, clear trends and indications in the investigated data appeared that proved the potential and applicability of the method combination. It was illustrated that quartz grains feature an extremely high diversity in both CL properties and trace element contents and distribution. Al and Ti could be confirmed as most common trace elements in natural quartz. Besides the two, the study focused on Li and Ge, all being common structurally bound trace elements in quartz and indicative for their crystallization environment.

Based on the CL and trace element characteristics, seven generic types of plutonic and metamorphic quartz grains were distinguished that were interpreted to represent different magmatic/metamorphic provinces. A supposedly large number of different crystalline basement provinces contributed to the sediments deposited on the Norwegian Shelf. The compositional variation within the samples is evidence for weathering and erosion acting on plutonic as well

as metamorphic rocks. The variety seems to represent the complex interplay of the Caledonian nappes with the Precambrian basement. Caledonian provinces may have contributed less sediments to the Molo Fm as most of the investigated grains were classified as plutonic originating from the Precambrian basement. Nevertheless, an overlap of quartz types within the cores and among the cores implies common sources and hence common sediment catchment areas for a depositional sink spanning at least 130 km horizontally and 500 m vertically.

The saprolitic outcrops on Hamarøy and Hadseløya are remains of weathered basement and represent Mesozoic weathering of previously much greater extent. The outcrops display weathering states close to the saprolite-basement transition (zone IV, see Fig. 4), which is in contrast to the basement sampled at the Froan and Ribban basins. The weathered basement here is protected by Mesozoic sedimentary rocks and sediments that are absent at the uplifted and glacially eroded mainland.

The geochemical and luminescence properties of the quartz grains sampled from the Molo Formation do not correspond to those studied in saprolitic sand and mangerite thin sections sampled from outcrops onshore on Hadseløya and Hamarøy. It is concluded that no significant amounts of weathering products from presently exposed saprolites are deposited in the Molo Fm. More distinct affiliation is identified among weathered bedrock samples from the Froan Basin (6408/12-U-01) and the sand from the Molo Fm. This suggests (1) an east-west sediment input from the mainland and subsequent distribution alongshore towards north-east and (2), assuming that Mesozoic deposits found offshore likewise existed on the basement that is eroded and uplifted above sea level today, stronger weathered (uppermost) saprolitic material can be expected in the Molo Fm.

The supposed absence of saprolite related sediments in the Molo Fm suggests that the material was significantly eroded when the Plio-Pleistocene glaciations commenced and glaciers removed the Mesozoic cover on the Baltic Shield. Consequently, remains of eroded saprolites are expected to be deposited in the Naust Formation. This hypothesis can be tested with the presented combination of methods.

6.2 Outlook

The techniques described in this Master thesis are highly sophisticated and are state of the art in geologic research. Potential for improvement concerns the implementation and, most importantly, the scope of the work. A compilation of quartz grain classes and subtypes was achievable but confined by a lack of data. It is inevitable to include a higher number of samples and grains per sample in order to establish statistically reasonable and consistent quartz grain categories.

Due to extensive oil and gas exploration on the Norwegian Sea continental shelf, an abundance of drill cores with a great deal of data from the shelf exists. Those potentially provide a repository for a large-scale provenance study using a similar approach. However, the availability of suitable onshore samples is limited by the sparse occurrence of weathered basement rocks or sediments on the mainland of Norway. A comprehensive study in a similar way requires a database with plenty of data of both CL scans and LA-ICP-MS data, preferably for the entire Norwegian coast.

In order to obtain a more comprehensive picture it would be reasonable to include further saprolites occurrences from different locations (e.g. Vestvågøya, Andøya, Inderøya, Vågsøy-Stad, see Olesen et al., 2012), especially samples from different weathering zones, preferably zone I and II (see Fig. 4). In order to confirm the source-sink connection between the basement of the Froan Basin and the Molo Fm, it is suggested to further investigate the wells located in the more southern parts of the Molo Fm (i.e. 6407/9-1, 6407/9-2, and 6407/9-5), which lie closer to well 6408/12-U-01 (sample 10) (see Fig. 22). Results obtained by the presented combined methods would provide validation or falsification for the suggested northward sediment transport direction and would give implications for the uplift history of the adjacent mainland. It is further suggested to include samples from more shallow depths within the range of the Naust Fm. Quartz grains within the Naust Fm can shed light on the erosion and deposition history of saprolites. Moreover, the assumed amounts of deposited saprolitic material in the Naust Fm has implications for the former extent of the weathered basement. The same wells as the ones sampled for this thesis can be used on that account: well 6610/7-1 reached the top of the Molo Fm at 890 m depth, well 6610/3-1 at 349 m, and well 6510/2-1 at 441 m depth. All wells penetrated the Naust Fm and are suitable for a vertical extension of the study.

Geologists have already mapped the mainland of Norway in terms of basement rock and Quaternary sediment cover. The basement is represented by several plutons that constitute unique magmatic provinces, which are further subdivided into countless sub-intrusions. Given that all plutons feature unique geochemical and luminescence properties, which can be illustrated by the presented methods, all sediments deposited on the shelf are theoretically assignable to specific plutons. A new dimension of geological mapping would emerge if sediment formations or even individual units of formations at the shelf could be directly assigned to specific magmatic provinces on the mainland. The diversity of the presented data suggests that several sources play a role for each depositional unit. The global and regional ocean current patterns further suggest expanding the potential provenance areas of sediments on the Norwegian shelf to adjacent continental masses, especially when deeper depositional areas are investigated. Comprehensive mapping of source-to-sink connections would significantly increase our knowledge of the influence of bottom currents and palaeo-bottom currents on sediment distribution, including contourite drifts.

The resistate mineral quartz is a useful object for provenance studies. This study distinctly illustrates the uniqueness of quartz grains and the associated practicality for provenance studies. This study was focused on quartz as the only examination object, while other minerals such as feldspar were also present in the samples. Quartz is stable in a large range of pressure and temperature conditions. This bears advantages, but also disadvantages. Stable minerals can outlast several sedimentary recycling phases which complicates the identification of the primary source. Less stable mineral groups such as feldspars can give a more straightforward indication under certain circumstances. The applicability of feldspar analyses for provenance studies has recently been re-evaluated by Scholonek & Augustsson (2016).

Müller & Knies (2013) introduced the combined methods presented in this study as a new proxy for IRD at Svalbard. The Svalbard area provides a convenient setting for comparison with the Norwegian mainland since the archipelago belongs to the Caledonian orogen (bed-rock comparability) and at the same time still possesses a well preserved sedimentological succession ranging from Archaean to present time (Dallmann, 2007). The quartz grain classification presented by Müller & Knies (2013) is restricted to their study area. The classification presented here is likewise restricted to the study area on the mid-Norwegian shelf. With an

increasing number of similar studies in and around both study areas, an overlap in quartz grain properties is expected to emerge. The high amounts of low-grade metamorphic grains with dull CL signals reported by Müller & Knies (2013) are in contrast to the low amounts of similar grains in this study. Transect-based sampling could potentially find some sort of border or defined transition area between both depositional areas.

The number of elements included in LA-ICP-MS studies is confined by the present technology of mass spectrometry. LOD's might reach closer to zero in the future which would allow the incorporation of more elements that usually lie below the present LOD. The more elements are included, the more accurate the mineralogical fingerprint becomes. Lattice-bound trace elements cannot be removed from quartz today (Müller et al., 2015) but might be removable in the future. Technological progress of the presented equipment is of interest not only for geologists, as high-purity quartz finds plenty of economically relevant fields of applications. Similar provenance studies are not restricted to sediments but can also be applied in archaeology (e.g. provenance of quartz-containing pottery, Picouet et al., 1999). In fact, the application of the methods, especially of CL scanning, is not even restricted to studies on Earth, as was pointed out by Schieber et al., 2002 (see also Gucsik, 2009).

7. REFERENCES

- Andersen, T. B., & Jamtveit, B., (1990): Uplift of deep crust during orogenic extensional collapse: A model based on field studies in the Sogn-Sunnfjord region of western Norway. *Tectonics*, 9, 1097-1111.
- Andersen, A. & Tull, J. F., (1983): The age of the Lødingen granite and its possible regional significance. *Norsk Geologisk Tidsskrift*, 4, 269-276.
- Andresen, A. & Tull, J., (1986): Age and tectonic setting of the Tysfjord gneiss granite, Eufjord, North Norway. *Norsk Geologisk Tidsskrift*, 66, 69-80.
- Andrews, J. T., (1979): The present ice age: Cenozoic. In: John, B. S. (ed.): *The winters of the world*: Newton Abbott, UK, David and Charles, 173-218.
- Andrews, J. T., (1982): New evidence from beneath the western North Atlantic for the depth of glacial erosion in Greenland and North America: Comment. *Quaternary Research*, 17, 123-124.
- Anell, I., Thybo, H. & Artemieva, I. M., (2009): Cenozoic uplift and subsidence in the North Atlantic region: Geological evidence revisited. *Tectonophysics*, 474, 78-105.
- Bell, M. & Laine, E. P., (1985): Erosion of the Laurentide region of North America by glacial and glaciofluvial processes. *Quaternary Research*, 23, 154-174.
- Bergh, S. G., Eig, K., Kløvjan, O. S., Henningsen, T., Olesen, O. & Hansen, J. A., (2007): The Lofoten-Vesterålen continental margin: a multiphase Mesozoic-Palaeogene rifted shelf as shown by offshore-onshore brittle fault-fracture analysis. *Norwegian Journal of Geology*, 87, 29-58.
- Bernet, M. & Bassett, K., (2005): Provenance Analysis by single-quartz-grain SEM/CL/Optical Microscopy. *Journal of Sedimentary Research*, 75, 492-500.
- Bingen, B., Nordgulen, Ø. & Viola, G., (2008): A four-phase model for the Sveconorwegian orogeny, SW Scandinavia. *Norwegian Journal of Geology*, 88, 43-72.
- Blankenburg, H.-J., Götze, J., Schulz, H., (1994): *Quarzzrohstoffe*. Deutscher Verlag für Grundstoffindustrie, Leipzig-Stuttgart, 296 pp.
- Blystad, P., Brekke, H., Færseth, R. B., Larsen, B. T., Skogseid, J. & Tøruðbakken, B., (1995): Structural elements of the Norwegian continental shelf. Part II: The Norwegian Sea Region, Plate I, *NPD-Bulletin*, 8.
- Boggs, S. & Krinsley, D., (2006): *Application of Cathodoluminescence Imaging to the Study of Sedimentary Rocks*. Cambridge University Press. New York.
- Brekke, H., (2000): The tectonic evolution of the Norwegian Sea Continental Margin with emphasis on the Vøring and Møre Basins. Geological Society, London, Special Publications, 167, 327-378.

- Bryn, P., Berg, K., Stoker, M. S., Hafliðason, H. & Solheim, A., (2005): Contourites and their relevance for mass wasting along the Mid-Norwegian Margin. *Marine and Petroleum Geology*, 22, 85-96.
- Büdel, J., (1982): Climatic geomorphology (translation from German of 1977). Princeton: Princeton University Press. 443 pp.
- Bugge, T., Lien, R. & Rokoengen, K., (1976): Kartlegging av de prekvartære lag utenfor Møre – Trøndelag (63°-65°N). Continental Shelf Institute, Norway, (IKU) 69, 1-47.
- Bullimore, S., Henriksen, S., Liestøl, F. M. & Helland-Hansen, W., (2005): Clinoform stacking patterns, shelf-edge trajectories and facies associations in Tertiary coastal deltas, o-shore Norway: Implications for the prediction of lithology in prograding systems. *Norwegian Journal of Geology*, 85, 169-187.
- Bungum, H., Olesen, O., Pascal, C., Gibbons, S., Lindholm, C. & Vestøl, O., (2010): To what extent is the present seismicity of Norway driven by post-glacial rebound? *Journal of the Geological Society*, 167, 373-384.
- Burov, E., Poliakov, A., (2001): Erosion and rheology controls on synrift and postrift evolution: Verifying old and new ideas using a fully coupled numerical model. *Journal of Geophysical Research*, 106 (B8), 16,461-16,481.
- Bøe, R., Smelror, M., Davidsen, B., & Walderhaug, O., (2008): Nearshore Mesozoic basins off Nordland, Norway: Structure, age and sedimentary environment. *Marine and Petroleum Geology*, 25, 235-253.
- Bøe, R., Fossen, H., and Smelror, M., (2010): Mesozoic sediments and structures onshore Norway and in the coastal zone: *Norges Geologiske Undersøkelse Bulletin*, 450, 15-32.
- Carstens, H., (2011): Reservoaranalog – midt inne i skauen. *GEO*, 8, 10-15.
- Cohen, K. M., Finney, S. C., Gibbard, P. L. & Fan, J.-X. (2013; updated): The ICS International Chronostratigraphic Chart. *Episodes*, 36, 199-204.
- Corfu, F., (2004): Pb Age, Setting and Tectonic Significance of the Anorthosite–Mangerite–Charnockite–Granite Suite, Lofoten–Vesterålen, Norway. *Journal of Petrology*, 45, 1799-1819.
- Dahlgren, K. I., Vorren, T. O. & Laberg, J. S., (2002). Late Quaternary glacial development of the mid-Norwegian margin - 65 to 68°N. *Marine and Petroleum Geology*, 19, 1089-1113.
- Dalland, A., (1975). The Mesozoic rocks of Andøy, northern Norway. *Norges Geologiske Undersøkelse Bulletin*, 316, 271-287.
- Dalland, A., (1981): Mesozoic sedimentary succession at Andøya, Northern Norway, and relation to structural development of the North Atlantic area. In Kerr, J. W. & Fergusson, A. J. (eds.): *Geology of the North Atlantic borderlands. Canadian Society Petroleum Geologist Memoir*, 7, 563-584.

- Dallmann, W. K., (2007): Geology of Svalbard. In: Geology of the land and sea areas of Northern Europe: a collection of short descriptions of the geology of countries and sea areas within the region covered by the 1:4 million bedrock geological map. Ellen M. O. Sigmond, E. M. O., & Roberts, D. (eds.). *Geological Survey of Norway, Special Publication*, 10, 87-89.
- Dennen, W. H., (1967): Trace elements in quartz as indicators of provenance. *Geological Society of America Bulletin*, 78, 125-130.
- Dowdeswell, J. A., & Siegert, M. J., (1999): Ice-sheet numerical modelling and marine geophysical measurements of glacier-derived sedimentation on the Eurasian Arctic continental margins. *Geological Society of America Bulletin*, 111, 1080-1097.
- Dowdeswell, J. A., Ottesen, D., Rise, L., & Craig, J., (2007): Identification and preservation of landforms diagnostic of past ice-sheet activity on continental shelves from three-dimensional seismic Evidence. *Geology*, 35, 359-362.
- Dowdeswell, J. A., Ottesen, D. & Rise, L., (2010): Rates of sediment delivery from the Fennoscandian Ice Sheet through an ice age. *Geology*, 38, 3-6.
- Drever, J. I. (1994): The effect of land plants on weathering rates of silicate minerals. *Geochimica et Cosmochimica Acta*, 58, 2325-2332.
- Dusel-Bacon, C., (2012): Petrology of metamorphic rocks associated with volcanogenic massive sulfide deposits. In: Pat Shanks, W. C. III & Thurston, R., (eds.) (2012): Volcanogenic massive sulfide occurrence model. *U.S. Geological Survey Scientific Investigations Report 2010–5070–C*, 345 pp. 275-288.
- Eidvin, T., Brekke, H., Riis, F. & Renshaw, D. K., (1998): Cenozoic Stratigraphy of the Norwegian Sea continental shelf, 64°N-68°N. *Norsk Geologisk Tidsskrift*, 78, 125-151.
- Eidvin, T., Bugge, T. & Smelror, M., (2007): The Molo Formation, deposited by coastal progradation on the inner Mid-Norwegian continental shelf, coeval with the Kai Formation to the west and the Utsira Formation in the North Sea. *Norwegian Journal of Geology*, 87, 75-142.
- Eidvin, T., Riis, F., Rasmussen, E. S. & Rundberg, Y., (2013): Investigation of Oligocene to Lower Pliocene deposits in the Nordic area. NPD Bulletin no 10. Available from the Internet: http://www.npd.no/engelsk/cwi/pbl/NPD_papers/Hyperlink-NPDBulletin-10.pdf (accessed 16.02.16).
- Eidvin, T., Riis, F. & Rasmussen, E. S., (2014): Oligocene to Lower Pliocene deposits of the Norwegian continental shelf, Norwegian Sea, Svalbard, Denmark and their relation to the uplift of Fennoscandia: A synthesis. *Marine and Petroleum Geology*, 56, 184-221.
- Eldholm, O. & Nysæther, E., (1968): Seismiske undersøkelser på den norske kontinentalsokkel 1968, del C. Seismol. Observ. University of Bergen, 29.
- Eskola, P. E., (1920): The mineral facies of rocks. *Norsk geologisk tidsskrift*, 6, 143-194.

- Faleide, J. I., Tsikalas, F., Breivik, A. J., Mjelde, R., Ritzmann, O., Engen, Ø., Wilson, J. & Eldholm, O., (2008): Structure and evolution of the continental margin off Norway and Barents Sea. *Episodes*, 31, 82-91.
- Fitzpatrick, E. A., (1963): Deeply weathered rock in Scotland, its occurrence, age and contribution to the soils. *Journal of Soil Science*, 14, 33-43.
- Fjeldskaar, W., Lindholm, C., Dehls, J. F., Fjeldskaar, I., (2000): Postglacial uplift, neotectonics and seismicity in Fennoscandia. *Quaternary Science Reviews*, 19, 1413-1422.
- Flem, B. & Müller, A., (2012): In Situ Analysis of Trace Elements in Quartz Using Laser Ablation Inductively Coupled Plasma Mass Spectrometry. In: Götze, J., & Möckel, R. (eds.): Quartz: Deposits, mineralogy and analytics: Berlin, Heidelberg, Springer Geology, 219-236.
- Fredin, O., Bergstrøm, B., Eilertsen, R., Hansen, L., Longva, O., Nesje, A. & Sveian, H., (2013): Glacial landforms and Quaternary landscape development in Norway. In: Olsen, L., Fredin, O. & Olesen, O. (eds.): Quaternary Geology of Norway, *Geological Survey of Norway Special Publication*, 13, 5-25.
- Gee, D. G., (1975): A tectonic model for the central part of the Scandinavian Caledonides. *American Journal of Science*, 275A, 468-515.
- Gee, D. G., Fossen, H., Henriksen, N., Higgins, A. K., (2008): From the Early Paleozoic Platforms of Baltica and Laurentia to the Caledonide Orogen of Scandinavia and Greenland. *Episodes*, 31, 44-51.
- Gee, D. G., Juhlin, C., Pascal, C. & Robinson, P., (2010): Collisional Orogeny in the Scandinavian Caledonides (COSC). *GFF*, 132, 29-44.
- Gee, D. G. & Sturt, B. A, (1985): The Caledonide Orogen – Scandinavia and Related Areas. John Wiley & Sons, Chichester, 1266 pp.
- Gerler, J., (1990): Geochemische Untersuchungen an hydrothermalen, metamorphen, granitischen und pegmatitischen Quarzen und deren Flüssigkeitseinschlüssen. Ph.D. Thesis, University of Göttingen, Germany, 169 pp.
- Google Earth ver. 7.1.5.1557 (2013): Scandinavia, North-Western Norway. Data SIO, NOAA, U.S. Navy, NGA, GEBCO Image Landsat. Accessed: 14.4.2016.
- Gorbatshev, R., & Bogdanova, S., (1993): Frontiers in the Baltic Shield. *Precambrian Research*, 64, 3-21.
- Gorbatshev, R., (2004): The Transscandinavian Igneous Belt - introduction and background. In: Högdahl, K., Andersson, U. B. & Eklund, O. (eds): The Transscandinavian Igneous Belt (TIB) in Sweden: a review of its character and evolution. *Geological Survey of Finland, Special Paper*, 37, 9-15.
- Götze, J., (2000): Cathodoluminescence in applied Geosciences. In: Pagel, M., Barbin, V., Blanc, P. & Ohnenstetter, D. (eds.): Cathodoluminescence in Geosciences. Springer Berlin Heidelberg, 457-479.

- Götze, J. & Zimmerle, W., (2000): Quartz and silica as guide to provenance in sediments and sedimentary rocks. *Contributions to Sedimentary Geology*, 21, 1-91.
- Götze, J., Plötze, M. & Habermann, D., (2001): Origin, spectral characteristics and practical applications of the cathodoluminescence (CL) of quartz - a review. *Mineralogy and Petrology* 71, 225-250.
- Götze J., Plötze, M., Graupner, T., Hallbauer, D. K. & Bray, C., (2004): Trace element incorporation into quartz: a combined study by ICP-MS, electron spin resonance, cathodoluminescence, capillary ion analysis and gas chromatography. *Geochimica et Cosmochimica Acta*, 68, 3741-3759.
- Götze, J., (2009): Chemistry, textures and physical properties of quartz - geological interpretation and technical application. *Mineralogical Magazine*, 73, 645-671.
- Götze, J., (2012a): Classification, Mineralogy and Industrial Potential of SiO₂ Minerals and Rocks. In: Götze, J., & Möckel, R. (eds.): Quartz: Deposits, mineralogy and analytics: Berlin, Heidelberg, Springer Geology, 71-118.
- Götze, J., (2012b): Application of Cathodoluminescence Microscopy and Spectroscopy in Geosciences. *Microscopy and Microanalysis*, 18, 1270-1284.
- Grant, W. H., (1963): Weathering of Stone Mountain Granite. In: Ingersoll, E. C., (ed): Clays and Clay Minerals, 11, 65-73.
- Gregersen, S., & Voss, P., (2010): Irregularities in Scandinavian postglacial uplift/subsidence in time scales tens, hundreds, thousands of years. *Journal of Geodynamics*, 50, 27-31.
- Gregersen, U. & Johannessen, P. N., (2007): Distribution of the Neogene Utsira Sand and Hutton Sand, and the succeeding deposits in the Viking Graben area, North Sea. *Marine and Petroleum Geology*, 24, 591-606.
- Griffin, W. L., Taylor, P. N., Hakkinen, J. W., Heier, K. S., Iden, I. K., Krogh, E. J., Malm, O., Olesen, K. I., Ormaasen, D. E., & Tveten, E., (1978): Archaean and Proterozoic crustal evolution in Lofoten-Vesterålen, N. Norway. *Journal of the Geological Society of London*, 135, 629-647.
- Griffin, W. L., & Brueckner, H. K., (1980): Caledonian Sm-Nd ages and a crustal origin for Norwegian eclogites. *Nature*, 285, 319-321.
- Gucsik, A. (ed.) (2009): Cathodoluminescence and its Application in the Planetary Sciences, Springer-Verlag Berlin, Heidelberg. 160 pp.
- Gustavson, M. & Bugge, T., (1995): Geologisk kart over Norge, berggrunnskart VEGA, M 1:250 000. *Norges geologiske undersøkelse*.
- Gutenberg, B., (1941): Changes in sea level, postglacial uplift and mobility of the Earth's interior. *Geological Society of America Bulletin*, 52, 721.
- Hall, A. M., (1985): Cenozoic weathering covers in Buchan, Scotland and their significance. *Nature*, 315, 392-395.

- Hall, A. M., Ebert, K., Kleman, J., Nesje, A. & Ottesen, D., (2013): Selective glacial erosion on the Norwegian passive margin. *Geology*, 41, 1203-1206.
- Hansen, B. & Østerhus, S., (2000). North Atlantic–Nordic Seas exchanges. *Progress in Oceanography*, 45, 109-208.
- Holbourn, A. E., Kuhnt, W., Kochhann, K. G. D., Andersen, N., & Meier, S., (2015): Global perturbation of the carbon cycle at the onset of the Miocene Climatic Optimum. *Geology*, 43, 123-126
- Holdaway, M. J., (1971): Stability of andalusite and the aluminum silicate phase diagram. *American Journal of Science*, 271, 97-131.
- Holtedahl, H., (1998): The Norwegian strandflat – a geomorphological puzzle. *Norsk Geologisk Tidsskrift*, 78, 47-66.
- Jansen, E., & Sjøholm, J., (1991): Reconstruction of glaciation over the past 6 Myr from ice-borne deposits in the Norwegian Sea. *Nature*, 349, 600-603.
- Jansen, E., (1993): Miocen og pliocen sedimentasjon og paleomiljø på Vøringplatået. Rapp. Oljedirektoratet. Univ. Bergen, 10 pp.
- Japsen, P. & Chalmers, J. A., (2000): Neogene uplift and tectonics around the North Atlantic: overview. *Global and Planetary Change*, 24, 165-173.
- Japsen, P., Bidstrup, T. & Lidmar-Bergström, K., (2002): Neogene uplift and erosion of southern Scandinavia induced by the rise of the South Swedish Dome. In: Doré, A. G., Cartwright, J. Stoker, M. S., Turner, J. P. & White N. (Eds.): Exhumation of the North Atlantic Margin: Timing, Mechanisms and Implications for Petroleum Exploration. *Geological Society, London, Special Publications*, 196, 183-207.
- Japsen, P., Bonow, J. M., Chalmers, J. A. & Rasmussen, E. S., (2008): Norges fjelde - rodløse realiteter. *Geologisk Nyt*, 2, 38-40.
- Jourdan, A.-L., Vennemann, T. W., Mullis, J., Ramseyer, K. & Spiers, C. J., (2009): Evidence of growth and sector zoning in hydrothermal quartz from Alpine veins. *European Journal of Mineralogy*, 21, 219-231.
- Kejonen, A., (1985): Weathering in the Wyborg rapakivi area, southeastern Finland. *Fennia*, 163, 309-313.
- Klein, A. & Steltenpohl, M. G., (1999): Basement-cover relations and late- to post-Caledonian extension in the Leknes group, west-central Vestvågøy, Lofoten, north Norway. *Norges Geologisk Tidsskrift*, 79, 19-31.
- Kleman, J., (1994): Preservation of landforms under ice sheets and ice caps. *Geomorphology*, 9, 19-32.
- Kleman, J. & Stroeven, A. P., (1997): Preglacial surface remnants and Quaternary glacial regimes in northwestern Sweden. *Geomorphology*, 19, 35-54.

- Krauss, W., (1986): The North Atlantic Current. *Journal of Geophysical Research*, 91, 5061-5074.
- Kwon, Y. I. & Boggs, S., (2002): Provenance interpretation of Tertiary sandstones from the Cheju Basin (NE East China Sea): a comparison of conventional petrographic and scanning cathodoluminescence techniques. *Sedimentary Geology*, 152, 29-43.
- Laberg, J. S. & Vorren, T. O., (2000): The Trænadjupet Slide, offshore Norway – morphology, evacuation and triggering mechanisms. *Marine Geology*, 171, 95-114.
- Laberg, J. S., Stoker, M. S., Dahlgren, K. I. T., de Haas, H., Hafliðason, H., Hjelstuen, B. O., Nielsen, T., Shannon, P., Vorren, T. O. & van Weering, T. C. E., (2005a): Cenozoic alongslope processes and sedimentation along the NW European Atlantic margin. *Marine and Petroleum Geology*, 22, 1069-1088.
- Laberg, J. S., Dahlgren, K. I. T. & Vorren, T. O., (2005b): The Eocene-late Pliocene paleoenvironment in the Vøring Plateau area, Norwegian Sea - paleoceanographic implications. *Marine Geology*, 269-285.
- Laberg, J. S., Eilertsen R. S. & Vorren, T. O., (2009): The paleo-ice stream in Vestfjorden, north Norway, over the last 35 k.y.: Glacial erosion and sediment yield. *Geological Society of America Bulletin*, 121, 434-447.
- Lahtinen, R., Garde, A. A. & Melezhik, V. A., (2008): Paleoproterozoic evolution of Fennoscandia and Greenland. *Episodes*, 31, 20-28.
- Lahtinen, R., Korja, A., Nironen, M. & Heikkinen, P., (2009). Palaeoproterozoic accretionary processes in Fennoscandia. In: Cawood, P. A. & Kröner, A. (eds.): *Earth Accretionary Systems in Space and Time. Geological Society of London, Special Publication*, 318, 237-256.
- Larsen, E. & Holtedahl, H., (1985): The Norwegian strandflat: A reconsideration of its age and origin. *Norsk Geologisk Tidsskrift*, 65, 247-254.
- Lidmar-Bergström, K., (1982): Pre-Quaternary geomorphological evolution in southern Fennoscandia. Meddelanden från Lunds Universitets Geografiska Institution. Avhandlingar 91/Sveriges Geologiska Understknig C 785.
- Lidmar-Bergström, K., (1988): Denudation surfaces of a shield area in south Sweden. *Geografiska Annaler*, 70A (4), 337-350.
- Lidmar-Bergström, K., (1995): Relief and saprolites through time on the Baltic Shield. *Geomorphology*, 12, 45-61.
- Lidmar-Bergström, K., (1999): Uplift histories revealed by landforms of the Scandinavian domes. In: Smith, B. J., Whalley, W. B. & Warke, P. A. (eds.): *Uplift, Erosion and Stability: Perspectives on Long-term Landscape Development*, 85-91. *Geological Society, London, Special Publications* 162, 85-91.

- Lidmar-Bergström, K., Olsson, S. & Roaldset, E., (1999): Relief features and palaeoweathering remnants in formerly glaciated Scandinavian basement areas. In: Thiry, M. & Simon-Coinçon, R. (eds.): Palaeoweathering, palaeosurfaces and related continental deposits, International Association of Sedimentologists (IAS) Special publication 27, 275-301.
- Lidmar-Bergström, K., Bonow, J. M. & Japsen, P., (2013): Stratigraphic Landscape Analysis and geomorphological paradigms: Scandinavia as an example of Phanerozoic uplift and subsidence. *Global and Planetary Change*, 100, 153-171.
- Lorentzen, T., (2015): A statistical analysis of sea temperature data. *Theoretical and Applied Climatology*, 119, 585-610.
- Løseth, H. & Henriksen, S., (2005): A Middle to Late Miocene compression phase along the Norwegian passive margin. In: Doré, A. G. & Vining, B. A. (eds.): Petroleum Geology: North-West Europe and Global Perspectives-proceedings of the 6th Petroleum Geology Conference, 845-859.
- Lundqvist, T., Bøe, R., Kousa, J., Lukkarinen, H., Lutro, O., Roberts, D., Solli, A., Stephens, M. & Weihed, P. (1996): Bedrock map of Central Fennoscandia. Scale 1:1000 000. Geological Surveys of Finland (Espoo), Norway (Trondheim) and Sweden (Uppsala).
- Magnitsky, V. A., (1967): Postglacial Uplift of Scandinavia and Physical Nature of Viscosity of the Earth's Upper Mantle. *Geophysical Journal of the Royal Astronomical Society*, 14, 245-249.
- McKerrow, W. S., Mac Niocaill, C. & Dewey, J. F., (2000): The Caledonian Orogeny redefined. *Journal of the Geological Society*, 157, 1149-1154.
- Meteorologisk institutt, (2016): The climate of Norway (Norwegian Meteorological Institute (http://www.met.no/English/Climate_in_Norway/) (accessed: 03.02.2016).
- Mosar, J., Lewis, G. & Torsvik, T. H., (2002a): North Atlantic sea-floor spreading rates: implications for the Tertiary development of inversion structures of the Norwegian–Greenland Sea. *Journal of the Geological Society*, 159, 503-515.
- Mosar, J., Eide, E. A., Osmundsen, P. T., Sommaruga, A. & Torsvik, T. H., (2002b): Greenland–Norway separation: a geodynamic model for the North Atlantic. *Norwegian Journal of Geology*, 82, 281-298.
- Müller, A., (2000): Cathodoluminescence and characterisation of defect structures in quartz with applications to the study of granitic rocks. Ph.D. Thesis, University of Göttingen, Germany, 228 pp.
- Müller A., Lennox P., Trzebski, R., (2002): Cathodoluminescence and micro-structural evidence for crystallization and deformation processes of granites in the Eastern Lachlan Fold Belt (SE Australia). *Contributions to Mineralogy and Petrology*, 143, 510-524.
- Müller A., Wiedenbeck, M., Van den Kerkhof, A.M., Kronz, A. & Simon, K., (2003): Trace elements in Quartz - a combined electron microprobe, secondary ion mass spectrometry, laser-ablation ICP-MS, and cathodoluminescence study. *European Journal of Mineralogy*, 15, 747-763.

- Müller, A., Wanvik, J. E. & Ihlen, P. M., (2012): Petrological and chemical characterisation of high-purity quartz deposits with examples from Norway. In: Götze, J., & Möckel, R., (eds.): *Quartz: Deposits, mineralogy and analytics*: Berlin, Heidelberg, Springer Geology, 71-118.
- Müller, A. & Knies, J., (2013): Trace elements and cathodoluminescence of detrital quartz in Arctic marine sediments – a new ice-rafted debris provenance proxy. *Climate of the Past*, 9, 2615-2630.
- Müller, A., Ihlen, P. M., Snook, B., Larsen, R. B., Flem, B., Bingen, B. & Williamson, B. J., (2015): The Chemistry of Quartz in Granitic Pegmatites of Southern Norway: Petrogenetic and Economic Implications. *Economic Geology*, 110, 1737-1757.
- Müller, A., (2015): Evaluation of samples from drill cores 6814-04-U-01 and 6408-12-U-01 at the contact of basement rocks and sediment cover. Unpublished NGU Report, 6 pp.
- Mørk, M. B. E. & Johnsen, S. O., (2005): Jurassic sandstone provenance and basement erosion in the Møre margin – Froan Basin area. *Norges geologiske undersøkelse Bulletin*, 443, 5-18.
- Nansen, F., (1922): The strandflat and isostasy. Skrifter Videnskapselskapet i Kristiania. *Matematisk-Naturvitenskaplig klasse*, 2, 1-313.
- Nesbitt, H. W. & Young, G. M., (1984): Prediction of some weathering trends of plutonic and volcanic rocks based on thermodynamic and kinetic considerations. *Geochimica et Cosmochimica Acta*, 48, 1523-1534.
- Nesbitt, H. W., Young, G. M., McLennan, S. M. & Keays, R. R., (1996): Effects of chemical weathering and sorting on the petrogenesis of siliciclastic sediments, with implications for provenance studies. *The Journal of Geology*, 104, 525-542.
- Nesbitt, H. W., Fedo, C. M., Young, G. M., (1997): Quartz and Feldspar Stability, Steady and Non-steady-State Weathering, and Petrogenesis of Siliciclastic Sands and Muds. *The Journal of Geology*, 105, 173-191.
- Nesbitt, H. W., (2003): Petrogenesis of siliciclastic sediments and sedimentary rocks. In: Lentz, D. R., (ed.): *Geochemistry of Sediments and Sedimentary Rocks: Evolutionary Considerations to Mineral Deposit-Forming Environments*. *Geological Association of Canada*, Vol. 41D - 38, 39-51.
- Nesje, A., Dahl, S. O., Anda, E. & Rye, N., (1988): Block fields in southern Norway: Significance for the Late Weichselian ice sheet. *Norsk Geologisk Tidsskrift*, 68, 149-169.
- NGU – Geological Survey of Norway (2016): Norway through time. (<https://www.ngu.no/en/topic/norway-through-time>) (accessed: 06.04.2016).
- Nielsen, S. B., Paulsen, G. E., Hansen, D. L., Gemmer, L., Clausen, O. R., Jacobsen, B. H., Balling, N., Huuse, M. & Gallagher, K., (2002): Paleocene initiation of Cenozoic uplift in Norway. In: Doré, A. E., Cartwright, J., Stoker, M. S., Turner, J. P. & White, N. (Eds.): *Exhumation of the North Atlantic Margin: Timing, Mechanisms and Implications for Petroleum Generation*. *Geological Society, Special Publications*, London, 196, 45-65.

- Nielsen, S. B., Gallagher, K., Leighton, C., Balling, N., Svenningsen, L., Jacobsen, B. H., Thomsen, E., Nielsen, O. B., Heilmann-Clausen, C., Egholm, D. L., Summerfield, M. A., Clausen, O. R., Piotrowski, J. A., Thorsen, M. R., Huuse, M., Abrahamsen, N., King, C. & Lykke-Andersen, H., (2009): The evolution of western Scandinavian topography: a review of Neogene uplift versus the ICE (isostasy-climate-erosion) hypothesis. *Journal of Geodynamics*, 47, 72-95.
- NPD - Norwegian Petroleum Directorate, (2016): Factpages. (<http://factpages.npd.no>) (accessed: 07.09.2015).
- Olesen, O., Torsvik, T. H., Tveten, E., Zwaan, K. B., Løseth H. & Henningsen, T., (1997): Basement structure of the continental margin in the Lofoten–Lopphavet area, northern Norway: constraints from potential field data, on-land structural mapping and palaeomagnetic data. *Norsk Geologisk Tidsskrift*, 77, 15-33.
- Olesen, O., Dehls, J. F., Ebbing, J., Henriksen, H., Kihle, O. & Lundin, E., (2007): Aeromagnetic mapping of deep-weathered fracture zones in the Oslo Region – a new tool for improved planning of tunnels. *Norwegian Journal of Geology*, 87, 253-267.
- Olesen, O., Gellin, J., Gernigon, L., Kihle, O., Koziel, J., Lauritsen, T., Mogaard, J. O., Myklebust, R., Skilbrei, J. R. & Usov, S., (2010): Magnetic anomaly map, Norway and adjacent areas, scale 1:3 millions. *Geological Survey of Norway*.
- Olesen, O., Bering, D., Brønner, M., Dalsegg, E., Fabian, K., Fredin, O., Gellein, J., Husteli, B., Magnus, C., Rønning, J. S., Solbakk, T., Tønnesen J. F. & Øverland, J. A., (2012): Tropical Weathering In Norway, TWIN Final Report. NGU Report 2012.005, 188 pp.
- Olesen, O., Kierulf, H. P., Brønner, M., Dalsegg, E., Fredin, O. & Solbakk, T., (2013): Deep weathering, neotectonics and strandflat formation in Nordland, northern Norway. *Norwegian Journal of Geology*, 93, 189-213.
- Olivarius, M., (2009): Provenance and facies of Miocene sand succession in western Denmark based on bulk geochemistry, heavy minerals and zircon dating. Master's thesis. Department of Geography and Geology, University of Copenhagen.
- Ottesen, D., Rise, L., Knies, J., Olsen, L., Henriksen, S., (2005a): The Vestfjorden-Trænadjupet palaeo-ice stream drainage system, mid-Norwegian continental shelf. *Marine Geology*, 218, 175-189.
- Ottesen, D., Dowdeswell, J. A. & Rise, L., (2005b): Submarine landforms and the reconstruction of fast-flowing ice streams within a large Quaternary ice sheet: The 2500-km-long Norwegian-Svalbard margin (57° - 80°N). *Geological Society of America Bulletin*, 117, 1033-1050.
- Ottesen, D., Rise, L., Andersen, E. S., Bugge, T. & Eidvin, T., (2009): Geological evolution of the Norwegian continental shelf between 61°N and 68°N during the last 3 million years. *Norwegian Journal of Geology*, 89, 251-265.

- Parducci, L., Jørgensen, T., Tollefsrud, M. M., Elverland, E., Alm, T., Fontana, S. L., Bennett, K. D., Haile, J., Matetovici, I., Suyama, Y., Edwards, M. E., Andersen, K., Rasmussen, M., Boessenkool, S., Coissac, E., Brochmann, C., Taberlet, P., Houmark-Nielsen, M., Larsen, N. K., Orlando, L., Gilbert, M. T. P., Kjær, K. H., Alsos, I. G. & Willerslev, E., (2012): Glacial survival of boreal trees in northern Scandinavia. *Science*, 335, 1083-1086.
- Pascal, C., Ebbing, J. & Reidar Skilbrei, J., (2007): Interplay between the Scandes and the Trans-Scandinavian Igneous belt: integrated thermo-rheological and potential field modelling of the Central Scandes profile. *Norwegian Journal of Geology*, 87, 3-12.
- Peulvast, J. P., (1985): In situ weathered rocks on plateaus, slopes and strandflat areas of the Lofoten-Vesterålen, North Norway. *Fennia*, 163, 333-340.
- Peulvast, J. P., (1988): Pre-glacial landform evolution in two coastal high latitude mountains: Lofoten-Vesterålen (Norway) and Scoresby Sund area (Greenland). *Geografiska Annaler* 70A, 351-360.
- Picouet, P., Maggetti, M., Piponnier, D. & Schvoerer, M., (1999): Cathodoluminescence Spectroscopy of Quartz Grains as a Tool for Ceramic Provenance. *Journal of Archaeological Science*, 26, 943-949.
- Plant, J. A., Whittaker, A., Demetriades, A., De Vivo, B. & Lexa, J., (2005): Geological and Tectonic Framework of Europe. In: Salminen, R. (ed): Geochemical Atlas of Europe part 1, Espoo, *Geological Survey of Finland*, 20 pp.
- Pound, M. J., Haywood, A. M., Salzmann, U. & Riding, J. B., (2012) Global vegetation dynamics and latitudinal temperature gradients during the Mid to Late Miocene (15.97–5.33 Ma). *Earth-Science Reviews*, 112, 1-22.
- Powers, M. C., (1953): A new roundness scale for sedimentary particles. *Journal of sedimentary petrology*, 23, 117-119.
- Ramberg, I. B., Bryhni, I., Nøttvedt, A. & Rangnes, K. (eds.) (2008): The Making of a Land – Geology of Norway. Trondheim: Norsk Geologisk Forening.
- Reusch, H. H., (1894): Strandflaten, et nyt trek i Norges Geografi. *Norges geologiske undersøkelse*, 14, 1-14.
- Reusch, H. H., (1901): Nogle bidrag til forstaaelsen af, hvorledes Norges dale og fjelde er blevne til. *Noregs Geologiske Undersøkingar*, 32, 124-217.
- Reusch, H. H., (1903): Betrachtungen über das Relief von Norwegen. *Geographische Zeitschrift*, 8, 425-435.
- Rise, L., Ottesen, D., Berg, K., Lundin, E., (2005): Large-scale development of the mid-Norwegian margin during the last 3 million years. *Marine and Petroleum Geology*, 22, 33-44.
- Riis, F. & Fjeldskaar, W., (1992): On the magnitude of the Late Tertiary and Quaternary erosion and its significance for the uplift of Scandinavia and the Barents Sea. In: Larsen, R. M., Brekke, H., Larsen, B. T. & Talleraas, E (eds.): Structural and Tectonic Modelling and its Application to Petroleum Geology. *Norwegian Petroleum Society Special Publications*, 163-185.

- Riis, F., (1996): Quantification of Cenozoic vertical movements of Scandinavia by correlation of morphological surfaces with offshore data. *Global and Planetary Change*, 12, 331-357.
- Roadset, E., Pettersen, E., Longva, O. & Mangerud, J., (1982): Remnants of preglacial weathering in western Norway. *Norges Geologisk Tidsskrift*, 62, 169-178.
- Roberts, D., (1998): High-strain zones from meso- to macro-scale at different structural levels, Central Norwegian Caledonides. *Journal of Structural Geology*, 20, 111-119.
- Rokoengen, K., Rise, L., Bryn, P., Frengstad, B., Gustavsen, B., Nygaard, E. & Sættem, J., (1995): Upper Cenozoic stratigraphy on the Mid-Norwegian continental shelf. *Norsk Geologisk Tidsskrift*, 75, 88-104.
- Romer, R. L., Kjøsnes, B., Korneliussen, A., Lindahl, I., Skyseth, T., Stendal, H. & Sundvoll, B., (1992): The Archaean-Proterozoic boundary beneath the Caledonides of northern Norway and Sweden: U-Pb, Rb-Sr, and eNd isotope data from the Rombak-Tysfiord. *Norges Geologiske Undersøkelse Rapport*, 91, 67.
- Rosby, T., (1996): The North Atlantic Current and surrounding waters: At the crossroads. *Reviews of Geophysics*, 34, 463-481.
- Rundberg, Y. & Eidvin, T., (2005): Controls on depositional history and architecture of the Oligocene-Miocene succession, northern North Sea Basin. In: Wandås, B. T. G., Nystuen, J. P., Eide, E. & Gradstein, F. M. (eds.): Onshore-Offshore Relationships on the North Atlantic Margin. *NPF Special Publication*, 12, 207-239.
- Rusk, B., (2012): Cathodoluminescent Textures and Trace Elements in Hydrothermal Quartz. In: Götze, J., & Möckel, R., (eds.): Quartz: Deposits, mineralogy and analytics: Berlin, Heidelberg, Springer Geology, 307-329.
- Seager, R., Battisti, D. S., Yin, J., Gordon, N., Naik, N., Clement, A. C. & Cane, M. A., (2002): Is the Gulf Stream responsible for Europe's mild winters? *Quarterly Journal of the Royal Meteorological Society*, 128, 2563-2586.
- Schetelig, J., (1918): Natur og fjeldgrund. Lorens Berg: Sandeherred. En bygdebok, 36-50. Kristiania.
- Schieber, J., Krinsley, D. & Tennison, E., (2002): Provenance Studies of Fine-Grained Sediments with Scanned Cathodoluminescence of Quartz: Potential Applications in Planetary Exploration. 33rd Annual Lunar and Planetary Science Conference, march 11-15, 2002, Houston, Texas, extended abstract, no. 1088.
- Scholonek, C. & Augustsson, C., (2016): Can cathodoluminescence of feldspar be used as provenance indicator? *Sedimentary Geology*, 336, 36-45.
- Seyedolali, A., Krinsley, D. H., Boggs Jr., S., O'Hara, P. F., Dypvik, H., Goles, G. G., (1997): Provenance interpretation of quartz by scanning electron microscope cathodoluminescence fabric analysis. *Geology*, 25, 787-790.
- Sippel R. F., (1968): Sandstone petrology. Evidence from luminescence petrography. *Journal of Sedimentary Petrology*, 38, 530-554.

- Smelror, M., Dehls, J., Ebbing, J., Larsen, E., Lundin, E. R., Nordgulen, Ø., Osmundsen, P. T., Olesen, O., Ottesen, D., Pascal, C., Redfield, T. F. & Rise, L., (2007): Towards a 4D topographic view of the Norwegian Sea margin. *Global and Planetary Change*, 58, 382-410.
- Smith J. V. & Stenstrom R. C., (1965): Electron-excited luminescence as a petrologic tool. *Journal of Geology*, 73, 627-635.
- Solli, A., & Nordgulen, Ø., (2008): Bedrock map of Norway and the Caledonides in Sweden and Finland – 1:2 000 000. *Geological Survey of Norway*.
- Spear, F. S., (1993): Metamorphic phase equilibria and pressure-temperature-time paths. Washington, D.C., *Mineralogical Society of America*, 799pp.
- Sprunt, E. S., Dengler, L. A., & Sloan, D., (1978): Effects of metamorphism on quartz cathodoluminescence. *Geology*, 6, 305-308.
- Steltenpohl, M. G., Hames, W. E. & Andresen, A., (2004): The Silurian to Permian history of a metamorphic core complex in Lofoten, northern Scandinavian Caledonides. *Tectonics*, 23, 1-23.
- Stuevold, L. M. & Eldholm, O., (1996): Cenozoic uplift of Fennoscandia inferred from a study of the mid-Norwegian margin. *Global Planetary Change*, 12, 359-386.
- Streckeisen, A. L., (1979): Classification and nomenclature of volcanic rocks, lamprophyres, carbonatites, and melilitic rocks: recommendations and suggestions of the IUGS sub-commission on the systematics of igneous rocks. *Geology*, 7, 331-335.
- Sturt, B. A., Dalland, A. & Mitchell, J. G., (1979): The age of the sub Mid-Jurassic tropical weathering profile of Andøya, northern Norway, and the implications for the Late Palaeozoic paleogeography in the North Atlantic region. *Geologische Rundschau*, 68, 523–542.
- Sørensen, R., (1988): In-situ Rock Weathering in Vestfold, Southeastern Norway. *Geografiska Annaler Series A*, 70, 299-308.
- Taylor, S. R., (1964): Abundance of chemical elements in the continental crust: a new table. *Geochimica et Cosmochimica Acta*, 28, 1273-1285.
- Thomas, M. F., (1966): Some Geomorphological Implications of Deep Weathering Patterns in Crystalline Rocks in Nigeria. *Transactions of the Institute of British Geographers*, 40, 173–193.
- Thomas, J. B., Watson, E. B., Spear, F. S., Shemella, F. S., Nayak, S. K. & Lanzirotti, A., (2010): Titanite under pressure: the effect of pressure and temperature on the solubility of Ti in quartz. *Contributions to Mineralogy and Petrology*, 160, 743-759.
- Torsvik, T., H. & Cocks, L. R. M., (2016): Earth History and Palaeogeography, Cambridge University Press.
- Tveten, E. (1978): Geologisk kart over Norge, berggrunnskart Svolvær 1:250 000. *Norges geologiske undersøkelse*.

- Vorren, T. O., Laberg, J. S., Blaume, F., Dowdeswell, J. A., Kenyon, N. H., Mienert, J., Rumohr, J. & Werner, F., (1998): The Norwegian Greenland Sea continental margins: Morphology and late Quaternary sedimentary processes and environment. *Quaternary Science Reviews*, 17, 273-302.
- Wahlström, R., (1993): Fennoscandian seismicity and its relation to the isostatic rebound. *Global and Planetary Change*, 8, 107-112
- Walker, G. & Burley, S., (1991): Luminescence petrography and spectroscopic studies of diagenetic minerals. In: Barker, C. E. & Kopp, O. C. (eds.): Luminescence Microscopy and Spectroscopy: Quantitative and Qualitative Applications, 83–96.
- Wark, D. A., & Spear, F. S., (2005): Titanium in quartz: cathodoluminescence and thermometry. *Geochimica et Cosmochimica Acta* Supplement, 69, A592.
- Wark D. A. & Watson, E. B., (2006): The TitaniQ: a Titanium-in-quartz geothermometer. *Contributions to Mineralogy and Petrology*, 152, 743-754.
- Wedepohl, K. H., (1995): The composition of the continental crust. *Geochimica et Cosmochimica Acta*, 59, 1217-1232.
- Weihed, P., Billström, K., Persson, P.-O. & Bergman Weihed, J., (2002): Relationship between 1.90–1.85 Ga accretionary processes and 1.82–1.80 Ga oblique subduction at the Karelian craton margin, Fennoscandian Shield. *Geologiska Föreningens i Stockholm Förhandlingar*, 124, 163-180.
- White A. F. & Blum A. E., (1995): Effects of climate on chemical weathering in watersheds. *Geochimica et Cosmochimica Acta*, 59, 1729-1747.
- White, A. F., Blum, A. E., Bullen, T. D., Vivit, D. V., Schulz, M. & Fitzpatrick, J., (1999): The effect of temperature on experimental and natural chemical weathering rates of granitoid rocks. *Geochimica et Cosmochimica Acta* 63 (19-20), 3277-3291.
- Wilson, C. J. N., Seward, T. M., Allan, A. S. R., Charlier, B. L. A. & Bello, L., (2012): A comment on: 'TitaniQ under pressure: the effect of pressure and temperature on the solubility of Ti in quartz', by Jay B. Thomas, E. Bruce Watson, Frank S. Spear, Philip T. Shemella, Saroj K. Nayak and Antonio Lanzirrotti. *Contributions to Mineralogy and Petrology*, 164, 359-368.
- Åm, K., (1975): Aeromagnetic basement complex mapping north of latitude 62°N, Norway. *Norges Geologiske Undersøkelse*, 316, 351-374.
- Ørvig, T., (1960): The Jurassic and Cretaceous of Andøya in Northern Norway. In: Høltedahl, O. (ed.) *Geology of Norway. Norges Geologiske Undersøkelse*, 208, 344-350.

8. APPENDIX

Table 4: Trace element concentrations of quartz grains in offshore sample 2 (well 6610/7-1, 900 m). Determined by LA-ICP-MS.

	Li	Be	B	Mn	Ge	Rb	Sr	Sb	Na	Al	P	K	Ca	Ti	Fe	Zn
LOD	0.08	0.11	0.40	0.14	0.32	0.01	0.01	0.01	9.32	8.53	4.53	2.38	6.15	0.84	0.69	2.29
grain no.																
1	<0.08	<0.11	9.07	1.47	1.49	<0.01	2.95	1.22	<9.32	65.76	6.49	10.70	<6.15	<0.84	1.81	4.14
3	4.99	0.09	0.44	0.36	0.93	0.20	0.13	0.08	48.85	21.86	5.15	7.00	43.86	18.63	0.67	<2.29
8	0.56	<0.11	1.92	0.36	0.59	0.01	0.06	0.07	<9.32	5.28	5.61	2.18	76.20	5.54	0.64	<2.29
9	0.44	0.09	0.74	0.61	0.83	<0.01	0.17	0.07	<9.32	62.81	<4.53	1.51	<6.15	13.24	14.50	<2.29
10	3.11	<0.11	1.16	0.52	0.86	<0.01	0.02	0.07	<9.32	17.77	6.98	3.10	<6.15	12.59	<0.69	<2.29
11	1.88	0.31	0.78	0.30	1.03	<0.01	0.07	0.12	<9.32	22.19	6.88	1.39	<6.15	4.44	1.32	<2.29
12	<0.08	<0.11	1.23	0.36	0.81	<0.01	0.79	0.25	<9.32	24.30	2.31	4.70	<6.15	<0.84	0.93	<2.29
13	3.36	0.01	0.92	0.71	0.49	<0.01	0.09	<0.01	<9.32	<8.53	<4.53	5.30	<6.15	10.37	1.24	<2.29
14	6.70	0.06	0.42	0.27	1.00	0.03	0.08	0.10	<9.32	26.31	3.61	3.64	20.53	38.45	4.56	0.53
15	4.30	<0.11	1.88	0.37	0.53	0.17	0.61	0.33	<9.32	80.51	4.54	10.81	3.40	34.37	7.70	1.57
17	5.44	0.05	0.78	0.32	1.05	<0.01	0.12	0.26	<9.32	13.01	<4.53	3.24	<6.15	2.94	0.31	1.52
18	1.01	0.16	0.79	0.31	0.92	<0.01	0.12	0.05	13.71	29.95	7.47	1.17	24.44	6.68	0.42	<2.29
20	0.05	<0.11	0.98	0.44	1.04	<0.01	0.17	0.63	<9.32	<8.53	21.93	2.38	<6.15	<0.84	9.72	<2.29
21	0.43	<0.11	3.65	1.58	0.75	0.05	0.88	1.42	<9.32	77.14	5.03	41.34	11.34	71.44	11.86	1.24
24	0.67	<0.11	0.73	0.56	0.62	0.03	0.10	0.08	<9.32	16.93	8.28	0.34	<6.15	3.66	1.12	<2.29
26	2.13	<0.11	2.17	0.71	1.00	0.09	0.14	0.19	7.37	30.27	11.75	7.70	35.26	19.99	5.08	<2.29
28	0.45	0.15	0.86	1.05	0.09	<0.01	0.20	0.17	4.04	<8.53	7.22	0.51	<6.15	<0.84	3.83	<2.29
29	0.51	<0.11	0.49	0.34	0.35	<0.01	0.14	<0.01	<9.32	<8.53	<4.53	<2.38	<6.15	28.64	0.40	<2.29
30	<0.08	<0.11	3.55	0.87	1.26	0.47	0.12	0.37	<9.32	20.61	10.12	4.58	<6.15	8.65	4.61	<2.29
31	0.14	0.46	1.89	0.28	0.94	0.07	0.36	0.17	<9.32	11.34	6.14	2.41	12.19	<0.84	2.61	<2.29
32	<0.08	<0.11	3.80	0.73	0.75	0.10	0.34	0.10	80.39	6.92	15.41	6.89	<6.15	10.33	2.30	<2.29
33	<0.08	0.09	0.61	0.36	1.19	0.13	0.09	<0.01	<9.32	39.78	<4.53	2.43	24.64	34.48	22.09	<2.29
35	2.91	<0.11	0.88	0.34	0.81	<0.01	0.07	0.08	<9.32	21.44	5.40	3.84	45.25	21.57	9.26	<2.29
36	4.27	0.20	0.47	0.53	1.02	0.09	0.11	0.10	<9.32	18.39	9.15	<2.38	<6.15	11.49	0.01	<2.29
37	<0.08	0.35	2.15	0.15	0.36	0.05	0.33	0.38	32.12	22.42	5.24	2.83	30.61	<0.84	10.27	3.05
38	6.59	0.09	1.28	0.33	1.05	<0.01	0.13	0.10	<9.32	42.66	6.44	2.11	43.63	21.89	1.67	<2.29
41	0.10	<0.11	7.15	0.84	1.16	0.04	1.63	0.84	<9.32	51.32	10.71	17.46	71.37	<0.84	9.66	<2.29
43	<0.08	<0.11	3.03	0.26	0.64	0.02	1.01	0.19	45.94	6.91	16.68	5.66	<6.15	<0.84	0.92	<2.29
47	6.79	0.06	0.68	0.30	0.68	0.06	0.16	0.03	<9.32	20.79	13.17	0.24	<6.15	10.51	0.44	<2.29
48	8.91	<0.11	0.43	0.32	1.56	0.01	0.07	0.09	<9.32	49.45	<4.53	2.91	19.04	55.12	0.72	<2.29
49	4.91	<0.11	0.71	0.32	0.54	<0.01	0.09	0.16	<9.32	30.56	1.52	1.99	10.18	8.90	1.28	<2.29
51	5.34	<0.11	1.55	0.14	0.35	<0.01	0.16	0.30	<9.32	36.98	<4.53	0.33	13.10	50.68	2.88	3.28
52	4.91	<0.11	0.64	0.41	1.10	0.06	0.10	0.04	<9.32	23.03	3.80	1.27	<6.15	7.41	1.05	<2.29
53	0.36	<0.11	3.57	0.50	0.72	<0.01	0.19	1.49	6.83	50.15	10.96	9.30	0.93	5.71	1.76	<2.29
55	5.58	0.42	1.69	0.34	0.87	0.01	0.14	0.33	<9.32	36.07	3.96	2.46	<6.15	19.65	6.75	<2.29
65	11.26	0.66	0.84	0.41	0.42	0.03	0.24	0.26	<9.32	38.27	6.67	4.63	<6.15	46.50	0.13	<2.29
66-A	2.34	<0.11	0.77	0.33	0.89	0.04	0.17	0.23	<9.32	23.61	14.49	0.49	42.86	27.78	9.26	<2.29
67	0.34	<0.11	1.05	0.26	0.59	0.01	0.11	0.07	<9.32	<8.53	11.43	7.32	<6.15	<0.84	0.84	<2.29
68	0.30	<0.11	5.34	1.01	0.64	0.23	1.48	0.15	42.85	27.61	14.04	20.50	66.64	<0.84	73.69	<2.29
69	5.82	0.26	0.63	0.27	1.26	<0.01	0.04	0.25	<9.32	16.89	10.41	0.07	<6.15	13.42	0.08	<2.29
73	0.39	0.98	2.84	0.35	0.90	<0.01	0.01	<0.01	<9.32	<8.53	7.67	2.91	14.45	<0.84	<0.69	<2.29
74-A	6.73	<0.11	1.24	0.16	0.79	0.09	0.05	0.15	<9.32	5.56	8.86	5.67	31.55	20.39	0.41	<2.29
74-B	5.87	<0.11	1.27	0.37	0.95	<0.01	0.13	0.18	<9.32	28.97	17.55	4.83	<6.15	16.31	1.94	<2.29
75	7.48	<0.11	1.56	0.59	1.54	0.04	<0.01	0.09	<9.32	23.66	0.97	<2.38	<6.15	12.52	0.47	<2.29

Table 5: Trace element concentrations of quartz grains in offshore sample 1 (well 6610/3-1, 460 m). Determined by LA-ICP-MS.

	Li	Be	B	Mn	Ge	Rb	Sr	Na	Al	P	K	Ca	Ti	Fe
LOD	0.14	0.10	0.39	0.06	0.08	0.02	0.00	9.15	5.21	6.07	16.88	5.37	0.92	1.65
grain no.														
1	13.45	0.03	3.10	0.38	0.42	< 0.02	0.05	< 9.15	19.98	2.15	0.54	2.29	40.75	0.13
3	16.89	0.04	4.45	0.32	0.91	0.02	0.03	< 9.15	71.84	< 6.07	0.40	< 5.37	37.45	4.10
5	6.47	< 0.10	3.83	0.33	0.98	0.07	0.07	< 9.15	109.64	1.56	20.74	< 5.37	44.35	6.04
7	2.75	< 0.10	3.40	0.17	1.07	0.02	0.05	< 9.15	10.42	5.55	0.65	< 5.37	3.36	0.20
8	5.23	< 0.10	2.98	0.22	0.47	< 0.02	0.08	< 9.15	17.58	0.37	2.06	1.31	29.73	0.50
12	7.53	0.09	3.37	0.31	0.80	0.06	0.11	< 9.15	95.40	5.01	11.60	< 5.37	38.99	1.18
14	6.32	< 0.10	1.79	0.13	0.41	0.02	0.02	< 9.15	21.46	3.19	0.55	7.09	28.12	0.18
15	1.15	0.02	1.92	0.32	0.63	0.02	0.17	2.69	19.12	6.60	1.45	5.79	29.56	1.60
16	< 0.14	0.01	2.62	0.19	0.48	< 0.02	0.10	< 9.15	19.36	11.11	1.05	14.60	20.59	3.73
17	10.61	0.01	2.84	0.28	0.45	< 0.02	0.11	< 9.15	47.12	0.44	0.93	< 5.37	27.73	0.43
18	16.82	< 0.10	1.90	0.16	0.66	< 0.02	0.03	< 9.15	48.88	4.35	0.61	< 5.37	22.05	0.40
19	< 0.14	< 0.10	2.17	0.16	0.82	< 0.02	0.02	< 9.15	6.36	1.05	< 16.88	< 5.37	5.67	0.44
21	6.72	< 0.10	2.29	0.18	0.72	< 0.02	0.04	< 9.15	17.76	0.46	1.10	5.89	6.01	< 1.65
23	< 0.14	0.03	4.11	0.38	1.14	< 0.02	0.01	< 9.15	6.82	3.85	< 16.88	< 5.37	2.49	0.20
28	3.14	0.03	2.34	0.25	0.79	0.06	0.04	< 9.15	27.17	0.97	1.65	4.52	12.96	0.23
29	3.50	< 0.10	2.14	0.24	0.37	< 0.02	0.07	< 9.15	37.37	< 6.07	< 16.88	< 5.37	23.99	0.26
30	< 0.14	0.04	2.60	0.16	0.69	< 0.02	0.05	< 9.15	12.68	11.61	< 16.88	< 5.37	5.92	6.65
31	< 0.14	< 0.10	2.29	0.36	1.36	0.01	0.28	1.81	8.29	< 6.07	0.39	5.59	< 0.92	1.13
32	3.13	0.09	2.31	0.20	1.07	< 0.02	0.03	< 9.15	10.69	1.49	0.59	< 5.37	6.88	0.14
33	0.11	< 0.10	1.78	0.65	0.50	0.09	1.02	14.13	28.55	< 6.07	4.69	18.70	24.50	0.61
34	3.38	< 0.10	2.12	0.21	0.65	0.01	0.05	< 9.15	16.87	3.04	0.46	7.07	18.11	< 1.65
37	4.70	0.06	1.90	0.25	0.70	< 0.02	0.03	< 9.15	20.47	0.94	0.57	4.76	19.27	< 1.65
40	12.33	0.10	2.20	0.24	0.75	< 0.02	0.05	< 9.15	30.95	< 6.07	1.21	0.65	20.19	0.35
42	1.43	0.01	2.53	0.30	0.65	0.02	0.03	< 9.15	17.26	8.03	< 16.88	12.71	4.25	3.38
43	4.85	0.07	1.13	0.17	1.03	< 0.02	0.06	< 9.15	19.01	2.59	0.17	< 5.37	15.97	0.05
44	9.23	0.08	1.49	0.17	0.91	< 0.02	0.05	< 9.15	36.62	< 6.07	1.55	5.41	8.35	0.20
45	2.76	0.08	1.42	0.13	0.91	< 0.02	0.05	< 9.15	9.62	5.11	< 16.88	4.17	1.12	0.05
46	11.56	0.08	1.58	0.18	0.95	< 0.02	0.04	< 9.15	24.60	1.93	< 16.88	< 5.37	11.10	0.20
47	7.36	0.02	2.02	0.27	0.88	< 0.02	0.05	< 9.15	57.70	0.70	3.89	< 5.37	30.61	1.93
48	5.65	< 0.10	1.58	0.17	1.08	< 0.02	0.04	< 9.15	17.22	< 6.07	< 16.88	< 5.37	7.64	< 1.65
49	1.35	0.06	2.24	0.20	0.83	0.02	0.03	< 9.15	15.05	0.27	1.45	3.44	8.31	4.03
52	17.25	0.22	2.45	0.29	0.40	0.02	0.04	< 9.15	58.79	1.47	< 16.88	< 5.37	43.99	0.99
53	2.51	< 0.10	2.99	0.37	0.83	< 0.02	0.07	< 9.15	54.84	0.58	2.25	< 5.37	56.81	1.11
56	0.36	0.12	3.50	0.27	0.71	< 0.02	0.05	< 9.15	15.37	15.31	< 16.88	< 5.37	17.66	0.61

Table 6: Trace element concentrations of quartz in sample 47802 (Hundholmen, Tysfjord). Determined by LA-ICP-MS.

	Li	Be	B	Mn	Ge	Rb	Sr	Na	Al	P	K	Ca	Ti	Fe
LOD	1.06	0.11	0.71	0.43	0.26	0.05	0.05	11.8	7.5	1.7	0.6	26.1	1.5	0.64
sample no.														
47802-A	6.57	0.53	2.06	< 0.43	0.87	< 0.05	< 0.05	12.6	18.0	< 1.7	1.3	69.7	4.5	< 0.64
47802-B	6.31	< 0.11	2.34	0.44	1.74	0.05	< 0.05	19.3	< 7.5	< 1.7	< 0.6	< 26.1	3.8	< 0.64

Table 7: Trace element concentrations of quartz grains in sample 89415 (Brennvinshaugen, Hadseløya) and sample 89421 (Stotland, Hamarøy). Determined by LA-ICP-MS.

	Li	Be	B	Mn	Ge	Rb	Sr	Na	Al	P	K	Ca	Ti	Fe
89415-1	5.80	0.18	4.60	0.31	0.68	0.00	0.06	0.00	119.00	3.83	1.44	5.47	7.11	0.45
89415-4	6.68	0.15	3.92	0.49	0.67	0.00	0.16	1.13	136.59	2.59	9.30	8.92	3.33	1.75
89415-7	6.69	0.00	3.79	0.39	0.56	0.04	0.13	0.49	178.89	0.83	7.00	2.50	5.05	0.64
89415-8	5.69	0.00	4.03	0.61	0.78	0.05	0.18	1.74	194.35	1.62	2.90	7.22	6.81	0.39
89415-9	5.92	0.00	4.10	0.56	0.64	0.03	0.06	7.79	91.66	7.23	9.74	7.42	4.40	1.55
89421-3	3.41	0.31	4.57	0.69	0.92	0.01	0.18	5.36	56.58	3.09	2.09	6.22	6.50	1.32
89421-4	3.86	0.00	3.53	0.16	0.70	0.20	0.11	5.78	88.59	2.83	6.04	0.00	6.06	0.75
89421-5	3.03	0.00	4.64	0.52	0.81	0.00	0.20	2.63	38.64	1.17	2.54	7.20	11.86	0.15
89421-6	4.04	0.00	2.82	0.14	0.76	1.22	0.14	0.00	17.86	3.60	1.51	2.64	6.23	0.05
89421-7	3.28	0.00	3.35	0.44	0.69	0.00	0.17	1.87	12.39	0.81	5.44	0.00	10.12	0.11